THÈSE

En vue de l'obtention du

DOCTORAT DE L'UNIVERSITÉ DE TOULOUSE

Délivré par *l'Institut National des Sciences Appliquées de Toulouse*
Discipline ou spécialité : *Traitement du Signal*

Présentée et soutenue par Mathieu RAIMONDI
Le 24 Octobre 2008

Titre : Développement et Caractérisation de techniques de réduction d'interférences pulsées pour récepteurs GNSS embarqués

(Development and Characterization of Pulsed Interference Mitigation Techniques for on-board GNSS Receivers)

JURY
Prof. Dr. Francis Castanié - Président
Prof. Dr. René Landry - Rapporteur
Prof. Dr. Emmanuel Duflos - Rapporteur
Dr. Christophe Macabiau - Directeur de thèse
Dr. Olivier Julien - Examinateur
Ing. Jean-Michel Perre - Examinateur

Ecole doctorale : *Mathématiques Informatique Télécommunications de Toulouse*
Unité de recherche : *Laboratoire de Traitement du Signal et des Télécommunications de l'ENAC*
Directeur(s) de Thèse : *Christophe Macabiau*

Résumé

Les organismes de standardisation de l'aviation civile (OACI, RTCA, EUROCAE) mènent actuellement des études sur l'utilisation des systèmes de navigation par satellite fournissant une couverture globale, tels GPS ou Galileo, en tant que moyen de navigation embarqué unique. L'OACI regroupe l'ensemble de ces systèmes de navigation satellitaires et de leurs systèmes d'augmentation sous la dénomination GNSS. Pour des raisons de sécurité évidentes, les performances des récepteurs GNSS embarqués doivent garantir des minima propres à chaque phase de vol et chaque procédure d'approche. Ces exigences de performances sont spécifiées dans les spécifications des performances opérationnelles minimales, documents publiés (ou en cours de publication) par les autorités sus-citées.
Le GNSS est en passe d'être amélioré par la diffusion de nouveaux signaux. Parmi eux, les signaux Galiléo E5 et GPS L5 devraient permettre l'amélioration du service de navigation par satellite. Cependant, ces signaux seront émis dans une bande déjà utilisée par des systèmes radiofréquences. Il est donc primordial de s'assurer de la possibilité de la cœxistence de ces systèmes. Plus particulièrement, il est nécessaire de s'assurer que les récepteurs GNSS embarqués utilisant les signaux sus-cités respectent les exigences de performance. La menace principale au bon fonctionnement des récepteurs GNSS utilisant les signaux E5/L5 a été identifiée comme étant les émissions pulsées des systèmes DME, TACAN, JTIDS et MIDS. Sans moyen de lutte contre ces interférences, les performances des récepteurs GNSS embarqués peuvent être dégradées de manières significatives, empêchant les récepteurs de se conformer aux exigences de sécurité sur l'ensemble du monde, et plus particulièrement sur des « points chauds » ayant été identifiés comme les lieux ou l'impact de ces interférences sur lesdits récepteurs est la plus importante. Deux techniques de réduction d'interférences ont été proposées pour lutter contre cette menace, le Blanker temporel et le Frequency Domain Interference Suppressor (FDIS).
Le Blanker temporel est une technique de traitement du signal consistant en un test de puissance, relativement simple à mettre en œuvre et dont la capacité de réjection des interférences a été démontrée suffisante pour assurer les exigences de l'aviation civile dans toutes les phases de vols sur l'ensemble du monde pour les récepteurs GPS et Galiléo utilisant respectivement les signaux L5 et E5, dans [Bastide, 2004]. Toutefois, cette technique permet de respecter les exigences avec une marge faible, dans les environnements les plus riches en interférences, autrement dit les « points chauds ».
En revanche, le FDIS est une technique de lutte contre les interférences pulsées beaucoup plus exigeante en termes de ressources, puisque basée sur l'excision des interférences dans le domaine fréquentiel. Cependant, elle permet une amélioration sensible des performances du récepteur, et donc une augmentation des marges vis-à-vis des exigences fixées par l'Aviation Civile.

Le FDIS a été proposé comme une alternative au blanker temporel, mais ses problèmes d'implantation et ses performances n'ont été que peu étudiés. La dissertation a pour but de participer à cette étude de performance afin de valider son intérêt. Le plan de la thèse est le suivant : tout d'abord, les signaux de navigation, Galileo E5a/E5b et GPS L5, les interférences pulsées, ainsi que leur impact sur les performances des récepteurs GNSS sont présentés. Ensuite, une description des techniques de suppression d'interférences (blanker temporel, FDIS), leurs caractéristiques théoriques et les dégradations de performances subies par un récepteur GNSS utilisant ces techniques en présence d'interférences pulsées sont présentées. Les conditions dans lesquelles ont été obtenues ces performances, c'est à dire le choix des scénarios joués ainsi que des paramètres observés, ou encore les outils de simulation sont décrits. La conclusion résume l'analyse des performances, les compare aux exigences de l'Aviation Civile, et propose des recommandations pour la conception de récepteurs GNSS embarqués.

Abstract

Civil Aviation standardisation bodies (ICAO, RTCA, EUROCAE) are currently investigating the use of the Global Navigation Satellite System (GNSS) as a stand-alone navigation solution for civil aircraft. For obvious safety reasons, on-board GNSS receivers must guarantee minimum performance requirements in given phases of flights. These requirements, dependent upon the system and signals used, are stated in the Minimum Operational Performance Specification (MOPS), published (or being published) by the corresponding authorities.
With that respect, the future use of Galileo E5 and GPS L5 bands has raised, among others, interference issues. Indeed, pre-existent RF systems emit in this band, thus interfering with the E5/L5 signals. The main threat was identified as being DME/TACAN ground beacons pulsed emissions. Without any mitigation capability, these systems can disturb the proper operation of on-board GNSS receivers, preventing them from complying with safety requirements. Two Interference Mitigation Techniques (IMT) have been proposed to fight this threat, the Temporal Blanker and the Frequency Domain Interference Suppressor (FDIS). The Temporal Blanker technique offers a fairly simple implementation and was shown to provide enough benefits to ensure that the specified requirements were met in all phases of flight for a GPS L5 or Galileo E5 receiver. However, it was also demonstrated that the resulting performances were meeting the requirements by only a small margin on the worst DME/TACAN interference environment that can be found in Europe and USA, so called the European and USA “hot spots”.
In contrast, the FDIS is a more demanding mitigation technique against pulsed interference in terms of required resources but improves the performances of the receiver, thus allowing larger margins with respect to the civil aviation requirements.
The core of the study is the analysis of the performances of GNSS receivers using FDIS as IMT. The dissertation architecture is the following: first, the navigation signals, Galileo E5a/E5b and GPS L5, as long as the interferences that constitute a threat for GNSS navigation and their impact on GNSS receivers operations are presented. Then, a description of the studied IMTs (Temporal Blanker, FDIS), their theoretical characteristics and the theoretical derivations of the post-correlation C/N_0 degradation suffered by a receiver using these techniques in presence of pulsed interference are depicted.

Afterwards, all the results obtained concerning the IMTs performance assessments are presented. Firstly, the Figures Of Merit chosen to analyze the performance of both techniques are presented and their choice is motivated. Then, the chosen interference and signal scenarios, along with the simulation tools and means are finely detailed. Finally, a confrontation of Temporal Blanker and FDIS performances is given using the previously described FOMs. The conclusion summarizes the performances analysis, compares them to

civil aviation performances requirements, and proposes recommendations for on-board GNSS receivers design.

Acknowledgments

First, I would like to acknowledge the European Commission, who funded my PhD thesis, through its 6th framework program and more particularly the Anastasia project. More generally speaking, I would like to thank the European Commission for funding ambitious research projects throughout Europe. I also thank some members of the ANASTASIA consortium, who I had the chance to meet. It was a pleasure to work with Kristne BIRKELAND and Reto TRÖNDLE from DATARESPONS, Luis NUNES from Skysoft, Gordana MIJIC from Ascom, Giovanni GROSSO from Selex communications, Stephane ROLLET and Jean-Yves CATROS from Thales Avionics.

En second lieu, j'aimerais remercier l'état Français, qui permet à chaque citoyen de suivre des études supérieures, sans distinction de classe sociale ni d'origine ethnique.

Je tiens aussi à remercier l'Ecole Nationale de l'Aviation Civile, et plus particulièrement le département EL et son Laboratoire du Traitement du signal et des Télécommunications, au sein duquel s'est déroulée ma thèse. Ces remerciements s'adressent aussi bien Monsieur Farid ZIZI, directeur des études de l'ENAC, qu'à Monsieur Lucien MAZET, chef du département EL, et qu'à tous les membres du LTST. Je remercie aussi Cathy MIGOT et Colette ROY, pour leur aide précieuse au secrétariat.

Je remercie aussi mon directeur de thèse Christophe MACABIAU, qui aurait pu figurer en premier dans cette liste. Il a su me communiquer sa passion pour la recherche, mais aussi instaurer une ambiance de travail détendue et agréable dans son laboratoire, tout en conservant une très bonne qualité technique ainsi qu'un grand sens de l'organisation. Il lui reste toutefois à améliorer son touché de balle.

Il m'est impossible de ne pas remercier Olivier JULIEN, mon « nègre », pour avoir suivi de très près mes travaux. Il est aussi doué d'une grande qualité technique et il est très agréable de travailler à ses côtés, il a donc été très précieux durant ces 3 ans et je le remercie mille fois. Son toucher de balle est bien meilleur que celui de Christophe MACABIAU.

Je remercie aussi les doctorants que je pu rencontrer et côtoyer au LTST. Tous sont animés d'une forte curiosité scientifique, et il a été agréable et motivant de travailler avec eux. Je remercie ainsi Philippe PAIMBLANC, Emilie REBEYROL, Damien KUBRAK, Hanaa ALBITAR, Audrey GIREMUS, Benjamin CHIBOUT, Anaïs MARTINEAU, Christophe OUZEAU, Na TAO, Marianna SPANGENBERG, Axel GARCIA, Paul THEVENON, Pierre NERI, Adrien CHEN, Damien SERANT, et Gaël.

Je remercie aussi Antoine BLAIS, enseignant à l'ENAC, pour son aide et ses connaissances en traitement numérique du signal. Il est, lui aussi, animé d'une grande curiosité scientifique, ce qui est fort agréable. Je lui souhaite bonne chance pour sa thèse.

Je remercie les professeurs LANDRY et DUFLOS, mes rapporteurs de thèse, ainsi que le professeur Francis CASTANIE, le président de mon jury de soutenance, ainsi que Jean-Michel PERRE. Je tiens à remercier ce dernier pour sa participation en tant que membre de mon jury, ainsi que pour sa collaboration tout au long du projet ANASTASIA. C'est un ingénieur de qualité, tant au niveau technique qu'humain.

Je remercie aussi mes parents, et de manière générale ma famille, qui m'ont permis de poursuivre mes études jusqu'au bout.

Enfin, je remercie ma femme, Nathalie, pour le bonheur que nous avons partagé durant ces années, et qui a contribué à me mettre dans de bonnes conditions de travail.

Table of Contents

List of Figures

List of Tables

List of Symbols and Acronyms

Acronyms

ADC	Analog-to-Digital Converter
AGC	Automatic Gain Control
AltBOC	Alternative Binary Offset Carrier
ANASTASIA	Airborne New Advanced Satellite Techniques and Technologies in a System Integrated Approach
ARNS	Aeronautical Radio Navigation Service
Bdc	Blanker Duty Cycle
BER	Bit Error Rate
C/N_0	Carrier to Noise density ratio
CW	Continuous Wave
DAC	Digital to Analog Converter
DFT	Discrete Fourier Transform
DME	Distance Measuring Equipment
DPU	Digital Processing Unit
DSP	Digital Signal Processor
DTI	Direction de la Technique et de l'Innovation
E5	E5 frequency band centred in 1191.18 MHz
EMLP	Early Minus Late Power
EUROCAE	EURopean Organization for Civil Aviation Equipments
FDAF	Frequency Domain Adaptive Filtering
FDIS	Frequency Domain Interference Suppressor
FEC	Forward Error Correction
FFT	Fast Fourier Transform
FIR	Finite Impulse Response
FOM	Figure Of Merit
FPGA	Field-Programmable Gate Array
GIRASOLE	Galileo Integrated Receivers for Advanced Safety Of Life Equipment
GNSS	Global Navigation Satellite System
GPS	Global Positioning System
I&D	Integrate and Dump filter
ICAO	International Civil Aviation Organization
ICD	Interface Control Document

IGEB	Interagency GPS Executive Board
IIR	Infinite Impulse Response
ILS	Instrument Landing System
IMT	Interference Mitigation Technique
ITU	International Telecommunication Union
JTIDS	Joint Tactical Information Distribution System
Kcps	Kilo chip per second
L5	
MIDS	Multifunctional Information Distribution System
MLS	Microwave Landing System
MMI	Man Machine Interface
MOPS	Minimum Operational Performance Specification
OS	Open Service
Pdf	Probability density function
Pfa	Probability of false alarm
Pmd	Probability of missed detection
P/NRZ/L	Polar-Non-Return-to-Zero-Level
PRF	Pulse Repetition Frequency
PRN	Pseudo Random Noise
PSD	Power Spectral Density
PULSAR	PULSe Assessment Routine
PVT	Position, Velocity and Time
QPSK	Quadra Phase Shift Keying
QZSS	Quasi-Zenith Satellite System
RCU	Receiver Control Unit
RF	Radio Frequency
RTCA	
SNR	Signal to Noise Ratio
SoL	Safety Of Life
TACAN	TACtical Air Navigation system
THAV	Thales Avionics
TTFF	Time To First Fix
VGA	Variable Gain Amplifier
VOR	Very high frequency Omnidirectional Range

Symbols

α	Elevation angle
β	Thermal noise power reduction at correlator output due to front-end filtering
C	Total signal transmitted power
C_I	Interference coefficient
d	Early-late spacing
D	Navigation message
ε_ϑ	Phase offset between the received and local

	carriers
$f_{carrier}$	Interference carrier frequency
$FDIS_{eq}$	FDIS Equivalent transfer function
f_P	Predetection bandwidth
f_S	Sampling frequency
G_{beacon}	Normalized DME/TACAN beacon antenna gain
$G_{aircraft}$	Normalized aircraft antenna gain
h	
H_0	Neyman-Pearson test hypothesis 0
H_1	Neyman-Pearson test hypothesis 1
H_{BB}	Frequency base-band equivalent filter of the front-end filter
H_{BB}	
L	Maximum quantization level
λ	Non-central chi-square distribution non-centrality parameter
λ	Parameter of the Poisson law
L_{free}	Free space loss
M	Number of non-coherent integrations
N	Number of samples used in FFT calculations
N_0	Thermal noise density
$N_{0,I}$	Interference equivalent noise density at correlator output
$P_{\text{int}erf}$	Received interference mean power after front-end filtering
R_f	Correlation of the local code with the filtered incoming code
S_C	Base-band normalized PRN code PSD
S_I	Base-band normalized interference PSD
Th	Threshold
T_0	Neyman-Pearson test criterion 0
T_1	Neyman-Pearson test criterion 1
T_S	Sampling period
w	Weighting windows coefficients

INTRODUCTION

MOTIVATION

Today's airliners use numerous and expensive ground navigation systems, such as Very high frequency Omnidirectional Range or Distance Measuring Equipments (VOR/DME) for en-route, or Instrument Landing System (ILS) for landing operations. The International Civil Aviation Organization (ICAO) current strategy for introducing advanced communication, navigation, and surveillance systems is to replace the ground navigation systems by satellite-based ones [European Community, 2003]. The Global Navigation Satellite System (GNSS) is defined by ICAO as "A worldwide position and time determination system that includes one or more satellite constellations, aircraft receivers and system integrity monitoring, augmented as necessary to support the required navigation performance for the intended operation" [ICAO]. Using GNSS as a unique navigation mean, whatever the phase of flight, would decrease airliners costs but also simplify the navigation procedures.

The already existing Global Positioning system (GPS) cannot guarantee the safety level required by the ICAO for the most critical phases of flight, such as landing operations. The performances of a GNSS can be observed along four criteria: accuracy, availability, continuity, and integrity. As part of the development of satellite-based positioning systems, (in particular GPS modernization or the development of Galileo), a certain number of new features were meant to allow GNSS receivers to match ICAO minimum performances required.

The Galileo E5a/E5b and GPS L5 signals were mainly designed for civil aviation purposes. They are located within the 960 - 1215 MHz frequency band, which was already allocated to Aeronautical Radio Navigation Services (ARNS). This provides a strong protection against out-of-band interferences and ensures that interference between systems present within this band respect the recommendations from the International Telecommunication Union (ITU). Because other aeronautical systems (such as Distance Measuring Equipment (DME), TACtical Air Navigation (TACAN), Joint Tactical Information Distribution System (JTIDS) and Multifunctional Information Distribution System (MIDS)) were already present in this band, it was necessary to ensure that the proposed GNSS signals could coexist with them without significantly degrade their performance. The particularity of these interferences is their

pulsed nature. [Tran, 2001] showed that the GPS L5 signal could not fully coexist with the current systems as it is, unless the DME/TACAN and JTIDS/MIDS frequencies are reassigned.

In particular, [Bastide, 2003''] and [Tran, 2001] stated that GNSS receivers could not comply with civil aviation performance requirements in the worst interference environments, using E5/L5 signals. It then appeared as a necessity to design antenna or receiver based Interference Mitigation Techniques (IMTs). Using current antennas and forecasts on future receivers architectures, [Bastide, 2004] showed that GNSS receivers could meet civil aviation requirements using an IMT called the Temporal Blanker, but with very slim margins and non negligible constraints on the receiver design. This technique blanks the parts of the signal that are above a certain threshold due to the presence of a pulsed interference.

[Bastide, 2004] is a PhD thesis sponsored by the "Direction de la Technique et de l'Innovation" (DTI), a French civil aviation institution. DTI is deeply involved in standardisation activities so that the interference impact assessment on E5/L5 was a topical subject needing a resolution. Notably, the DTI is linked member of the EURopean Organisation for Civil Aviation Equipment Working Group 62 (EUROCAE WG-62), which is in charge of Galileo standardization for civil aviation in Europe. In particular, the results proposed in [Bastide, 2004] largely inspired EUROCAE WG-62 works and were also used by the RTCA SC-159, which is the US equivalent for EUROCAE WG-62. The quoted PhD thesis concluded that link budgets for GPS L5 and Galileo E5a/E5b signals were positive over both Europe and the U.S.A. following a conservative worst-case approach and assuming the use of the temporal blanker. However, the E5a/L5 margins are slight and the degradation results sensitive to the blanking threshold. Finally, 1500 to 2500 hardware correlators are required to meet the civil aviation acquisition time requirements.

[Monnerat, 2000] also studied an alternative IMT: the Frequency Domain Adaptive Filtering (FDAF). This technique detects and removes the interferences in the frequency domain, which is expected to be more efficient than the temporal blanking technique, the counter part being a significantly higher required processing power. This technique has also been studied in [DiPietro, 1989], where the algorithm is called a Frequency Domain Interference Suppressor (FDIS), and not FDAF. Indeed, the name FDAF is used in [Kinjo, 1997], where the proposed technique is completely different from the algorithm proposed in [Monnerat, 2000]. In this PhD thesis, the denomination FDIS has been preferred to FDAF. [Monnerat, 2000] also provided FDIS and temporal blanker performance assessments, through simulation results and theoretical derivations. These results showed that FDIS was a more efficient IMT than the temporal blanker.

The temporal blanker was thoroughly investigated by civil aviation certification bodies (RTCA, EUROCAE, ICAO) as a fairly simple method to mitigate DME/TACAN and JTIDS/MIDS pulsed interference while still allowing civil aviation operations anywhere anytime. The FDIS was only briefly investigated in a second time, mostly due to its significant complexity with respect to the temporal blanker. However, with the increase in the processing power, the FDIS is more seducing because if applied correctly, it could lead to more comfortable margins for civil aviation users, thus relaxing constraints on the other receiver parameters.

The European Commission funded through the 6th framework programme the ANASTASIA project ([ANASTASIA, 2008]) which core is to provide on-board Communication, Navigation and Surveillance (CNS) solutions to cope with the foreseen doubling of air traffic by 2020. More particularly, the objective of the Navigation Subproject SP3 "Navigation and space based technologies", was to define the new satellite-based technologies able to fulfil the civil aviation requirements in the Navigation domain, and to validate their performance ([ANASTASIA]). One of the outcomes of this project is a Galileo E1/E5 dual-frequency receiver mock-up incorporating innovative signal processing techniques, mostly to fight multipath and in-band interferences. An important part of the receiver was the implementation of both the temporal blanker and the FDIS techniques to mitigate pulsed interference. The present PhD thesis was conducted in the framework of the ANASTASIA project, which funded the PhD.

The objectives of the PhD were thus:

- To deepen the FDIS analysis given in [Monnerat, 2000], to propose a theoretical derivation of the technique's expected performances, and to study the benefits brought by this technique with respect to the temporal blanker in the context of civil aviation considerations,
- To take into account hardware solutions that have been proposed to implement the FDIS and temporal blanker techniques, and the effect of implementation constraints, which have been neglected in [Bastide, 2004],
- To design, based on the previous analysis, the temporal blanker and the FDIS that will be implemented in the ANASTASIA mock-up receiver, taking into account the receiver constraints,
- To participate to the testing of the ANASTASIA receiver and assess the resulting performance,
- To conclude about the worthiness of the FDIS implementation on airborne GNSS receivers through theoretical derivations, simulations, and tests.

THESIS CONTRIBUTION

Based on the previous section, the major contributions of the present Ph.D. thesis are the following:

- Consolidation of the results on pulsed interferences impact on GNSS receivers performances,

- Consolidation of the results on GNSS receivers using the Temporal Blanker as IMT,

- Analysis of FDIS algorithm against pulsed interference,

- Theoretical derivation of post-correlation C/N_0 degradation in pulsed interference environment using FDIS as a mitigation technique,

- Analysis of the impact of pulsed interference on Automatic Gain Control (AGC) device accuracy,

- Implementation and test of a distribution based AGC showing good pulsed interference robustness on a Galileo mock-up receiver,

- Implementation and test of Temporal Blanker and FDIS algorithms as IMTs on a Galileo mock-up receiver,

- Analysis of the impact of the FDIS algorithm on PRN codes isolation and tracking loops accuracy,

- Matching of the mock-up receiver with civil aviation requirements.

THESIS ORGANIZATION

The core of the study is the analysis of the performances of GNSS receivers using FDIS as IMT. The dissertation architecture is the following.

First, the navigation signals, Galileo E5a/E5b and GPS L5, are presented in Chapter I. The interferences that constitute a threat for GNSS navigation are also presented in Chapter I, along with their impact on GNSS receivers operations. Finally, it presents the performances required by the civil aviation authorities to certify a GNSS receiver as a primary navigation mean, relevant in the scope of the study.

Chapter II describes the studied IMTs (Temporal Blanker, FDIS), their theoretical characteristics and the theoretical derivations of the post-correlation C/N_0 degradation suffered by a receiver using these techniques in presence of pulsed interference. It also proposes an analysis of the implementation constraints susceptible to degrade the algorithms performances, and study their impact on them.

The analysis approach, the Figures Of Merit chosen to analyse the performance of both techniques, the chosen interference and signal scenarios, and the simulation tools (theoretical derivation tool, PULSAR, Galileo receiver mock-up, GIRASOLE receiver mock-up, acquisition time simulator) used to obtain the results are finely detailed in Chapter III.

Chapter IV gathers all the results obtained concerning the IMTs performance assessments. A confrontation of Temporal Blanker and FDIS performances is given using the previously described FOMs and simulation tools. The results are also compared with civil aviation requirements.

The conclusion summarizes the performances analysis, and proposes recommendations for on-board GNSS receivers design. Finally, alternative interference mitigation techniques are introduced, and perspectives for future work are proposed.

CHAPTER I: GALILEO E5A/E5B AND GPS L5 SIGNALS AND THEIR INTERFERENCE ENVIRONMENT

This chapter describes the GPS L5 and Galileo E5 signals, along with the interference that threatens their correct use by GNSS users. Those new GNSS signals were chosen to be broadcast in an Aeronautical Radio Navigation Services frequency band (ARNS), as it is protected by the International Telecommunication Union (ITU). However, this ARNS band was already occupied by radio navigation systems such as DME, TACAN, JTIDS, and MIDS, which impact on GNSS receivers cannot be ignored.
The first section of this chapter is dedicated to the description of the GPS L5 signal, and the second one to the Galileo E5a/E5b signals. The third section describes the other signals already present in the E5 band, while the fourth section briefly introduces typical GNSS receivers' architecture. Finally, the fifth section describes the impact of these interferences on GNSS receivers operations.

I.1. GPS L5 SIGNAL STRUCTURE

The GPS L5 signal was originally introduced in order to support the civil aviation community. It brings several important features with respect to the GPS L1 C/A signal alone: it allows dual frequency measurements, and thus precise ionospheric delay corrections; it is also a precise signal due to its wide bandwidth (10 times the bandwidth of the GPS C/A); finally, it also provides a backup to the L1 signal, improving the service availability.

The GPS L5 signal can be modelled at the receiver antenna port as follows:

$$\begin{aligned} s_{L5}(t) = \sqrt{C}\cdot d\left(t-\tau_g\right)\cdot XI\left(t-\tau g\right)\cdot NH_{10}\left(t-\tau_g\right)\cdot\cos\left(2\pi f_{L5}t-\vartheta\right) \\ +\sqrt{C}\cdot XQ\left(t-\tau_g\right)\cdot NH_{20}\left(t-\tau_g\right)\cdot\sin\left(2\pi f_{L5}t-\vartheta\right) \end{aligned} \qquad \text{I.1}$$

Where:

- The signal is composed of two components in phase quadrature: the data component (in-phase), and the pilot component (in quadrature),
- τ_g is the time-varying group delay,
- ϑ is the GPS signal carrier phase shift,

- C is the total signal transmitted power,
- d is the Polar-Non-Return-to-Zero-Level (P/NRZ/L) materialisation of the navigation message. Only the Inphase component carries this message,
- XI and XQ are respectively the P/NRZ/L materialisation of the Inphase and Quadraphase Pseudo Random Noise (PRN) codes,
- NH_{10} and NH_{20} are respectively the P/NRZ/L materialisation of the Inphase and Quadraphase Neuman-Hoffman codes (also called secondary codes or synchronisation sequences),
- t is the time in seconds,
- f_{L5} =1176.45 MHz is the L5 carrier frequency.

The main characteristics of the GPS L5 signal shown in Table 1 introduce the major improvements brought in this new signal (compared to the L1 C/A signal): the increase of the chip rate, the presence of two different components (Pilot + Data), and the introduction of secondary codes and of Forward Error Correction (FEC) codes. The latter ones are meant to reduce the Bit Error Rate (BER).

Table 1: L5 signal characteristics

Channel	Modulation type	Chip Rate [Mcps]	Code Period	Symbol Rate [sps]	FEC period [sps]	Secondary Code Rate	Secondary Code Period
L5 data	QPSK	10.23	1 ms	50	100	1 kHz	10 ms
L5 pilot				N/A	N/A		20 ms

A more detailed description of the L5 signal can be found in the GPS L5 Interface Specification (IS) [ARINC, 2005].

I.1.1. **GPS L5 PRN Codes**

The major interest of the GPS L5 signal is its use of high chipping rate: it induces a wider spectrum compared to L1 C/A which results in a better robustness against narrow-band interference, a better mitigation of long-delay multipath, and lower tracking noise jitter. The spreading sequence used by GPS L5 are also significantly longer than the GPS C/A sequences, which provide a better isolation with cross-correlation peaks ([Van Dierendonck, 1999]). 74 PRN codes (37 XI used on the Data channel, and 37 XQ used on the Pilot one) were chosen from the GPS L5 codes generating process, provided in [ARINC, 2005]. For each satellite, the code pair (XI and XQ) was chosen to be as orthogonal as possible. Figure 1 shows the power spectral density of a typical GPS L5 PRN code. The main lobe is 20 MHz wide, which well illustrates the better robustness of such codes to interference.

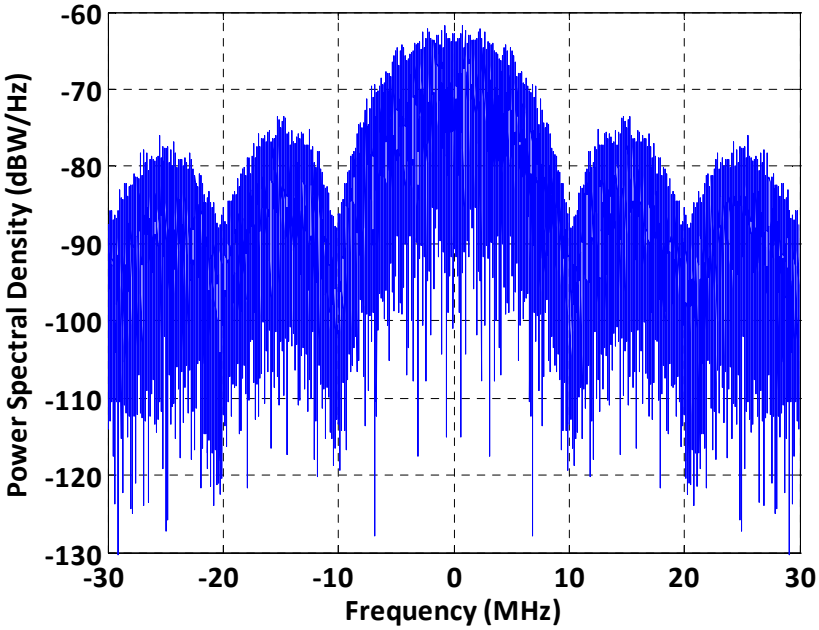

Figure 1 : Normalized GPS L5 PRN 1 XI code PSD.

A summary of the cross-correlation isolation with respect to the autocorrelation function main peak, extracted from [Macabiau, 2002], is given in Table 2, where Doppler frequency offsets are neglected. GPS L1 C/A PRN codes isolations are also given, to show the improvement brought by the new GPS L5 codes.

Table 2: 1 ms XI and XQ codes properties

	XI/XI	XQ/XQ	XI/XQ (same satellite)	L1 C/A
Maximum crosscorrelation sidelobe (dB)	-26.4	-26.5	-62.1	-21.0

I.1.2. **Navigation Message and Synchronisation sequence**

The navigation message carries essential information for user position determination. As presented in Table 1, only the data component of the L5 signal broadcasts the required data, the pilot component being meant only for ranging.
As it will be clarified later, the present investigation does not require the generation of the navigation message, thus it will not be described further herein. However, the complete description of the transmitted navigation message can be found in [ARINC, 2005].
Both components (data and pilot) are also encoded respectively with a 10-bit and a 20-bit Neuman-Hoffman code. One code chip of the secondary code has the same duration as the whole primary code period, 1 ms. These codes are used notably for bit synchronisation

improvement, and also to fight against narrow-band interference. They are also extensively described in [ARINC, 2005].

I.2. GALILEO E5A/E5B SIGNAL STRUCTURE

The Galileo system will propose numerous navigation signals broadcasted on 3 bands: E1, E5 and E6. The E5 signal, which is emitted within 1164 and 1215 MHz is composed of the E5a and E5b signals, modulated coherently using an AltBOC(15,10) modulation ([Rebeyrol, 2005]). The ALTBOC(15,10) modulation is described in [GSA, 2008]. It can be noted that its PSD is constituted of two main side-lobes, one centred around 1176.45 MHz representing the E5a component, and one centred around 1207.14 MHz representing the E5b component. Note that the E5a signal PSD superimposes with the GPS L5 signal [Rebeyrol, 2007].
The E5a and E5b signals are both composed of a data and a pilot component. The navigation data carried by the E5a signal corresponds to the Galileo Open Service (OS), while the E5b signal carries the Galileo Safety-of-Life service data.
The E5 signal can be processed in 2 different ways:

- As a single wide bandwidth signal,
- Or considering each of the two signals separately. In this case, both E5a and E5b signals can be considered as QPSK-modulated with a minimal degradation. However, this configuration imposes a high level of filtering between the 2 signals, as it will be seen later on.

The latter strategy has been chosen by the EURopean Organization for Civil Aviation Equipment (EUROCAE) in [EUROCAE, 2007], in order to avoid interferences in one band to degrade the Galileo signal in the other band. For example, interferences received in either band might cause the loss of both signals in case they are simultaneously tracked. Otherwise, if the signals are separately tracked, only the one concerned by the interference might be lost. Moreover, it is important to keep in mind that the E5b signal is the only one to carry the Safety-of-Life message, and thus the integrity message necessary to civil aviation.
Both signals are modulated by PRN ranging codes, secondary codes. The major characteristics of the E5 signal are summarized in Table 3. Because E5b transmits the integrity message, the data rate is higher than on E5a.

Table 3 : E5 signal characteristics

Channel	Modulation type	Chip Rate [Mcps]	Symbol Rate [sps]
E5a data	AltBOC(15,10)	10.23	50
E5a pilot			N/A
E5b data			250
E5b pilot			N/A

The E5a normalized power spectrum (XQ - PRN 1) is represented in Figure 2, while the E5b one (XQ - PRN 1) is shown in Figure 3.

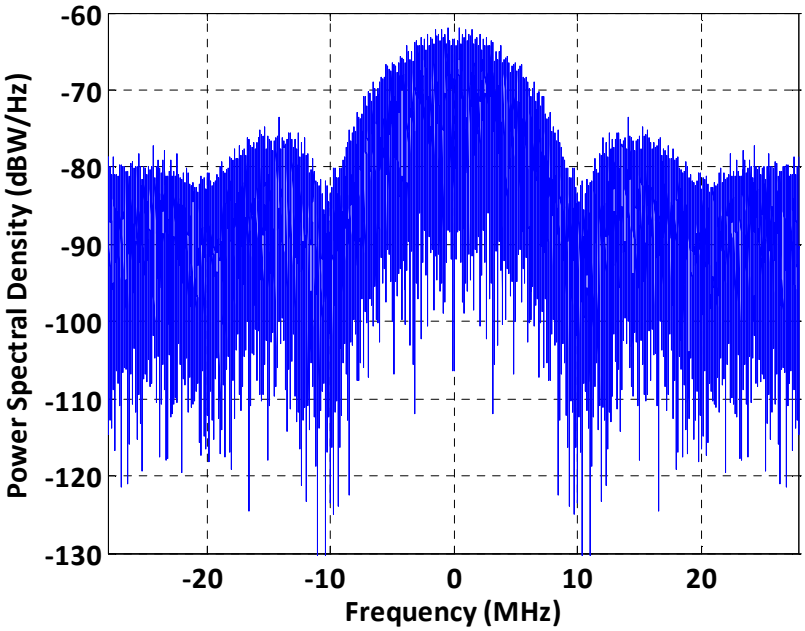

Figure 2: Normalized Galileo E5a PRN 1 code PSD.

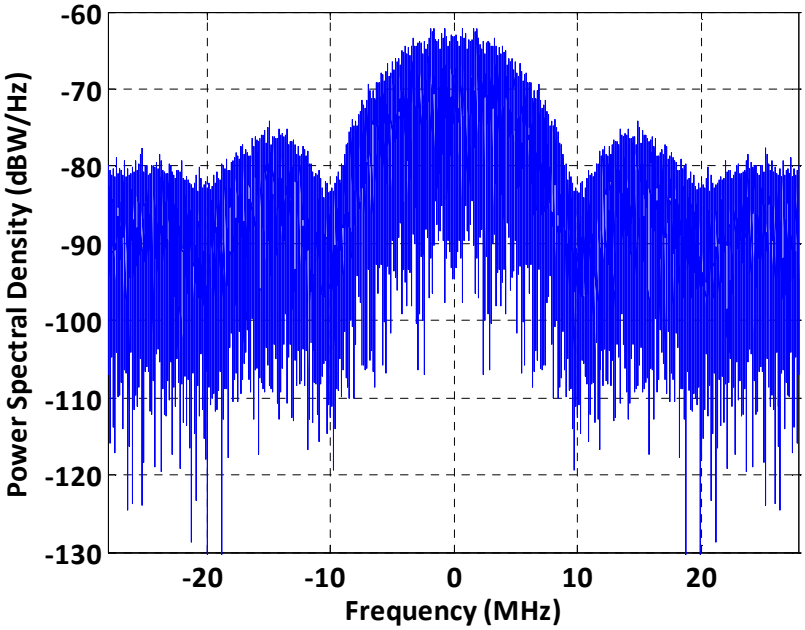

Figure 3: Normalized Galileo E5b PRN 1 code PSD.

I.2.1. **GALILEO E5 Spreading Codes Characteristics**

The Galileo E5 primary codes have the same properties than the L5 ones: chipping rate of 10.23 Mcps, period of 1 ms. The major difference between E5 and L5 codes lies in the length of the secondary codes (or synchronisation sequences), as shown in Table 4.

Table 4: Galileo E5 PRN codes caracteristics

Channel	Code Length (ms)	Code length (chips)	
		Primary	Secondary
E5a-I	20	10230	20
E5a-Q	100	10230	100
E5b-I	4	10230	4
E5b-Q	100	10230	100

Galileo E5 PRN code isolation properties are expected to be similar to those of GPS L5.

I.2.2. **Navigation Message and Synchronization Sequence**

Two different types of navigation messages are transmitted by the E5 signal: the F/NAV message on the E5a data component, and the I/NAV message on the E5b data component. The major difference between these two messages is their emission rate: 50 symbols per second for F/NAV, 250 symbols per second for I/NAV. Moreover, E5a is part of the Open and the Commercial Services (OS and CS), while E5b is part of the Open, the Commercial and the Safety of Life (SoL) services ([ESA, 2008]). Indeed, the E5b signal (I/NAV message) broadcasts navigation and integrity data applicable to E1/E5b dual-frequency measurements (the integrity information is not valid for E1/E5a measurements). This is the reason why, from the civil aviation community point of view, at this time the E5b signal is of greater interest than the E5a one. This situation may change as the possibility of broadcasting integrity data on the E5a signal is still under discussion.
As for GPS L5, Galileo E5 secondary codes are used to improve bit synchronization, solve pseudorange measurements ambiguities, and also improve the signals' robustness to narrow-band interference. Their chip rate also equals 1 kilo chip per second (kcps), but their period is longer, as shown in Table 4.
A full description of Galileo OS signals can be found in [GSA, 2008].

I.3. INTERFERENCE THREATS IN THE E5 BAND

The L5/E5 band occupation has already been extensively studied, in [RTCA, 2004], or [Anon, 1997]. DME/TACAN and JTIDS/MIDS signals have been identified as the only systems – excepted unintentional emissions – emitting in the band of interest. Out-of-band and spurious emissions such as military radars impact on GNSS receivers have been assessed negligible for the GPS L5 and Galileo E5a signals [RTCA, 2004]. It is slightly different for the E5b signal, since the military radar band finishes very close to the E5b upper limit (1217 MHz). Because military radars emit very powerful signals, they are a potential threat to GNSS reception due to a potential lack of filtering. This problem was thoroughly investigated by the EUROCAE ([EUROCAE, 2007]) and the solution was to specify a sharp E5b filter that has a cut-off frequency well within the E5b band, as shown in paragraph I.6.2.

I.3.1. **DME/TACAN Signals**

DME, and its military equivalent, TACAN, are two systems used by aircrafts to know their distance to a ground station, which position is known. The systems operate as follows ([Borden, 1951]): the aircraft DME equipment (called interrogator) sends pulses to ground stations. Once the interrogation is detected, the station transponder replies to the interrogator. The distance is then determined by measuring the time elapsed between each pulse transmitted by the interrogator and the reception of its corresponding reply pulse from the transponder. This time corresponds to twice the distance between the aircraft and the station, plus fixed processing time inside the ground station.
According to [RTCA, 2004], only the signals emitted in the band of interest of the study disturb GNSS receivers operations. Indeed, the band of interest is either the E5a/L5 one and equals [1164 MHz; 1191 MHz], or the E5b one which equals [1191 MHz; 1215 MHz]. The aircraft's DME interrogators emitting their signals between 1025 and 1151 MHz, they are ignored herein. The study focuses on DME ground stations, as they emit their signals between 962 and 1213 MHz, which includes the above defined band of interest. The emitted signal is composed of a pair of Gaussian pulses modulated by a cosine, which can be modelled as:

$$s(t) = \sqrt{P} \times \sum_{k=1}^{N} \left(e^{\frac{-\alpha(t-t_k)^2}{2}} + e^{\frac{-\alpha(t-t_k-\Delta t)^2}{2}} \right) \times \cos\left(2\pi f_l t + \theta_l\right) \qquad \text{I.2}$$

Where:

- P is the interference beacon transmitting peak power (dBW),
- f_l is the carrier frequency of the DME/TACAN signal (Hz),
- $\alpha = 4.5 \times 10^{11} s^{-2}$,
- $\Delta t = 12 \mu s$ is the inter pulse time separation,
- t_k is the emission time of the kth pulse pair and
- ϑ_l is the DME/TACAN signal initial carrier phase shift.

Figure 4 represents a normalized DME/TACAN pulse pair, modulated at 14 MHz. This carrier was chosen as it is the Intermediate Frequency (IF) used in the simulators and the mock-up receiver.

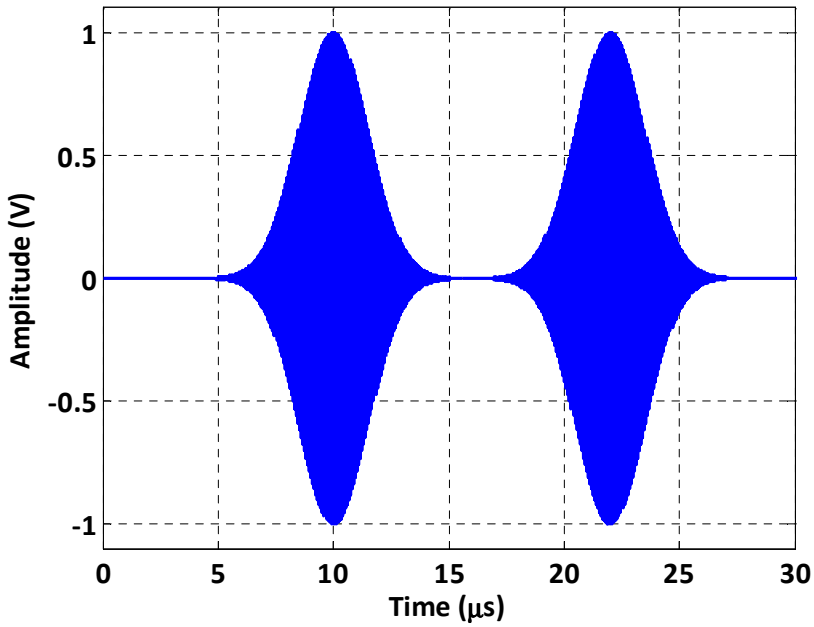

Figure 4: DME signal pattern.

Theoretically, the Fourier transform (FT) of a DME/TACAN signal as expressed in I.2 has the following expression:

$$TF(DME/TACAN) = A\sqrt{\frac{2\pi}{\alpha}}\frac{\left(e^{-\frac{2\pi^2}{\alpha}(f+f_l)^2}+e^{-\frac{2\pi^2}{\alpha}(f-f_l)^2}\right)}{2}\times\left(1+e^{-2i\pi f\Delta t}\right)\times e^{-2i\pi f\left(t_k+\frac{\vartheta_l}{2\pi f_l}\right)} \qquad \text{I.3}$$

Moreover, signal's FT are calculated on a bounded support, which is materialized by a rectangular window of duration *T*. Then, the FT of a windowed DME/TACAN signal has the following expression:

$$TF(DME_{[0;T]}) = \left(A\sqrt{\frac{2\pi}{\alpha}}\frac{\left(e^{-\frac{2\pi^2}{\alpha}(f+f_l)^2}+e^{-\frac{2\pi^2}{\alpha}(f-f_l)^2}\right)}{2}\times\left(1+e^{-2i\pi f\Delta t}\right)\times e^{-2i\pi f\left(t_k+\frac{\vartheta_l}{2\pi f_l}\right)}\right)\otimes T\,\mathrm{sinc}(\pi fT) \qquad \text{I.4}$$

Figure 5 shows that the energy of a DME/TACAN pulse pair is spectrally constrained. Indeed, more than 99.99% of its energy is contained in a bandwidth of 1 MHz. It can be noticed that this band is much narrower than the studied GNSS signals' ones.

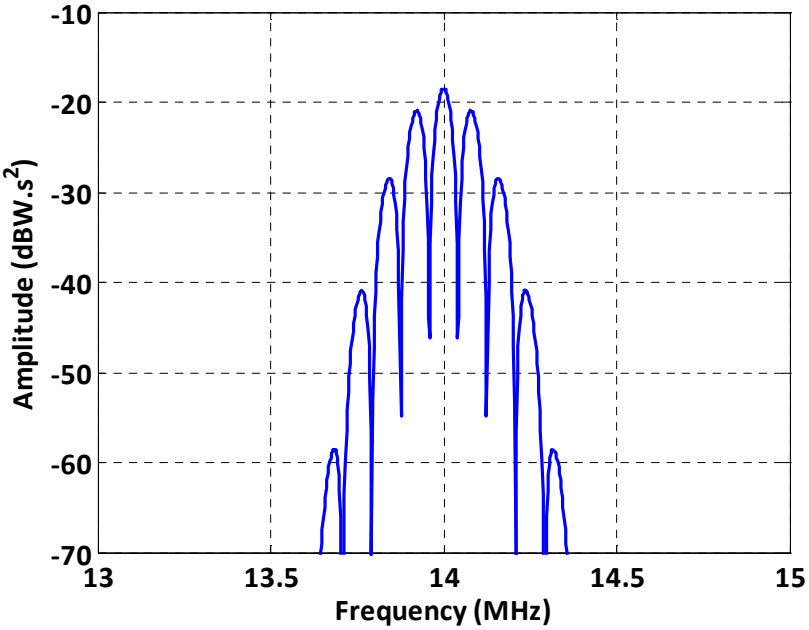

Figure 5: Normalized DME/TACAN Signal Energy Spectral Density.

The answers of each and every beacon located in the radio-electric range are received at the airplane level. The number of beacons and their characteristics are therefore a function of the position (latitude, longitude, altitude) of the aircraft. The DME/TACAN stations located in Europe are represented on Figure 6 by red (DME) and blue (TACAN) dots.

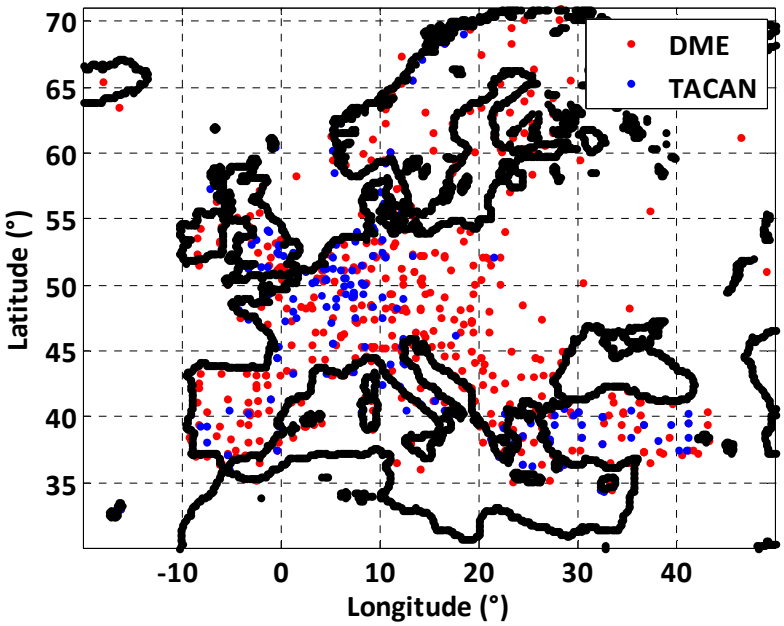

Figure 6 : European DME/TACAN ground stations.

Figure 7 provides the same information in the United States of America. The study focuses on these areas as most DME/TACAN beacons are concentrated in Europe and USA.

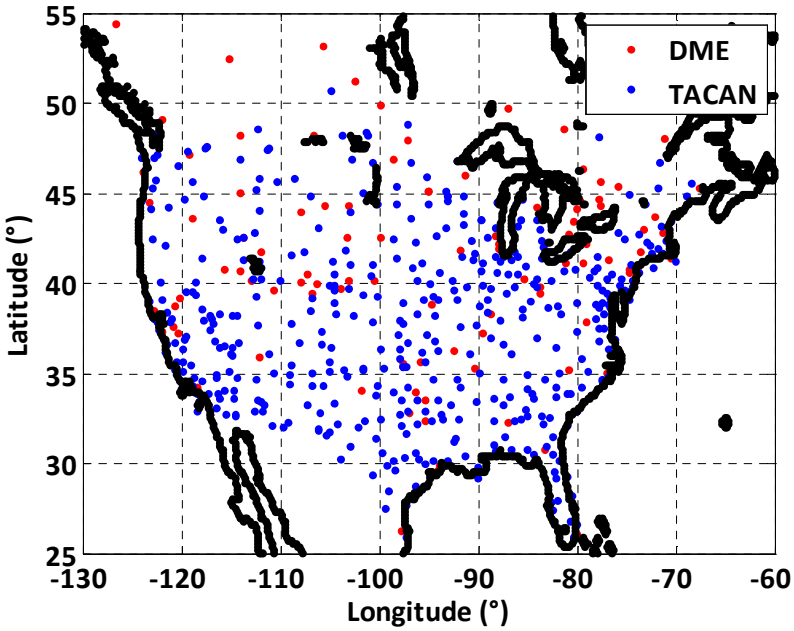

Figure 7: US DME/TACAN ground stations.

Each DME/TACAN ground beacon can respectively emit up to 2700/3600 pulse pairs per second. This number depends upon the number of aircrafts sending interrogations to the station, so upon the air traffic.

I.3.2. **JTIDS/MIDS Signals**

JTIDS is an L band TDMA network radio system used by the United States armed forces and their allies to support data communications needs, principally in the air and missile defence community. It provides high-jam-resistance, high-speed, crypto-secure computer-to-computer connectivity in support of every type of military platform from Air Force fighters to Navy submarines. JTIDS is one of the family of radio equipment implementing what is called Link 16.

Multifunctional Information Distribution System (MIDS) is the NATO name for the communication component of Link-16. An older MIDS is the JTIDS.

JTIDS/MIDS signals are composed of pulses that last 13 µs (6.4 µs active and 6.6 µs passive). Those pulses are modulated by a chip sequence, which is 32 chips long and each chip lasts 200 ns. A typical JTIDS/MIDS pulse is represented in Figure 8.

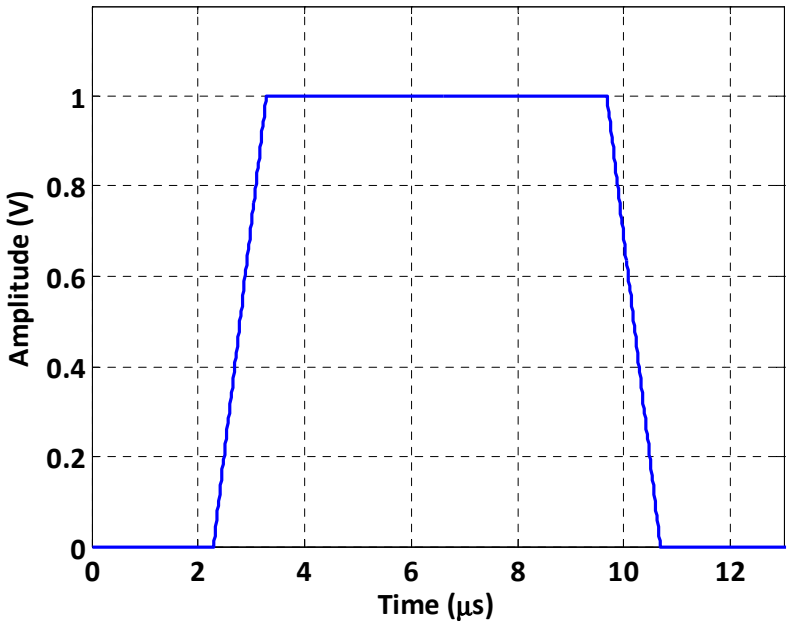

Figure 8 : Normalized JTIDS/MIDS pulse.

More details about JTIDS/MIDS signals can be found in [Nisner, 2003].

I.4. GNSS RECEIVERS ARCHITECTURE

In this paragraph, GNSS receivers' architecture is briefly described. This description is required to introduce how the interferences described in paragraph I.5 impact these receivers. Figure 9 shows a simplified scheme of generic GNSS receivers' architecture, which is detailed in [Van Dierendonck, 1996].

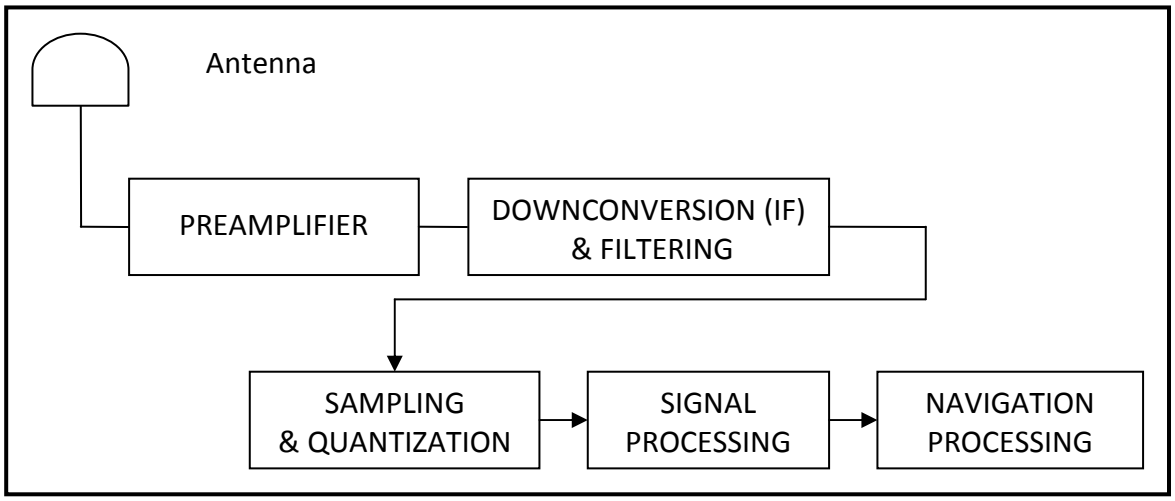

Figure 9 : GNSS Receiver Architecture.

I.4.1. **Antenna and Preamplifier**

The RF front-end is mainly composed of an antenna and a preamplifier.
There are many important factors entering in the assessment of an antenna performance (antenna gain pattern, front-to-back ratio, polarization, etc…). In the present case, it is interesting to spend time discussing the antenna gain pattern. Indeed, it is crucial to be able to receive the useful signal with a high gain while rejecting the interference. It has to be kept in mind that DME/TACAN and JTIDS/MIDS signals are coming from ground stations and thus from negative elevations. In general, in the civil aviation context, antenna gains are not specified for such negative elevations, but RTCA and EUROCAE proposed assumptions about maximum aircraft antenna gain patterns, which are provided in paragraph I.6.2. These assumptions are necessary to assess the performance of the receiver in the worst case scenario.
The preamplifier is usually composed of a preselector filter, a burnout protection and a Low Noise Amplifier (LNA). The LNA is used to amplify the signal, while limiting the level of noise entering the receiver. They can process signals linearly only within a specified range, this range being chosen according to the incoming signal specifications. In this study, it has been assumed that the preamplifier was designed to stand the most powerful interference that could be received. Thus, the effect on the preamplifier is considered to be negligible.

I.4.2. **Down-conversion and Filtering**

GNSS signals are transmitted at Radio Frequencies (RF), and need to be down-converted to an Intermediate Frequency (IF) before sampling and processing. The down-conversion is required to lower signal processing complexity, and is performed by mixing the incoming signal with local oscillators. The local oscillators are usually derived from the receiver reference oscillator, thus stressing the importance of the oscillator quality.
Filtering is then required to keep only the frequency band of interest, and remove out of-band interference, as well as local oscillators feed-through and harmonics. In particular, the quality of the filter and its design highly impact the receiver performance. Indeed, the sharpness of the filter edges is of tremendous importance because of the presence of near-band interferences, as already mentioned for the case of Galileo E5b, or the case of a separate processing of E5a and E5b. Moreover, filtering degrades both the useful signal and the thermal noise powers. At correlator output, the SNR degradation due to equivalent front-end filtering is:

$$\deg(SNR) = \frac{\left(\int_{-\infty}^{+\infty} S_C(f) H_{BB}(f) df \right)^2}{\int_{-\infty}^{+\infty} S_C(f) \left| H_{BB}(f) \right|^2 df} \qquad \text{I.5}$$

Where:

- S_c is the base-band normalized PRN code PSD,
- $H_{BB}(f)$ is the frequency response base-band equivalent filter of the front end filter.

I.4.3. **Sampling and Quantization**

This stage transforms the analog signal into a digital one. In this study, attention will be paid on the quantization process which is highly impacted by interference. A typical sampling and quantizing architecture is given in Figure 10.

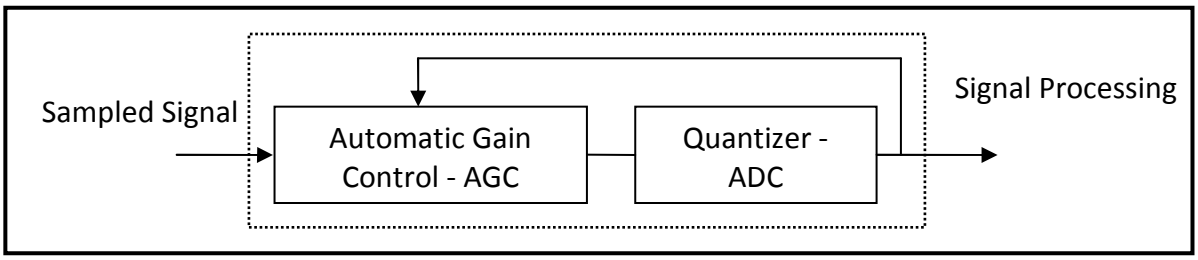

Figure 10 : Close-up to Quantization: AGC-ADC block.

Quantization is achieved by an Analog to Digital Converter (ADC), which turns voltages into bit trains. Quantization laws can be centred (0 is a possible output value) or non-centred (0 is not a possible output value).
Figure 11 presents the example of a uniform centred 8-bit quantization law. As it will be seen later on, this law is used in the ANASTASIA mock up receiver. The input voltages included in the range [-L; +L] volts are turned into bit trains which decimal representation lies in the range [-127; +127]. If the input values do not lie in the [-L; +L] range, the ADC is saturated and the output value equals -127 or +127.

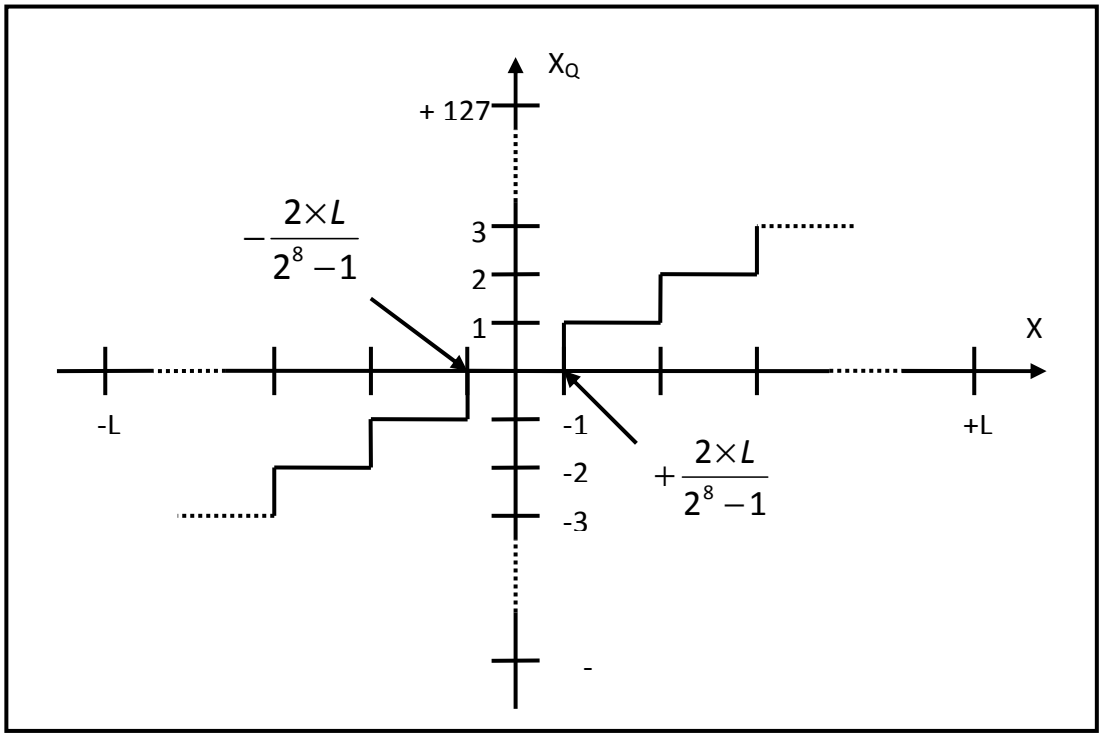

Figure 11: Example of uniform centred 8-bit quantization law.

The quantization process creates a degradation that is usually referred to as quantization noise. This noise is typically modelled as an additive white noise. It results in a decrease of the Signal-to-Noise Ratio (SNR), which will degrade further signal processing performance.
The SNR degradation due to quantization is a function of the ADC input signal and the converter characteristics (number of bits and quantization law). In this study, the ADC input signal is composed of:

- Thermal noise (assumed Gaussian and white), which power depends upon the receiver temperature, the cable losses and amplifications operated between the antenna and the ADC,
- The GNSS signal of interest. Referring to the link budget in [Bastide, 2004], which considers the same operational conditions, it can be seen that the level of this signal is significantly below the noise floor,
- Interference, if received. As exposed in section I.3, mainly pulsed interference (DME/TACAN and JTIDS/MIDS) will be considered.

In the nominal case, interferences are not considered so that the signal entering the ADC is dominated by thermal noise. The distribution and power of the observed signal are therefore almost completely set by the thermal noise. The SNR degradation suffered because of quantization is then a function of the number of bits used in the ADC, the quantization law, the maximum quantization level (L), and the noise standard deviation. Figure 12 shows the SNR degradation suffered at the correlator output due to quantization (assumed uniform and centred), for different number of bits, as a function of k, defined as the ratio between the maximum quantization level (L) and the input signal standard deviation. Moreover, the results were obtained assuming infinite front-end equivalent

bandwidth and infinite sampling frequency [Van Dierendonck, 1996]. Otherwise, the degradation is larger, as shown in [Chang, 1982].

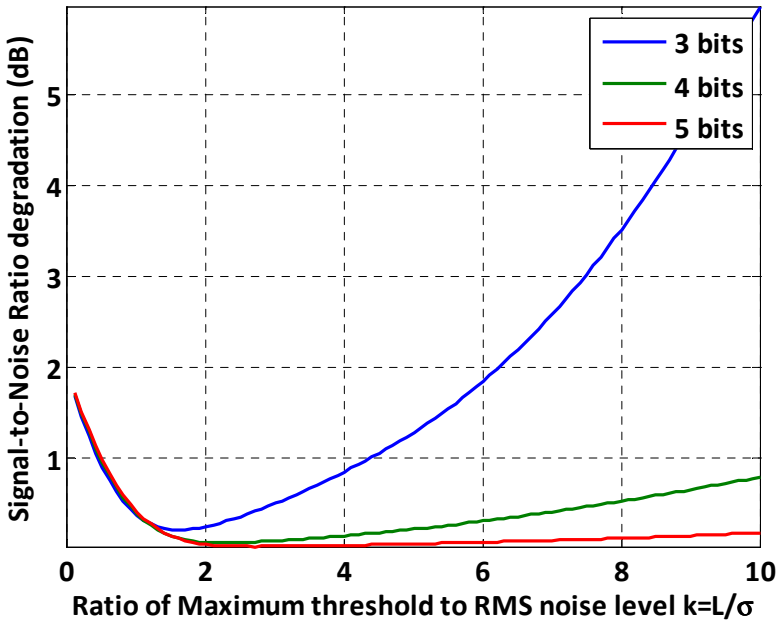

Figure 12 : SNR degradation at correlator output in presence of thermal noise only.

According to Figure 12, for a given ADC implementation (number of bits, quantization law, maximum quantization level), the signal standard deviation can be set so as to minimize quantization losses.

As mentioned earlier, the thermal noise entering the ADC varies with time, mainly because of temperature variations. Therefore, the standard deviation at ADC input cannot be predicted, so that it is not possible to preset amplifiers gains that will minimize the quantization loss during the receiver design. The total gain applied to the signal needs to be adapted during the operation of the receiver, requiring the implementation of a specific amplifier: the AGC. This module amplifies the signal before the ADC (see Figure 10), and adapts its gain using a feedback loop. The classical implementation estimates the signal standard deviation at ADC output, calculates the difference between the standard deviation minimizing quantization loss and the current estimate, and sends a command to the AGC. The performances of such AGCs depend upon the quality of the standard deviation estimator, the real distribution of the received signal, and the design of the loop (filters, time constant).
More particularly, the reception of interferences modifies the distribution and the power of the signal. AGCs sensitivity to interferences is described in paragraph I.5.1.

I.4.4. **Signal Processing**

The signal processing stage is composed of two main functions: acquisition and tracking. The acquisition is meant to roughly estimate the signal propagation delay and the Doppler

frequency. The tracking process consists in a refined estimation of the code and carrier phases. Both processes use correlators, which are described below. In addition, other modules can be added. This is the case in the context of this thesis, since a specific emphasis is given to the mitigation of pulsed interference. These modules will be introduced later in the dissertation.

I.4.4.1. Correlators' output modelling

The correlators process the signal as follows:

- The signal is multiplied by a locally generated carrier,
- The obtained signal is multiplied by a locally generated PRN code,
- The signal is then integrated over one or several code length.

The correlator scheme, provided in Figure 13, represents the 3 processes described above.

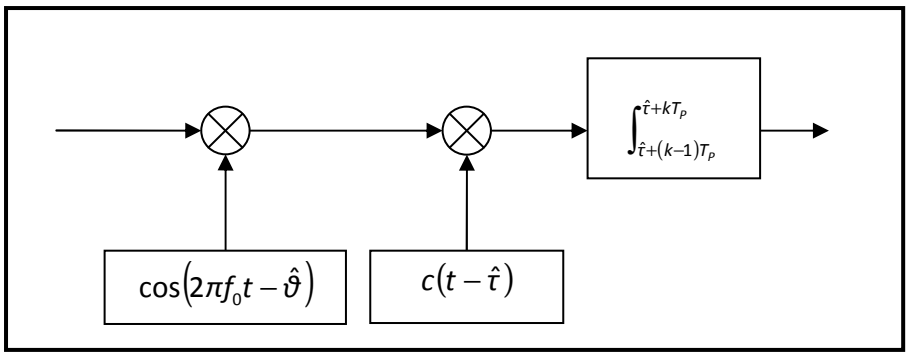

Figure 13: Architecture of a correlator.

Because GPS L5, and Galileo E5a and E5b have a data and a pilot component using different spreading sequences, it is necessary to represent separately the correlator output of each component. The In-phase and Quadraphase correlators output can be modelled as follows [Bastide, 2004]:

$$
\begin{aligned}
I_{data}(k) &= \sqrt{\frac{C}{4}} D(k) \frac{\sin(\pi \Delta f T_P)}{\pi \Delta f T_P} \cos(\varepsilon_\vartheta(k)) R_{data,f}(\varepsilon_\tau(k)) + n_{I,data} \\
Q_{data}(k) &= \sqrt{\frac{C}{4}} D(k) \frac{\sin(\pi \Delta f T_P)}{\pi \Delta f T_P} \sin(\varepsilon_\vartheta(k)) R_{data,f}(\varepsilon_\tau(k)) + n_{Q,data} \\
I_{pilot}(k) &= \sqrt{\frac{C}{4}} \frac{\sin(\pi \Delta f T_P)}{\pi \Delta f T_P} \sin(\varepsilon_\vartheta(k)) R_{pilot,f}(\varepsilon_\tau(k)) + n_{I,pilot} \\
Q_{pilot}(k) &= \sqrt{\frac{C}{4}} \frac{\sin(\pi \Delta f T_P)}{\pi \Delta f T_P} \cos(\varepsilon_\vartheta(k)) R_{pilot,f}(\varepsilon_\tau(k)) + n_{Q,pilot}
\end{aligned}
\qquad \text{I.6}
$$

Where:

- $D(k)$ is the navigation data bit sign over the kth coherent integration,
- $\Delta f = f_{DOP} - f_{DOP,loc}$ is the frequency offset between the received and local carriers,

- ε_{ϑ} is the phase offset between the received and local carriers,
- $\varepsilon_{\tau} = \tau_g - \tau$ is the phase offset between the received and local codes,
- $R_{data,f}$ and $R_{pilot,f}$ are respectively the data and pilot cross-correlations between the filtered received codes and the unfiltered local ones. A representation of this cross-correlation functions is given in Figure 14,
- $n_{I,data}$, $n_{Q,data}$, $n_{I,pilot}$, $n_{Q,pilot}$, are respectively the in-phase/quadraphase correlator output noise contribution of the data and pilot components. These noise samples are centred and have a power of $\sigma_n^2 = \beta \frac{N_0 f_P}{4}$,
- f_p is the predetection bandwidth and equals $1/T_p$, where T_p is the coherent integration time,
- $\beta = \int_{-\infty}^{+\infty} S_C(f) \left| H_{BB}(f) \right|^2 df$ is the thermal noise power reduction at correlator output due to front-end filtering.

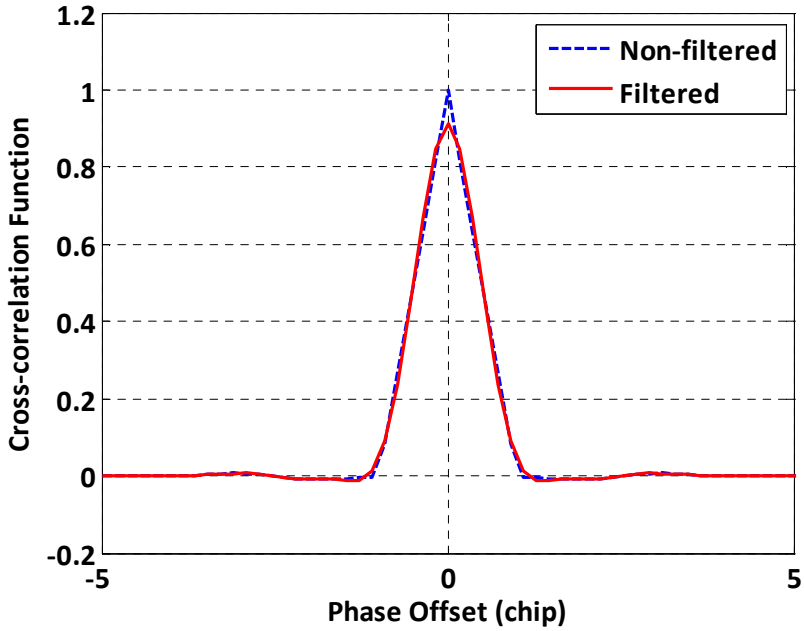

Figure 14: Cross-correlation functions between received and local E5/L5 codes.

There are several important results linked to the expression of the correlator output. First, it can be noticed that the useful component of the In-phase and Quadraphase correlator output are very similar:

- There is a dependence with the code delay error following the correlation function between the incoming and the locally generated spreading code. Note that because Galileo E5a and E5b are processed as BPSK(10) signals with minimal degradation, the associated correlation function can be assumed similar to that of GPS L5.

- There is a dependence with the frequency error following a sinc function. The first zero of this sinc function appears at $1/T_p$ which means that a correlation done over a long integration time will require a small frequency error to function properly.

On the other hand, the impact of the phase error is different between the I and Q components: the first one has a cosine dependence, while the second one has a sine dependence.

Finally, note also that a longer coherent integration results in a higher SNR. Thus, it is interesting to use a long integration time if possible. However, several reasons limit the choice of the integration time, such as:

- The presence of a navigation data bit transition,
- The drift of the receiver clock,
- A strong dynamic stress.

I.4.4.2. Acquisition Process Principle

The objectives of the acquisition process are to detect the signal of interest, and if successful, to roughly assess its characteristics:

- The delay between the incoming spreading code and the local spreading code, τ_g,
- The Doppler frequency, f_{DOP}.

A basic acquisition strategy consists in searching sequentially all the possible values of τ_g and f_{DOP} until the acquisition criterion is maximized and reaches a pre-defined threshold. In order to do so, a range of values and a search step are defined for the two parameters. This range usually depends upon the available information regarding the signal of interest (availability of the time, ephemeris, etc). This defines the size of the two-dimensional search space composed of code/frequency bins. For each bin, or code/frequency combination $\left(\tau, f_{DOP,loc}\right)$, the following criterion is calculated:

$$T\left(\tau, f_{DOP}\right) = \sum_{k=1}^{M} I_{data}^2(k) + Q_{data}^2(k) + I_{pilot}^2(k) + Q_{pilot}^2(k) \qquad \text{I.7}$$

Where M is the total number of non-coherent integrations.

The above criterion was used by [Bastide, 2004] to take advantage of the pilot/data structure of the considered signals, and thus gather the energy of the whole signal. It can be noticed that this acquisition detector removes the dependence with the phase error.

The criterion is then compared to a threshold, in order to determine if the searched signal is present or not. The test can lead to four different cases:

- The signal is present (understand the good code/frequency bin is found) but the criterion does not exceed the threshold. The detection is missed.

- The signal is present and the criterion does exceed the threshold. The detection succeeds.
- The signal is not present and the criterion is exceeded. A false alarm occurs.
- The signal is not present and the criterion is not exceeded.

The missed detection and false alarm events are likely to happen because the tested criterion is affected by noise, multipath or interference. The issue raised by these events is that they slow down the acquisition process, or, in the worst case, could lead to erroneous measurements.

The considered acquisition process is sequential, which means that each bin is tested successively. If no detection occurred when the entire span has been tested, the process starts over. Thus, a missed detection results in an augmentation of the acquisition time equalling at least the time required to search the entire search space, which is represented in Figure 15.

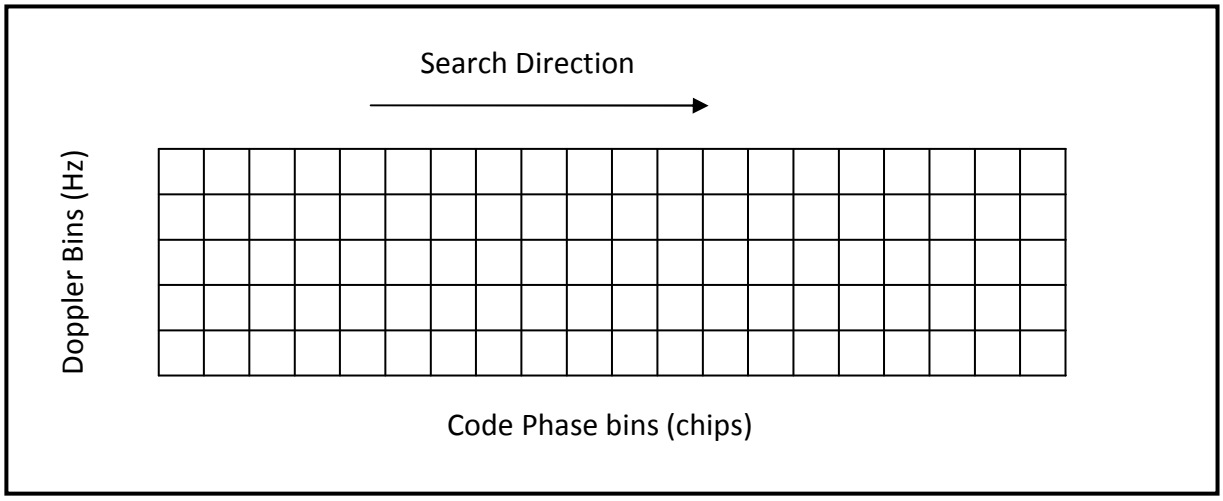

Figure 15 : Acquisition process uncertainty region.

The time required to test one bin is the dwell time. The time required to cover the entire search space is therefore:

$$T_{tot} = \frac{M \times T_p \times N_{bin}}{N_{corr}} \qquad \text{I.8}$$

Where:

- $M \times T_p$ is the dwell time,
- N_{bin} is the number of bins constituting the uncertainty region,
- N_{corr} is the number of correlators allocated to the search.

Two hypotheses are used to assess the acquisition performance:

- H_0: The signal is not present in the currently searched bin. In this case, the detector equals T_0,

- H_1: The signal is present in the currently searched bin. In this case, the detector equals T_1.

Assuming H_0, the correlators' output is composed of noise and potentially interference. In particular, there might be other GNSS signals present. If the correlator output is assumed centred and Gaussian, the distribution of the detector is a central chi-square distribution with 4M degrees of freedom. If it is assumed that there is also a high cross-correlation peak coming from a strong interfering GNSS signal, the distribution of the normalized detector $\frac{T_0}{\sigma_n^2}$ becomes a non-central chi-square distribution with 4M degrees of freedom, the non-centrality parameter being:

$$\lambda = \frac{2}{f_p} \times \left(\frac{C}{N_0} \right)_{cross-corr} \times \frac{1}{B} \times M \qquad \text{I.9}$$

Where $\left(\frac{C}{N_0} \right)_{cross-corr}$ is the carrier to noise ratio (C/N_0) of a high cross-correlation peak.

The civil aviation certification bodies usually consider the latter case, as described in [Bastide, 2004]. Then, knowing the detector distribution and a given probability of false alarm Pfa, it is then possible to define a threshold Th using the Neyman-Pearson lemma.

Considering now hypothesis H_1, $\frac{T_1}{\sigma_n^2}$ follows a non-central chi-square distribution with 4.M degrees of freedom, which non-centrality parameter equals:

$$\lambda = \frac{2}{f_p} \times \frac{C}{N_0} \times \left(\frac{\sin(\pi \Delta f T_p)}{\pi \Delta f T_p} \right)^2 \times \frac{1}{B} \times M \times R_f^2(\varepsilon_\tau) \qquad \text{I.10}$$

One can derive the probability of missed detection (Pmd) from the threshold and T_1 pdf.

Figure 16 represents the Pdf of $\frac{T_0}{\sigma_n^2}$ considering a cross-correlation C/N_0 of 19 dB.Hz, and $\frac{T_1}{\sigma_n^2}$ considering a C/N_0 of 32 dB.Hz. Finally, the threshold has been defined with respect to a Pfa of 10^{-3}. In this particular example, the Pmd equals 0.12.

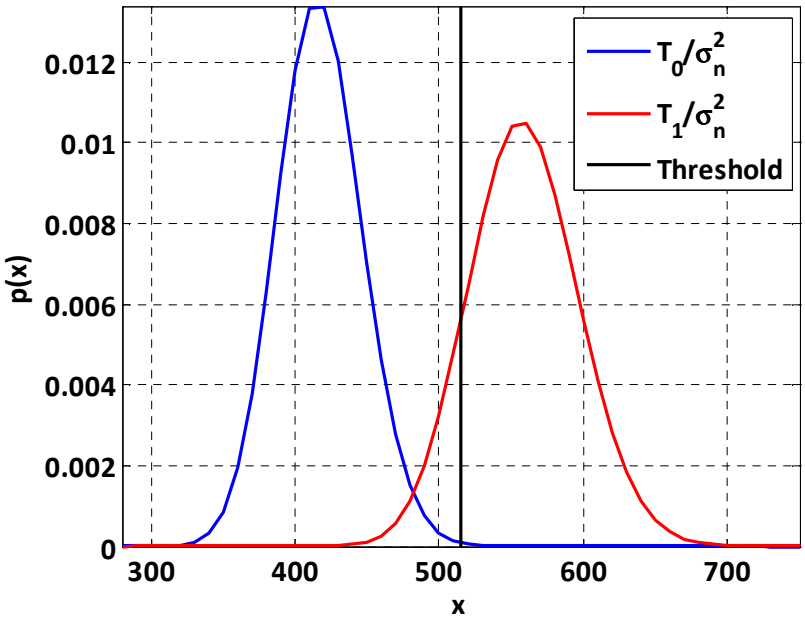

Figure 16: Test criteria Pdf.

I.4.4.3. Tracking Process

The tracking process is started after a successful acquisition. It is composed of the following:

- The signal is multiplied by a locally generated carrier, which phase is controlled by the feedback of the carrier tracking loop,
- The obtained signal is multiplied by a locally generated PRN code, which delay is controlled by the feedback of the code tracking loop,
- The signal is then integrated over one or several code length. The output value is used to feed the code and phase discriminators and to determine the navigation message bits. The collection of these outputs (bits) constitute the navigation message,
- The code and carrier discriminators calculate the error made on the previous estimates, and send the correction to the code and carrier generators.

A scheme of this signal processing module is provided in Figure 17. The scheme, as well as the description given above, is largely simplified. The details of the implementation are not required in this section, as the objective is to introduce the effects of pulsed interference on these modules operation. More details can be found in [Van Dierendonck, 1996] or [Kaplan, 2006]. The actual implementation chosen during the simulations will be given in paragraphs III.3.1 and III.3.2.

The locally generated carrier is controlled by a Phase-Locked Loop (PLL), which estimates the carrier phase error. The phase error estimation is performed by a discriminator, which is fed by correlators' outputs. PLL discriminators are characterized by their robustness (their capacity to keep tracking) and their accuracy. Then, the carrier phase error estimates are

passed through the carrier loop filter, which smoothes the carrier phase estimates. The filter is required to improve tracking accuracy, which depends upon the noise bandwidth of the filter. However, this bandwidth also impacts the time constant of the PLL.

The locally generated PRN code is controlled by a Delay-Locked Loop (DLL), which estimates the delay error. This error is estimated by a discriminator, fed by correlators' outputs. The choice of DLL discriminators is driven by accuracy considerations, the robustness being less critical for DLLs than for PLLs. Finally, the delay estimates are filtered by a code loop filter, which improves the tracking accuracy.

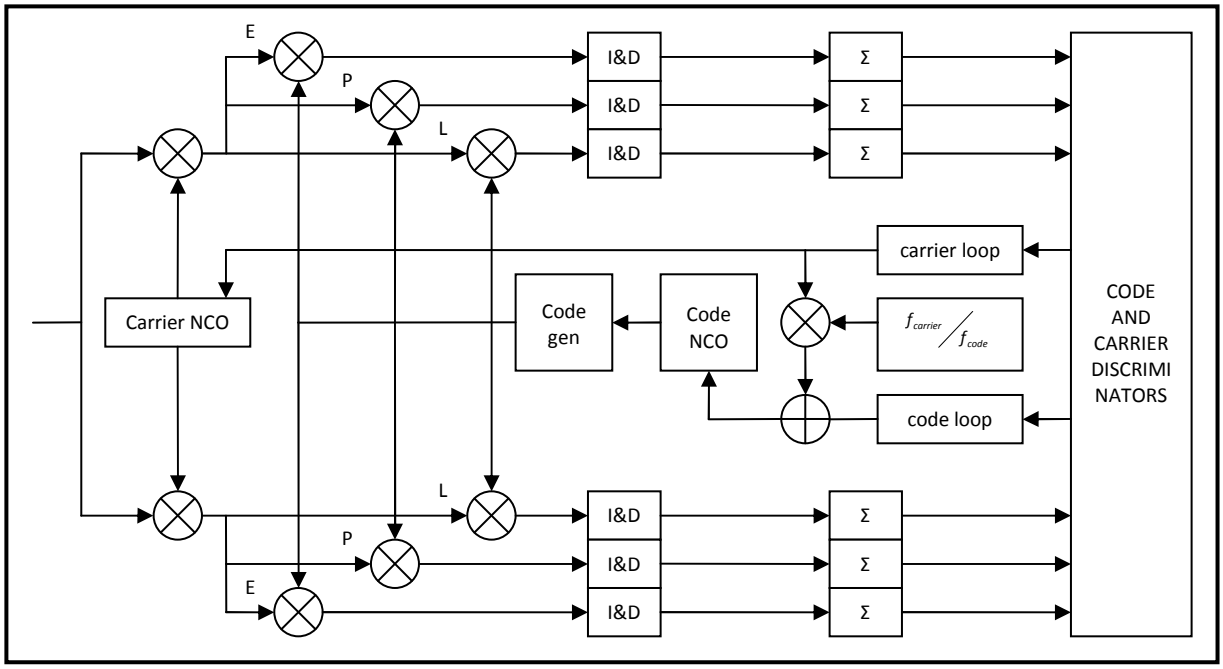

Figure 17: GNSS Receiver's signal processing module scheme.

The code and carrier phase tracking and the data demodulation performance highly depend upon their design, disturbances such as interference or multipath, and the SNR. When the interferences described in paragraph I.3 are received, the SNR is decreased (see details in section I.5.2), and the performances of the signal processing module are worsened. Generally speaking, tracking loops integrate the signal as long as possible. Indeed, the integration time increases the SNR, which improves the tracking performances.

Other types of interference induce other types of disturbances, which are not detailed in this study.

In Chapter IV, the assessment of the degradations caused by pulsed interference justifies the need to mitigate pulsed interferences. In the following, two Interference Mitigation Techniques (IMTs) are proposed: the temporal blanker and the Frequency Domain Interference Suppressor (FDIS). The first one detects and removes interferences by comparing the signal amplitude to a threshold. The second one detects and removes interferences by comparing an estimation of the signal spectrum to a threshold. The underlying theory is given in Chapter II.

I.4.5. **Navigation Processing**

The obtained navigation message and pseudorange measurements are then processed to compute the position, velocity and time solution (PVT).
The navigation message provides the satellites positions, their onboard clock biases, estimates of the ionospheric and tropospheric correction parameters. Atmospheric (ionospheric, tropospheric) corrections and satellite clock biases are required to adjust the pseudorange measurements, while the position is determined by combining the corrected measurements and the satellites positions.

I.5. PULSED INTERFERENCE IMPACT ON GNSS RECEIVERS OPERATION

The AGC and the correlators are the elements the most sensitive to interference. The present paragraph describes the impact of the studied interferences on GNSS receivers.

I.5.1. **Automatic Gain Control Sensitivity to Interference**

As mentioned in paragraph I.4.3, classical AGCs use standard deviation estimators to control their gain. These systems show good performance in nominal cases, which is when thermal noise only is received. In case interference signals are received, the SNR degradation derivation proposed in Figure 12, paragraph I.4.3 is not applicable anymore, as the properties of the signal are modified.

In this study, the approach consists in assuming that the presence of interferences does not affect the SNR degradation due to quantization. As a matter of fact, the optimal k value is the same whether interferences are present or not.

Therefore, the optimal k value must be calculated taking into account the thermal noise standard deviation only, not the interfering signal. Considering that the interference is not correlated with the thermal noise, the variance of the total signal is then:

$$\sigma^2_{noise+\text{int}\,erf} = \sigma^2_{noise} + \sigma^2_{\text{int}\,erf} \qquad \text{I.10}$$

The AGC will then adapt its gain to obtain the optimal variance $\sigma^2_{optimal}$, and so apply a gain equalling:

$$\begin{aligned} G_{interference} &= \sqrt{\frac{\sigma^2_{optimal}}{\sigma^2_{noise+interf}}} \\ &= \sqrt{\frac{\sigma^2_{optimal}}{\sigma^2_{noise}} \times \frac{\sigma^2_{noise}}{\sigma^2_{noise+interf}}} = \sqrt{\frac{\sigma^2_{optimal}}{\sigma^2_{noise}}} \times \sqrt{\frac{\sigma^2_{noise}}{\sigma^2_{noise+interf}}} \\ &= G_{nominal} \times \sqrt{\frac{\sigma^2_{noise}}{\sigma^2_{noise} + \sigma^2_{interf}}} \end{aligned} \quad \text{I.11}$$

Where $G_{nominal}$ is the theoretical optimal gain, in presence of thermal noise only. Then, the parameter k can be written:

$$\begin{aligned} k_{interference} &= \frac{L}{G_{interference} \times \sigma_{noise}} \\ &= \frac{L}{G_{nominal} \times \sqrt{\frac{\sigma^2_{noise}}{\sigma^2_{noise} + \sigma^2_{interf}}} \times \sigma_{noise}} \\ &= \frac{L}{\sigma_{optimal} \times \sqrt{\frac{\sigma^2_{noise}}{\sigma^2_{noise} + \sigma^2_{interf}}}} \\ &= k_{optimal} \times \sqrt{\frac{\sigma^2_{noise} + \sigma^2_{interf}}{\sigma^2_{noise}}} \end{aligned} \quad \text{I.12}$$

The introduced bias $\sqrt{\frac{\sigma^2_{noise} + \sigma^2_{interf}}{\sigma^2_{noise}}}$ on the parameter k will decrease the ADC performance as a function of the received interference variance. This bias gets larger with the power of the received interference.

Moreover, this bias disturbs the IMTs performances. As said in paragraph I.4.4, IMTs process the signal in order to remove pulsed interference, using a threshold. This threshold is chosen to optimize the algorithms performances, assuming a perfect AGC. The introduced bias will therefore decrease the IMTs performance.

I.5.2. **Correlators sensitivity to DME/TACAN Signals**

The correlator output sensitivity to interference has already been extensively studied. [Van Dierendonck, 1996] proposes to model interference at correlator output as an equivalent additive white noise, which density equals:

$$\begin{aligned} N_{0,I} &= P_{interf} \times C_I \\ C_I &= \int_{-\infty}^{+\infty} S_I(f) \times S_c df \end{aligned} \quad \text{I.13}$$

Where:

- P_{interf} is the received interference mean power after front-end filtering,
- C_I is the interference coefficient,
- S_I is the base-band normalized interference PSD.

The density of this noise depends on the mean power of the interference, but also on the resemblance of the interference power spectrum with the GNSS signal PSD, through the interference coefficient. This density directly impacts the satellite acquisition process, as it decreases the SNR, which is one of the decisive parameters of acquisition performance (see paragraph I.4.4.2 on the acquisition process). For the same reasons, the code and carrier phase tracking and data demodulation performance are impacted by interference, through the SNR.

I.6. CIVIL AVIATION REQUIREMENTS

Airborne navigation systems must present performances better or equal to the ones specified in the Minimum Operational Performance Standards or Specifications (DO, MOPS) documents issued by civil aviation standardization bodies (RTCA, EUROCAE). In order to fully certify a navigation system, its performances are confronted to four main criteria defined by the ICAO: continuity, availability, integrity, and accuracy. During operations, airplanes fly different phases of flight, each of them requiring a different level of performance.

GNSS MOPS documents define the assumptions that must be considered in each phase of flight, and derive minimum performance for the different components of GNSS receivers.

The final objective of the civil aviation community is to define minimum operational performances that should be fulfilled by any GNSS embarked in an aircraft.

I.6.1. **Context**

GNSS receivers must guarantee minimum performances even in harsh interference environments, in all phases of flight. The impact of pulsed interferences on GNSS receivers has been identified to be the largest while flying at Flight Level (FL) 400 (40.000 feet), which corresponds to en-route. This is due to the fact that at this altitude, the number of DME/TACAN in the radio-electric range of the GNSS receiver is the maximum. Hence, in the following the performances are observed during en-route operations, assuming worst case interference scenarios. These scenarios, defined in [EUROCAE, 2007], are introduced in paragraph I.6.5.

I.6.2. **Antenna and RF front end requirements**

The power of the received interferences is affected by the antenna pattern of the transmitting beacon, free space losses, and receivers' antennas gain. The interferences being

received below the horizon, civil aviation authorities had to specify the aircraft antenna gain pattern for negative elevations. Different patterns were proposed by RTCA in [RTCA, 2004] and EUROCAE in [EUROCAE, 2007]. The impact of interferences being obviously higher for high interferences power, the worst case corresponds to the specified maximum aircraft antenna gain, see Figure 18. From the receiver point of view, the EUROCAE assumption is much more pessimistic as interferences coming from negative elevations can be less attenuated by the antenna. On the other hand, such assumptions allow loosening antenna manufacturer's constraints, and so decrease antennas' costs.

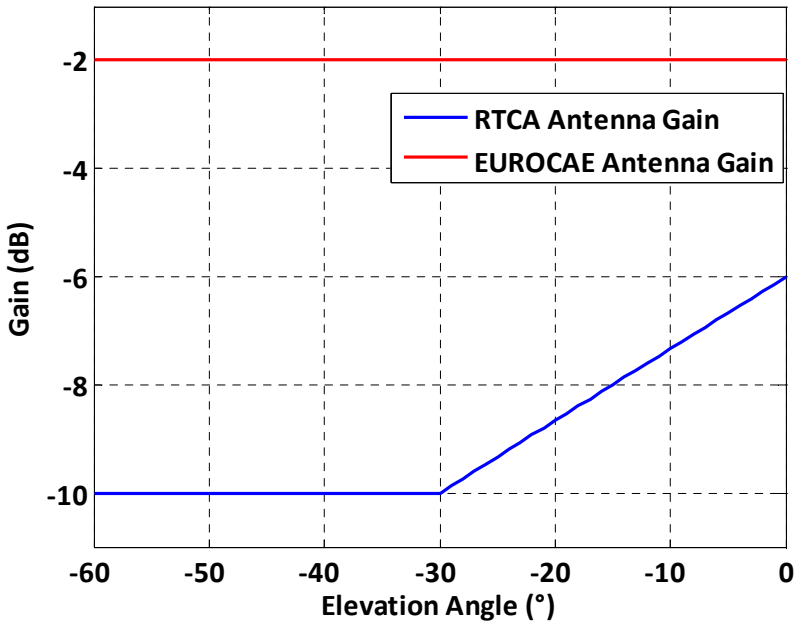

Figure 18: RTCA and EUROCAE antenna gain patterns worst case assumptions.

According to RTCA and EUROCAE, GNSS receivers must also achieve the minimum performances described in [EUROCAE, 2007], in the presence of out-of-band interfering signals, which levels can be as high as the ones shown in Figure 19.

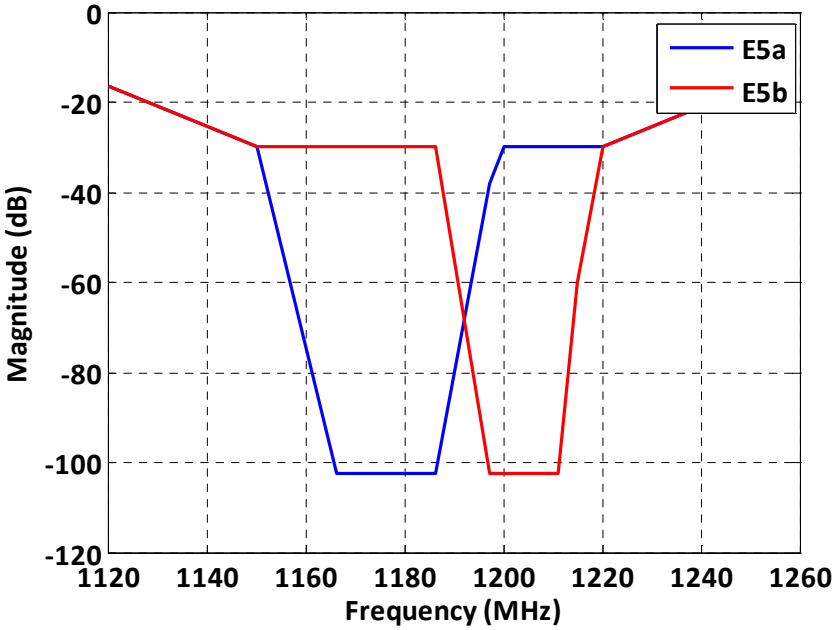

Figure 19: E5 maximum out of band RFI levels.

This requirement is then used to design front end filters. In-band Continuous Waves (CW) interferences are supposed to be supported by the receiver signal processing chain, so that a peak power of -102.5 dBW represents the nominal level. Expected out-of-band CW interferences being stronger than in band ones, filters are required to guarantee a maximum CW power of -102.5 dBW, whatever its carrier frequency. The E5a, E5b and L5 filter masks required to guarantee this are shown in Figure 20.

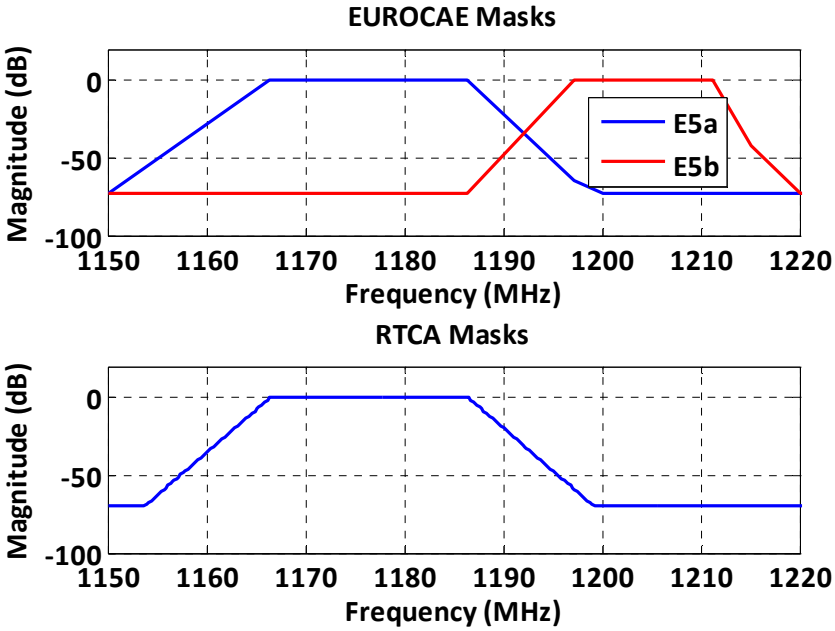

Figure 20: E5/L5 Interference masks.

These equivalent filter templates model not only the RF front-end filter but also the antenna induced filtering and the preamplifier. In this study, all these components are modelled by a unique intermediate frequency filter.
One can notice the asymmetry of the E5b interference mask, justified by the presence of radars right above the band.

I.6.3. **Acquisition, Tracking and Data demodulation Thresholds**

The objective of the study is to design a GNSS receiver capable of performing signal acquisition, signal tracking and data demodulation processes such that they meet the civil aviation requirements, in a specified interference environment. During en-route operations, the requirements are met if the C/N_0 thresholds indicated in Table 5, which is extracted from [Macabiau, 2008], are respected. The acquisition threshold is required to comply with the TTFF requirements given in paragraph I.6.4. In [Bastide, 2004], the tracking threshold is defined as the lowest C/N_0 for which the tracking loop still performs tracking. However, [RTCA, 2004] showed that the most limiting requirement was the cycle slip rate. The same methodology is being adopted by the EUROCAE, but the results are not consolidated yet [Macabiau, 2008], and therefore not available in this PhD Thesis. This lack is not of tremendous importance as [Bastide, 2004] stated that the tracking threshold was not the dimensioning process.
The data demodulation threshold is defined as the lowest C/N_0 for which the Word Error Rate (WER) is lower than 10^{-3} for [RTCA, 2004], and 10^{-4} for [EUROCAE, 2007]. However, the limiting phenomenon has also been identified as the cycle slip rate, not purely noise. Nevertheless, the data demodulation thresholds provided in [EUROCAE, 2007] were obtained considering noise was the limiting phenomenon. Thus, the data demodulation thresholds provided in Table 5 were derived following the noise approach for E5 signals, and the cycle slip rate approach for L5.

Table 5: C/N_0 Thresholds for GPS L5 and Galileo E5a and E5b signals.

	Acquisition	Tracking	Data Demodulation
L5	29 dB.Hz	27 dB.Hz	27 dB.Hz
E5a	29 dB.Hz	N/A	22.5 dB.Hz
E5b	29 dB.Hz	N/A	29.7 dB.Hz

Finally, the dimensioning process has been identified as signal acquisition for the Galileo E5a and GPS L5 signals, and data demodulation for the Galileo E5b signal.

I.6.4. **TTFF Requirements**

The Time To First Fix (TTFF) is defined as the time required by the GNSS receiver to acquire satellites and determine a valid position. The position is declared “valid” if *the determined*

position meets accuracy/integrity requirements for at least one minute following the first position fix (extracted from [EUROCAE, 2007], this definition is equivalent to the RTCA one).
GNSS receivers shall comply with the following requirements:

- TTFF<15 minutes in “cold start” conditions 95% of the time,
- TTFF<5 minutes in “warm start” conditions 95% of the time.

The difference between cold and warm start lies in the initialization information: in cold start conditions, no information is available. In warm start condition, the latitudes and longitudes are known within 60 nautical miles, time within 1 minute; and almanac data (part of the navigation message providing orbital information for all satellites), is available.
Conditions on satellites acquisition time can be derived from this TTFF requirement. [Bastide, 2004] proposes the following requirements on satellite acquisition time, assuming warm start conditions:

- The probability of acquiring the first satellite within 60 seconds shall be higher than 99%,
- The probability of acquiring each of the three subsequent satellites within 30 seconds shall be higher than 99%,
- These statements are equivalent to the following one: the probability that 4 satellites are acquired within 2.5 minutes is higher than 95%.

The 2.5 remaining minutes are allocated to verification, tracking convergence and data demodulation. This requirement and its derivation will be applied to the scope of the study in subsequent chapters.

During en-route operation, the receiver can undergo a power outage. In this particular case, the receiver is in warm start conditions, and shall provide a valid fix within 5 minutes.

I.6.5. **Interference Scenarios**

Onboard receivers must achieve the quoted minimum performances under the interference conditions defined in [RTCA, 2004]. From the C/N_0 degradation point of view, the worst European location is located over Frankfurt area (Germany) (longitude 9° East, Latitude 50° North) at flight level 400, as numerous and powerful DME/TACAN ground beacons are in the radio-electric range of the receiver. The location of this place, called hot spot, depends on the assumed aircraft antenna gain pattern. In the present PhD thesis, RTCA assumptions are considered rather than EUROCAE ones. First because previous studies about the coexistence of GPS L5 and Galileo E5 signals with DME/TACAN and JTIDS/MIDS systems took the RTCA assumptions into account. Then because the RTCA antenna gain assumptions were validated by antenna manufacturers, while EUROCAE assumptions were not.
The worst JTIDS/MIDS environment is defined as IGEB case VIII scenario. The DME/TACAN scenario corresponds to the case where all the ground stations in the radio-electric range of the aircraft emit at their maximum Pulse Repetition Frequency (PRF), which is the number of pulse pair they emit each second ([EUROCAE, 2007], [RTCA, 2004]).

The JTIDS/MIDS worst case scenario has been defined by the Interagency GPS Executive Board (IGEB) to test the systems compatibility. Its characteristics are given in Table 6. This scenario is considered as the worst case over US and Europe. Thus degradations due to these interfering signals are assumed equal over the US and Europe.

Table 6 : IGEB WG1 case VIII JTIDS/MIDS scenario

	RING	Power level (dBm)	TSDF (%)
Case VIII	FG	-35	50
	R1	-60	50
	R2	-90	300
	R3	-100/-120	300

Column *"RING"* pertains to the Geographical Area (GA) management concept [IGEB, 2000]. Geographically there are the following separation distances between JTIDS/MIDS terminals (FG, R1, R2 and R3) and the GPS L5 user:

- Foreground user (FG): 1000 feet,
- the background user 1 (R1): 5 nautical miles,
- the background user 2 (R2): 100 nautical miles,
- the background user 3 (R3) is an aggregate of the remainder of the JTIDS net: between 100 and 200 nautical miles.

Power levels indicated in the previous table equate powers at the GNSS receiver antenna port.

A Time Slot Duty Factor (TSDF) of 100% corresponds to the number of pulses resulting from transmitting 258 pulses in 128 time slots each second.

CHAPTER II: PULSED INTERFERENCE MITIGATION TECHNIQUES THEORETICAL STUDY

According to the previous chapter the pulsed interference present in the E5/L5 band might prevent the GNSS receivers from operating safely. It is necessary to integrate pulsed interference mitigation techniques into these receivers. Two different techniques have been developed for that purpose and have received a specific emphasis for L5 and/or E5 GNSS receivers: the Temporal Blanker and the FDIS.

II.1. REVIEW OF EXISTING TECHNIQUES

Only two interference mitigation techniques have been studied in order to address pulsed interference issues on GNSS receivers: the temporal blanker and the FDIS. The temporal blanker was proposed by the time the L5 signal was introduced in [Hegarty, 2000], while the FDIS was proposed a little bit after, in [Monnerat, 2000] or [Lesthievent, 2000] (patent). Other techniques, which are so far used to address other issues such as narrow band interference mitigation or not used in direct sequence spread spectrum systems, could be investigated.
Among them, filter bank based methods might be relevant. A filter bank is an array of band-pass filters that separates the input signal into several components, each one carrying a single frequency subband of the original signal. It also is desirable to design the filter bank in such a way that subbands can be recombined to recover original signal. The first process is called analysis, while the second is called synthesis. The output of analysis is referred as a subband signal with as many subbands as there are filters in filter bank. Each subband could be used to detect pulsed interference, by estimating the signal power and comparing it to a threshold for example, and the interference suppression would be performed during the signal synthesis.

More particularly, the use of polyphase representations leads to computationally efficient implementations of filter banks [Vaidyanathan, 1993]. The implementation of a polyphase filter is proposed in Figure 21. First, the signal is decomposed in its polyphase components:

$$x_l(n) = x(nM + l)$$

The process is equivalent to a decimation by a factor M, and a delay, different for each component x_l. Then, each component x_l is filtered by $E_l(z)$ and $\bar{E}_l(z)$, which can be defined in the time domain as $\bar{e}_l(m)=\bar{h}(mM+l)$ and $e_l(m)=h(mM+l)$, where $h(n)$ and $\bar{h}(n)$denote the impulse responses of the analysis and synthesis low pass filters, respectively.

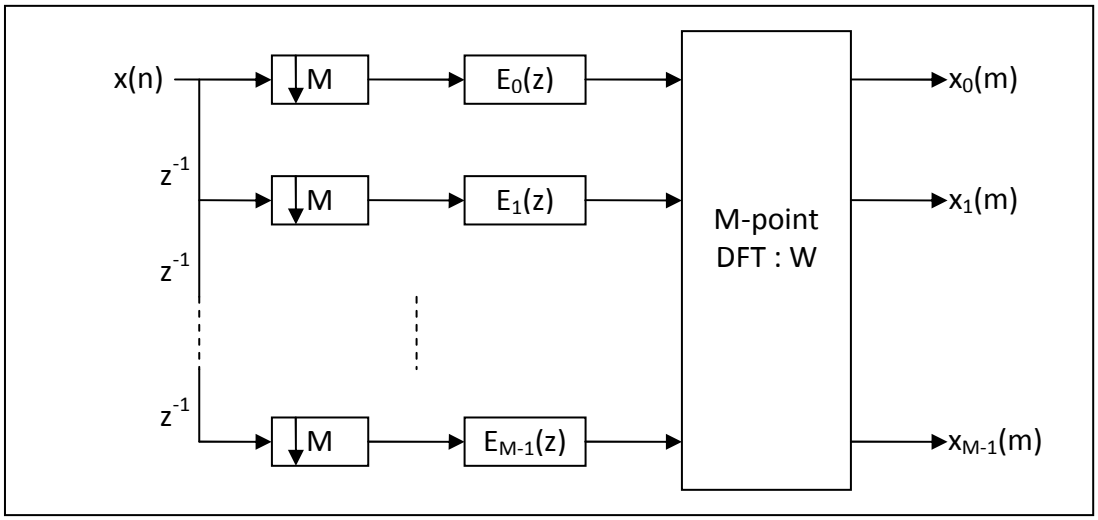

Figure 21: Polyphase Filter Implementation Scheme.

The output signal is then composed of M channels x_l, decimated with a factor M. Each channel represents the input signal filtered at a different frequency, and interference detection can be performed at this stage. Then, the interference can be suppressed between this analysis stage and the signal reconstruction, which is performed using the implementation presented in Figure 22.

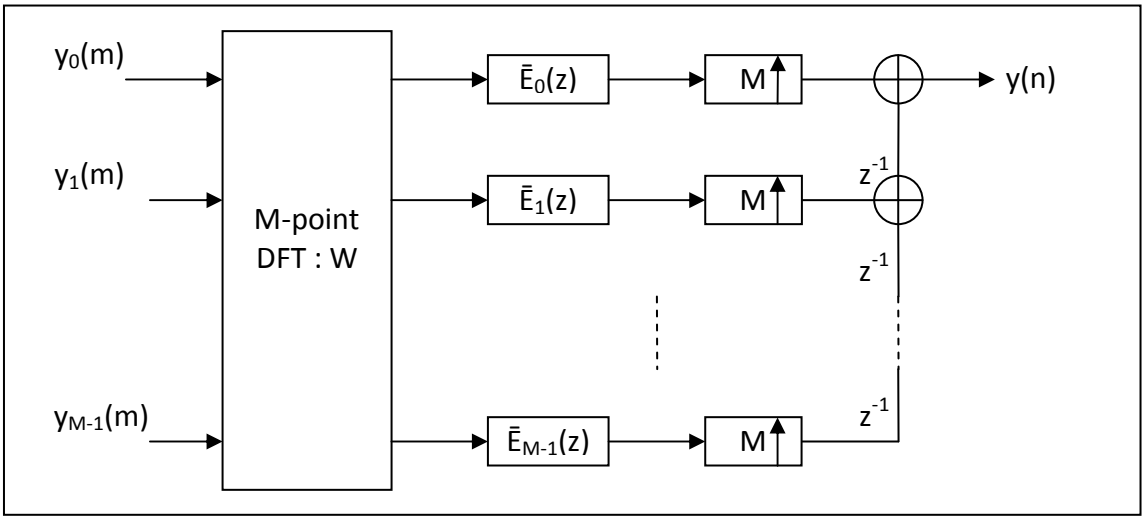

Figure 22 : Synthesis bank Implementation Scheme.

This kind of processing is well adapted to pulsed interference mitigation. Indeed, the received interference can be received over the band of interest in slots of 1 MHz. Therefore, the filter banks should be designed to process 1 MHz wide subbands, each of them being centred on the expected interference carrier frequency. This technique is not studied in the

present PhD thesis, as it requires more computations than the FDIS, which is also a frequency based interference mitigation technique.

[Landry, 1998] proposed a notch filter-based interference mitigation technique. The designed rejection filter is of recursive prediction error (RPE) form and uses a special constrained model of infinite impulse response (IIR) with a minimal number of parameters. The so-called PIRANHA filter is made up of independent cascaded adaptive cells realising high rejection at certain frequencies. The convergent filter is characterised by highly narrow-bandwidth and uniform notches of desired shape. Results from simulations illustrate the performance of the algorithm used in the PIRANHA filter under a wide range of conditions and situations. The PIRANHA filter is an efficient solution for detection, tracking and elimination of multiple high-power CWI and narrowband jammers. However, the efficiency of this algorithm against pulsed interference has not been studied, which would be interesting.

Many other interference mitigation techniques can be used, such as multicorrelators based techniques [Ouzeau, 2008]. However, this technique is better suited to CW or narrow band interference mitigation.

To conclude, many interference mitigation techniques can be used to fight pulsed interference. In this PhD thesis, only the temporal blanker and the FDIS are studied. The choice of these techniques was imposed by the ANASTASIA project, which defined the techniques to investigate before the beginning of the PhD, and more particularly during the initialization of the project. Indeed, frequential techniques are adapted to pulsed and narrowband interference mitigation, so the choice of the FDIS is natural.

II.2. TEMPORAL BLANKER DESCRIPTION

II.2.1. **Overview**

The Temporal Blanker was the first pulsed interference mitigation technique proposed to solve the issue of pulsed interference present on E5/L5 band. First, an analogue implementation of the temporal blanker was proposed in [Hegarty, 2000]: a circuitry detecting the beginning and the end of each pulse is implemented before the ADC. [Hegarty, 2000] concludes that the implementation requires great care to achieve maximum blanking performance especially for short duration pulses. The digital implementation of the technique has been preferred for cost and complexity reasons. The digital blanker thus operates at the ADC output.
[Grabowski, 2002] proposes a very simple implementation of the digital blanker: individual samples are compared against user specified threshold and zeroes the samples that exceed the threshold. More complex implementations [Perre, 2008] were then proposed, where power estimation approaches are preferred to individual sample approach. This kind of implementation is more complex but expected to provide better performance.

This kind of signal processing technique is adapted to pulsed interference mitigation, because of the nominal input signal Gaussian distribution. Indeed, in absence of interference, the GNSS signal is dominated by thermal noise. Figure 23, which was obtained using a dedicated Matlab routine, shows the probability that a signal exceeds a threshold, the threshold being expressed as a function of the standard deviation of the thermal noise. Two plots are drawn: (1) one corresponding to an input thermal noise, which represents the nominal signal (GNSS signals are drown in thermal noise), and (2) one representing a pulsed interference generated using the DME/TACAN signal model provided in paragraph I.3.1. The pulsed interference has a power of -100 dBW and is modulated at 5 MHz.

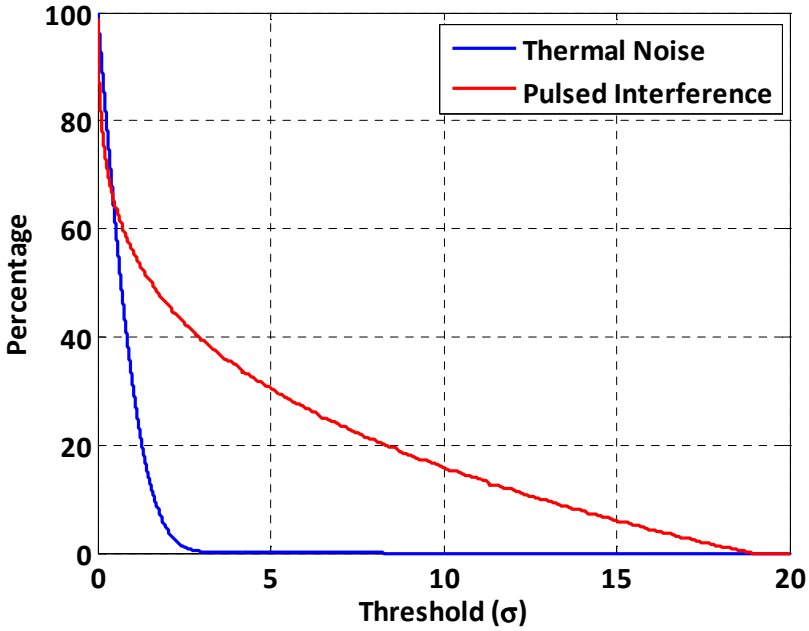

Figure 23 : Probability of exceeding a threshold.

According to the respective distributions of thermal noise and pulsed interference, the amplitude based detection approach seems judicious: for example, 40% of the samples of the simulated pulse pair exceed 3σ of the considered thermal noise, while only 3% of thermal noise samples do.

The performance of this technique highly depends upon the choice of the threshold: a trade-off between interference detection capability and false alarm rate is required.

II.2.2. **Blanker Duty Cycle**

The Blanker Duty Cycle (Bdc) is a measure of the blanker activity. It equals the ratio of the portion of time the blanker is activated (samples are zeroed) to the total observation time.

$$Bdc = \frac{T_{blanker}}{T_{tot}} \qquad \text{II.1}$$

It equals the percentage of time during which the signal is lost. Thus, the degradation on the useful signal or the amount of interference energy removed by the technique are directly impacted by the Bdc.

II.2.3. **Temporal Blanker Threshold Determination**

Pulsed Interference Mitigation Techniques (IMTs) are not supposed to be switched on and off during aircraft operation. Hence, the temporal blanker shall be configured so as to:

- Show good pulsed interference mitigation performance in harsh interference environments,
- Be a negligible source of loss in interference-free environments.

In the scope of the study, the techniques shall cope with the following conditions:

- The temporal blanker minimizes the C/N_0 degradations over hot spots,
- It induces less than 0.5 dBs of degradation on the C/N_0 in absence of interference. This limit has been decided in this PhD thesis.

According to the C/N_0 degradation derivation proposed in paragraph II.4, in absence of interference the degradation due to the Temporal Blanker processing equals $1-Bdc$. Moreover, the Bdc can be deduced from the threshold and the knowledge of the signal distribution. In absence of interference, the signal being dominated by thermal noise, its distribution is Gaussian. Figure 24 shows the Bdc as a function of the threshold, assuming a thermal noise of density -200 dBW/Hz and a sampling frequency of 56 MHz. The thermal noise density has been derived assuming a 100 K sky noise and following the recommendations of RTCA SC-159 WG1 members about the receiver noise figure (see [Hegarty, 1999] or [Bastide, 2004]). The Bdc has been obtained from the signal probability density function (pdf).

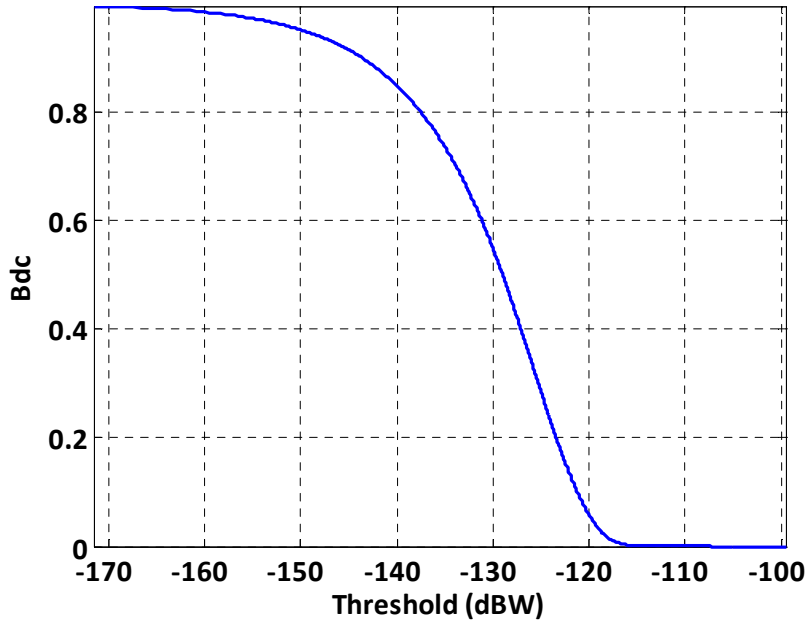

Figure 24: Bdc as a function of the threshold, assuming a thermal noise of density -200dBW/Hz.

Then, the degradation is easily deduced using the relation:

$$\deg_{dB} = 10\log_{10}(1 - Bdc) \qquad \text{II.2}$$

Figure 25 confronts the degradation as a function of the threshold to the 0.5 dB limit degradation fixed at the beginning of this paragraph. The condition is fulfilled for thresholds higher than -121.3 dBW.

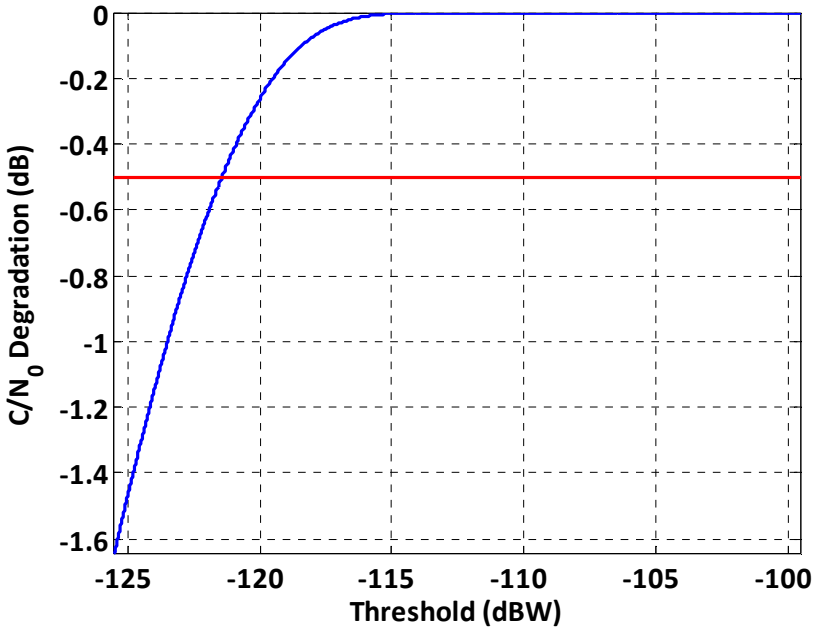

Figure 25: C/N_0 degradation as a function of the threshold, assuming thermal noise only.

In [Bastide, 2004], the performances of the temporal blanker have been extensively studied. The techniques performances were tested while flying over the hot spot, at FL 400. It is reminded that the hot spot is defined as the location where the impact of DME/TACAN on the victim GNSS receiver is the largest. The study proposed a theoretical derivation of the performances, validated by simulations results. Both revealed that the techniques performances were optimized considering a threshold of -117.1 dBW for E5a/L5 and -120 dBW for E5b signals. In the following, these values will be used as references.

II.3. FDIS DESCRIPTION

II.3.1. **Overview**

The FDIS technique is an interference removal technique operating in the frequency domain, firstly proposed in [DiPietro, 1989]. This paper proposes to use a Fast Fourier Transform (FFT) based narrow-band interference suppression filter for use in spread spectrum communication systems. The narrow-band interfering signals are materialized by CWs, as in [Young, 1998], where the performance of several types of FDIS algorithms are presented. [Capozza, 2000] also proposes a hardware implementation of such algorithms, as a mean of fighting CW effects on GPS receivers.
The detailed analysis proposed in this paragraph is one of the main studies conducted during this PhD thesis.
The FDIS algorithm consists in translating the input signal into the frequency domain using the FFT algorithm. Then, a detection/excision module detects and eliminates interferences, and the signal is calculated back in time domain using the inverse FFT. This processing is performed using the digitalized signal, at the ADC output. The discrete Fourier transform (DFT) is calculated for each block of N samples, and is expressed as:

$$X(k) = \sum_{n=0}^{N-1} x(n) e^{-\frac{j2\pi kn}{N}}, k = 0,1,...,N-1 \qquad \text{II.3}$$

Interferences are detected by comparing each of these N frequency bins to the same threshold. Indeed, in the nominal case (no interference) the signal at FDIS input is dominated by thermal noise, which can be assumed white. Thus, any bin that exceeds the thermal noise floor can be considered as interference, and removed. In practice, the DFT being a noisy estimator of the Fourier transform of the considered signal, a threshold slightly higher than the noise floor shall be used. If a frequency bin exceeds the threshold, its value is zeroed. The architecture of the algorithm is given in Figure 26.

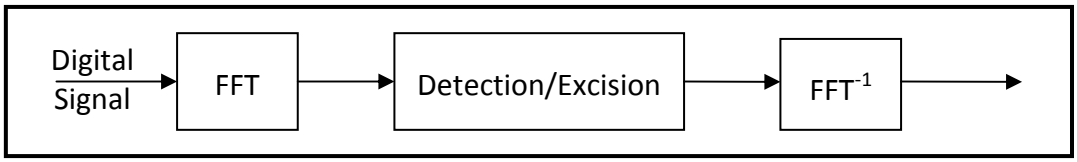

Figure 26: FDIS Architecture.

The power spectral density of the FDIS input signal can be estimated using the periodogram:

$$\hat{PSD}(k) = \frac{|FFT(k)|^2}{N} \qquad \text{II.4}$$

In Figure 27, the blue curve represents the thermal noise PSD estimate which noise density has been set to -200 dBW/Hz, while the red one represents a CW PSD estimate which peak power equals -100 dBW and frequency 14 MHz. Theoretically, one can discriminate both signals using the amplitude of the periodogram, for each frequency bin. In this case, the CW spectrum is very thin and can be easily detected and removed. However, this operation also distorts GNSS signals.

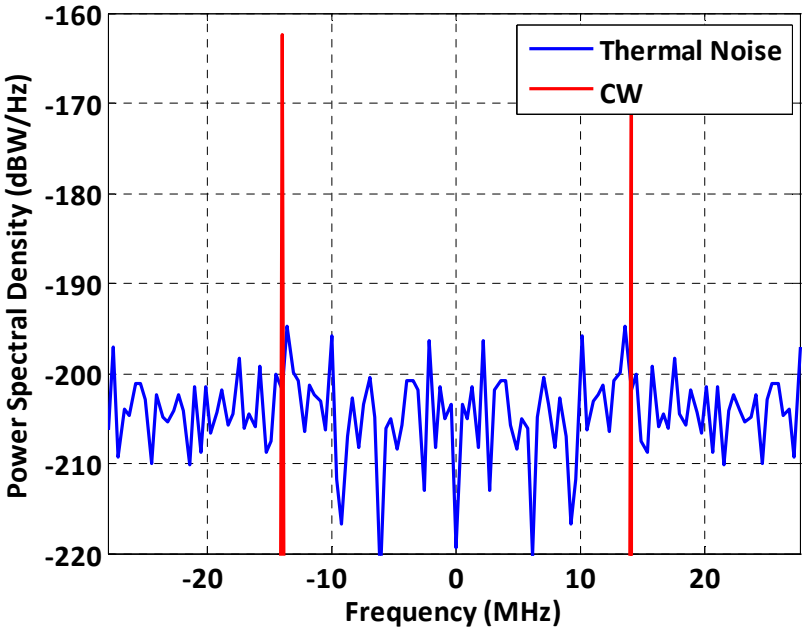

Figure 27 : PSD estimates of thermal noise and CW using the periodogram.

The FDIS algorithm performance depends on its configuration: the number of samples N used in the FFT calculation and the excision threshold. The chosen number of samples, also referred as window size (in samples) and its impact on FDIS algorithm is discussed in paragraph II.3.2.

II.3.2. **Window Size Effect on FDIS Performance**

The FDIS algorithm estimates the input signal FT using a finite number of samples, N. This is equivalent to the weighting of the input signal by a rectangular window. The effect of such windows on the FT estimation is the convolution of the observed signal PSD by a dirichlet kernel. This effect can be easily modelled for stationary signals such as CWs, but it is more difficult considering sparse signals such as pulsed interferences.

Indeed, for stationary signals, the number of bins set to zero is constant from one window to another. This kind of metrics, which was used in previous studies on DFT-based frequency excision algorithms ([Young, 1998], [Capozza, 2000]), cannot be used to study pulsed signals. The metrics used to assess the effect of the window size on the algorithm performances will be described in paragraph II.3.2.2.
Basically, the increase of the window length should improve the FT estimation, and so the algorithm performance. However, increasing it being costly, this idea needs to be validated. The analysis process is the following: first, the window length theoretical effects on FT estimation are presented. Then, simulations are run to assess the performance improvement in terms of C/N_0.

II.3.2.1. Algorithm Configuration

In the following, the FDIS threshold has been set to -195 dBW/Hz, which guarantees a maximum C/N_0 degradation of 0.5 dB in absence of interference (details on threshold choice and implementation are given in section II.3.4).

II.3.2.2. Windowing Effects on FT Estimate

The algorithm calculates the FT estimate from a discrete, windowed signal. Windowing has two main effects: spectral leakage and sampling.

Multiplying the signal by a rectangular window induces a convolution of the Fourier transform by a dirichlet kernel, which width depends upon the window duration in seconds. Short windows induce wide dirichlet kernels, leading to a spreading of the interference energy, which is generally referred as spectral leakage [Harris, 1978].

$$FFT\left(Int(t) \times rect\left(\frac{t - T/2}{T} \right) \right) = T \times FFT(Int(t)) \otimes \left(\frac{\sin(\pi f T)}{\sin(\pi f)} \right) \qquad \text{II.5}$$

Where:

- T is the window duration is seconds ($T = N \times T_s$ for a window size of N samples),
- $Int(t)$ is the interference signal.

Spectral leakage corresponds to the spreading of the observed signal energy over a wider band than the original one. The power contained in the signal being the same, the main lobe is wider and lower than expected, as shown in Figure 28. The spectrum of a CW of amplitude one is estimated using 128 samples (red curve) and a very large number of samples (blue curve), which represents the real spectrum estimate. The figure shows the two drawbacks of spectral leakage: first, the maximum value of the main lobe is lowered, which can lead to missed detections. Then, the main lobe is widened, which means that a wider part of the spectrum of the processed signal has to be zeroed by the algorithm, which also means that more of the useful signal is zeroed as well.

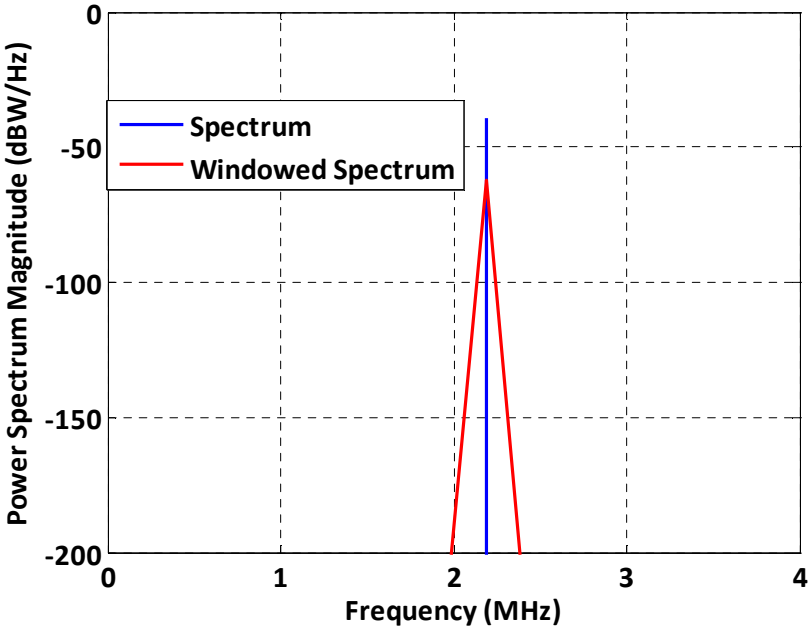

Figure 28: Spectral Leakage on a CW.

Another effect of the observation window size is related to the energy contained in one window. Indeed, when estimating the signal power spectral density using the periodogram, the underlying theory assumes that the observed signal is stationary, and so that the energy contained in the observed window is the same than in any other, which is wrong when considering pulsed interferences. Figure 29 shows the PSD estimate of a Gaussian pulse considering two consecutive windows of 128 samples, and compares it with the PSD estimate obtained using a window of 256 samples (which corresponds to the 128 ones concatenated). It is clear that the amount of energy observed in the windows is different, and it leads to two different PSD estimates. Moreover, it appears that the main lobe is not higher using the large (256 samples) window than the second narrow (128 samples) window. In fact, two effects explain this phenomenon:

- First, the increase of the window size diminishes the spectral leakage effect, which should raise the main lobe,
- The total power contained in the wide window corresponds to the average power contained in the two narrow windows. The power contained in the first narrow window being relatively low, the average is lower than the power in the second window. This effect should lower the main lobe.

Figure 29 shows that these two effects do not exactly compensate: the averaging effect is stronger than the spectral leakage reduction.

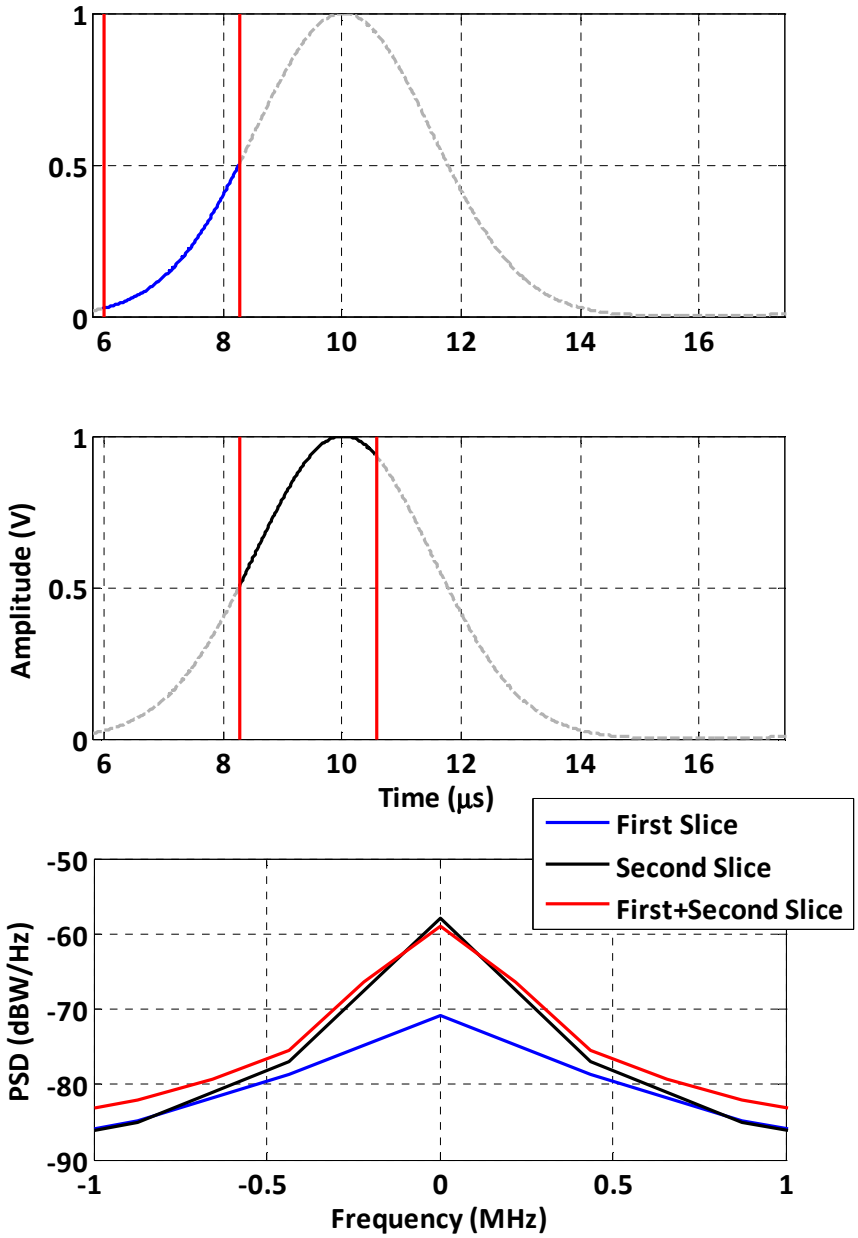

Figure 29: PSD estimates of slices of signal.

This observation shows that it is very difficult to analyse the effect of the size of the window on the PSD estimation: in this particular case, the power averaging effect is stronger than the spectral leakage decrease, but it is not always the case. The power averaging depends upon the portion of the pulse that is observed. However, the diminution of the spectrum spread due to the use of long windows does not suffer from such considerations, as shown in Figure 30.

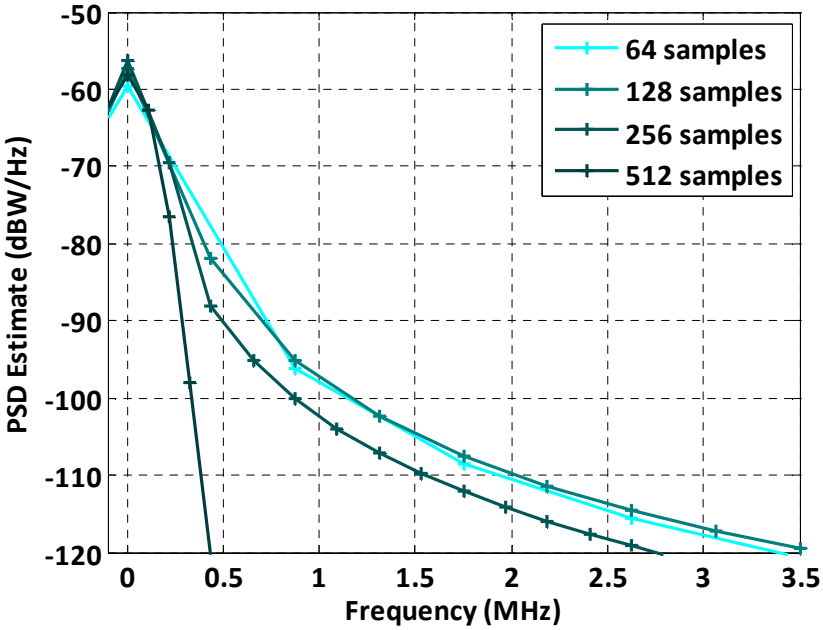

Figure 30 : Close up on the spectral leakage mechanism pulsed interference PSD estimate, using observation windows located around the centre of one pulse, modulated at 0 Hz.

The second effect of windowing (sampling) is due to the use of a finite number of samples. In the present case, the Fourier Transform (FT) is sampled every $\frac{f_s}{N}$ hertz. Then, the choice of *N* directly impacts the FT resolution. More particularly, the poor resolution offered by short duration windows is problematic when the interference carrier frequency does not match one of the frequencies sampled by the algorithm ($f_{CW} \neq k \times \frac{f_s}{N}$). Indeed, the maximum amplitude of the FT of a windowed CW is reached when the frequency shift between the CW frequency and the closest frequency bin $k_0 \times \frac{f_s}{N}$ is minimized. This amplitude equals:

$$\max\left(FFT\left(CW \times rect\left(\frac{t - T/2}{T}\right)\right)\right) = T \times \frac{\left(\frac{\sin\left(\pi \times \left(k_0 \frac{f_s}{N} - f_{CW}\right)T\right)}{\sin\left(\pi \times \left(k_0 \frac{f_s}{N} - f_{CW}\right)\right)} + \frac{\sin\left(\pi \times \left(k_0 \frac{f_s}{N} + f_{CW}\right)T\right)}{\sin\left(\pi \times \left(k_0 \frac{f_s}{N} + f_{CW}\right)\right)}\right)}{2}$$

The worst case is reached for $f_{CW} = \left(k_0 + \frac{1}{2}\right)\frac{f_s}{N}$. The corresponding minimum frequency shift equals $\frac{f_s}{2N}$. The decrease of *N* induces an increase of this frequency shift, which corresponds to a decrease of the dirichlet kernel, as illustrated by Figure 31. For example, the maximum amplitude of a FT of a CW which carrier frequency would be as far as 250 kHz from the closest frequency bin would be divided by two. This is an issue from the algorithm's detection capability point of view.

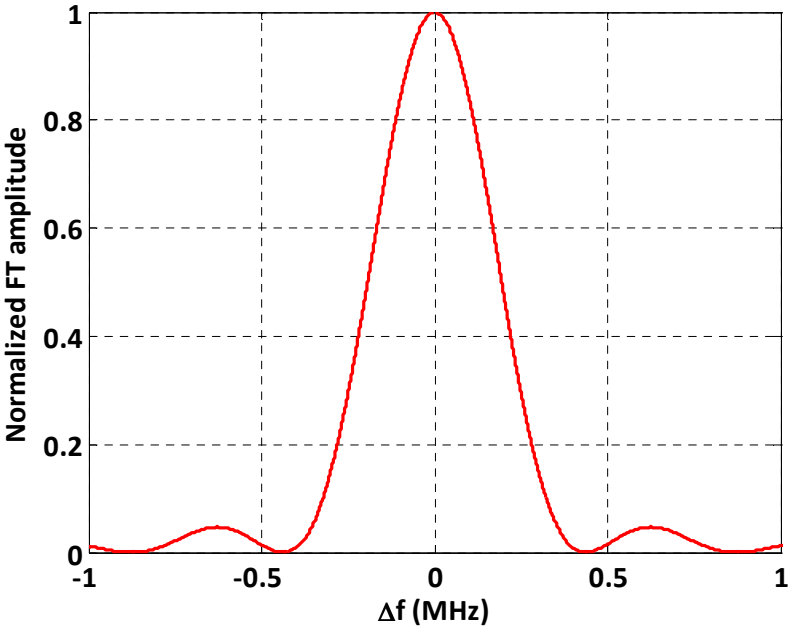

Figure 31: Dirichlet Kernel amplitude around zero.

In the targeted application, which is DME/TACAN or JTIDS/MIDS signals mitigation, this issue could be solved by adapting the algorithm. Indeed, the quoted signals carrier frequencies are known (1160 to 1211 MHz by step of 1 MHz). Therefore, the algorithm could be adapted in such a way that the signal power spectrum density is estimated every megahertz, thus minimizing the issue induced by the sampling of the Fourier Transform. This optimization has not been studied herein.

II.3.2.3. Simulations

The mechanisms described and analyzed in the previous paragraphs have to be confirmed by Matlab simulations. The first test is conducted observing a noise free signal, only composed of one pulse pair. This signal is processed by FDIS, using the threshold defined in paragraph II.3.4 (-195 dBW/Hz), and the output is analyzed. Two Figures of Merit (FOMs) are observed:

- the pulse pair energy, after being processed by FDIS,
- The total number of excisions induced by the presence of the pulse pair. This will help understanding the amount of useful signal lost because of FDIS.

Figure 32 shows the results obtained for a pulse pair presenting a peak power of -100 dBW and modulated at 1176 MHz, which represents the most disturbing configuration, from the correlators point of view, see paragraph I.5.2. Indeed, the correlation process rejects signals modulated at carrier frequencies far from the tracked GNSS signal one.
In this particular configuration, the interference removal efficiency seem very good (>98%), and not dependent upon the window duration (here in samples). However, the number of excisions highly depends upon this duration, and shows that small windows (N=64) perform three times worse than biggest ones (128, 256, 512). The reader would notice that the total

number of excisions exceeds the number of frequency bins contained in each window (*N*). Indeed, as shown in Figure 29, a pulse pair lasts longer than one window. Then, the excisions performed on each window are summed, and their total number can exceed *N*.
The performances being constant the same for the three last configurations, the least computationally expensive one can be considered the best configuration (128 samples) in this particular example. Nevertheless, the considered interference scenario is not yet representative of real interference scenarios.

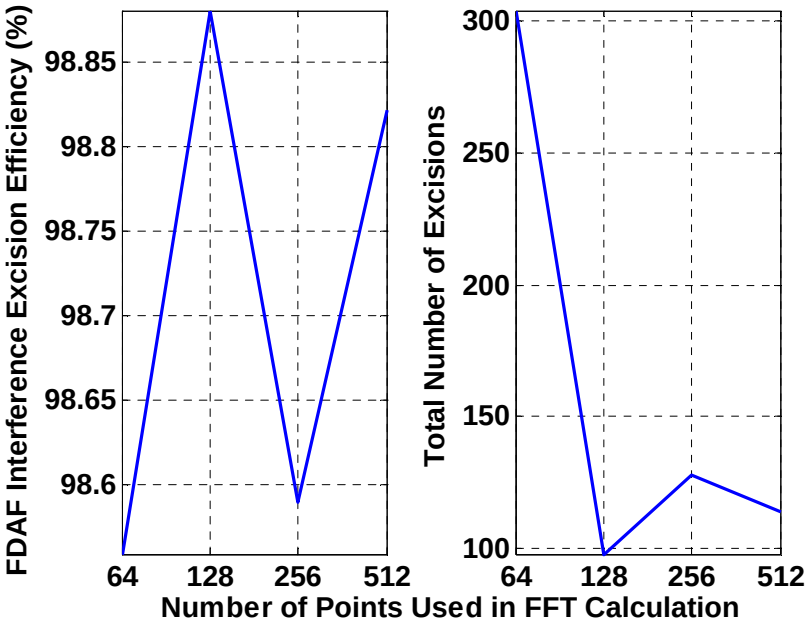

Figure 32 : FDIS efficiency as a function of the number of points used in FFT calculation, considering a pulse pair modulated at 1176 MHz.

The unwanted pulsed interferences are emitted in the entire E5 band, so the technique shall mitigate their effect, whatever their carrier frequency, including the Doppler effect. The FOMs presented in Figure 32 are re-calculated for each in-band carrier frequency (instead of 1176 MHz only), and the average results are presented in Figure 33. Differently from the previous test, this one leads to the conclusion that using as much samples as possible (512 here) is the best choice. Indeed, the interference excision percentage is somewhat constant (≈98.5%), while the number of excisions decreases while *N* increases.

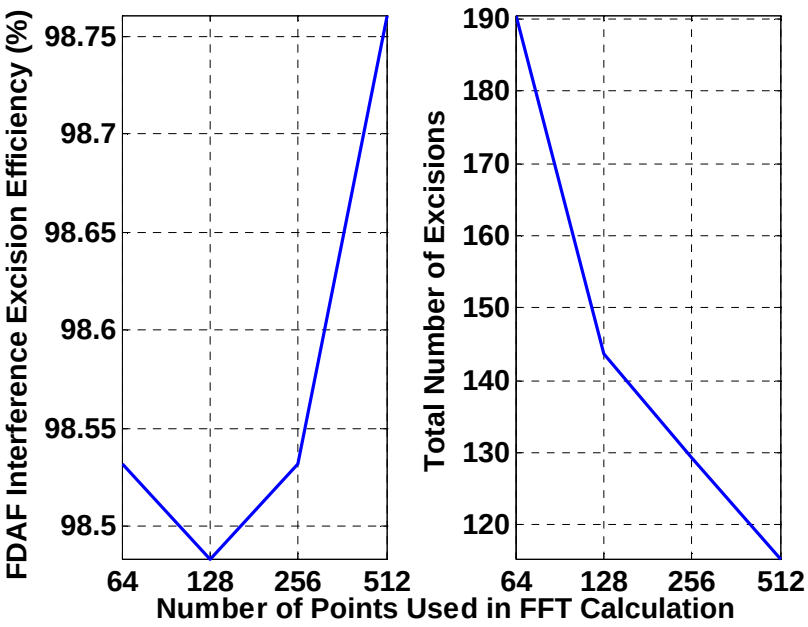

Figure 33 : FDIS efficiency as a function of the number of points used in FFT calculation, averaged for pulsed interference modulated at frequencies going from 1166 MHz to 1186 MHz by steps of 1 MHz.

The second scenario seems more relevant than the first one as it takes into account all the possible carrier frequencies. Nevertheless, the interference impact on GNSS signal tracking highly depends upon the frequency offset between the GNSS signal carrier frequency and the interference one (see paragraph II.4.2.3), so upon the interference environment, which might be different from the one proposed.

II.3.2.4. C/N_0 Simulations

In order to validate the previous analysis, the performance of the algorithm is assessed in terms of post-correlation C/N_0 as a function of the window duration. In the simulations, which were performed using a Matlab routine, the C/N_0 is obtained using the estimator described in paragraph III.3.1.2.7. The interference scenario was the following: only one DME beacon is assumed to be visible from the receiver point of view, and emits 2700 pulse pairs per seconds. The pulses are randomly emitted, and their reception instants follow a Poisson distribution. Then, the signal is processed by FDIS, and the post-correlation C/N_0 of the processed signal is estimated. The interference is modulated at 1176 MHz, and its peak power equals -100 dBW.

The results shown in Table 7 agree with previous analyses: the performance of the algorithm is somewhat improved when the duration of the window is increased, excepted when using 256 samples, but as already said this is specific to the carrier frequency. Moreover, the performance improvement seems negligible, but it is due to the fact that quite few signals are generated.

Table 7 : Post-Correlation C/N_0 Degradation as a Function of the Number of Samples Used in FFT Calculation.

IMT	No FDIS	64	128	256	512
C/N_0 Degradation	8.6 dB	0.6 dB	0.42 dB	0.63 dB	0.32 dB

II.3.2.5. Conclusion

The performance of the FDIS algorithm depends upon the window duration choice. Theoretical analyses show that estimating the PSD with more samples is more accurate, because the spectral leakage is mitigated and the frequency resolution is improved. Thus, the technique should be more efficient using large windows, what must be validated through simulations. The simulations showed in the most challenging case; high level interference modulated at the tracked signal carrier frequency; that the performance of the technique was optimum using a 512 samples wide window, which is the largest tested one. Nevertheless, the relation between the performance and the window width is not monotonous, as the highest degradation is reached using 256 samples.

II.3.3. **Use of weighting windows**

The described FDIS algorithm simply calculates the FFT of the incoming signal. As explained in the previous paragraph, spectral estimations are distorted by spectral leakage issues. These issues can be mitigated by the use of weighting windows. The use of classical windows such as Hamming, Hanning, or Blackman-Harris windows is likely to reduce the signal energy frequency spreading due to spectral leakage. However, the use of such windows also distorts the investigated signal. The following section theoretically assesses the interest of implementing weighting windows in the FDIS algorithms.

II.3.3.1. Weighting windows theory

When a weighting window is used, the FFT is not convoluted by a dirichlet kernel anymore, but by the Fourier transform of the chosen window. Then, weighting windows are chosen from the following criteria:

- The width of its Fourier transform main lobe,
- The height of the secondary lobes.

Both characteristics impact the final spectrum estimation. In this study, the objective is to suppress interferences as efficiently as possible: reduce the interference power to its minimum while preserving the useful signal. Then, the best window to use is the one that gathers the most important part of the interference energy in the smallest possible band. The Fourier Transforms of three classical windows (Hamming, Hanning and Blackman-Harris) are provided in Figure 34.

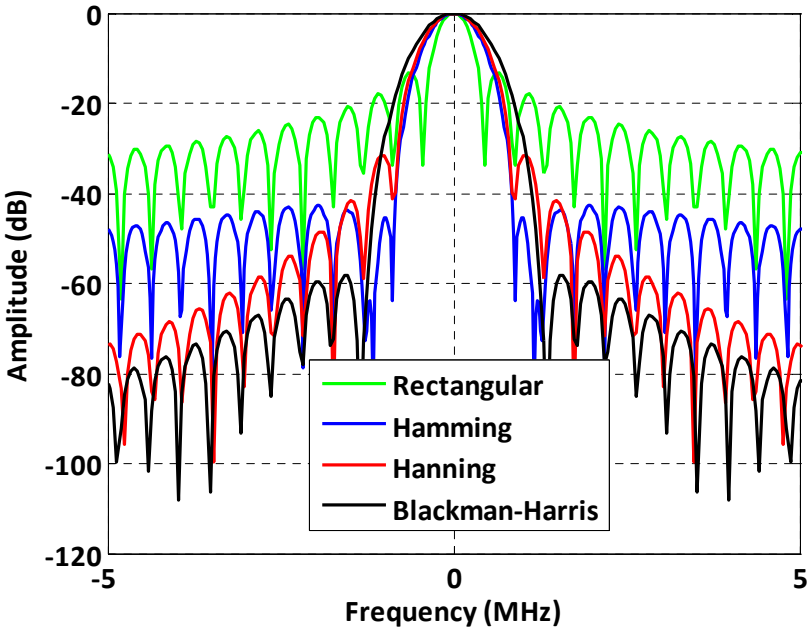

Figure 34: Weighting Windows Fourier Transforms.

The spectral characteristics of the weighting windows are summarized in Table 8, considering windows of 128 samples, and a sampling frequency of 56 MHz. The Blackman-Harris window has the lowest secondary lobes, but has the widest main lobe. The Hamming window has the narrowest lobe.

Table 8: Weighting Windows Characteristics.

	Hamming	Hanning	Blackman-Harris
Main Lobe Width (-3 dB, kHz)	570	622	722
Secondary Lobes fading (dB)	-45.5	-31.5	-58.3

Another characteristic of weighting windows is the distortion they induce in the signal. Usually, this characteristic is not important, as many applications use these windows for spectrum analysis only. In our case, the signal is kept and used for further signal processing. The distortion induces non-negligible SNR degradations, which can be calculated as follows [Harris, 1978]:

$$SNR_{\deg} = \frac{\left(\sum_{k=1}^{N} w(k)\right)^2}{N \times \left(\sum_{k=1}^{N} w^2(k)\right)} \qquad \text{II.7}$$

Where $w(k)$ are the windows coefficients. Table 9 shows the SNR degradation due to the studied weighting windows, assuming they are defined on 128 coefficients. The largest degradation is suffered using the Blackman-Harris window. Nevertheless, this degradation can be easily mitigated by using overlapped windows. [Calmettes, 1999] showed that the degradations were minimized when using a 50% overlap. The SNR degradations suffered in this case are also provided in Table 9. The Blackman-Harris is still the worse choice but, for the three windows, the degradation is somewhat negligible (0.3 dB or less). The counterpart of using overlapped windows is the computation load increase.

Table 9: SNR degradation due to weighting windows.

	Hamming	Hanning	Blackman-Harris
No overlap	1.71 dB	1.37 dB	3.05 dB
50% overlap	0 dB	0 dB	0.3 dB

At this point, it is difficult to determine the best choice in terms of weighting window. Therefore, it is necessary to test the three proposed windows using more complex simulations and to compare their efficiency. The corresponding results can be found in paragraph IV.2.1.

II.3.3.2. Additional Calculation Induced

The use of weighting windows makes the FDIS a more demanding algorithm from the resources point of view:

- Considering a N-point FDIS, the multiplication by the window induces N additional multiplications,
- N/2 additions are also required because of overlap,
- The FFT calculation is performed twice more often (every N/2 samples), because of overlap.

Nevertheless, the calculations are made in the time interval separating two samples arrival, which depends upon the sampling frequency. Thus, only considering that the calculations have to be made twice more often is not a dimensioning parameter. The processor will be busier (calculation-free times will be smaller), the power consumption will be increased, but the processor does not have to be more powerful.

Assuming a butterfly algorithm, the number of calculations required to perform an N points FFT equals $N \times \log_2(N)$. In case weighting windows are used, this number becomes $N \times \log_2(N) + \frac{3}{2}N$.

As forecasted, the use of such windows increases the calculation load, but by $\frac{3}{2}N$ operations only. If their use is expected to improve the FDIS performances, section II.3.2 also shown that the increase of the number of point used to compute the FFT brought improvements. Assuming the FFT is calculated using a fixed number of samples N, one can determine which of the two evoked solutions is more costly in terms of calculations:

$$\begin{aligned} N_{calc,2N} - N_{calc,weighting} &= 2N \times \log_2(2N) - \left(N \times \log_2(N) + \frac{3}{2}N \right) \\ &= 2N \times \log_2(N) + 2N - \left(N \times \log_2(N) + \frac{3}{2}N \right) \\ &= N \times \log_2(N) + \frac{3}{2}N \geq 0 \end{aligned} \qquad \text{II.8}$$

It appears that the introduction of weighting windows costs less than doubling the number of FFT points. The performances of these two solutions are assessed in paragraph IV.2.

II.3.4. **FDIS Threshold Determination**

As the Temporal Blanker, the FDIS is not supposed to be turned off during aircraft operation. Hence, the threshold must be chosen so as to:

- Show good pulsed interference mitigation performance in harsh interference environments,
- Be a negligible source of loss in interference free environments.

These performances shall respect the same requirements as the ones already given for the Temporal Blanker:

- The FDIS minimizes C/N_0 degradations over hot spots,
- It induces less than 0.5 dBs C/N_0 degradation in absence of interference.

The FDIS algorithm detects interferences in the Fourier domain, using the FFT algorithm. Indeed, this is equivalent to detecting it using the periodogram and an adapted threshold:

$$\left|FFT(k)\right|^2 \leq Th \Leftrightarrow \frac{\left|FFT(k)\right|^2}{N} T_s \leq Th_{perio} = \frac{Th}{N} T_s \qquad \text{II.9}$$

In absence of interference, the FDIS excise frequency bins which noise component exceed the chosen threshold. The periodogram of a white Gaussian noise follows a non-centred chi square distribution with one degree of freedom and of parameter λ.

$$\lambda = \frac{-(2-4A) + \sqrt{\Delta}}{2} \qquad \text{II.10}$$

Where:

- $\Delta = -(2-4A)^2 - 4 \times (1-2A)$,

- $A = \frac{\mu_{perio}}{\sigma^2_{perio}}$,
- $\mu_{perio} = \sigma^2_{noise}$ is the periodogram mean,
- $\sigma^2_{perio} = \sigma^4_{noise}$ is the periodogram variance.

Thermal noise being an ergodic process, its periodogram is assumed to be so. Knowing the distribution of the random variable, or more exactly its repartition function and the threshold used, one can derive a false alarm rate.

$$P_{fa}(Th) = 1 - P(Perio \leq Th_{perio}) \quad \text{II.11}$$

The repartition function of the periodogram is represented in Figure 35, as a function of the periodogram standard deviation.

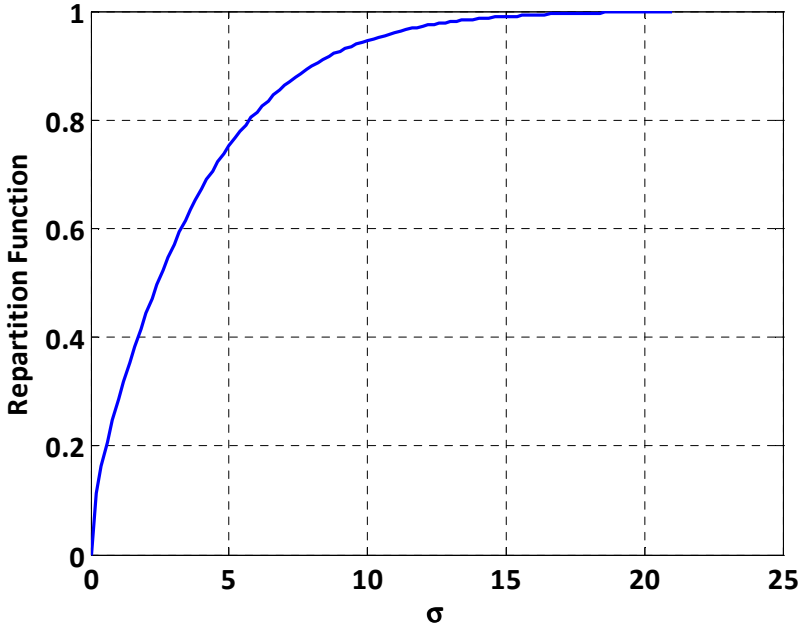

Figure 35: Thermal Noise Periodogram Repartition Function.

Moreover, assuming a probability of false alarm P_{fa}, and that the false alarms (excisions) are randomly distributed over the entire spectrum, the thermal noise density after being processed by FDIS in absence of interference equals:

$$N_{0,FDIS} = N_0 \times (1 - P_{fa}) \quad \text{II.12}$$

With the same assumptions, the GNSS code power equals (see details in paragraph II.4):

$$C_{FDIS} = C \times (1 - P_{fa})^2 \quad \text{II.13}$$

Then, the C/N_0 equals:

$$\frac{C}{N_{0\ FDIS}} = \frac{C}{N_0} \times (1 - P_{fa}) \quad \text{II.14}$$

The degradation limitation having been fixed to 0.5 dB, one can derive the P_{fa} limit, and then the threshold from Figure 36.

$$P_{fa} = 1 - \frac{\frac{C}{N_{0\ FDIS}}}{\frac{C}{N_0}} = 1 - 10^{-0.05} = 0.11 \qquad \text{II.15}$$

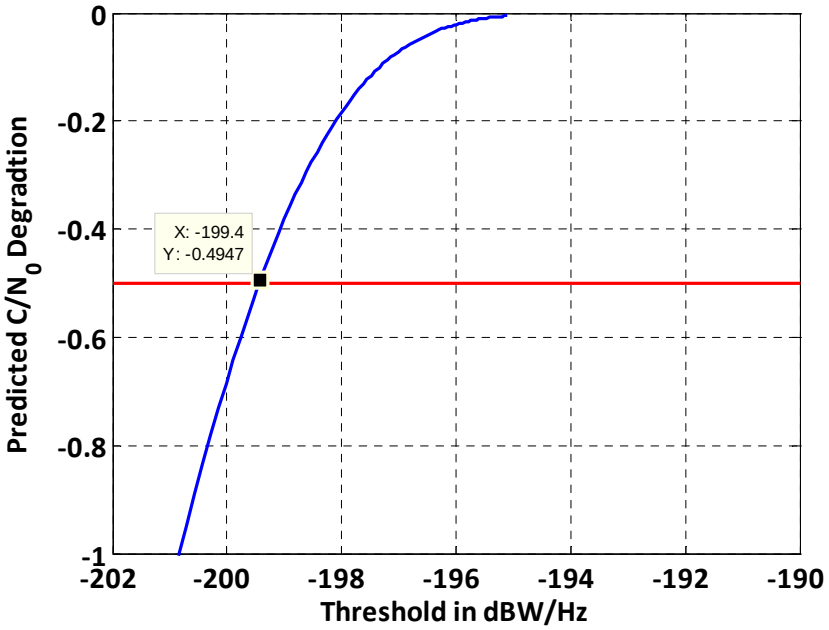

Figure 36 : C/N_0 degradation due to FDIS as a function of its threshold.

According to Figure 36, the 0.5 dB degradation corresponds to a threshold of -199.4 dBW/Hz. Largest thresholds can be used, but the performance of the technique will a priori be optimum for thresholds relatively close to the thermal noise floor, as the objective is to remove as much interference as possible. However, a threshold of -195 dBW/Hz is used in the following. Indeed, the chosen threshold (-195 dBW/Hz) shows the same performances than the lowest acceptable threshold (-199.4 dBW/Hz) in presence of interference, and induces a lower C/N_0 degradation in interference-free environments.

The reader would notice that the threshold derivation has been conducted assuming a rectangular window. In case the weighting windows presented in paragraph II.3.3 are used, the threshold might require an adaptation, or a normalization of the obtained FFT.

II.3.5. **Quantization impact on FDIS operation**

In a first approximation, FDIS has been studied assuming non quantized signals. The quantization induces a degradation of the quality of the signal, which might affect FDIS performances. The purpose of this paragraph is to assess the impact of quantization on FDIS algorithm performances. The study decomposes in two parts:

- Study of the impact of quantization in absence of interference,
- Study of the impact of quantization when receiving interference.

II.3.5.1. No interference

In case no interference is present, noise only enters the ADC and so the FDIS. Basically, the FDIS should not remove frequency channels since no interference is present, but depending on the chosen threshold, false alarms can occur (as seen in paragraph II.3.4). In presence of noise only, the quantization effect is modelled as an additive white noise, which PSD equals:

$$S_\varepsilon(f) = \frac{1}{f_s}\frac{q^2}{12} rect\left(\frac{f - B/2}{B}\right) \quad \text{II.16}$$

Where:

- $\varepsilon = x - x_Q$ is the quantization noise,
- q is the quantization step,
- f_s is the sampling frequency,
- B is the front end filter bandwidth.

Then, assuming the input signal (thermal noise) and the noise induced by the quantization are not correlated, the quantized signal PSD becomes:

$$\begin{aligned} S_{x_Q}(f) &= S_x(f) + S_\varepsilon(f) \\ &= N_0 \times rect\left(\frac{f - B/2}{B}\right) + \frac{1}{f_s}\frac{q^2}{12} \times rect\left(\frac{f - B/2}{B}\right) \\ &= \left(N_0 + \frac{1}{f_s}\frac{q^2}{12}\right) \times rect\left(\frac{f - B/2}{B}\right) \end{aligned} \quad \text{II.17}$$

The observed effect is an increase of the noise floor, which imply an increase of the false alarm rate, and so of the C/N_0 degradation in absence of interference.

II.3.5.2. Pulsed Interference

In presence of pulsed interference, the quantization process will have the same impact on the input signal, as long as the ADC is not saturated by the interference.

$$\begin{aligned} x_Q(t) &= x(t) + \varepsilon(t) \\ &= n(t) + Int(t) + \varepsilon(t) \end{aligned} \quad \text{II.18}$$

Where n is the thermal noise and Int the interference signal. Quantization noise has the same PSD as in previous section. The PSD of the quantized signal is then:

$$S_{X_Q}(t) = S_X(f) + S_\varepsilon(f)$$
$$= S_I(f) + \left(N_0 + \frac{1}{F_s}\frac{q}{12}\right) \times rect\left(\frac{f - B/2}{B}\right) \quad \text{II.19}$$

Where $S_I(f)$ is the PSD of the interference signal. Quantization results in an increase of the noise floor, resulting in an increase of the false alarm rate.

Figure 37 shows the FDIS excision rate, considering a signal composed of thermal noise of density -200 dBW/Hz and one pulse pair (peak power of -100 dBW, carrier frequency equals 16 MHz, sampling frequency is 56 MHz, IF=14 MHz), as a function of the FDIS threshold. Two configurations are represented: first the signal is quantized prior FDIS processing (blue curve), and then it is not (red curve). The quantization is performed according to the quantization law described in paragraph I.4.3. These results were obtained using a Matlab routine developed during the PhD thesis.

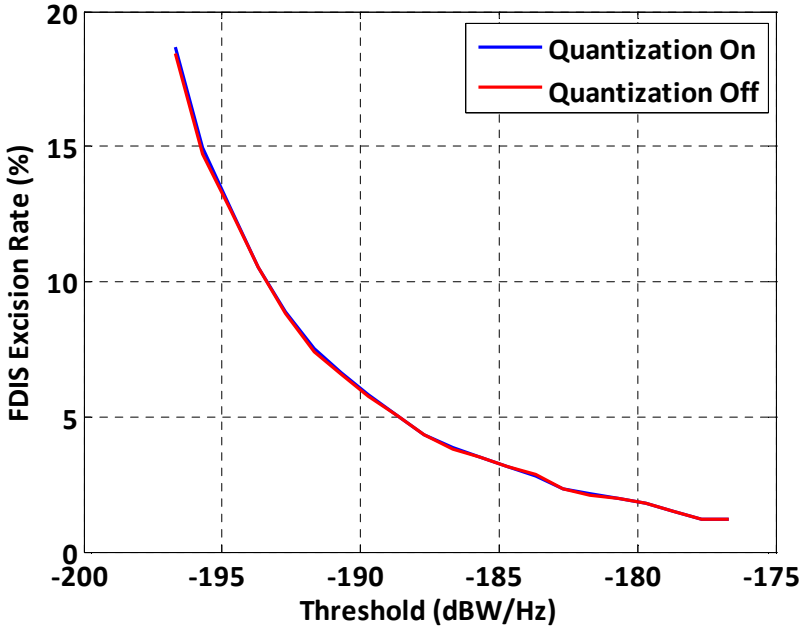

Figure 37: Comparison of FDIS Detection Rates, assuming a FFT window size of 128 samples.

Figure 38 shows a close up of Figure 37. In case quantization is activated, the noise floor is increased, inducing an increase of the false alarm rate, and so of the excision rate. This increase is observed for low threshold values, where false alarm rates become non-negligible. Nevertheless, the impact of the quantization process is somewhat negligible (increase of the FDIS excision rate by a few tenths of percents).

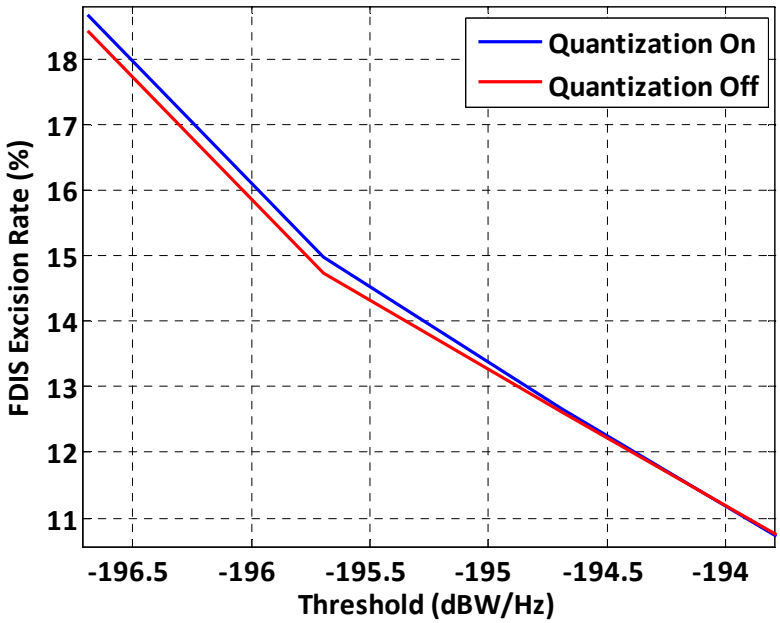

Figure 38: Figure 37 close up.

To conclude, the quantization process results from the FDIS point of view, in an increase of the noise floor, and so of the false alarm rate. This false alarm rate increase will have two main effects:

- In the absence of interference, the C/N_0 loss increases of a few tenth of dB,
- In the presence of interference, the non-corrupted parts of the spectrum will suffer an increased false alarm rate also, and so a loss higher by a few tenth of dB.

As long as the interference does not saturate the ADC, the distortions induced by the quantization should not significantly disturb the proposed algorithm.

II.3.6. **FDIS System Characterization**

FDIS has been presented as an algorithm detecting and removing interferences in the frequency domain. Indeed, this system can be decomposed in two subsystems:

- The detection algorithm is indeed a time frequency analysis, performed by a short-time Fourier transform. A description of this kind of analyses is available in [Cohen, 1995]. It notably discusses the necessity of a trade-off between time and frequency resolution, as both notions are, in this case, competing.
- The suppression stage is an FFT filter: if classical filters convolute the input signal to their coefficients, FFT filters multiply the input signal FFT by a transfer function. This transfer function is a function of the input signal and of the threshold, so that it varies with time.

On each block of N samples, the impulse response can be retrieved from the filter transfer function, but special care has to be taken because of circular convolution issues. Indeed, the signal, at FDIS output, can be written:

$$y(n) = \frac{1}{N}\sum_{k=0}^{N-1} H(k) X_{FFT}(k) e^{j\frac{2\pi}{N}nk} \qquad \text{II.20}$$

Where:

- H is the FDIS transfer function,
- N is the number of samples used in the FFT estimation,
- X_{FFT} is the FFT of the FDIS input signal.

Writing the FDIS function and the input signal FFT as a function of their temporal expressions:

$$y(n) = \frac{1}{N}\sum_{k=0}^{N-1}\left(\sum_{n_1=0}^{N-1} h(n_1) e^{-j\frac{2\pi}{N}n_1 k}\right)\left(\sum_{n_2=0}^{N-1} x(n_2) e^{-j\frac{2\pi}{N}n_2 k}\right) e^{j\frac{2\pi}{N}nk} \qquad \text{II.21}$$

Where:

- h is the inverse Fourier transform of the FDIS transfer function H,
- x is the input signal.

Then, it comes

$$\begin{aligned} y(n) &= \frac{1}{N}\sum_{n_1=0}^{N-1}\sum_{n_2=0}^{N-1} x(n_2) h(n_1) \sum_{k=0}^{N-1} e^{-j\frac{2\pi}{N}(n_1+n_2-n)k} \\ &= \sum_{n_1=0}^{N-1}\sum_{n_2=0}^{N-1} x(n_2) h(n_1) \delta_{n_1+n_2-n}^{i\cdot N} \\ &= \sum_{n_1=0}^{N-1} h(n_1) x\left((n-n_1)_{\mathrm{mod}uloN}\right) \qquad \text{II.22} \\ &= \sum_{n_1=0}^{N-1} h(n_1) x(n-n_1) + \sum_{n_1=0}^{N-1} h(n_1) x(n-n_1+N) \\ &= \sum_{n_1=0}^{N-1} h(n_1) x(n-n_1) + \sum_{n_1=N}^{2N-1} h(n_1-N) x(n-n_1) \end{aligned}$$

Where δ is Kronecker's symbol.

The FDIS output, re-written as above, is expressed as the convolution between the input signal and the inverse FFT of the filter function:

$$y(n) = \sum_{n_1=0}^{2N-1} \left(h(n_1) + h(n_1-N)\right) \cdot x(n-n_1) \qquad \text{II.23}$$

Then, one can write that the FDIS is a time-varying filter which impulse response equals:

$$\begin{aligned} &h_l'(n) = h_l(n) + h_l(n-N) \\ &n \in [(l-1)\times N + 1; l\times N[, l \in \mathbf{Z} \end{aligned} \quad \text{II.24}$$

II.3.6.1. FDIS phase

The FDIS processes noise, interference, but also the useful signal. Therefore, the phase of the signal can be distorted by the process, which is not bearable. Indeed, the fact that abrupt changes (interference corrupted frequency bins are set to zero whatever the vicinity frequency bins values) are created in the signal spectrum might induce distortions in the signal phase, such as ringing artefacts (Gibbs phenomenon). FDIS phase properties can be deduced from the parity of its impulse response. The FDIS function $H\left(\frac{k}{N}\right)$ equalling one if the threshold is not exceeded and zero if so, it is real. Its impulse response is therefore even. Then:

$$h(N-1-n) = h(n) \quad \text{II.25}$$

Moreover, on one hand:

$$\begin{aligned} h'(n-1) &= h(n-1) + h(n-1+N) \\ &= h(N-1) \quad if\ n = 0 \\ &= h(n-1) \quad if\ n \geq 1 \end{aligned} \quad \text{II.26}$$

And on the other hand:

$$\begin{aligned} h'(-n) &= h(-n) + h(N-n) \\ &= h(0) = h(N-1) \quad if\ n = 0 \\ &= h(N-n) \quad if\ n \geq 1 \end{aligned} \quad \text{II.27}$$

So $h'(n-1) = h(n-1) = h(N-1-n+1) = h(N-n) = h'(-n)$, the impulse response h' of the FDIS filter is even. According to [Kunt, 1999], a filter which impulse response is even is linear in phase. As a conclusion, FDIS does not distort GNSS signals.

II.4. THEORETICAL POST-CORRELATION C/N_0 DEGRADATION PREDICTIONS

The post-correlation C/N_0 (or carrier-to-noise ratio) is a measure of the ratio between the signal carrier power, C, and the noise density ratio, N_0. Its degradation is the main figure of merit used to characterize pulsed interference mitigation techniques performance, for two main reasons:

- The post-correlation C/N_0 degradation is the figure of merit that has been studied in previous work about pulsed interference impact on GNSS receivers, and temporal blanker efficiency as a pulsed interference mitigation technique. Using the same

figure of merit allow validating our results and simulators by comparison with previous studies' results,
- It is a good indicator of GNSS receivers' performances. For example, it can be used to compute the mean acquisition time, the tracking errors standard deviation, or the word error rate.

The theoretical derivation of this degradation for the temporal blanker presented in this PhD thesis is extracted from [Bastide, 2004], while the derivation for the FDIS has been developed for this PhD.

II.4.1. **Temporal Blanker post-correlation C/N$_0$ degradation derivation**

The Temporal Blanker is extensively studied in [Bastide, 2004], which derived the post-correlation C/N$_0$ degradation suffered by a GNSS receiver in presence of pulsed interference, using the temporal blanker as mitigation technique. The degradation expression is:

$$\deg\left(\frac{C}{N_{0\ eq}}\right)=\frac{1-Bdc}{1+\frac{\sum_i P_{Interf,i}\cdot C_I(\Delta f_i)}{\beta\cdot N_0}} \qquad \text{II.28}$$

Where:
- $P_{Interf,i}$ is the i^{th} mean power of the interference signal at correlator input,
- Δf_i is the frequency offset between the tracked GNSS signal and the received interference,
- $C_I(\Delta f_i)$ is the interference coefficient at the frequency offset Δf_i, which is written:

$$C_I(\Delta f)=\int_{-\infty}^{+\infty}\left|H_{BB}(f)\right|^2\times S_I(f-\Delta f_i)\times S_c(f)df \qquad \text{II.29}$$

Indeed, the degradation can be decomposed as follows:
- The useful signal power degradation, which equals $(1-Bdc)^2$,
- The thermal noise power degradation, which equals $(1-Bdc)$,
- The contribution of DME/TACAN signals to noise floor, which equals $(1-Bdc)\frac{f_p}{4}\sum_i P_{Interf,i}\cdot C_I(\Delta f_i)$.

According to [Bastide, 2004], the Bdc can be predicted from the DME/TACAN environment knowledge. The mean activation time of the temporal blanker, when a pulse pair is received, equals:

$$T_{blanker}=\gamma\left(\frac{J}{Th}\right)\cdot\left(T_{eq}e^{-\lambda T_{eq}}+\frac{T_{eq}}{2}\frac{(\lambda T_{eq})}{1!}e^{-\lambda T_{eq}}+\frac{T_{eq}}{3}\frac{(\lambda T_{eq})^2}{2!}e^{-\lambda T_{eq}}+\ldots\right) \qquad \text{II.30}$$

Where:

- $T_{eq} = 2.64\mu s$ is the equivalent duration of a pulse,
- λ is the parameter of the Poisson law characterizing the DME/TACAN signals reception times,
- J is the amplitude of the DME/TACAN signals at correlator input,
- Th is the temporal blanker threshold,
- $\gamma\left(\frac{J}{Th}\right)$ is the ratio of the real mean blanker activation time to the theoretical mean blanker activation time as a function of $\frac{J}{Th}$.

The blanker duty cycle is then obtained by combining (adding) the mean activation time of the blanker for each received pulse pair:

$$Bdc = \frac{T_{blanker}}{T_p} = \frac{2 \cdot \left(2700 \cdot \sum_{i=1}^{n_{DME}} T_{blanker,DME}(i) + 3600 \cdot \sum_{i=1}^{n_{TACAN}} T_{blanker,TACAN}(i) \right)}{T_p} \quad \text{II.31}$$

The interference signal mean power at correlator input P_{Interf} has been calculated from the signal autocorrelation function evaluated in zero [Bastide, 2003']. Using the DME/TACAN signal autocorrelation function model derived in [Bastide, 2004], this value equals:

$$P_{Interf} = P_{RF}\left(\lambda T_{eq}\right)e^{-\lambda T_{eq}} \cdot \left(1 + \left(\lambda T_{eq}\right)e^{-\lambda T_{eq}}\right) \quad \text{II.32}$$

Where P_{RF} is the interference power at RF level (dBW). However, this is true for weak pulse (peak power below the blanking threshold). If the peak power of the received pulse exceeds the threshold, its power after temporal blanking is approximated as the power of a pulse which peak power would equate the blanking threshold. In this case, P_{RF} is replaced by the threshold value.

II.4.2. **FDIS post-correlation C/N$_0$ degradation derivation**

This study constitutes an original contribution of the present PhD thesis. At correlator output, the effect of pulsed interference is equivalent to the effect of a white Gaussian noise which density equals $N_{0,I}$ ([Van Dierendonck, 1996]).

$$\frac{C}{N_{0\ equ}} = \frac{C}{N_0 + N_{0,I}} \quad \text{II.33}$$

FDIS processes all the components of the signal. Thus, C, N_0 and $N_{0,I}$ are modified.

$$\frac{C}{N_{0\ equ,FDIS}} = \frac{C_{FDIS}}{N_{0,FDIS} + N_{0,I,FDIS}} \quad \text{II.34}$$

Thus, the present paragraph proposes a derivation of the C/N$_0$ degradation based on the derivation of each of the three components C_{FDIS}, $N_{0,FDIS}$, and $N_{0,I,FDIS}$.

II.4.2.1. Useful Signal Power Degradation

The power of a GNSS signal, processed by FDIS, can be written as the product of the useful signal power C by the PRN code autocorrelation function evaluated in zero, processed by FDIS:

$$C_{FDIS} = C \times K^2_{c,f,FDIS}(0) \quad \text{II.35}$$

Where $K_{c,f,FDIS}$ is the correlation function between the locally generated PRN code and the received code, taking into account front end filtering and FDIS processing. In absence of FDIS it equals:

$$C_f = C \times K^2_{c,f}(0) \quad \text{II.36}$$

Where $K_{c,f}$ is the correlation function between the locally generated GNSS code and the received code, taking into account front-end filtering.

Thus, the useful signal power degradation induced by FDIS processing is:

$$\deg(signal) = \frac{K^2_{c,f,FDIS}(0)}{K^2_{c,f}(0)} \quad \text{II.37}$$

The autocorrelation function, evaluated in zero, equals the total power of the considered signal. It can be written as a function of the signal's PSD:

$$K^2_{c,f,FDIS}(0) = \left(\int_{-\infty}^{+\infty} S_{c,f,FDIS}(f) df \right)^2$$
$$K^2_{c,f}(0) = \left(\int_{-\infty}^{+\infty} S_{c,f}(f) df \right)^2 \quad \text{II.38}$$

Then, assuming that the FDIS, which is a time-frequency FFT filter, processes the GNSS signal as a filter which transfer function equals $FDIS_{eq}(f)$ would do, one can write:

$$\deg(signal) = \frac{\left(\int_{-\infty}^{+\infty} S_{c,f,FDIS}(f) df \right)^2}{\left(\int_{-\infty}^{+\infty} S_{c,f}(f) df \right)^2} = \frac{\left(\int_{-\infty}^{+\infty} S_c(f) \times FDIS_{eq}(f) \times H_{BB}(f) df \right)^2}{\left(\int_{-\infty}^{+\infty} S_c(f) \times H_{BB}(f) df \right)^2} \quad \text{II.39}$$

The corresponding demonstration is provided in paragraph II.4.2.5.

II.4.2.2. Thermal Noise density degradation

At correlator output, the power of thermal noise is:

$$P_n \approx \frac{1}{4}\frac{N_0}{2}\int_{-\infty}^{+\infty}\left[S_c(f-f_0)+S_c(f+f_0)\right]\times\left|H_{BB}(f)\right|^2\times\left|FDIS_{eq}(f)\right|^2 df \qquad \text{II.40}$$

Where f_0 is the GNSS signal carrier frequency.

Without FDIS, noise power at correlator output is:

$$P_n \approx \frac{1}{4}\frac{N_0}{2}\int_{-\infty}^{+\infty}\left[S_c(f-f_0)+S_c(f+f_0)\right]\times\left|H_{BB}(f)\right|^2 df \qquad \text{II.41}$$

Then, the degradation suffered by thermal noise because of FDIS processing, expressed at correlator output is:

$$\deg(noise)=\frac{\int_{-\infty}^{+\infty}S_c(f)\times\left|H_{BB}(f)\right|^2\times\left|FDIS_{eq}(f)\right|^2 df}{\int_{-\infty}^{+\infty}S_c(f)\times\left|H_{BB}(f)\right|^2 df} \qquad \text{II.42}$$

Once again, this expression assumes that the FDIS processing of the thermal noise can be resumed to a filter which transfer function equals $FDIS_{eq}(f)$.

II.4.2.3. Interference induced noise density

The equivalent noise spectral density $N_{0,DME/TACAN}$ of a single DME/TACAN signal equates [Van Dierendonck, 1996]:

$$N_{0,DME/TACAN} = P_{Interf}\times C_I\left(\left|f_{carrier}-f_{GNSS}\right|\right) \qquad \text{II.43}$$

Where:

- $f_{carrier}$ is the carrier frequency of the received interference,
- f_{GNSS} is the carrier frequency of the tracked GNSS signal.

The expression of the mean power of the DME/TACAN signal at correlator output is given in paragraph II.4.1.

In case the interference has been processed by FDIS, this noise spectral density can be written:

$$N_{0,I,FDIS} = P_{interf}\times C_{I,FDIS}\left(\left|f_{carrier}-f_{GNSS}\right|\right) \qquad \text{II.44}$$

The interference coefficient expression extracted from [Van Dierendonck, 1996], adapted to the case where FDIS is applied gives:

$$C_{I,FDIS}\left(\left|f_{carrier}-f_{GNSS}\right|\right)=\int_{-\infty}^{+\infty}\left|H_{BB}(f)\right|^2\times S_{I,FDIS}\left(f-\left|f_{carrier}-f_{GNSS}\right|\right)\times S_c(f)df \qquad \text{II.45}$$

Where $S_{I,FDIS}(f)$ is the base-band normalized interference PSD, when processed by FDIS. This coefficient depends upon the FDIS settings, the received interference power and its carrier frequency. A table containing these coefficients as a function of the quoted parameters have been pre-processed and stored, assuming the FDIS threshold equals -195 dBW. For this calculation, the signal is composed of a pulse pair only, and assuming 128 samples rectangular windows (neither weighting nor overlap). Figure 39 shows these interference coefficients, calculated for carrier frequencies ranging from 1160 MHz to 1210 MHz (entire E5 band), and DME powers from -80 to -140 dBW.

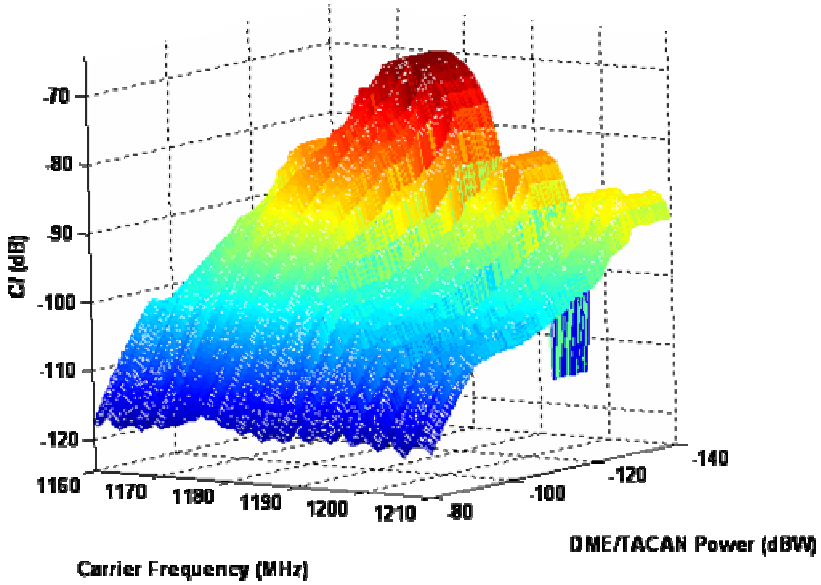

Figure 39: Interference Coefficient as a function of the carrier frequency and power, considering a FDIS threshold of -195 dBW.

Indeed, the coefficients only depend upon the carrier frequency and the offset between the interference peak power and the threshold. If the threshold is set to another value, the coefficients can be used as follows:

$$CI(Th, P, f_{carrier}) = CI(Th', P + Th - Th', f_{carrier}) \qquad \text{II.46}$$

Finally, the interference induced noise spectral density can be written:

$$N_{0,I,FDIS} = P_{RF} \times (\lambda \times T_{eq}) \times e^{-\lambda \times T_{eq}} \times (1 + (\lambda \times T_{eq}) \times e^{-\lambda \times T_{eq}}) \times CI(Th, P, f_{carrier}) \qquad \text{II.47}$$

II.4.2.4. Carrier to noise density ratio degradation

Given the carrier-to-noise density ratio expression in the beginning of this section:

$$\frac{C}{N_{0\ equ,FDIS}} = \frac{C_{FDIS}}{N_{0,FDIS} + N_{0,I,FDIS}} \qquad \text{II.48}$$

And the expression of each of the three components in paragraphs II.4.2.1, II.4.2.2, and II.4.2.3, the effective post correlation C/N_0 degradation due to DME/TACAN interference and FDIS processing with respect to the nominal case (front-end filtering but no interference) is:

$$\frac{C}{N_{0\,\deg}} = \frac{\frac{\left(\int_{-\infty}^{+\infty} S_c(f)\times FDIS_{eq}(f)\times H_{BB}(f)df\right)^2}{\left(\int_{-\infty}^{+\infty} S_c(f)\times H_{BB}(f)df\right)^2}}{\frac{\int_{-\infty}^{+\infty} S_c(f)\times\left|H_{BB}(f)\right|^2\times\left|FDIS_{eq}(f)\right|^2 df}{\int_{-\infty}^{+\infty} S_c(f)\times\left|H_{BB}(f)\right|^2 df} + \frac{\sum_i P\sum Interf\times CI(Th,P,f_{carrier})}{N_0}} \quad \text{II.49}$$

II.4.2.5. FDIS Equivalent transfer function calculation

The FDIS has been presented as a time-frequency FFT filter, which transfer function varies from one block to another. Nevertheless, the following approach demonstrates that an average transfer function exists with respect to stationary signals. By definition, if $FDIS_{eq}(f)$ exists, its square module equals the ratio between the power spectral density of the FDIS output signal and the PSD of the FDIS input signal. Assuming s is stationary:

$$\left|FDIS_{eq}(f)\right|^2 = \frac{S_{GNSS,FDIS}(f)}{S_{GNSS}(f)} \quad \text{II.50}$$

The PSD of the FDIS input and output signals can be estimated using the periodogram. Considering a stationary signal:

$$\begin{aligned} E\left[\frac{\left|FFT_k(s(t))\right|^2}{N}\right] &= S_s(f) * N\left(\frac{\sin(\pi fN)}{N\sin(\pi f)}\right)^2 \\ E\left[\frac{\left|FFT_k(s_{FDIS}(t))\right|^2}{N}\right] &= S_{s,FDIS}(f) * N\left(\frac{\sin(\pi fN)}{N\sin(\pi f)}\right)^2 \end{aligned} \quad \text{II.51}$$

By definition of FDIS, the Fast Fourier Transform of the signal at FDIS output equals:

$$FFT_k(s_{FDIS}(t)) = FFT_k(s(t))\times FDIS(k,f) \quad \text{II.52}$$

FDIS functions $FDIS(k,f)$ are obtained by comparing the input signal to a threshold. The threshold has been chosen so as to induce negligible false alarm rate, so that interferences only determine the FDIS functions shape. Therefore, thermal noise and GNSS signals, which are stationary, are independent with the FDIS functions.

$$E\left[\frac{\left|FFT_k\left(s_S(t)\right)\times FDIS(k,f)\right|^2}{T}\right]=E\left[\frac{\left|FFT_k\left(s_S(t)\right)\right|^2}{T}\right]\times E\left[\left|FDIS(k,f)\right|^2\right]$$
$$=\left(S_S(f)*N\left(\frac{\sin(\pi fN)}{N\sin(\pi f)}\right)^2\right)\times E\left[\left|FDIS(k,f)\right|^2\right] \quad \text{II.53}$$

Then, neglecting the periodogram induced bias, which is common to the FDIS input and output signals, the square module of the FDIS equivalent transfer function can be written:

$$\left|FDIS_{eq}(f)\right|^2=E\left[\left|FDIS(k,f)\right|^2\right] \quad \text{II.54}$$

FDIS functions depend upon pulsed interference characteristics (number, power, carrier frequency), and their arrival times. A DME/TACAN pulse pair received by a GNSS receiver, which previously described characteristics are known, always produce the same effect on FDIS functions. In other words, the random behaviour of FDIS functions can be resumed to the random behaviour of pulsed interference arrival times, as all the other characteristics are a-priori known.

The impact of one DME/TACAN signal is derived as follows: a DME/TACAN pulse pair is generated, with random arrival time, and the FDIS functions are calculated assuming the input signal is composed of the pulse pair only (thermal noise, GNSS signals, and other interference signals are ignored). The number of excisions is then calculated. This process is realized for each visible DME/TACAN ground station.

If $FDIS(k,f)$ equals 1, the signal is not modified, while if $FDIS(k,f)$ equals 0, $1-FDIS(k,f)$ equals 1, which corresponds to the case where a frequency bin have been excised.

An example of this calculation is given below. Figure 40 shows the generated pulse pair used to obtain FDIS functions. This pulse pair has a carrier frequency of 1170 MHz (6 MHz after downconversion), and a power of -110 dBW.

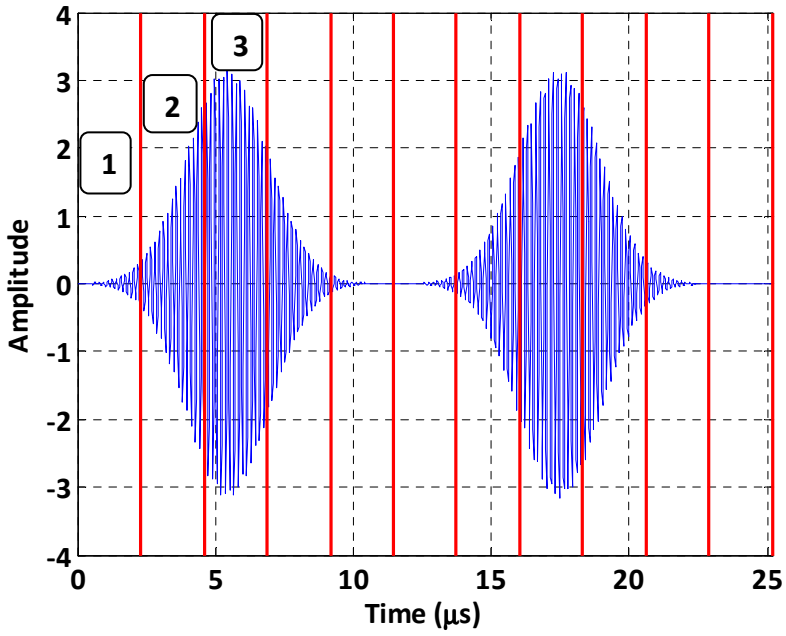

Figure 40: DME Pulse Pair.

The excision function is calculated on each slice, which are marked out by the red lines. Figure 41 shows the quantity $1-FDIS(k,f)$ for slice number 1 to slice number 3.

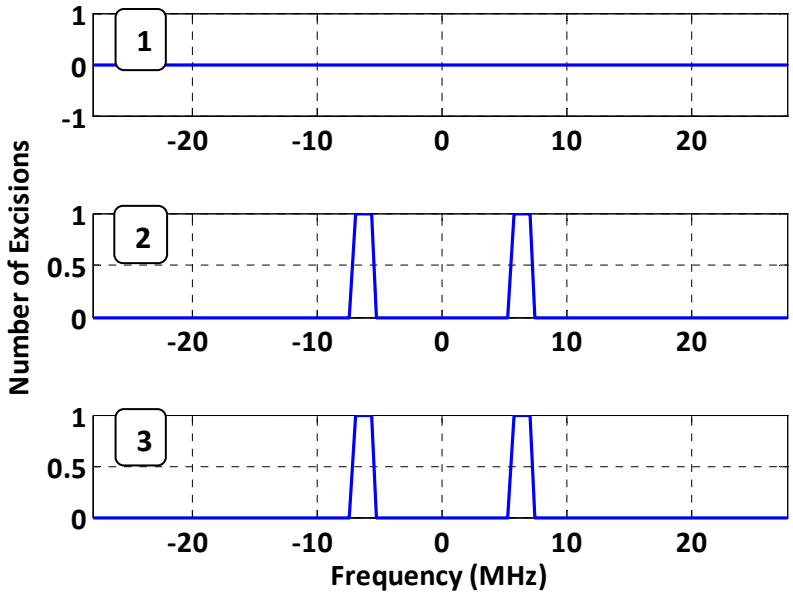

Figure 41: Number of Excisions for windows 1 to 3.

The objective being to calculate FDIS functions expectation, these excision functions are summed so as to obtain the total number of excisions made because of one pulse pair, as shown in Figure 42.

$$\begin{aligned} E[FDIS(k,f)] &= E[1-(1-FDIS(k,f))] \\ &= E[1-N_{excision}(k,f)] \\ &= 1-E[N_{excision}(k,f)] \end{aligned} \qquad \text{II.55}$$

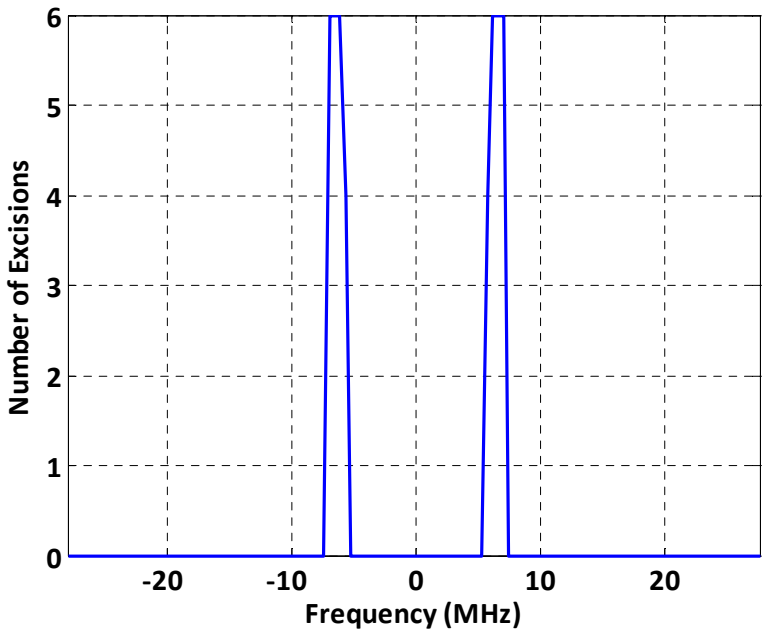

Figure 42: Total Number of Excisions due to the simulated pulse pair.

This calculation is possible assuming the FDIS function random variable is stationary and ergodic. Therefore, our calculation should consider an average case, which requires an observation window of at least one second, for example.
During one second, a given ground station emits 3600/2700 ppps (TACAN/DME). It is possible to predict, using the previous calculation, the average number of excisions made by FDIS when one ground station is visible:

$$E\left[N_{excision}(k,f)\right]=\frac{\sum_{k} N_{excision}(k,f)\times PRF\times T}{N_{win,T}} \qquad \text{II.56}$$

When flying over Europe, for example, several ground stations are in visibility of the receiver. Thus, the total number of excisions is:

$$E\left[N_{excision,tot}(k,f)\right]=\sum_{i}\frac{\sum_{k} N_{excision}(k,f,i)\times PRF(i)\times T}{N_{win,T}} \qquad \text{II.57}$$

Where:

- i is the ground station index,
- $N_{win,T}$ is the number of windows gathered in T seconds.

In case several ground stations are visible, one could assume that collisions can occur, possibly resulting in a decrease of the number of excisions. Indeed, if two pulse pairs inducing the same excisions (understand at the same frequency bins), the effective number of excisions will be lower than the one given by the above formula.
Given the frequency of transmission of the received DME/TACAN beacons, the probability that two pulses emitted with the same carrier frequency reach the receiver in the same time

is very low. Assuming that a collision occurs if less than T_{eq} (2.64 µs) separate the arrival of two pulse pairs, and that the pulse pairs arrival times follow a Poisson distribution, the probability that one collision occurs equals:

$$P(1\,collision) = \frac{(\lambda T_{eq})^2}{2} e^{-\lambda T_{eq}} \qquad \text{II.58}$$

Where λ is the Poisson law parameter. Assuming that from the FDIS point of view a collision occurs if the pulse pairs have the same carrier frequency, and given that the number of beacons emitting at the same carrier frequency can not exceed 5 over the hot spots (see Figure 43, Figure 44, Figure 45, and Figure 46), the Poisson law parameter does not exceed 5 times the PRF of a TACAN beacon (3600). Then, the maximum probability that this kind of collision occurs equals 10^{-3}.

In other words, collisions are neglected in the average number of excisions calculation process. Figure 43 to Figure 46 show the carrier frequency repartition of the DME/TACAN beacons transmitting within the E5a/L5 or E5b bands and which are in the radio-electric range of the European or US hot spot. The maximum number of beacons emitting at the same carrier frequency equals 5. These figures were obtained from the data contained in Table 27 which is extracted from [EUROCAE, 2007].

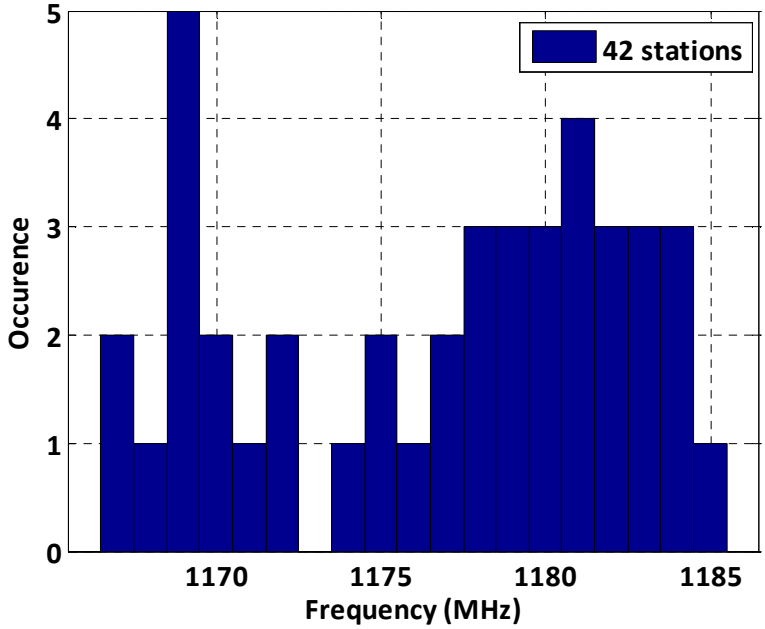

Figure 43: Frequency repartition of DME/TACAN beacons within the E5a/L5 band, in the radio-electric range of the European hot spot.

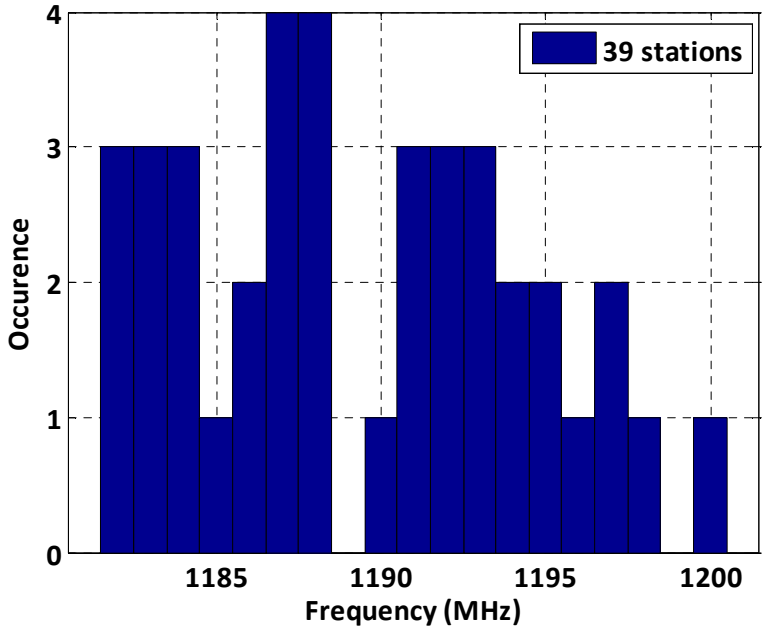

Figure 44: Frequency repartition of DME/TACAN beacons within the E5b band, in the radio-electric range of the European hot spot.

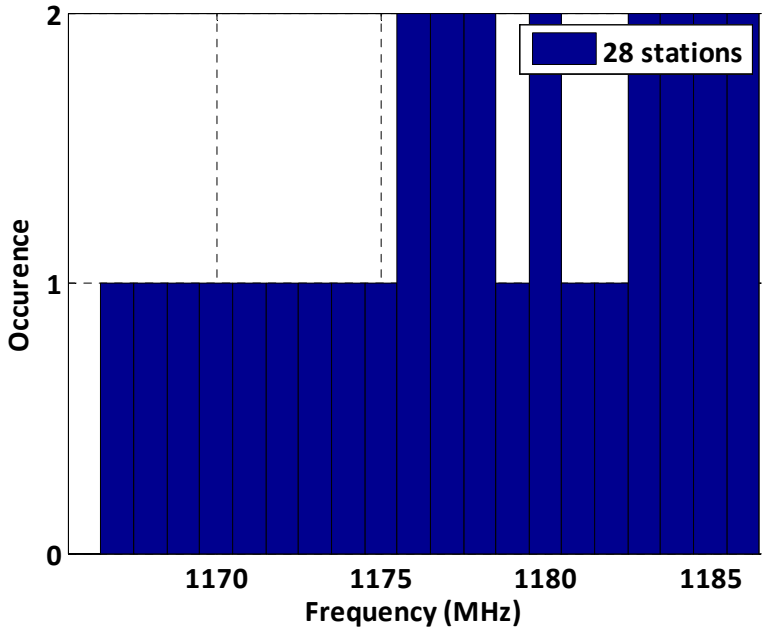

Figure 45: Frequency repartition of DME/TACAN beacons within the E5a band, in the radio-electric range of the US hot spot.

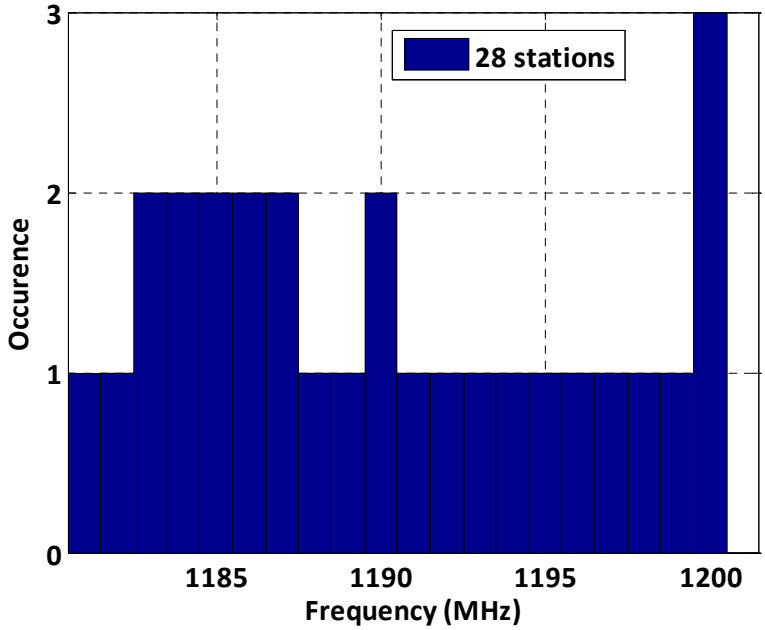

Figure 46: Frequency repartition of DME/TACAN beacons within the E5b band, in the radio-electric range of the US hot spot.

The number of excisions $\sum_k N_{excision}(k,f,i)\times PRF(i)$ realized by FDIS when receiving a signal from beacon i only depends upon the received interference PRF, carrier frequency, and power. Thus, a table gathering this information as a function of the quoted parameters have been pre-processed and stored, assuming a threshold of -195 dBW. In the degradation formula proposed in section II.4.2.4, the equivalent FDIS transfer function is thus replaced by:

$$\begin{aligned} FDIS_{eq}(f) &= E[FDIS(k,f)] \\ &= 1-E[N_{excision,tot}(k,f)] = 1-\sum_i \frac{\sum_k N_{excision}(k,f,i)\times PRF(i)\times T}{N_{win,T}} \\ &= 1-\sum_i \frac{Tab_{excision}(P,f_{carrier},f)\times T}{N_{win,T}} \end{aligned} \qquad \text{II.59}$$

As explained in paragraph II.4.2.3, the table is valid for any other chosen threshold, using the table as follows:

$$Tab_{excision}(Th,P,f_{carrier},f) = Tab_{excision}(Th',P+Th-Th',f_{carrier},f) \qquad \text{II.60}$$

Figure 47 shows an extract of the table corresponding to a signal which carrier frequency equals 1209 MHz.

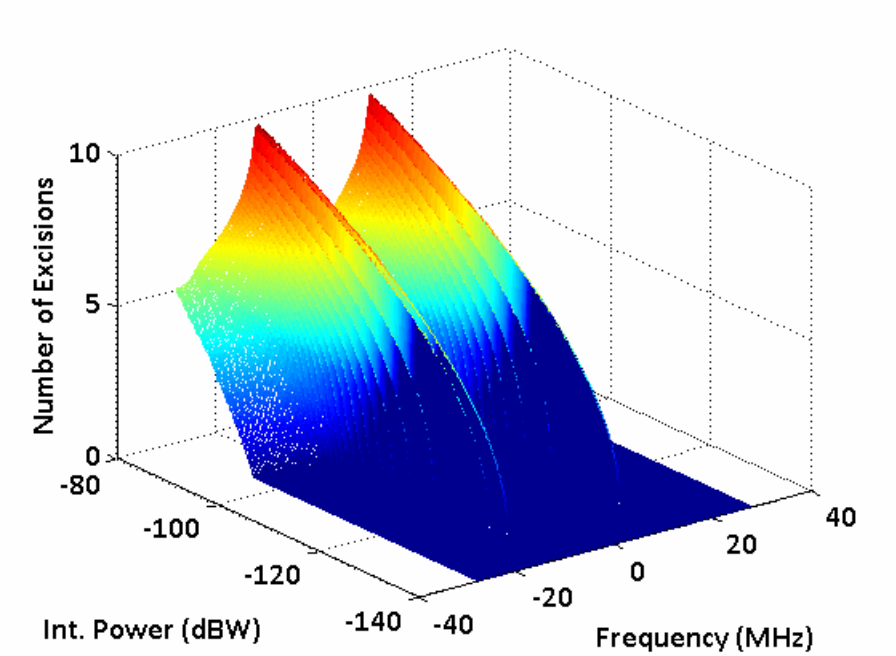

Figure 47: Number of excisions as a function of the frequency and the interference received power.

CHAPTER III: SIMULATION ENVIRONMENT

This chapter first presents the scenarios of interest, which were designed with respect to civil aviation test procedures. Then, the Figures of Merit chosen to assess their performances are presented. Finally, the simulation tools used to obtain these performances are described.

III.1. SCENARIO OF INTEREST

As stated in paragraph I.6, the tests should be performed during en-route operations, while flying over the hot spot. Moreover, GPS L5, Galileo E5a or Galileo E5b signals are simulated, assuming a received power of -155 dBW, considering the pilot channel only. Finally, thermal noise is generated with a noise density of -200 dBW/Hz (this choice is motivated in paragraph II.2.3).

III.2. STUDIED FIGURES OF MERIT (FOM)

The performances of the IMTs are evaluated using several FOMs, which were chosen for their relevance with respect to the civil aviation performances requirements. The chosen FOMs are:

- The C/N_0 degradation: it is a good indicator of acquisition and data demodulation performances, which are critical operations for onboard GNSS receivers. Moreover, the value will be used in link budgets so as to be compared to the C/N_0 thresholds presented in paragraph I.6,
- The mean acquisition time: this performance being a function of the receiver architecture (number of correlators) and the C/N_0 (but also the acquisition strategy or PRN codes isolation), the improvement of the latter can be turned into a loosening of the constraints on the receiver architecture,
- Code and Carrier Phase tracking accuracy: paragraph I.6 showed that it was not the limiting performances. Nevertheless, monitoring these FOMs will be done so as to check that the theoretical derivations proposed in II.3 about IMTs phase linearity are correct,

- AGC Gain bias: As stated in paragraph I.5.1, pulsed interferences induce a bias on the AGC gain, and this bias increases the C/N_0 degradation brought by the same interferences. Monitoring the amplitude of this bias is then interesting.

III.3. SIMULATION TOOLS DESCRIPTION

The following section describes the tools used to observe the previously described FOMs:

- PULSAR for C/N_0, code and carrier phase and AGC gain bias,
- the ANASTASIA and GIRASOLE Galileo mock-up receivers for C/N_0 and AGC gain bias,
- A Matlab routine for the mean acquisition time.

III.3.1. **PULSAR**

The performances of the techniques were obtained using a software simulator called PULSAR. The simulator is developed under Labview and is composed of:

- A signal generation block. This block generates E5a/E5b or L5 signals, thermal noise, and pulsed interferences (DME/TACAN and JTIDS/MIDS),
- A signal processing block composed of a front-end filter, an AGC/ADC, the IMTs described in Chapter II and the correlators, and the code and carrier phase tracking loops.

The simulator has been developed in the framework of [Bastide, 2004], a PhD thesis funded by the DTI. In the framework of the present PhD thesis, some modifications were brought to PULSAR in order to obtain a simulator as close as possible to the Galileo mock-up receiver developed for the ANASTASIA project. For example, the previous PULSAR version did not gather FDIS algorithm, which was implemented in PULSAR during the PhD thesis. Another important modification concerns the AGC loops, and more particularly the loop filters and the loop estimator.

III.3.1.1. Signal Generation Module

III.3.1.1.1. Galileo/GPS Signals Generation

Galileo E5 and GPS L5 signals are generated as described in Chapter I, with some simplifications:

- E5a and E5b signals are generated separately, as if modulated by a QPSK modulation,
- The pilot channel only is generated,
- The used PRN codes are the following ones: E5aQ code number 1 for E5a, E5bQ code number 1 for E5b, and XQ1 for L5,
- Secondary codes are neglected.

The signal generation scheme is given in Figure 48. The GNSS signals are first generated in base-band, and passed through an anti-aliasing filter which bandwidth equals 20 MHz (double sided), and which order equals 50 and transfer function is represented in Figure 49. The coefficients of the filter are determined using a Labview Finite Impulse Response (FIR) filter design function. This filtering induces the following delay:

$$\tau_{anti-alias} = \frac{N-1}{2} \times T_s \qquad \text{III.1}$$

Where N is the filter order.

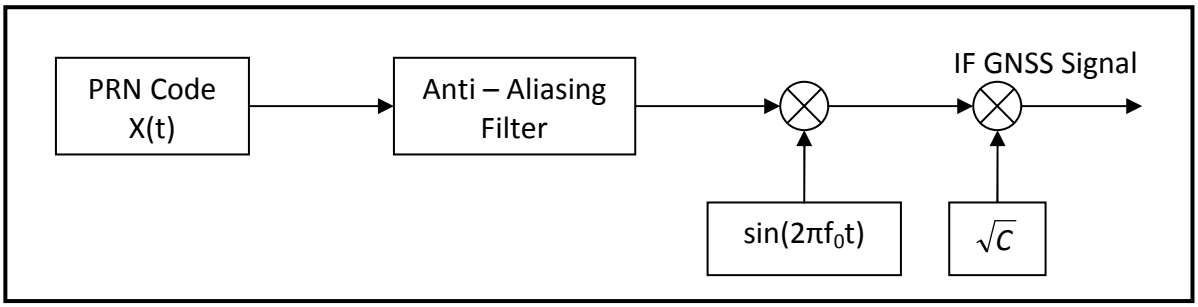

Figure 48: PULSAR GNSS Signal Generation Process.

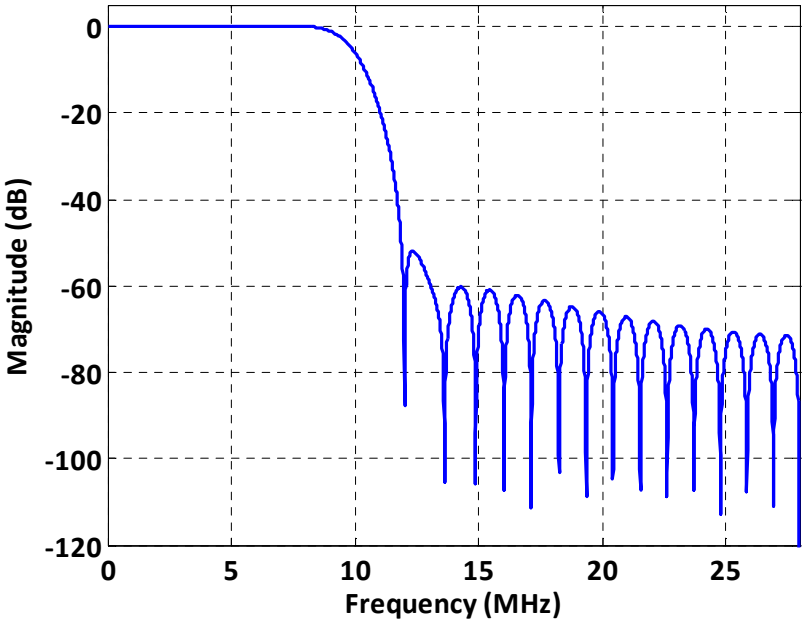

Figure 49: GNSS Signal Anti-Aliasing Filter.

Originally, the Galileo mock-up receiver developed for the ANASTASIA project was supposed to use a sampling frequency of 56 MHz. The same sampling frequency was used in the simulator, in order to compare the results. At last, the mock-up receiver sampling frequency uses a sampling frequency of 62.5 MHz, but the simulator configuration was not updated. Using a higher sampling would be more comfortable from the Shannon's theorem point of view, but it would require much more calculation load. Therefore, the GNSS codes previously

obtained are modulated at IF, which equals 14 MHz. Finally, the signal is multiplied by the amplitude.

III.3.1.1.2. Thermal noise generation

Thermal noise is generated using the Labview white Gaussian noise function. It generates pseudo random sequence which distribution is Gaussian, thanks to a random numbers algorithm generator based on the central limit theorem. The algorithm is designed so as to be close to the following probability density function (pdf):

$$f(x) = \frac{1}{s\sqrt{2\pi}} e^{\left(-\frac{x^2}{2s^2}\right)} \quad \text{III.2}$$

Where *s* is the noise standard deviation, which equals:

$$\sigma_{noise} = \sqrt{N_0 \times f_s} \quad \text{III.3}$$

Where f_s is the sampling frequency (56 MHz).

III.3.1.1.3. Interference generation

The DME/TACAN signals are generated using the theoretical formula given in paragraph I.3.1.

$$s_{DME/TACAN}(t,\alpha) = \sqrt{P} \times \sum_{k=1}^{N} \left(e^{\frac{-\alpha(t-t_k)^2}{2}} + e^{\frac{-\alpha(t-\Delta t-t_k)^2}{2}} \right) \times \cos(2\pi f_l t + \vartheta_l) \quad \text{III.4}$$

In the scenario of interest, the interference signal is a combination of the emissions of all the beacons visible from the airplane. The DME/TACAN beacons located in the radio-electric range of the aircraft are determined using a Matlab routine and a database encompassing the following information:

- the coordinates of each DME/TACAN ground station emitting in Europe/USA (latitude, longitude, altitude),
- their emission power,
- their carrier frequency,
- their Pulse Repetition Frequency.

Then, the routine calculates the distance between each DME/TACAN station and the user, which location has previously been provided. This distance is compared to the radio-electric horizon $D_{\max}$, which represents the maximum distance within which the aircraft GNSS antenna can receive signals.

$$D_{\max} = a\cos\left(\frac{R}{R + Alt_{user}}\right) \times R \quad \text{III.5}$$

Where:

- R equals 4/3 the earth radius,
- Alt_{user} is the altitude of the user (FL400 in our case, see paragraph I.6.5).

All the ground stations closer than this range are declared visible, and gathered in a list giving the carrier frequency, the pulse repetition frequency and the peak power at front-end level for each visible beacon. The power is calculated using the following formula:

$$P_{RF} = P + G_{beacon}(\alpha) + L_{free} + G_{aircraft}(-\alpha) \qquad \text{III.6}$$

Where:

- P_{RF} is the interference power at RF level (dBW),
- P is the interference beacon transmitted peak power (dBW),
- G_{beacon} is the normalized DME/TACAN beacon antenna gain (dB),
- α is the elevation angle of the aircraft from the beacon point of view (°),
- L_{free} is the free-space propagation loss term (dB),
- $G_{aircraft}$ is the normalized aircraft antenna gain (dB).

The free space losses are a function of the signal's wavelength (λ, in meters), and the radio-electric range between the aircraft and the beacon (d, in meters):

$$L_{free} = \left(\frac{\lambda}{4\pi d}\right)^2 \qquad \text{III.7}$$

The normalized DME/TACAN beacon antenna gain is applied using the model given in Figure 50 (extracted from [Bastide, 2004]).

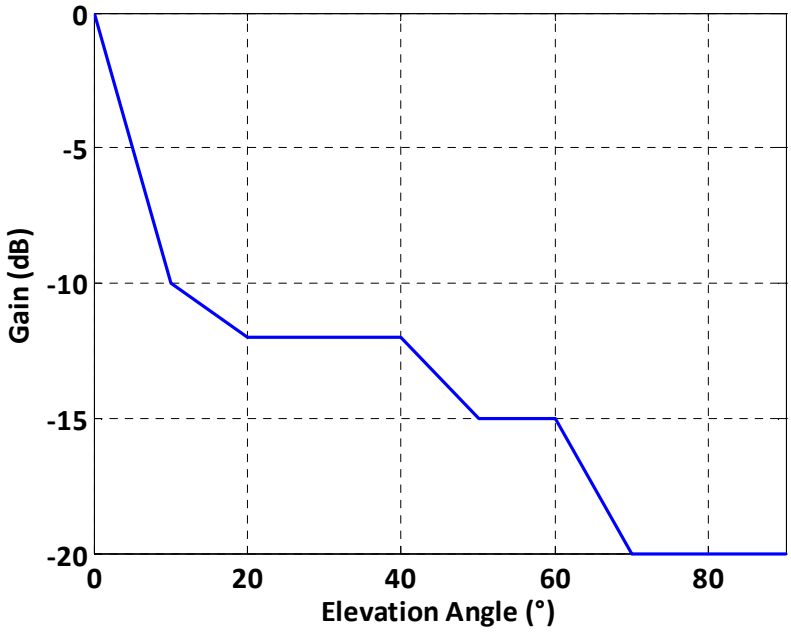

Figure 50: DME/TACAN normalized antenna gain vs. elevation angle.

The normalized aircraft antenna gain is considered to equal the EUROCAE specification given in paragraph I.6.2.
A Matlab routine uses the obtained characteristics to generate a 10 ms long signal which is a combination of all the interferences received by the GNSS device:

$$Interf = \sum_{k=1}^{N_{vis}} \sqrt{\frac{P_{RF}}{P}} s_{DME\,/\,TACAN}(t) \qquad \text{III.8}$$

Where N_{vis} is the total number of visible beacons. The duration of the signal (10 ms) has been chosen as it corresponds to the duration of the integration (10 coherent integrations of 1 ms, see paragraph I.4.4 for more details).
The arrival times are assumed to follow a Poisson law ([Bastide, 2004]) which parameter equals $\sum_{k=1}^{N_{vis}} PRF(k)$.

III.3.1.2. Receiver Module

PULSAR gathers a comprehensive GNSS receiver, from the RF front-end to the signal processing module. The antenna has not been implemented but its effects have already been taken into account at the signal generation stage. The navigation processing module has neither been implemented, as the functions it fulfils were not part of the initial objectives of the simulator, but it would constitute the finalization of it. All the modules constituting the simulator have been briefly introduced in paragraph I.4, however the details of their implementation are given hereafter.

III.3.1.2.1. Front-end filter

The signals are generated at IF. Therefore, the front end filters have also been designed so as to filter the signals around the chosen IF (14 MHz). The magnitude of the E5a/L5 filter transfer function is represented in Figure 51. The E5b filter magnitude is shown in Figure 52. Both magnitudes are transposed at RF so as to compare them to EUROCAE masks.

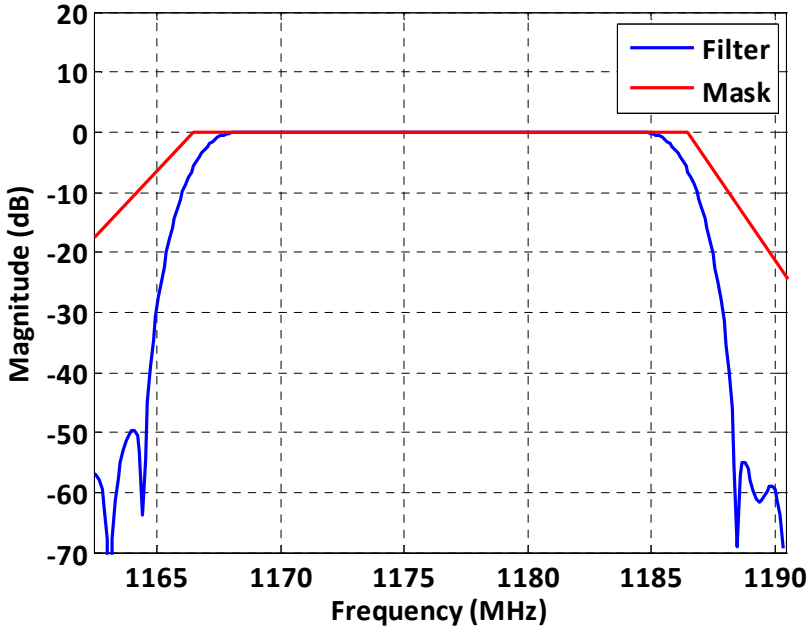

Figure 51: E5a/L5 Front-end Filter Magnitude.

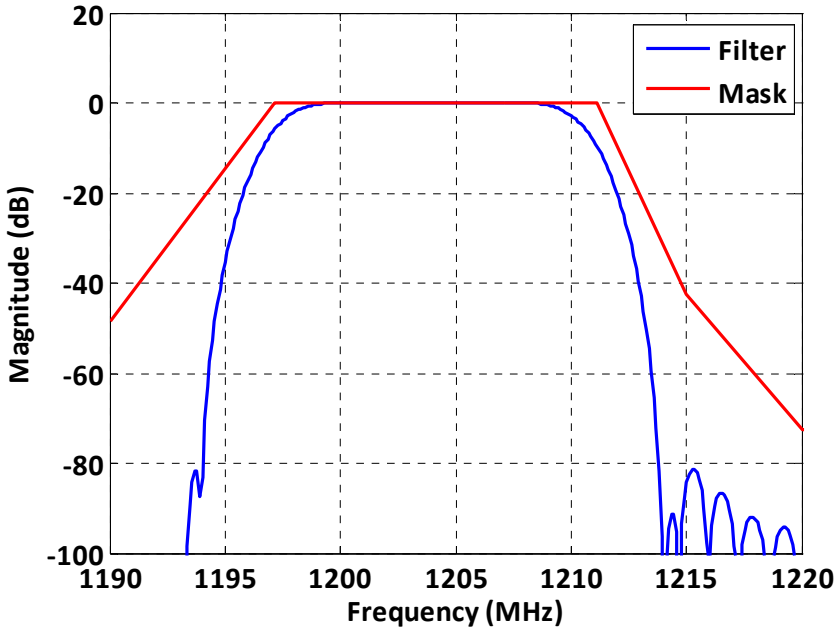

Figure 52: E5b Front-end Filter Magnitude.

The front-end filters are modelled using band-pass FIR Filters with 50 coefficients, which bandwidth equals 20 MHz for E5a/L5, and 14 MHz for E5b. The coefficients were determined using a dedicated Labview function. FIR filters are linear in phase, and induce a delay of $\tau_{RF} = \frac{N-1}{2} \times T_s$ seconds. The preamplifier is simply modelled by an amplifier which gain equals 29 dB.

III.3.1.2.2. Analog to Digital Converter

In the simulator, the ADC is preceded by the AGC, but the description of its implementation requires some details about the ADC.
The ADC is simply simulated by applying the quantization law given in paragraph I.4.3, Figure 11 (uniform centred 8-bit quantization law). The input voltages included in the range [-0.125; +0.125] volts are turned into bit trains which decimal representation lies in the range [-127; +127]. If the input values do not lie in the [-0.125; +0.125] range, the ADC is saturated and the output value equals -127 or +127.

III.3.1.2.3. Automatic Gain Control Loop

As stated in paragraph I.5.1, AGC loop operations are disturbed by interferences. Notably, AGCs using standard deviation estimators to determine the gain suffer the following bias:

$$\sqrt{\frac{\sigma_{noise}^2 + \sigma_{interf}^2}{\sigma_{noise}^2}} \qquad \text{III.9}$$

In PULSAR, the AGC gain estimation is based on a distribution estimator. This kind of estimators is for example proposed in [Bastide, 2003], for non-centred quantization laws. Basically, the estimator makes a histogram of the ADC output signal. Figure 53 shows the distribution of the samples at ADC output assuming a thermal noise which power equates -45 dBm at its input.

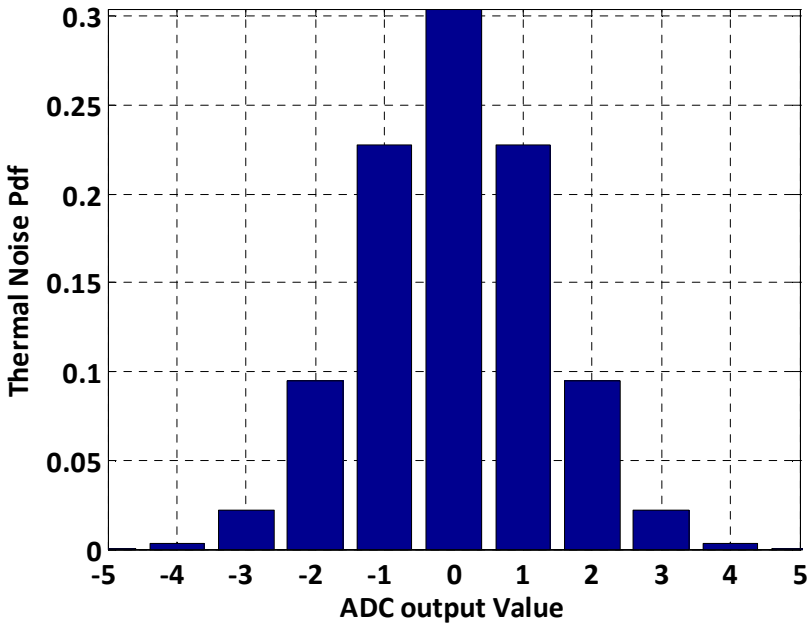

Figure 53: Close up of an 8-bits ADC output values distribution.

100 µs of signal (5600 samples at 56 MHz) are observed and the number of 0s, 1s and -1 are counted, so as to calculate the following value:

$$dist = 2 \times N_0 - N_1 - N_{-1} \qquad \text{III.10}$$

The value of this estimator is represented in Figure 54 as a function of the thermal noise power at ADC input. The chosen estimator has the interesting property of being a bijection with the thermal noise power. Therefore, one can derive the estimator value corresponding to the thermal noise power at the ADC input in order to minimize quantization losses. This value has been set to -45 dBm, accordingly to the specifications of the Galileo mock-up receiver developed for the ANASTASIA project. This choice, corresponding to a value of 861 from the AGC distribution estimator point of view, is motivated in paragraph III.3.2.

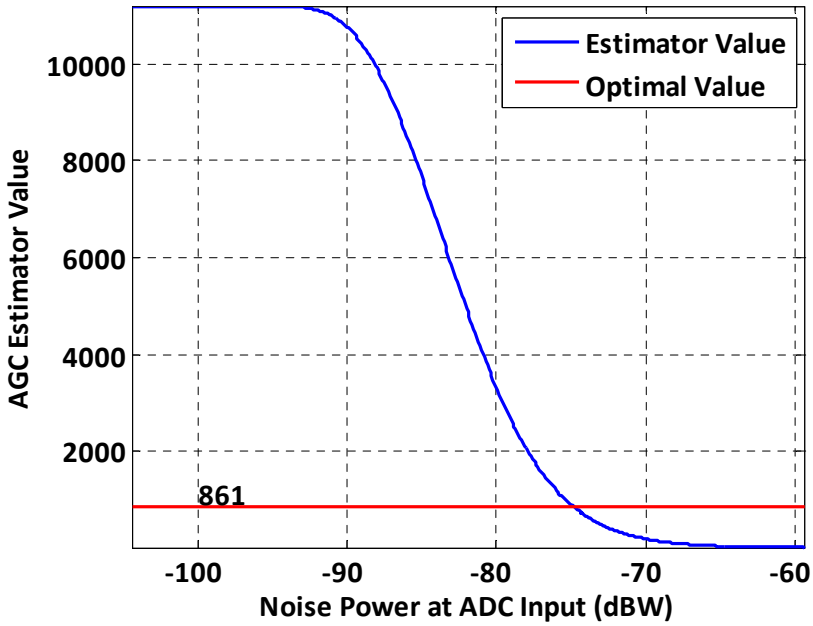

Figure 54: Distribution estimator as a function of thermal noise power at ADC input.

This estimator is compared to the optimal value (red line in Figure 54), and the resulting error tension is sent to an integrator. In the receiver mock-up, the integrator output is transformed into an analogue value thanks to a Digital to Analog Converter (DAC) and passed through a low pass RC filter (description provided in paragraph III.3.2.2). The integrator output is coded using 32 bits, which can be represented by the range [0; 2^{32}], while the DAC output lie in the range [0; 2] volts. In the simulator, the analog-to-digital conversion is simply modelled using a division by the factor 2^{31}. The RC filter is modelled by an Infinite Impulse Response (IIR) filter using the impulse invariance technique. The obtained filter transfer function equals:

$$H(z) = \frac{1}{1 + \frac{R_1}{R_2}} \times \frac{1 - e^{-\frac{T_s}{\tau}}}{1 - e^{-\frac{T_s}{\tau}} z^{-1}} \qquad \text{III.11}$$

Where:

- T_s is the sampling period,

- $\tau = \frac{R_1 R_2 C}{R_1 + R_2}$ is the filter time constant.

The implemented loop is represented in Figure 55.

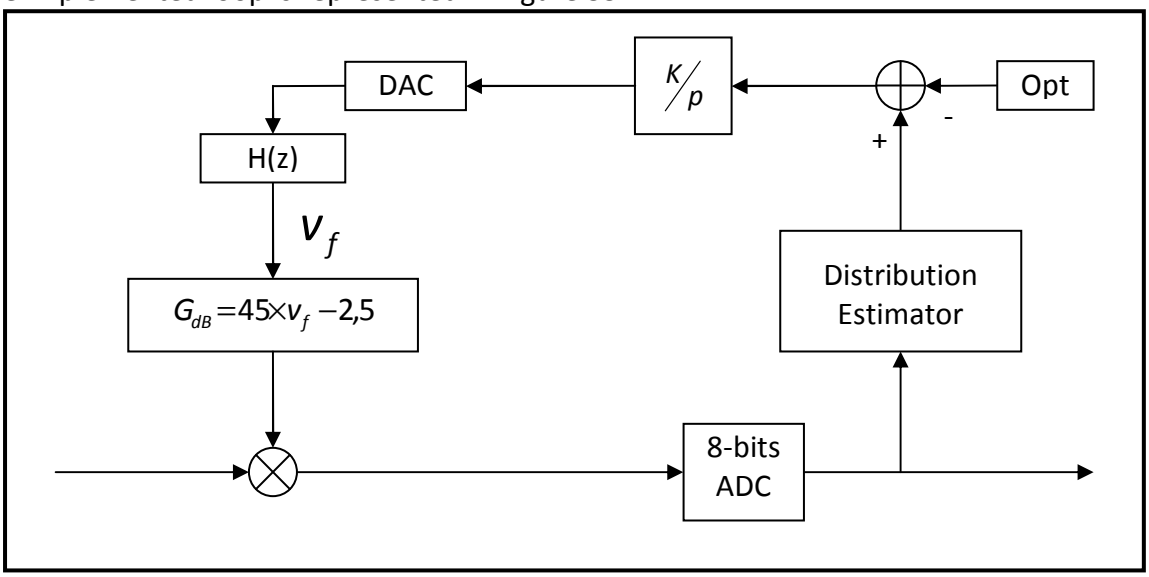

Figure 55: AGC Loop Pulsar Model Scheme.

The loop characteristics, such as stability and convergence time are detailed in Appendix A.

III.3.1.2.4. IMTs

The two IMTs presented in Chapter II are implemented in the simulator. The simulator man machine interface (MMI) offers the possibility of choosing between three options: no IMT, Temporal Blanker, and FDIS.

The temporal blanker is very easy to implement: the absolute value of the signal is compared to a threshold defined by the user in the MMI. This threshold is chosen in the "digital" domain, but can be associated to an analog value, using the following relation:

$$Th_{dBW} = 20\times\log_{10}\left(\frac{Th_{simu}}{G_{AGC}\times G_{Preamp}\times G_{Quantif}}\right) \qquad \text{III.12}$$

Where:

- Th_{dBW} is the threshold in the analog domain, in dBW,
- Th_{simu} is the threshold as set by the user in the MMI,
- G_{AGC} is the AGC gain,
- G_{Preamp} is the gain applied by the preamplifier, taking into account cable losses,
- $G_{Quantif}$ is the gain induced by quantization.

Assuming that the AGC performs perfectly, G_{AGC} equals G_{opt}, the desired gain. G_{Preamp} has been set to 24 dB: a typical value of 29 dB for preamplifier gain, and 5 dB of cable losses. $G_{Quantif}$ represents the gain induced by quantization: the analogic signal ranging between plus and minus 125 mV is represented by digital values ranging between plus and minus 127. This is equivalent to applying a gain of 1016. PULSAR TB thresholds are represented in Figure 58, as a function of the corresponding theoretical thresholds.

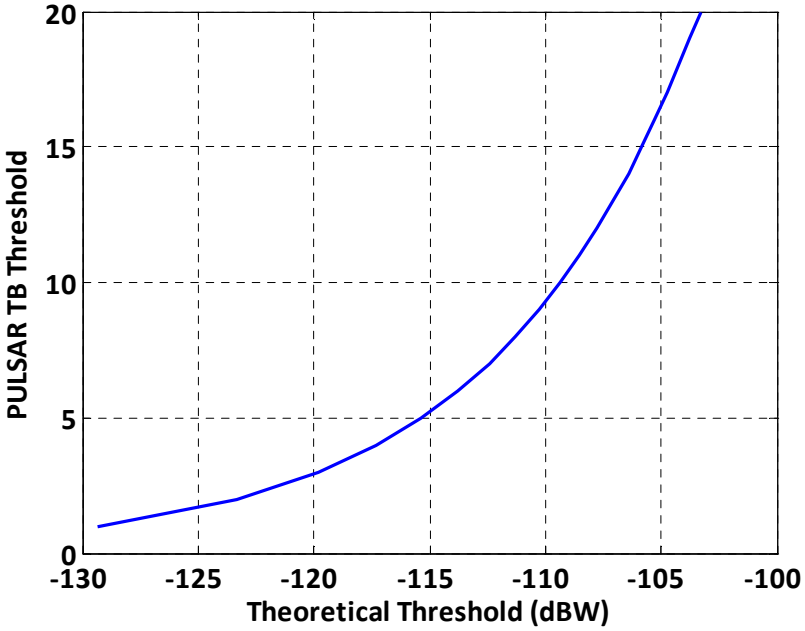

Figure 56: PULSAR vs. Theoretical TB thresholds.

If the threshold is exceeded, the ADC output sample is replaced by a zero. Otherwise, nothing happens. A scheme summarizing these steps is given in Figure 57.

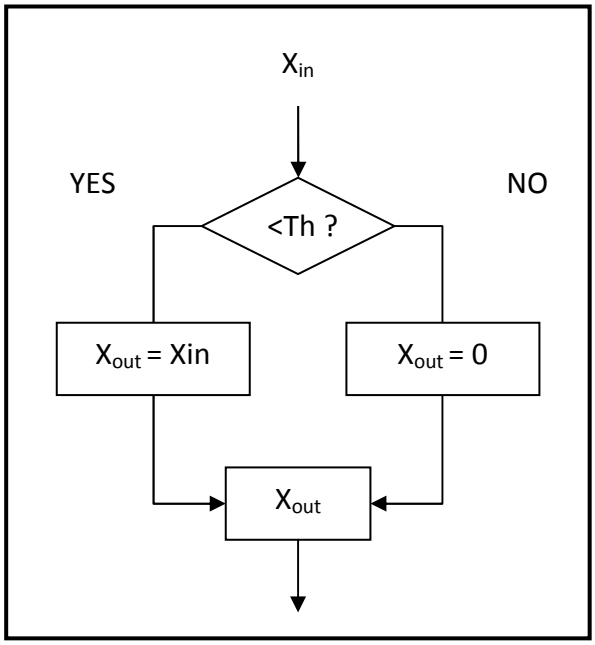

Figure 57: Temporal Blanker Scheme.

The algorithm is also able to calculate the Bdc. A counter is incremented each time the test result is “NO”.

The second implemented technique is the FDIS. First, the number of samples corresponding to the FDIS window size N specified by the user in the MMI is stored in a vector. In the meantime, the samples that have been previously processed by FDIS are released, with the same rate they are collected, thus introducing a delay of $N \times T_s$ seconds between the input and the output signal.
When the last sample is collected, a Matlab script calculates the square module of the signal’s FFT, which is obtained using the Matlab fft function. Then, the function is compared against a pre-defined threshold. The points exceeding the threshold are set to zero and the inverse FFT of the obtained signal is calculated using the Matlab ifft function.
The threshold is specified in the “digital” domain by the user in the simulator’s MMI. The formula linking this threshold to the analog one is:

$$Th_{dBW/Hz} = 10 \times \log_{10}\left(\frac{Th_{simu} \times T_s}{G_{AGC} \times G_{Preamp} \times G_{Quantif} \times N}\right) \qquad \text{III.13}$$

PULSAR thresholds are represented in Figure 58, as a function of the corresponding theoretical thresholds.

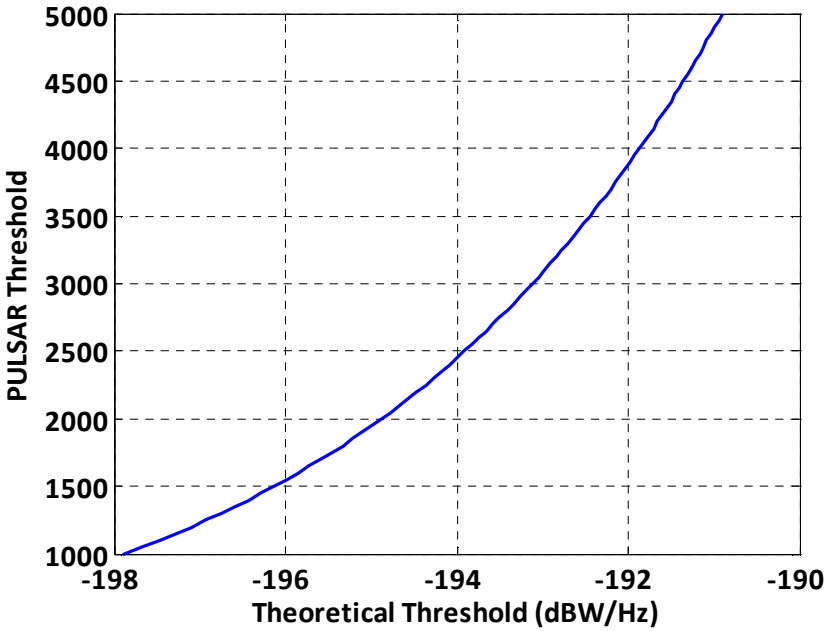

Figure 58: PULSAR vs. Theoretical FDIS thresholds.

III.3.1.2.5. Second quantization

Classical GNSS receivers tracking loops process signals coded on 1 or 2 bits. Upcoming receivers will likely process signals coded on 3 or 4 bits. The 8-bit ADC considered here and

implemented in the ANASTASIA Galileo mock-up receiver are meant to allow IMTs operation. Hence, after the processing by the IMTs, only the four least significant bits are kept, so that the new signal lies in the range [-7; +7]. The values exceeding this range are clipped.

III.3.1.2.6. Code and Phase Tracking Loops

The code and phase tracking loops are implemented as described in paragraph I.4.4. The implementation choices were not driven by the ANASTASIA project, as the simulator was created before the project. The loops were designed to match onboard receivers as well as possible. The considered overall tracking channel structure is simply an extension of the L1 classical one having twice more correlator and two different local codes generators: one for the data component and the other one for the pilot component.

First, the signal is multiplied by the locally generated carrier provided by the corresponding tracking loop. Then, the obtained I and Q channels are multiplied by the locally generated prompt, early and late code replica. The spacing between the early and late channels is set to 1 chip.
The following stage is the integrate and dump (I&D) filter: each channel (in-phase early, prompt, and late and quadra-phase early, prompt and late) is accumulated during the coherent integration time which has been set to 1 ms. This corresponds to one code period. Then, the I&D filter outputs are accumulated 10 times, resulting in an integration time of 10 ms. The correlators output are then provided to the discriminators.

Code tracking uses an Early Minus Late Power (EMLP) discriminator, 1.5-Hz equivalent loop noise bandwidth and 0.5 chips early/late chip spacing. Moreover, the loop is aided by the carrier tracking loop. To do so, the phase control value from the carrier tracking loop is multiplied by a scaling factor of 115 for E5a/L5, and 118 for E5b, corresponding to the ratio between the carrier frequency (1176.45 MHz for E5a/L5 and 1207.14 MHz for E5b) to the code one (10.23 Mcps).
Carrier tracking loop uses an extended arctangent discriminator, which linear range is $[-\pi,+\pi]$. The carrier loop filter is a Stephens loop of the third order [Stephens, 1995], which noise bandwidth is set to 10 Hz.

Theoretically ([Kolodziejski, 1999]), the tracking error variance in presence of white noise is:

$$\sigma_\tau^2 \approx \frac{2.B_{DLL}.(1-0.5.B_{DLL}.T_P)\int_{-\infty}^{+\infty} S_{c,f}(f)\times\sin^2(\pi f d T_c)df}{\frac{C}{N_0}\left(2\pi\int_{-\infty}^{+\infty} f\times S_{c,f}(f)\times\sin(\pi f d T_c)df\right)^2}\left(1+\frac{\int_{-\infty}^{+\infty} S_{c,f}(f)\times\cos^2(\pi f d T_c)df}{\frac{C}{N_0}T_P\left(\int_{-\infty}^{+\infty} S_{c,f}(f)\times\cos(\pi f d T_c)df\right)^2}\right)(chip^2) \quad \text{III.14}$$

Where:

- $B_{DLL}\ (Hz)$ is the one sided bandwidth of the equivalent loop filter,
- C/N_0 is the carrier to noise ratio,
- d is the chip spacing.

Theoretically ([Julien, 2005]), the tracking error variance in presence of white noise is:

$$\sigma^2_{PLL} = \frac{B_{PLL}\left(1-0.5B_{PLL}T_P\right)}{\frac{C}{N_0}\int_{-\infty}^{+\infty} S_{c,f}(f)df}\left(1+\frac{1}{2\frac{C}{N_0}T\int_{-\infty}^{+\infty} S_{c,f}(f)df}\right) \quad \left(rd^2\right) \qquad \text{III.15}$$

Figure 59 shows the architecture of the implemented code and carrier phase tracking loops.

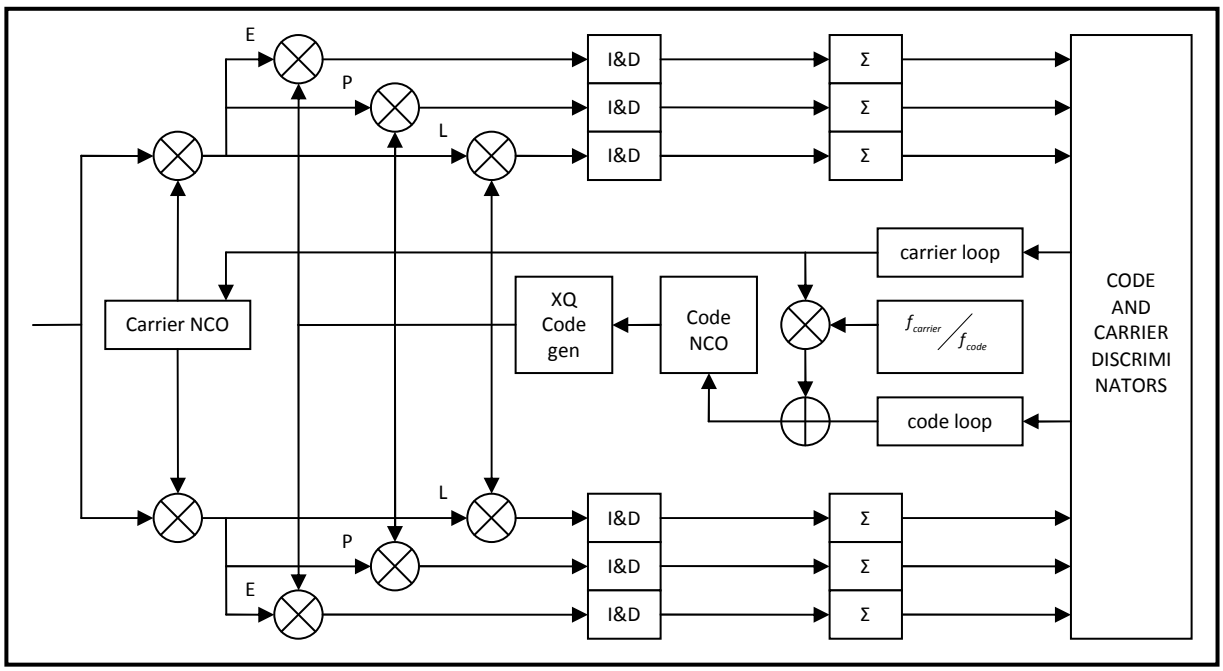

Figure 59 : Proposed L5 receiver architecture.

III.3.1.2.7. Carrier-to-noise ratio estimator

Carrier-to-noise ratio estimation is based on the formula provided in [Betz, 2000], which uses the prompt Inphase correlator output:

$$\frac{C}{N_0} = \frac{E\left[I_p\right]^2}{Var\left[I_p\right]} \times f_P \qquad \text{III.16}$$

The expectation and the variance are calculated using as many prompt inphase correlator output samples as possible, so that the carrier-to-noise ratio estimation will be calculated at the end of the simulation using all the samples.

III.3.2. **Anastasia's Galileo Receiver Mock-up**

III.3.2.1. Signal Generation Devices

III.3.2.1.1. Galileo signals

The ANASTASIA Galileo mock-up receiver was tested using a GNSS signal generator developed by NAVIS for the Girasole project, called CH-3806 (see Figure 60).
Further tests will be performed using a modified Spirent simulator owned by the German national research centre for aeronautics and space (DLR). The simulator, called Multi-output Advanced Signal Test Environment for Receivers (MASTER) can generate both GPS and Galileo constellations through the use of two modified Spirent GSS7790. The main specificity of MASTER is its capability of simulating multi-antenna receivers thanks to its multiple outputs. These tests are not analyzed in this document because of schedule issues.

Figure 60: NAVIS GNSS Signal Generator.

III.3.2.1.2. Thermal noise

The Galileo mock-up receiver is plugged to an LNA, which is linked to the GNSS signal generator. The sky noise and the antenna are simulated by the GNSS signal generator. The preamplifier is at ambient temperature, approximately 20°C (293 K).

III.3.2.1.3. Interferences

Interferences are generated using an Agilent E4438C (see Figure 61). A Matlab file is provided to the signal generator which generates the corresponding interference signals. A description of the scenario generated along with the procedure to follow is given in [THAV, 2007]. The played scenario is the hot spot one: the aircraft is assumed to fly over the

European hot spot (longitude 9° East, Latitude 50° North) at flight level 400 (40.000 feet). The characteristics of the beacons emitting in the radio-electric range of this particular location are provided in Appendix B. The peak powers are given at antenna port, and must be decreased by 2 dB, according to the aircraft antenna gain pattern proposed by EUROCAE (see paragraph I.6.2). The pulse pairs' reception times are randomly generated. The inter-arrival times follow a uniform distribution. This is different from the methodology proposed in [Bastide, 2004], and followed in PULSAR simulations. This highly modifies the interference signal received, mainly because several pulses can not arrive in the same time with this kind of assumption, and the number of pulse pairs collision decreases.

Figure 61 : Agilent E4438C.

III.3.2.2. Mock-up Receiver

The mock-up receiver is composed of four parts: the antenna, the RF unit (RFU), the Digital Processing Unit (DPU), and the Receiver Control Unit (RCU). A full description of the receiver can be found in [WP333, 2007].

III.3.2.2.1. Antenna

The antenna was designed by ERA technologies, a UK-based company notably working on antenna new technologies. The antenna is not used in the simulations, but is assumed to comply with EUROCAE performances requirements.

III.3.2.2.2. RF Unit

The RF unit used in the ANASTASIA mock-up receiver was developed by THAV. It performs the front-end filtering, downconversion and amplification operations. The RF unit can deliver three Galileo signals: L1, E5a, and E5b. Nevertheless, the whole E5 signal cannot be obtained

simultaneously, and the user has to choose between E5a and E5b. The selection is made by a mechanical switch. The unit, contained in a rack, is shown in Figure 62 (front view).

Figure 62: Front view of the RFU rack.

The main RFU characteristics are the following ones:

- For each frequency channel (L1, E5a, E5b), a filter fulfilling the EUROCAE requirements presented in I.6.2 has been implemented,
- Internal PLLs down-convert the incoming signals around 14 MHz,
- A Voltage Gain Amplifier (VGA) independently amplifies the frequency channels and is controlled by a voltage commanded by the Digital Processing Unit (DPU).

III.3.2.2.3. Digital Processing Unit (DPU)

The DPU was designed and developed by Data Respons, Norway. The functionalities of the DPU are the following ones:

- The DPU performs the sampling and the quantization of the signal,
- It uses the quantized signal to estimate the VGA control voltage,
- It performs IMTs algorithms,
- It performs acquisition, tracking, and data demodulation operations.

A picture of the DPU board is shown in Figure 63.

Figure 63 : Front view of the DPU.

The quantization is performed by an ADC DC782A-R. The IMTs along with the AGC loop are implemented in an ALTERA EP2S160F1020C3 Field-Programmable Gate Array (FPGA), while the acquisition and tracking process are performed by a Digital Signal Processor (DSP).

More particularly, the quantization is performed using 8 bits of a 14 bits +/- 0.125 V full scale ADC.

The AGC loop is spread over the RFU and the DPU, as shown in the AGC loop scheme, Figure 64. The signal is amplified by a VGA commanded by a control voltage which results from the low pass filtering of a DAC output which input is issued by the DPU. The estimators presented in the following were implemented according to the results obtained in this PhD thesis.

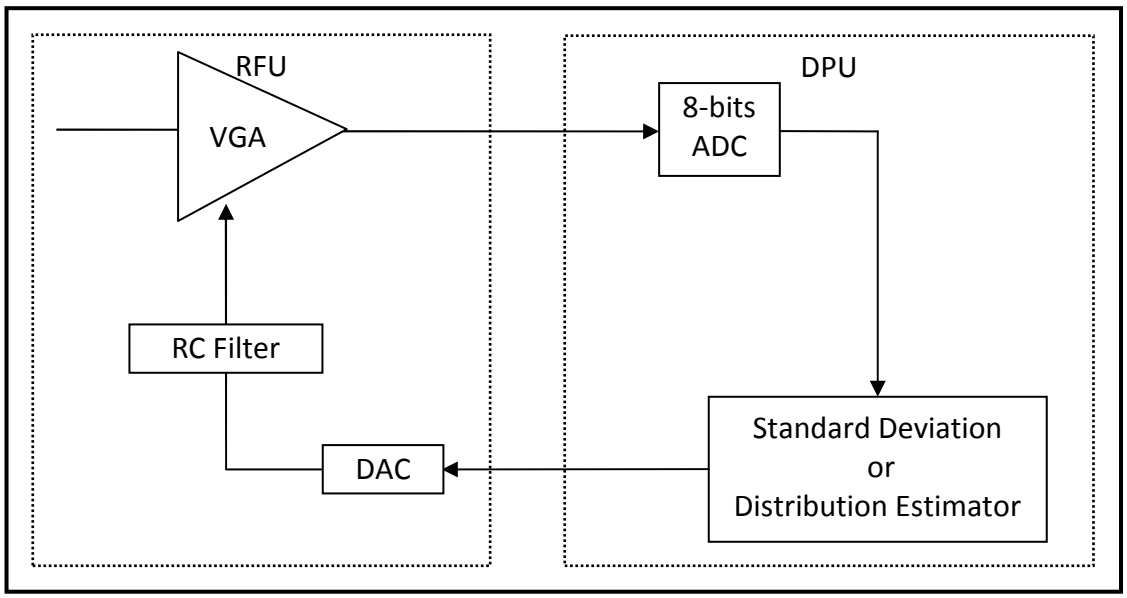

Figure 64 : ANASTASIA mock-up AGC Loop scheme.

The first estimator is based on the input signal standard deviation. This estimator is implemented according to the scheme provided in Figure 65.

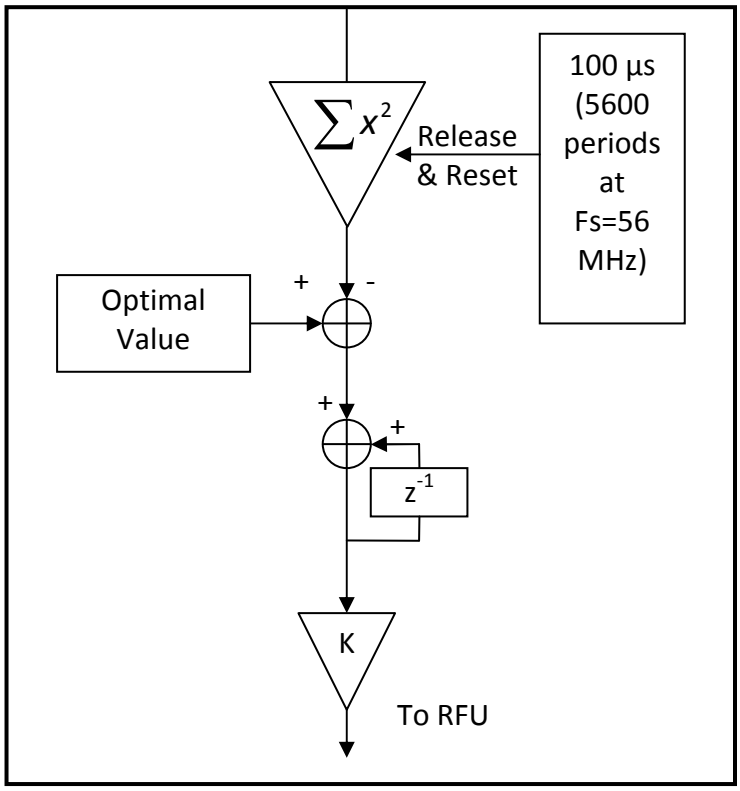

Figure 65 : Standard Deviation Estimator Scheme.

The input signal is squared and then summed, resulting in a value slightly different from the standard deviation:

$$\sum_{k=1}^{5600} x^2 = V\hat{a}r(x) \times 5600 \qquad \text{III.17}$$

This estimator is subtracted to the optimal value, and the result is passed through an integrator. The integrator shown in Figure 65 is different from classical ones (the integrator gain K should be placed before the integration), because an error occurred during the DPU implementation. This error does not prevent the loop from converging towards the correct value and in the correct convergence time. However, the loop will have difficulties to recover from unexpected events such as the reception of very wide band interferences. Indeed, the loop will take a very long time to converge towards the correct value.

The second AGC gain estimator is based on the output signal distribution. This estimator is implemented according to the scheme provided in Figure 66. It corresponds to the distribution estimator proposed in paragraph III.3.1.2.3:

$$dist = 2 \times N_0 - N_1 - N_{-1} \qquad \text{III.18}$$

The estimator is calculated during 100 µs or equivalently 5600 samples, as shown in Figure 66. The estimator is compared to an optimal value, and the difference is sent to an integrator. For the same reasons than for the standard deviation estimator, the integrator gain is misplaced.

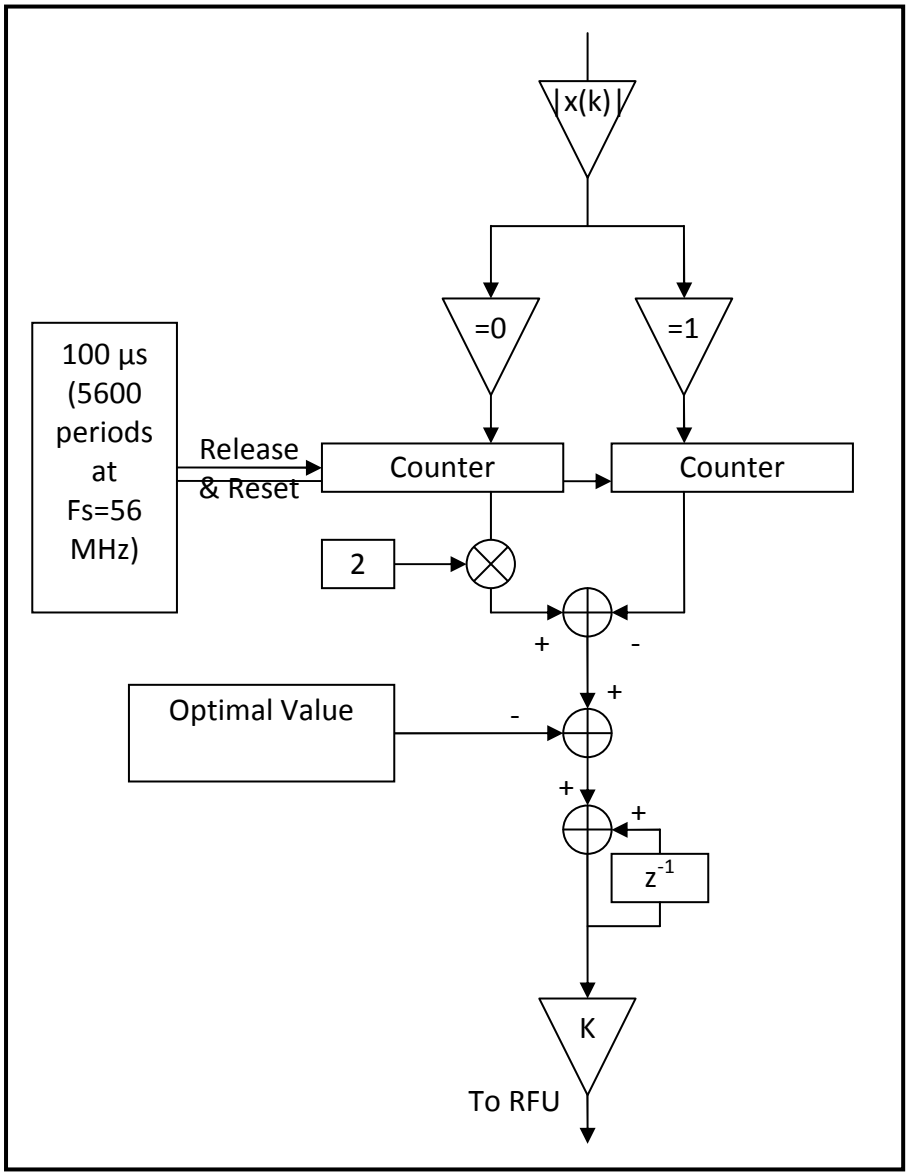

Figure 66 : Distribution Estimator Scheme.

The presented estimators should converge towards the optimal value set in the loop. It has been set so as to regulate the noise power at AGC output (or ADC input) to -37 dBm, which corresponds to a k value of 0.8 ($k = \frac{L}{\sigma}$, see details in paragraph I.4.3). As shown in Figure 67, this clearly does not correspond to the theoretical optimal value, inducing a SNR degradation of 0.5 dB, while it could be easily reduced to 0.1 dB. Indeed, there might be some differences between theoretical expectations and hardware implementation explaining this. In PULSAR, optimal values are set so as to obtain a k value of 1.95 which corresponds to a noise power at AGC output of -45 dBm.

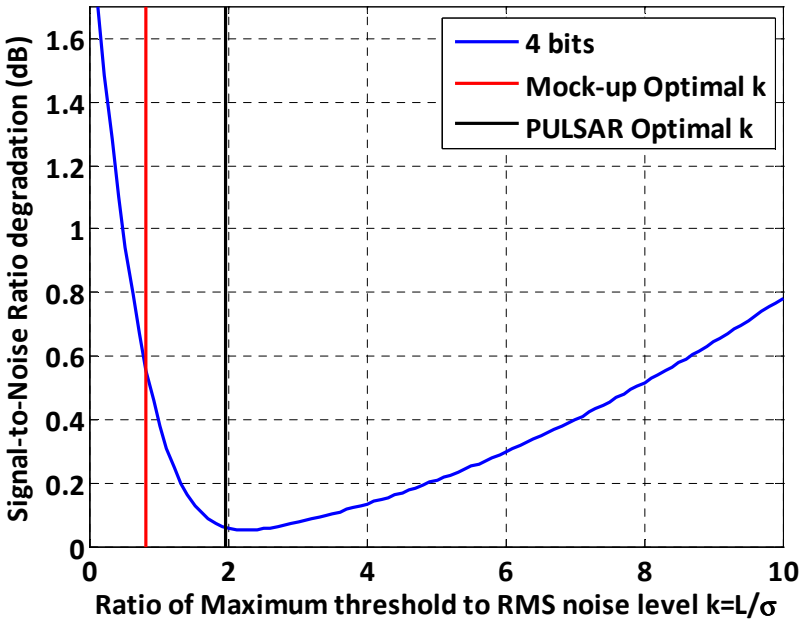

Figure 67 : SNR degradation at correlator output in presence of thermal noise only.

Moreover, the AGC gain regulation is not based on quantization SNR degradation minimization only. Indeed, the objective is to regulate the signal for a 4 bit ADC, taking into account that strong pulses will be received. In order to optimize IMTs processing, interference signals should not be distorted by the receiver (ADC saturation for example). Hence, AGC regulation is a trade-off between quantization losses minimization and adaptation to pulsed interferences. Table 10 sums up the noise power values and the corresponding distribution estimator regulated value. Standard deviation values are not provided as this method has not been tested, as it is not robust enough to pulsed interferences.

Table 10: AGC Loop Settings

	PULSAR	ANASTASIA mock-up receiver
Noise Power at AGC output	-45 dBm	-37 dBm
Distribution estimator regulated value	861	50

Then, the signal enters one of the two proposed IMTs, or any of them. The temporal blanker consists in a simple comparison between the threshold specified by the user and the absolute value of the incoming sample (the sign bit is removed). The sample is replaced by zero if the threshold is exceeded. Otherwise, the output equals the input sample (with the sign bit). The relation between the threshold specified by the user and the analog one is the one given in paragraph III.3.1.2.4.

The FDIS is implemented as follows: N samples are stored in a dedicated register. When the N samples are received, the FFT is calculated using an Altera-specific algorithm. The square module is then calculated:

$$\left|FFT\right|^2 = \mathrm{Re}(FFT)^2 + \mathrm{Im}(FFT)^2 \qquad \text{III.19}$$

This is then compared to the threshold specified by the user in the MMI. If the threshold is exceeded, both real and imaginary parts of the considered FFT value are set to zero. Finally, the inverse FFT is calculated also using an Altera-specific algorithm. The relation between the user specified threshold and the analog one is given in paragraph III.3.1.2.4.

III.3.2.2.4. Receiver Control Unit

The RCU receives measurements and navigation messages from the DPU and calculates Position, Velocity and Time (PVT) solutions. Moreover, the RCU constitutes the DPU MMI, allowing DPU configuration and DPU information display and record. A snapshot of the RCU MMI is provided in Figure 68.

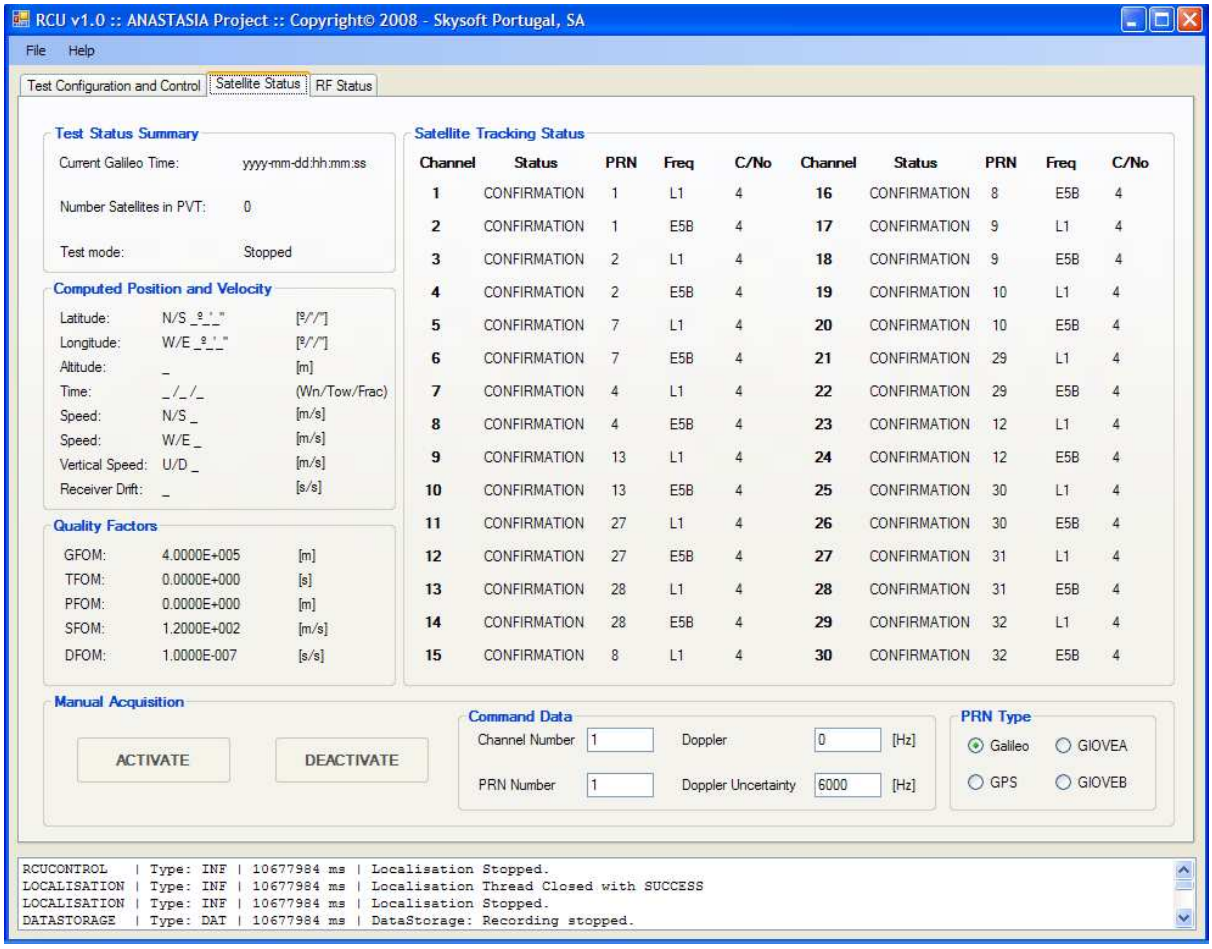

Figure 68: Test Configuration and Control MMI.

III.3.3. **GIRASOLE Mock-up receiver**

One of the objectives of the Galileo Integrated Receivers for Advanced Safety Of Life Equipment (GIRASOLE) project, which is another research project funded by the 6th European Commission Framework Program, was also to realize a Galileo mock-up receiver. The objectives of the project, which started in September 2005 are:

- To develop technologies and basic elements of a SoL Galileo receiver,
- To develop a receiver prototype for railway, avionics, maritime safety-critical applications,
- To support standardization.

One of the major contributors of this project is, as for ANASTASIA, Thales Avionics. Therefore, the results obtained for both projects could be exchanged and compared.

The design of the GIRASOLE receiver is different from the design of the ANASTASIA one. Nevertheless, this receiver uses an AGC which is based on the distribution properties of the input signal, a temporal blanker and an FDIS. However, the implementation of these modules is different from the ANASTASIA one, and no details about it can be provided because of intellectual property rights issues.
The GIRASOLE receiver mock-up is also intended to be an onboard receiver, so that it has to be confronted to the same interferences tests. Therefore, some results obtained with the GIRASOLE mock-up receiver are presented in paragraph IV.4.

III.3.4. **Acquisition Time Simulator Description**

III.3.4.1. Acquisition Time Simulations

The objective of these simulations is to determine the number of correlators required to match the civil aviation requirements presented in paragraph I.6.4. Indeed, the acquisition time is directly proportional to the number of correlators carrying out the acquisition process. The process is therefore:

- Monte-Carlo simulations are run, assuming one correlator and the desired C/N_0.
- For each try, the code/frequency bin is randomly chosen, and the test is performed using the acquisition strategy detailed above,
- If a false alarm occurs, the process starts over and 1 second is added to the acquisition time,
- The acquisition time cumulative density function (cdf) is calculated,
- The cdf is used to determine the time corresponding to the 99th percentile.

99% of the trials found the correct code/frequency bin in less than $T_{99,first}$ seconds for the first satellite acquisition, and $T_{99,subsequent}$ seconds for the subsequent satellites acquisitions. The acquisition of the first and the subsequent satellites are calculated differently, as explained in paragraph I.4.4.2.

99% of the trials being acquired in less than $T_{99,first}$ or $T_{99,subsequent}$ using N_{cor_simu} correlators, the number of correlators required to achieve the same performance in less than 60 seconds N_{cor_req} equals:

$$N_{cor\_req} = \max\left(\frac{T_{99,first}}{60}, \frac{T_{99,subsequent}}{30}\right) \times N_{cor\_simu} \quad \text{III.20}$$

The Monte-Carlo simulations are run using a Matlab routine based on [Bastide, 2004] works.

III.3.4.2. Assumptions

First, the search step has been defined as follows for the first acquired satellite:

- The entire code length is searched (10230 chips). The code search step equals 0.5 chip. 20460 code bins must therefore be explored,
- The Doppler uncertainty is +/- 200 Hz. The Doppler search step equals 500 Hz, thus only one Doppler bin has to be explored,
- Several dwell times are tested: 100, 200, 300, 400 or 500 ms.

Then, the acquisition threshold is defined assuming the following values:

- The desired Pfa equals 10^{-4},
- The worst cross-correlation peak has C/N_0 of 19 dB.Hz, as proposed in [Hegarty, 2003].

Afterwards, the calculation of the non-centrality parameter is performed following a worst-case approach:

- The Doppler misalignment equals half the search step (250 Hz),
- The acquisition time study is restricted to E5a/L5 signals, as justified in paragraph I.6. Therefore, the front-end filter noise power density attenuation factor equals 0.4 dB,
- The code phase offset is time-varying: Indeed, the Doppler misalignment induces the code phase offset changes with time.

Relatively long dwell times being considered (up to 500 ms), the code phase offset can correspond to one bin at the beginning of the integration and to another one at the end of it. Indeed, the code phase offset ε_τ between the received and local codes can be expressed as follows:

$$\varepsilon_\tau(t) = \tau(t) - \tau_{loc}(t) = (\tau_0 - \tau_{0loc}) - \frac{\Delta f \times f_{code}}{f_{carrier}} \times t \quad \text{III.21}$$

In [Bastide, 2004], the worst case has been defined as the case where the initial code phase offset is null ($\tau_0 = \tau_{0loc}$). Then, for a dwell-time of M milliseconds, the offset can be written:

$$\varepsilon_\tau(k) = -\frac{\Delta f \times f_{code}}{f_{carrier}} \times k \times 10^{-3}, k \in [1, M] \quad \text{III.22}$$

The last assumption induces that the non-centrality parameter has to be re-written:

$$\lambda = \frac{2}{f_p} \times \frac{C}{N_0} \times \left(\frac{\sin(\pi \Delta f T_p)}{\pi \Delta f T_p} \right)^2 \times \frac{1}{\beta} \times \sum_{k=1}^{M} R_f^2(\varepsilon_\tau(k)) \qquad \text{III.23}$$

The cross-correlation function R_f^2 has been evaluated and then summed over 100 to 500 ms. The result, provided in Figure 69, is compared to the static case: the code phase offset is constant during the entire dwell time, and equals a quarter of chip, which corresponds to the worst case. It is to be noticed that both curves are obtained assuming the received code is filtered by a 20 MHz double-sided bandwidth filter for E5a/L5 signals, and a 14 MHz double-sided bandwidth (IF-10MHz, IF+4 MHz) for E5b signals. For short dwell time durations, the static case is the worst one as it assumes the worst possible code misalignment. However, the difference between the two cases is not significant. For dwell time longer than 400 ms, the dynamic case is the worst one. Therefore, in the simulations the latter one is considered to determine the non-centrality parameter.

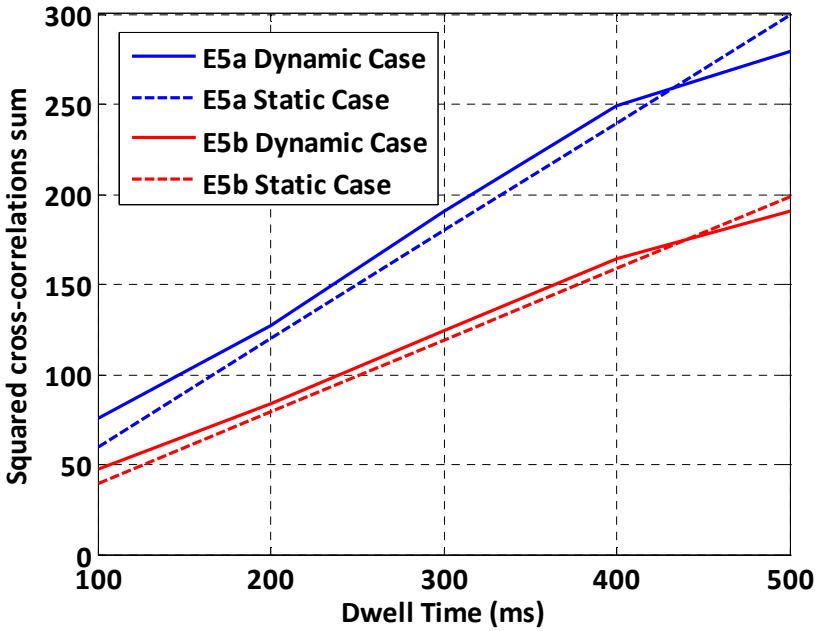

Figure 69: Squared cross-correlations sum assuming time-varying code phase offset.

Moreover, it is important to notice that the C/N_0 used in the non-centrality parameter is not the effective C/N_0 at correlator output, as correlation losses are considered separately ($\frac{1}{\beta}$, $\sum_{k=1}^{M} R_f^2(\varepsilon_\tau(k))$). Indeed, the equivalent C/N_0 expression is:

$$\frac{C}{N_{0\ eff}} = \frac{C}{N_0} \times \frac{1}{\beta} \times R_f^2(0) \qquad \text{III.24}$$

The acquisition time results must be related to the effective C/N_0 value, as it will be compared to the civil aviation effective C/N_0 thresholds proposed in paragraph I.6.3. This

comparison is made in paragraph IV.6. For readability reasons, the non-centrality parameter can be rewritten as follows:

$$\lambda = \frac{2}{f_p} \times \frac{C}{N_{0\ eff}} \times \left(\frac{\sin(\pi \Delta f T_p)}{\pi \Delta f T_p} \right)^2 \times \frac{\sum_{k=1}^{M} R_f^2(\varepsilon_\tau(k))}{R_f^2(0)} \qquad \text{III.25}$$

In addition, the fact that the code phase offset varies with time is taken into account in the simulations. First, the code-phase offset is randomly determined, uniformly over the entire code search space. Then, code bins are tested, 10 by 10, and after each trial, the code phase offset is modified, using the following formula:

$$\varepsilon_\tau(k) = \pm \frac{250 \times f_{code}}{f_{carrier}} \times k \times 10^{-3}, k \in [1, M] \qquad \text{III.26}$$

Where the sign of the Doppler offset is randomly determined, equally distributed between plus and minus. The Doppler offset sign will determine if the code phase offset goes away from the currently searched bins (the process is slowed down), or closer to them (the process is sped up). The reader would notice that the presence of the searched signal carrier frequency induces differences between E5a/L5 and E5b signals.

The last assumption concerns the subsequent acquired satellites. Indeed, the first satellite was acquired under “cold start” conditions (without any information). After that, the user clock uncertainty drops, and the code search space is reduced to 4092 chips [RTCA, 2001].

III.3.4.3. IMTs impact on Cross-correlation peaks

In the simulations, the acquisition threshold is calculated assuming a Pfa of 10^{-4} and a cross-correlation peak of 19 dB.Hz. This value represents the strongest possible correlation peak (worst case approach) between the searched PRN and any other PRN of the constellation. However, in case IMTs are used, cross-correlation functions can be modified, and so it might impact the acquisition performance. In GNSS receivers, acquisition thresholds are calibrated during its conception and not modified during operations. Therefore, the IMTs impact on cross-correlation peaks might have two different effects:

- If the maximum value of the cross-correlation function is decreased (the PRN isolation is improved), the Pfa decreases and the receiver performs better than expected (less false alarms occur),
- In case the maximum value is increased (the PRN isolation is degraded), the Pfa increases and the receiver performs worse than expected.

It is to be noticed that the degradation of the autocorrelation peak is not considered in this approach. Here, the absolute amplitude of the cross-correlation functions is considered, not the isolation between auto and cross correlations.

Hence, simulations are proposed to monitor the impact of IMTs on cross-correlation functions $K_{i,j,IMT}$, for every satellite couple (i, j). First, a GNSS signal is generated, according

to the expressions provided in paragraphs I.1 and I.2, for each PRN code. Then, thermal noise and pulsed interferences are added to the signal. The interference generation process is the same as the one used in PULSAR. The composite signal, generated at IF, is passed through a 20 MHz double-sided bandwidth filter.

The obtained signal is passed through the two presented IMTs. Then, only the GNSS signals, processed by one of the two proposed IMTs, is used to calculate the cross-correlation function, with each PRN code. The maximum value of the cross-correlation peak is then search, and compared to the same value in case no IMT has been applied.

Finally, the process is redone several thousand times, in order to obtain statistically valid results. The maximum value is averaged over all the simulations. The results are provided and commented in section IV.6.

CHAPTER IV: RESULTS ANALYSIS

IV.1. THEORETICAL DERIVATION TOOL

The theoretical derivation tools described in paragraph II.4 are used to estimate the C/N_0 degradations due to the presence of DME/TACAN interferences over Europe and the U.S.A. for two main reasons:

- It allows validating the results obtained with the ANASTASIA and GIRASOLE projects mock-ups,
- It shows the degradations all over Europe, not over the hot spot only, without being time demanding.

All the results presented in this paragraph (IV.1) were obtained during this PhD thesis. Some contributions from [Bastide, 2004] are presented in paragraph IV.2, as a mean of comparison with the results obtained during this PhD.

The tool has first been used without any IMT, in order to assess the degradation caused by pulsed interferences while flying all over Europe, at FL 400. Figure 70 shows a map of Europe, where C/N_0 degradations due to DME signals are represented, considering the E5a/L5 band. The maximum degradation equals 12 dB, which can cause tracking loss in case the received signal strength is low. Moreover, this degradation should severely increase the in-flight acquisition time, meaning that the receiver might not respect the civil aviation requirements. The maximum degradation is suffered while flying over the hot spot, which is consistent with the hot spot definition. It is reminded that the results presented in this paragraph were obtained considering RTCA antenna gain assumptions.

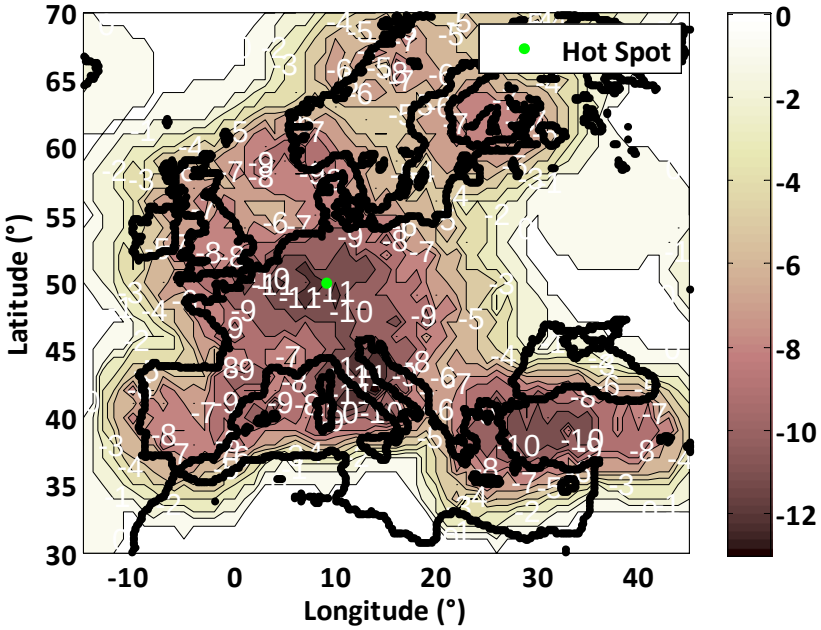

Figure 70 : E5a/L5 C/N_0 degradation due to DME/TACAN beacons over Europe at FL400, considering RTCA antenna gain assumptions.

The same map has been drawn assuming E5b was the tracked signal. The results are shown in Figure 71. The same conclusions as for the E5a/L5 signal can be drawn: the maximum suffered degradation equals 12.5 dBs is observed while flying over the hot spot.

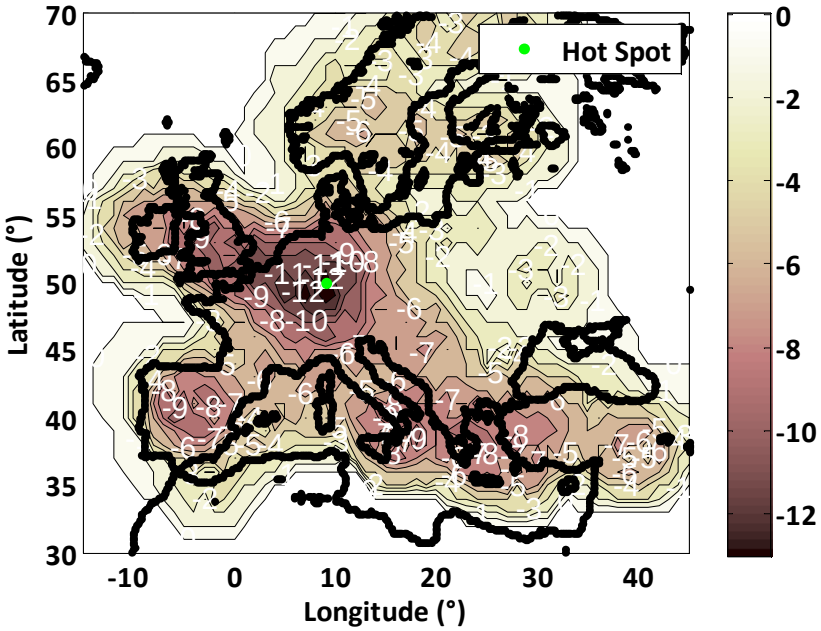

Figure 71: E5b C/N_0 degradation due to DME/TACAN beacons over Europe at FL400, considering RTCA antenna gain assumptions.

According to these two figures, the hot spot corresponds to the maximum C/N_0 degradation in both bands, but some other places are also strongly impacted by DME/TACAN signals: Spain for E5b, Turkey and Italia for E5a/L5.

IV.1.1. **Temporal Blanker**

The performances of the temporal blanker over Europe are assessed at FL400, for the Ea5/L5 signals, using a threshold of -117.1 dBW and the same theoretical derivation tool than in [Bastide, 2004]. Indeed, this threshold has been derived in [Bastide, 2004] as the one showing the best performances for the E5a/L5 signal. The maximum degradation is reached while flying over the hot spot, which is consistent with its definition. This degradation equates 9 dB, which is a few tenths of dBs higher than the values presented in [Bastide, 2004] (8.2 dB). The corresponding map is shown in Figure 72. The discrepancies between the two results are due to differences in the DME/TACAN characteristics. In [Bastide, 2004], the DME/TACAN powers received at aircraft antenna port are slightly less powerful than in this PhD.

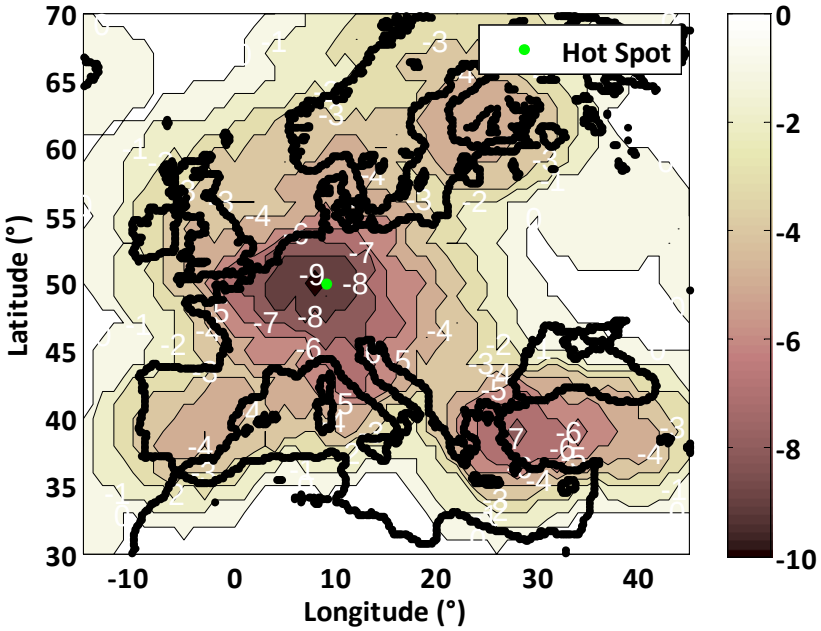

Figure 72: E5a/L5 C/N_0 degradation due to DME/TACAN beacons over Europe at FL400 , considering RTCA antenna gain assumptions and a blanking threshold of -117.1 dBW.

The tool has also been used to assess the temporal blanker performances for the E5b signal, using a threshold of -120.0 dBW and the same theoretical derivation tool than in [Bastide, 2004]. This threshold has also been chosen as it has been derived in [Bastide, 2004] as the one showing the best performances for the E5b signal. It also confirms that the hot spot is the place where the most important degradations are suffered. The degradation, which equals 6 dB, is also a few tenths of dBs higher than the value given in [Bastide, 2004] (5.1 dB), for the same reason as above.

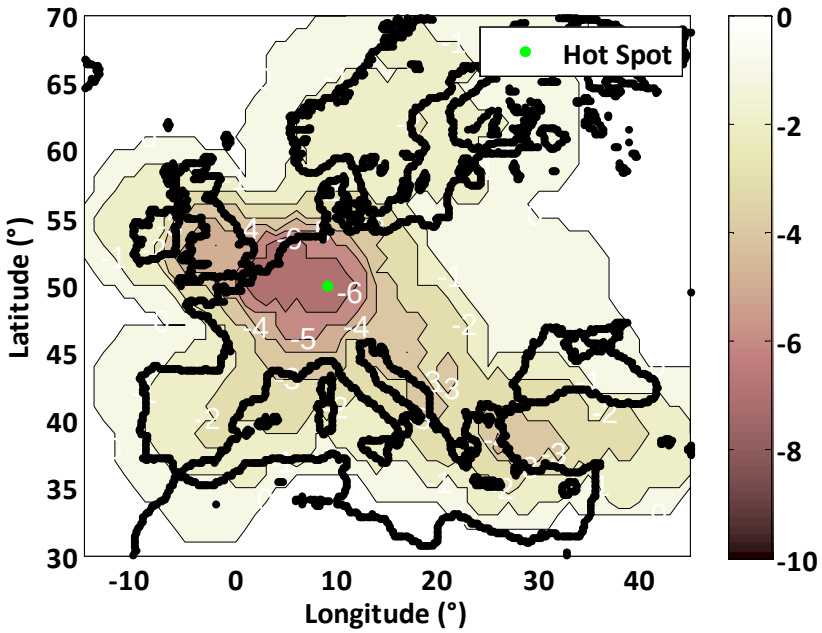

Figure 73 : E5b C/N_0 degradation due to DME/TACAN beacons over Europe at FL400, considering RTCA antenna gain assumptions and a blanking threshold of -120 dBW.

The use of the temporal blanker reduces the C/N_0 degradation by 3 dB for E5a/L5 and 6 dB for E5b. The difference in the improvement is due to the differences in the interference environment. The same interference power is received on both bands. However, few powerful beacons are emitted in the E5b band, while numerous and weaker beacons emit in the E5a/L5 band (see Figure 43 and Figure 44, paragraph II.4.2.5). According to the formula provided in paragraph II.4.1, the algorithm shows better performance if fewer but stronger pulses are received: the interference power after temporal blanker processing is the same for those who exceed the threshold, whatever their initial power. Then, the improvement brought by the algorithm is more important for very strong pulses. On the other side, when two pulses are received, the bdc is increased (not doubled since collisions are considered). The bdc increase results in an increase of the degradation suffered by the GNSS signal (see degradation formula in paragraph II.4.1). To conclude, the temporal blanker is well designed for strong short-duration, and rare interferences.

IV.1.2. **FDIS**

The same tests were run using the FDIS performances derivation tool, first in the E5a/L5 band (Figure 74), and then in the E5b band (Figure 75). The window size has been set to 128 samples and the threshold has been set to the same value in both cases: -195 dBW (see paragraph II.3.4).

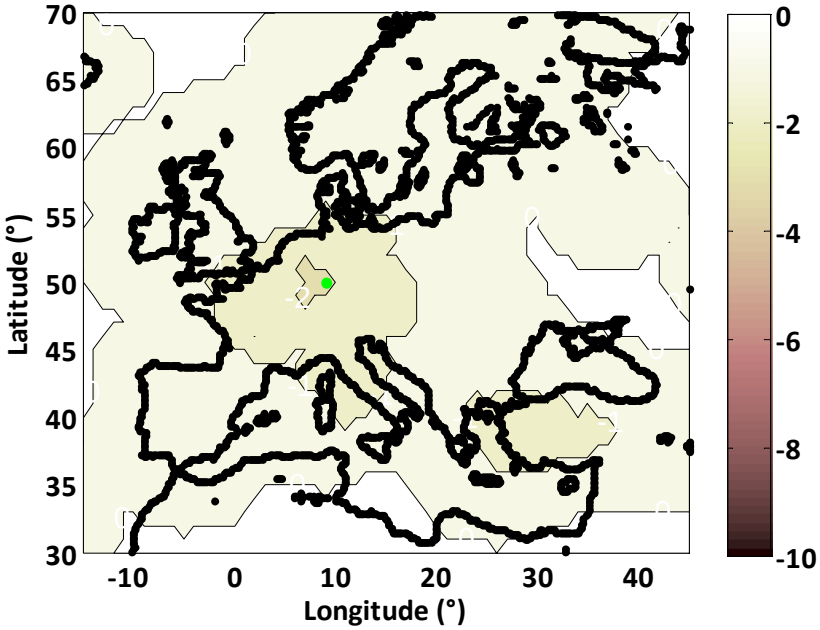

Figure 74: E5a/L5 C/N_0 degradation due to DME/TACAN beacons over Europe at FL400, considering RTCA antenna gain assumptions, using FDIS and a threshold of -195 dBW/Hz.

Here again, the hot spot corresponds to the location where the greatest degradation is suffered, in both E5a and E5b bands. In the E5a band, the degradation equals 2.2 dBs, and 1.9 dBs in the E5b band.

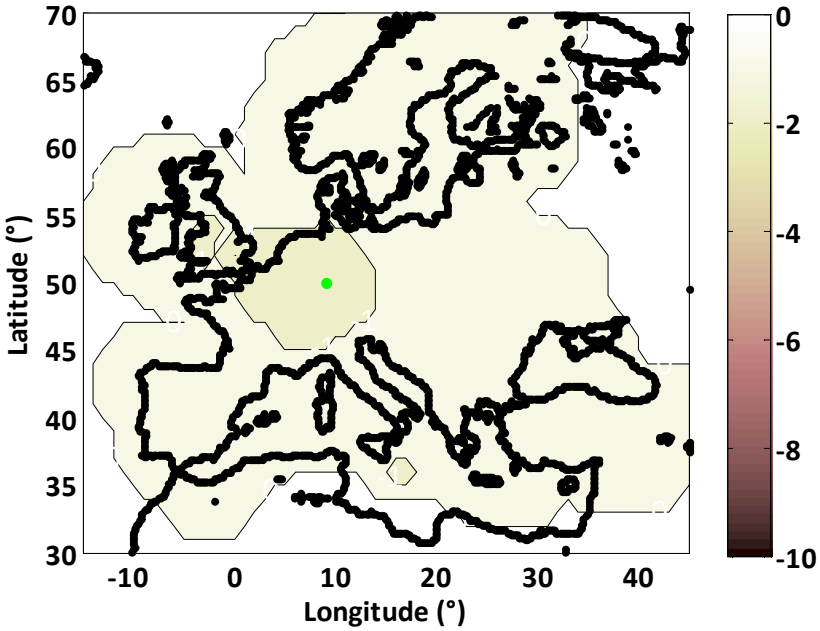

Figure 75: E5b C/N_0 degradation due to DME/TACAN beacons over Europe at FL400, considering RTCA antenna gain assumptions, using FDIS and a threshold of -195 dBW/Hz.

According to the theoretical derivation tools, the FDIS improves the temporal blanker performances by 7 dB in the E5a band, and 5 dB in the E5b band, while flying over the hot spot. Nevertheless, the tool does not take into account AGC imperfections, and the performances of the temporal blanker and FDIS might be degraded in a different way. To conclude, the theoretical derivation tool confirms the performances benefits brought by the FDIS, while flying all over Europe.

IV.2. PULSAR

As explained in paragraph III.1, the simulations are run assuming a GNSS signal power of -155 dBW and a thermal noise density of -200 dBW/Hz. Thus, the simulated C/N_0 equals 45 dB.Hz considering the pilot channel only, so that the total C/N_0 equals 48 dB.Hz. However, the implemented front-end filters induce correlation losses, which are indicated in Table 11. Then, the pilot channel C/N_0 at correlator output should equal 44.6 dB.Hz considering E5a/L5 signals and 44.1 dB.Hz considering the E5b signal.

Table 11: Front-end filter correlation losses for E5a/L5 and E5b signals.

E5a/L5	E5b
0.4 dB	0.9 dB

IV.2.1. C/N_0 degradation simulation results

This paragraph presents the C/N0 degradations measured through PULSAR simulations. The major characteristics of the simulations are reminded herein: each channel (in-phase early, prompt, and late and quadra-phase early, prompt and late) is accumulated during the coherent integration time which has been set to 1 ms. Then, the I&D filter outputs are accumulated 10 times, resulting in an integration time of 10 ms. Code tracking uses an Early Minus Late Power (EMLP) discriminator, 1.5-Hz equivalent loop noise bandwidth and 0.5 chips early/late chip spacing. Moreover, the loop is aided by the carrier tracking loop. Carrier tracking loop uses an extended arctangent discriminator, and the carrier loop filter is a Stephens loop of the third order, which noise bandwidth is set to 10 Hz. Finally, the simulation time is set to 5 seconds.

The simulator is tested in 4 different interference environments:

- Assuming no interference signals are received,
- Assuming the DME/TACAN hot spot scenario,
- Assuming the JTIDS/MIDS IGEB case VIII scenario,
- Assuming the DME/TACAN and JTIDS/MIDS signals hot spot scenario.

In all these simulations, RTCA aircraft antenna gain assumptions are considered. However, the DME/TACAN hot spot scenario has also been tested with EUROCAE aircraft antenna gain assumptions, in order to compare PULSAR results to ANASTASIA and GIRASOLE ones.

In each case, 3 different IMTs configurations were tested:

- using no interference mitigation techniques,
- using temporal blanker,
- using FDIS. If not mentioned, the FDIS window size is set to 128 samples.

In the absence of interference, the objectives are:

- To assess the nominal C/N_0 value when no IMTs are used,
- To assess the degradation brought by the use of the IMTs in absence of interference, and verify that it does not exceed the 0.5 dB limit given in paragraphs II.1 and II.3.

All these tests are run assuming a constant AGC gain. However, the DME/TACAN hot spot scenario and the DME/TACAN + JTIDS scenario were also performed using a regulated AGC, as described in paragraph III.3.1.2.3. These results are required to provide realistic results about pulsed interferences induced C/N_0 degradations, and will be used in the link budgets proposed in paragraph IV.5.

It is to be noticed that, excepted the results provided in Table 12, all the C/N_0 degradations provided in this paragraph do not take into account front-end correlation losses. Only the effect of received interferences and IMTs are considered.

IV.2.1.1. IMTs Performances in absence of interference

Table 12 shows the C/N_0 measurements in absence of interference. It shows that the effective C/N_0, without using IMTs, equals the nominal C/N_0 (45 dB.Hz) minus the front-end filtering induced degradation presented in Table 11. In addition, the 0.5 dB degradation limit defined to fix the IMTs minimum thresholds is not exceeded using both IMTs, on both bands. Note that the temporal blanker threshold is set to -117.3 dBW for E5a and L5 signals, and -119.8 dBW for the E5b signal. These thresholds were chosen to be as close as possible from the optimal thresholds defined in [Bastide, 2004].

Table 12: C/N_0 Measurements in Interference free environment with fixed AGC.

	No IMT	Temporal Blanker	FDIS
L5	44.6 dB.Hz	44.4 dB.Hz	44.3 dB.Hz
E5a	44.3 dB.Hz	44.4 dB.Hz	44.0 dB.Hz
E5b	44.1 dB.Hz	43.5 dB.Hz	43.3 dB.Hz

IV.2.1.2. DME/TACAN Signals Only, RTCA antenna gain assumptions

In this paragraph, the performances of the receiver are tested assuming the interfering signal is composed of DME/TACAN signals only, and that RTCA antenna gain assumptions are considered for negative elevations. The first set of results (Table 13) is obtained considering a fixed AGC, in order to obtain results in the same conditions as in [Bastide, 2004], while the

second set of results (Table 14) is obtained considering a regulated AGC, in order to assess the impact of the AGC regulation on the performances of the tested IMTs.

Table 13 shows the C/N_0 degradations suffered over the European hot spot with RTCA aircraft antenna gain assumptions, for L5, E5a and E5b signals, using different IMTs, with a fixed AGC gain. FDIS outperforms the temporal blanker, increasing the C/N_0 by 5.8 dB on L5, 6.3 dB on E5a, and 3.1 dB on E5b. Moreover, the degradations suffered without IMT do not match the results obtained with the theoretical derivation tools (the corresponding results are provided in Figure 70 and Figure 71). Indeed, in Pulsar the signals are quantized twice: once on 8 bits before IMTs, and once on 4 bits after IMTs. Theoretically, the AGC loop is set in order to avoid saturations during the first quantization step. In case IMTs are turned off, the signal entering the second quantizer can contain strong pulses. Then, the second quantizer is saturated by these signals. This is equivalent to a modified temporal blanker which threshold would equal the maximum quantization level, and which would replace the samples by this maximum level instead of zeros. This feature is not modelled in the theoretical derivation tool.
As a mean of comparison, the results obtained in [Bastide, 2004] for the temporal blanker are also provided in Table 13, in red. The degradations obtained for this PhD thesis are different from the ones proposed by [Bastide, 2004]: + 0.7 dB on L5, + 1.7 dB on E5a and – 0.3 dB on E5b. These discrepancies can be explained by the differences between the two studies: the quantization law used (centred for this PhD, non-centred in [Bastide, 2004]), and the sampling frequency (56 MHz in this PhD, unknown in [Bastide, 2004]). This means that the performances of the temporal blanker technique are very sensitive to implementation details. Moreover, the DME/TACAN ground stations database used in [Bastide, 2004] is slightly different from the one used in this PhD thesis.

Table 13: C/N_0 Degradations in DME/TACAN European hot spot environment with RTCA antenna gain assumptions and optimally fixed AGC.

	No IMT	Temporal Blanker / extract from [Bastide, 2004]	FDIS
L5	8.7 dB	8.8 / 8.1 dB	3.0 dB
E5a	8.6 dB	9.8 / 8.1 dB	3.5 dB
E5b	8.3 dB	6.1 / 6.4 dB	3.0 dB

The same simulations were performed considering a regulated AGC, in order to assess its impact on the performances. The results, provided in Table 14, show that the AGC imperfection has a non-negligible effect on both temporal blanker and FDIS performances. The performances of the FDIS can be degraded up to 1 dB (L5).

Table 14 : C/N_0 Measurements in DME/TACAN European hot spot environment with RTCA antenna gain assumptions and regulated AGC.

	No IMT	Temporal Blanker	FDIS
L5	9.9 dB	9.2 dB	4.0 dB
E5a	10.4 dB	9.2 dB	3.7 dB
E5b	8.4 dB	6.3 dB	3.8 dB

The following conclusions are drawn from these results:

- Compared to the temporal blanker, the FDIS largely decreases the C/N_0 degradation due to the reception of DME/TACAN signals, considering a fixed or a regulated AGC,
- the C/N_0 degradation results obtained with PULSAR match the results obtained with the theoretical derivation tool, using either the temporal blanker or the FDIS as IMT, with an accuracy of 1 dB,
- the C/N_0 degradation results obtained with PULSAR do not match the results obtained with the theoretical derivation tool, if no IMT is applied. This is due to the fact that the second quantization is not taken into account in the theoretical derivation tool,
- The C/N_0 degradations due to the reception of DME/TACAN signals obtained with PULSAR for this PhD thesis are higher than the ones provided in [Bastide, 2004]. This might be explained by the fact that the DME/TACAN beacons characteristics are not generated in the same manner, and that PULSAR was modified between the two studies,
- The additional degradations induced by the regulated AGC cannot be neglected. The performances of FDIS can be degraded by almost 1 dB.

IV.2.1.3. DME/TACAN Signals Only, EUROCAE antenna gain assumptions

The performances of the receiver were also tested considering the current EUROCAE antenna gain assumptions so as to compare PULSAR with the Galileo receiver mock-ups realized for the ANASTASIA and GIRASOLE projects, which were tested under these conditions. Moreover, the obtained results can be compared to the ones obtained in paragraph IV.2.1.2, where the interference scenario is the same but the antenna gain assumptions are different (RTCA instead of EUROCAE, see Table 13).

Table 15 shows the C/N_0 measurements over the European hot spot with EUROCAE aircraft antenna gain assumptions, for E5a and E5b signals. Obviously, the degradation suffered with EUROCAE assumptions is far higher than the one suffered with RTCA ones, see Figure 18. Compared to the temporal blanker, the FDIS is the best solution, and increases the C/N_0 by 6.6 dB on E5a and 3.2 dB on E5b compared to the temporal blanker. These results must be compared to the results obtained with the receiver mock-up, which are presented in paragraph IV.3.

Table 15: C/N_0 Measurements in DME/TACAN European hot spot environment with EUROCAE antenna gain assumptions and optimally fixed AGC.

	No IMT	Temporal Blanker	FDIS
E5a	11.9 dB	11.3 dB	4.7 dB
E5b	11.0 dB	7.5 dB	4.3 dB

The following conclusions are drawn from these results:

- The degradations do not match the results obtained with the ANASTASIA Galileo mock-up receiver presented in paragraph IV.3.2. The reasons of these discrepancies are exposed in the same paragraph,
- The degradations do not match the results obtained with the GIRASOLE Galileo mock-up receiver presented in paragraph IV.4. The reasons of these discrepancies are exposed in the same paragraph,
- The FDIS performances are largely better than the temporal blanker's ones: +6 dB on E5a, + 3 dB on E5b,
- The degradations are increased by 3 to 5 dB considering no IMT is applied, and by 1 to 2 dB considering an IMT is applied, with respect to the values obtained considering RTCA antenna gain assumptions.

IV.2.1.4. Weighting windows

As stated in paragraph II.3.3, the use of weighting windows should improve FDIS performances. Therefore, the following paragraph analyses the performances of the FDIS using weighting windows.

Table 16 compares the performances obtained using the FDIS algorithm and weighting windows of 128 samples with 50% overlap to the ones obtained using the algorithm and rectangular windows of 128 and 256 samples. On one hand, when Blackman instead of rectangular windows are used, the performances are improved by 1 dB on L5, 2 dB on E5a and 2.5 dB on E5b. On the other hand, when the rectangular window size is doubled, the performances are improved by a 0.7 dB on L5, 1 dB on E5a and 1.3 dB on E5b only. Moreover, it has been shown in paragraph II.3.3 that doubling the window size is more complex than using Blackman windows.

Table 16: C/N_0 Measurements in DME/TACAN European hot spot environment with RTCA antenna gain assumptions and optimally fixed AGC using FDIS and weighting windows.

	FDIS 128 Blackman	FDIS 128 Rectangular	FDIS 256 Rectangular
L5	2.1 dB	3.0 dB	2.8 dB
E5a	1.3 dB	3.5 dB	2.3 dB
E5b	1.3 dB	3.8 dB	2.6 dB

The following conclusions are drawn from these results:

- The use of Blackman windows improves the FDIS performances by 1 to 2 dB, depending on the considered signal,
- The increase of the window size to 256 samples improves the FDIS performances by 0.7 to 1.3 dB,
- The use of weighting windows being less expensive than doubling the window size, using Blackman windows is better than doubling the window size.

IV.2.1.5. JTIDS/MIDS Signals Only

The C/N_0 degradation suffered by GNSS receivers if JTIDS/MIDS signals only are received are showed herein so as to compare the results of this PhD thesis to the ones obtained in [Bastide, 2004]. For this reason, the conditions are the same as in [Bastide, 2004]: fixed AGC, RTCA antenna gain assumptions.

Table 17 shows the C/N_0 measurements in case only JTIDS/MIDS signals are received. The impact of JTIDS/MIDS signals on GNSS receivers is far lower than DME/TACAN, because of their low duty cycle. The degradations are compared to the results presented in [Bastide, 2004], which were obtained in the same conditions. The discrepancies between this study and [Bastide, 2004] are quite high, for the three considered signals is lower than 0.2 dB. In case JTIDS/MIDS only are receiver, using either the temporal blanker or the FDIS is not relevant, as the performances are decreased by a few tenth of dB.

Table 17: C/N_0 Measurements in JTIDS/MIDS IGEB case VIII environment with RTCA antenna gain assumptions and optimally fixed AGC.

	No IMT	Temporal Blanker / extract from [Bastide, 2004]	FDIS
L5	2.0 dB	1.1 / 1.9 dB	1.2 dB
E5a	1.9 dB	1.1 / 1.9 dB	0.8 dB
E5b	0.7 dB	0.5 / 1.2 dB	0.4 dB

The following conclusions are drawn from these results:

- JTIDS/MIDS signals are not sufficient to justify the implementation of FDIS,
- The results obtained in this PhD thesis are not consistent with the ones presented in [Bastide, 2004].

IV.2.1.6. DME/TACAN + JTIDS/MIDS Signals

The total impact of pulsed interferences is presented in this paragraph. First, the impact is assessed considering a fixed AGC, in order to compare the results obtained in this PhD thesis to the one provided in [Bastide, 2004], which calculated the degradation considering a fixed

AGC. Then, the results are presented considering a regulated AGC, so as to be used in the link budget, paragraph IV.5.

Table 18 shows the C/N_0 degradations suffered in the worst case interference scenario defined by civil aviation authorities over Europe: DME/TACAN European hot spot environment and JTIDS/MIDS IGEB case VIII scenario. Again, some discrepancies are observed between the results obtained for this PhD and [Bastide, 2004]. However, they do not exceed 1.1 dB, which is acceptable. Finally, the FDIS is the best IMT for all signals, and improve the temporal blanker performances by 6 dB on E5a/L5, and 3.4 dB on E5b.

Table 18: C/N_0 Measurements in DME/TACAN + JTIDS/MIDS environment with RTCA antenna gain assumptions and optimally fixed AGC.

	No IMT	Temporal Blanker / extract from [Bastide, 2004]	FDIS
L5	9.4 dB	10.2 / 8.9 dB	4.0 dB
E5a	9.6 dB	9.9 / 8.9 dB	4.0 dB
E5b	9.1 dB	6.6 / 7.3 dB	3.2 dB

Finally, the test corresponding to Table 18 is also done assuming a regulated AGC. The played scenario corresponds to the worst case, which is the one to be played in MOPS tests. The results, presented in Table 19, show what should be kept as the degradation due to pulsed interferences, and used in link budgets to check if the requirements could be matched or not. These values are to be used in the link budget proposed in paragraph IV.5.

Table 19: C/N_0 Measurements in DME/TACAN + JTIDS/MIDS environment with RTCA antenna gain assumptions and regulated AGC.

	No IMT	Temporal Blanker	FDIS
L5	11 dB	10.8 dB	5.0 dB
E5a	10.8 dB	10.5 dB	4.7 dB
E5b	9.1 dB	6.9 dB	3.9 dB

The following conclusions are drawn from these results:

- The degradations observed in this PhD thesis are higher than the one provided in [Bastide, 2004]. This is due to discrepancies between the two DME/TACAN beacons characteristics generation modules, as explained in paragraph IV.1.1,
- The regulated AGC decreases the performances of the tested IMTs. This phenomenon cannot be neglected,
- The FDIS performs 7 dB on E5a and L5 signals and 3 dB on E5b signal better than the temporal blanker.

IV.2.2. **AGC Gain**

The AGC loop gain values have been recorded in 2 different interference environments: first in an interference-free environment, and then in the European hot spot environment. In absence of interference and considering the E5a/L5 signals, the AGC loop converges towards the value defined as optimal, 10.6 dB, in approximately 10 ms. In the DME/TACAN hot spot environment, the loop converges towards 8.2 dB, which is 2.4 dB lower than the optimal gain.

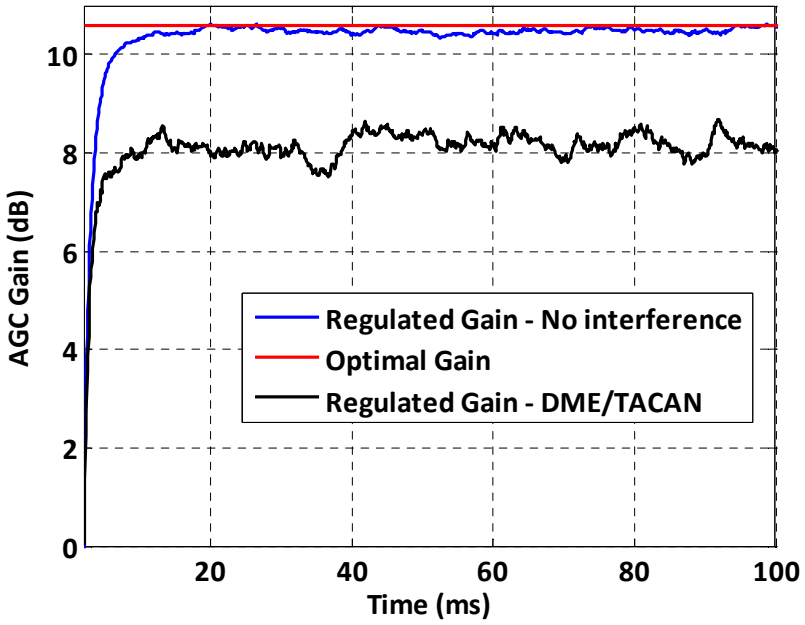

Figure 76: E5a/L5 AGC Loop Gain in various interference conditions.

The same tests were performed for the E5b signal. In this case, the interference environment is more clement, and the bias on the AGC loop convergence value equals 0.5 dB only. In this case, the impact of DME/TACAN signals on the AGC loop is somewhat negligible.

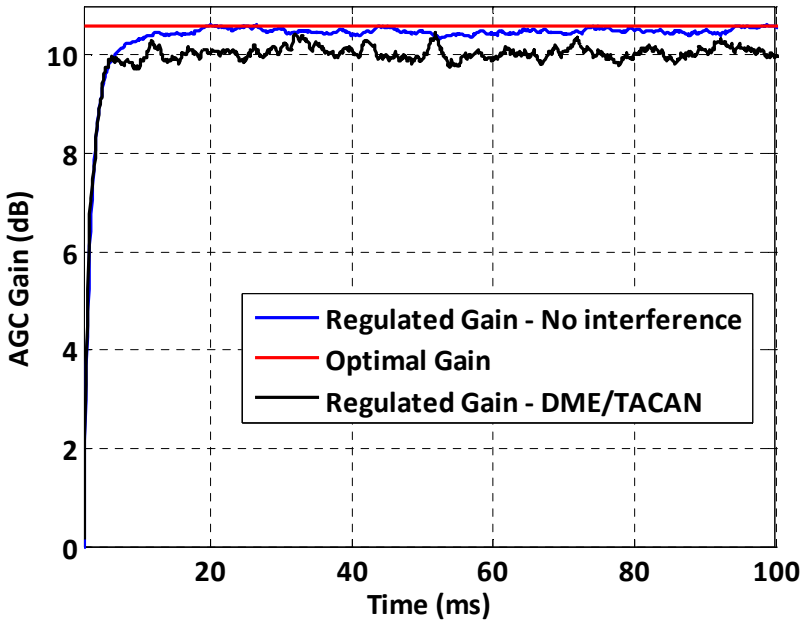

Figure 77: E5b AGC Loop Gain in various interference conditions.

IV.2.3. **Code and Phase tracking accuracy**

The code and carrier phase tracking accuracies are presented in order to check that the used IMTs do not introduce discontinuities in signal's code and carrier phases. Table 20 shows the code phase measurements standard deviation results obtained assuming the same interference scenario than in paragraph IV.2.1.2: the interference signal is composed of DME/TACAN signals only, the RTCA antenna gain assumption is considered, and the AGC is fixed. The measurements are then compared to theoretical results obtained using the formulas given in Chapter III, and the C/N_0 measurements obtained in the same interference conditions. As a matter of fact, these C/N_0 measurements take into account interference and correlation losses.

Table 20: Code phase Standard Deviation (chips)

	No IMT		Temporal Blanker		FDIS	
	Measured	Theory	Measured	Theory	Measured	Theory
L5	0.014	0.013	0.016	0.013	0.008	0.007
E5a	0.013	0.013	0.017	0.015	0.008	0.007
E5b	0.016	0.014	0.015	0.011	0.006	0.005

Carrier phase statistics are shown in Table 21.

Table 21: Carrier phase Standard Deviation (rad)

	No IMT		Temporal Blanker		FDIS	
	Measured	Theory	Measured	Theory	Measured	Theory
L5	0.073	0.073	0.086	0.075	0.039	0.038
E5a	0.084	0.073	0.094	0.084	0.040	0.040
E5b	0.080	0.075	0.059	0.058	0.031	0.030

The following conclusions are drawn from these results:

- The fact that the theoretical and measured code and carrier phase standard deviations match reveals that the temporal blanker does not introduce discontinuities in code and carrier phase measurements,
- The fact that the theoretical and measured code and carrier phase standard deviations match reveals that the FDIS does not introduce any major discontinuities in code and carrier phase measurements,
- As expected, the use of FDIS improves the code and carrier phase accuracies.

IV.3. ANASTASIA GALILEO MOCK-UP RECEIVER

Only AGC command tensions and C/N_0 degradation measurements were collected using the ANASTASIA Galileo mock-up receiver. More complete simulations, gathering code and carrier phase measurements and position solutions analyses are to be performed in a next step of the ANASTASIA project.

IV.3.1. **AGC Performances**

The AGC amplifies the signal with a gain commanded by a command tension. As explained in paragraph III.3.1.2.3, this tension is determined by the AGC loop. The loop has been tested under various interference conditions, in order to assess its robustness to pulsed interference. Indeed, the AGC command tension was measured and the observations were collected in Table 22. It is reminded that the AGC amplifier is linear in dB, which means that the gain (in dB) applied to the signal is proportional to the command tension. During this test, the AGC loop was set to regulate the signal power to -37 dBm.
In the interference test, the played scenario is the E5b DME/TACAN hot spot scenario, assuming an aircraft antenna gain of -2 dBi whatever the angle of arrival of the interference (EUROCAE assumption). In case pulsed interferences are simulated, the gain bias equals -10 dB in the standard deviation estimation mode, and only -1.35 dB in the distribution estimation mode. These results were expected, and show that the best and only acceptable solution is the distribution method.

This is consistent with the implementation choices made in PULSAR and the ANASTASIA Galileo mock-up, where the AGC loops are based on distribution estimators.

Table 22: AGC Sensitivity to Pulsed Interference

	AGC Command Tension		AGC Gain difference
	No Interference	Interference	
Standard Deviation Mode	2.20 V	0 V	-10 dB
Distribution Mode	2.08 V	1.96 V	-1.35 dB

To conclude, the distribution-based estimators are more robust to pulsed interference than standard deviation-based estimators, and must be used in GNSS E5/L5 receivers.

IV.3.2. C/N_0 degradation simulation results

The results presented in Table 23 were obtained using the receiver in various configurations:

- Each IMTs are tested, with different thresholds,
- The AGC gain is either controlled by the loop, or fixed to the value minimizing quantization losses.

The reader would notice that the nominal C/N_0 is 5 dB lower than in the PULSAR tests, and that only E5b signals were tested, because at the time the receiver was tested the RF unit could not process E5a signals. The degradation suffered by the receiver equals the ones provided by PULSAR in the conditions is about 12.5 dB.
The performances of the temporal blanker, considering a fixed AGC, equals approximately 9.7 dB, which is significantly higher (+2.3 dB) than the results obtained with PULSAR (Table 15). As explained in paragraph III.3.2.1.3, the pulsed interference generation process used to test the ANASTASIA prototype is not the same as the one used to test PULSAR. Indeed, in PULSAR, the DME/TACAN signals arrival times follow a Poisson law distribution, while it follows a uniform distribution in the ANASTASIA simulations. The arrival time distribution determines the number of collisions than can occur during the simulation, and so modify the Bdc, as stated in [Bastide, 2004]. Finally, as shown in paragraph II.4.1, the C/N_0 degradation is a function of the Bdc.
Considering a regulated AGC, the performances of the temporal blanker are degraded by almost 2 dB. The AGC robustness to pulsed interference can therefore not be ignored, as the induced degradation can not be neglected.
The FDIS performances are also presented. The main conclusions are the following ones:

- FDIS performs better than the temporal blanker, by almost 6 dB for E5b signals,
- The results are consistent with PULSAR ones,
- The AGC loop sensitivity to pulsed interference degrades the overall performance by 1 dB,
- The increase of the window size does not improve FDIS performances.

This last point was not expected: PULSAR results showed that the increase of the window size improves the performances of the algorithm. This is due to the fact that it is subject to implementation constraints, which were not modelled in PULSAR.
As stated in paragraph III.3.2.2.3, the FDIS algorithm is implemented in an FPGA, and the calculations are performed using quantized signals and coefficients. Due to the finite number of bits allocated to the FFT calculation (each frequency bins is represented with 12 bits), a great calculation noise affects the FFT/IFFT computations. This fact might explain the behaviour of the algorithm when the number of samples is increased, but also suggests that this issue could be solved by increasing the resources allocated to the FFT computation.
Finally, in absence of interference, the degradation caused by the mitigation techniques is negligible (<0.1 dB). The thresholds indicated in Table 23 were derived from the digital threshold set in the receiver and assuming a thermal noise density of -200 dBW/Hz. The FDIS thresholds are much higher than the one used in PULSAR (-195 dBW/Hz). The receiver tests showed that decreasing the threshold did not result in a significant improvement of the performances.

Table 23 : ANASTASIA Galileo Mock-up receiver: E5b simulations under EUROCAE interference conditions.

IMT / Threshold	Nominal C/N_0 (no interference simulated)	C/N_0 degradation (Hot Spot, regulated AGC)	C/N_0 degradation (Hot Spot, fixed AGC)
No IMT	40.0 dB	12.5 dB	N/A
TB /-120 dBW	40.0 dB	11.5 dB	9.7 dB
FDIS 64 /-160 dBW/Hz	40.0 dB	5.5 dB	4.7 dB
FDIS 128 /-160 dBW/Hz	40.0 dB	6.4 dB	N/A
FDIS 256 /-163 dBW/Hz	39.9 dB	5.7 dB	4.7 dB
FDIS 512 /-163 dBW/Hz	39.9 dB	5.7 dB	4.2 dB

IV.4. GIRASOLE MOCK-UP RECEIVER

The Galileo mock-up receiver produced for the GIRASOLE project has been tested in the same conditions (same interference scenario, same antenna gain assumptions) as the ANASTASIA mock-up receiver. However, as explained in paragraph III.3.3, in the GIRASOLE receiver, the temporal blanker, the FDIS, and the AGC loop estimator are implemented differently than in the ANASTASIA receiver. The obtained results are presented in Table 24, for both E5 signals, using a regulated AGC. Here again, the degradation suffered on the E5a band is higher than the one suffered on the E5b band. Moreover, the performances are better than the one obtained in PULSAR or the ANASTASIA mock-up receiver, on both studied bands, which is not surprising given that the GIRASOLE prototype implementation is different from PULSAR and ANASTASIA ones.

Table 24 : GIRASOLE Mock-up receiver Performances over European hot spot, with EUROCAE aircraft antenna gain assumptions.

IMT / Signal	Temporal Blanker	FDIS
E5a	9.3 dB	3.5 dB
E5b	7 dB	3.3 dB

The following conclusions can be drawn from the obtained results:

- The GIRASOLE mock-up receiver performs better than the ANASTASIA mock-up receiver. The IMTs implemented in GIRASOLE are more efficient than the one implemented in ANASTASIA,
- The E5b signal is less impacted by pulsed interference than the E5a signal. This is due to the fact that less DME/TACAN beacons emit in the E5b band than in the E5a band over the European hot spot (see Figure 43 and Figure 44, paragraph II.4.2.5).

IV.5. LINK BUDGET

In this section, the C/N_0 thresholds provided in paragraph I.6.3 are compared to the results obtained in paragraphs IV.1, IV.2, IV.3, and IV.4. According to [Bastide, 2004], the number of hardware correlators that will be available in future GNSS receivers should be about a few thousands, what leads to a minimum C/N_0 of 29 dB.Hz for acquisition. This threshold must be compared to the C/N_0 derived under the following conditions:

- The received signal power equals -155 dBW (at antenna input),
- The GNSS antenna gain equals -4.5 dB, which corresponds to the lowest gain an antenna can present at lowest elevation (0°),
- The thermal noise has a density of -200 dBW/Hz,
- Implementation induced losses equal -2.5 dB. These losses are due to front-end filtering, sampling, quantization or hardware components imperfections. More details on the subject are provided in [Chang, 1982].
- The effective thermal noise density is increased of 0.2 dB for L5 and 0.1 dB for for E5a due to inter-system interferences.
- The effective thermal noise density is increased by the degradations due to Pulsed interferences. The contributions of pulsed interferences are extracted from PULSAR simulation results presented in Table 16, where both DME/TACAN and JTIDS/MIDS signals are considered. The DME/TACAN played scenario is the European hot spot one, while the JTIDS/MIDS played scenario is the IGEB case VIII one. The aircraft antenna gain is assumed to follow RTCA antenna gain assumptions. Finally, the degradation values are obtained taking into account a regulated AGC.

The corresponding margins are provided in Table 25. It shows that an onboard GNSS receiver without IMT implemented would not match the requirements. Moreover, the temporal blanker cannot guarantee the minimum required performances for E5a and L5 signals. On the opposite, in [Bastide, 2004] the C/N_0 thresholds are respected for the three signals, using

the temporal blanker. This difference might be explained by the differences observed in the simulations conducted in [Bastide, 2004] and in this PhD thesis, notably concerning the quantization law and the generation of the DME/TACAN signals. Finally, the margins are positive for the three considered signals using FDIS as IMT. These margins exceed 4 dB, which is quite comfortable.

Table 25: Link Budget for several IMTs.

	No IMT			Temporal Blanker			FDIS		
Signal	L5	E5a	E5b	L5	E5a	E5b	L5	E5a	E5b
Signal Power (dBW)	-155	-155	-155	-155	-155	-155	-155	-155	-155
Implementation loss (dB)	-2.0	-2.0	-2.5	-2.0	-2.0	-2.5	-2.0	-2.0	-2.5
Minimum antenna gain	-4.5	-4.5	-4.5	-4.5	-4.5	-4.5	-4.5	-4.5	-4.5
Effective noise density (dBW/Hz)	-188.8	-189.1	-190.9	-189	-189.4	-193.1	-194.8	-195.2	-196.1
Effective C/N_0 (dB.Hz)	27.3	27.6	28.9	27.5	27.9	31.1	33.3	33.7	34.1
Required C/N_0	29.0	29.0	29.7	29.0	29.0	29.7	29.0	29.0	29.7
Margin	-1.7	-1.4	-0.8	-1.5	-1.1	+1.4	+4.3	+4.7	+4.4

To conclude:

- GNSS receivers cannot cope with civil aviation requirements while flying over the European hot spot, if not IMT is implemented,
- Only the E5b signal copes with civil aviation requirements while flying over the European hot spot, if the temporal blanker is used as IMT,
- GNSS receivers can cope with civil aviation requirements while flying over the European hot spot, if FDIS is implemented as IMT, with comfortable margins, for the three E5/L5 signals.

IV.6. ACQUISITION TIME SIMULATIONS

The acquisition time simulations have been performed following the approach described in paragraph III.3.4, and assuming 160 hardware correlators are available for acquisition. Indeed, the correlators are used as follows:

- 4 correlators are allocated to each code/frequency bin (2 for the pilot channel and 2 for the data channel),
- Only one Doppler frequency is tested,
- Consequently, 40 code bins are searched at once.

Then, the number of correlators required to achieve the minimum operational performances required by EUROCAE described in paragraph I.6.4 is derived using the formula given in paragraph III.3.4:

$$N_{cor\_req} = \max\left(\frac{T_{99,first}}{60}, \frac{T_{99,subsequent}}{30}\right) \times N_{cor\_simu} \qquad \text{IV.1}$$

Simulations were run using C/N_0 equalling values derived from the link budgets given in Table 25, paragraph IV.5. First, a value of 28 dB.Hz was considered. It represents the minimum C/N_0 value that can be achieved when no IMT is implemented in the receiver. Then, the same simulation was performed considering a C/N_0 value of 29 dB.Hz, which corresponds to the minimum C/N_0 value that can be achieved when the temporal blanker is implemented in the receiver, according to [Bastide, 2004]. Finally, a value of 33.5 dB.Hz was tested, as it constitutes the lower C/N_0 value that can be achieved when FDIS is implemented, according to this PhD thesis, and more particularly Table 25.

The number of correlators required to meet civil aviation TTFF requirements is represented in Figure 78, as a function of the dwell time, and the presented C/N_0 values. First, it shows that for high C/N_0 values, the number of required hardware correlators increases with the dwell time. Theoretically, the dwell time increase should improve the acquisition process performance: the probability of detecting the signal when present increases with the dwell time. However, for high C/N_0 values, the detection probability improvement due to the dwell time increase is negligible (Pd ≈ 1 for a dwell time of 100 ms and a C/N_0 of 33.5 dB.Hz). In the meantime, the time required to sweep the entire search span is proportional to the dwell time, so that the overall process is slowed down. Therefore, short dwell times should be used in high C/N_0 environments.

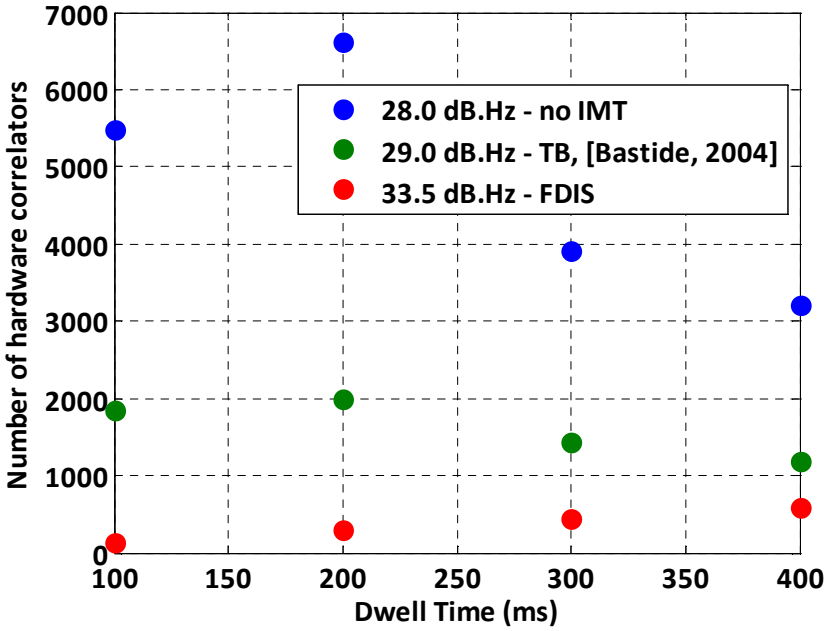

Figure 78: Required Number of Correlators vs. dwell time for the first satellite acquisition.

Figure 79 represents the same information for the acquisition of subsequent satellites. As explained in paragraph III.3.4, subsequent satellites acquisition is facilitated by the acquisition of the first satellite, through the knowledge of the navigation message. Then, even if the acquisition of subsequent satellites must be performed twice faster than the first one (30 seconds instead of 60 according to the approach proposed in paragraph I.6.4), the number of correlators necessary to achieve the required minimum performances for subsequent satellites acquisition is smaller than for the first satellite, whatever the dwell time and the C/N_0. Therefore, the dimensioning parameter is the number of correlators required for the first satellite.

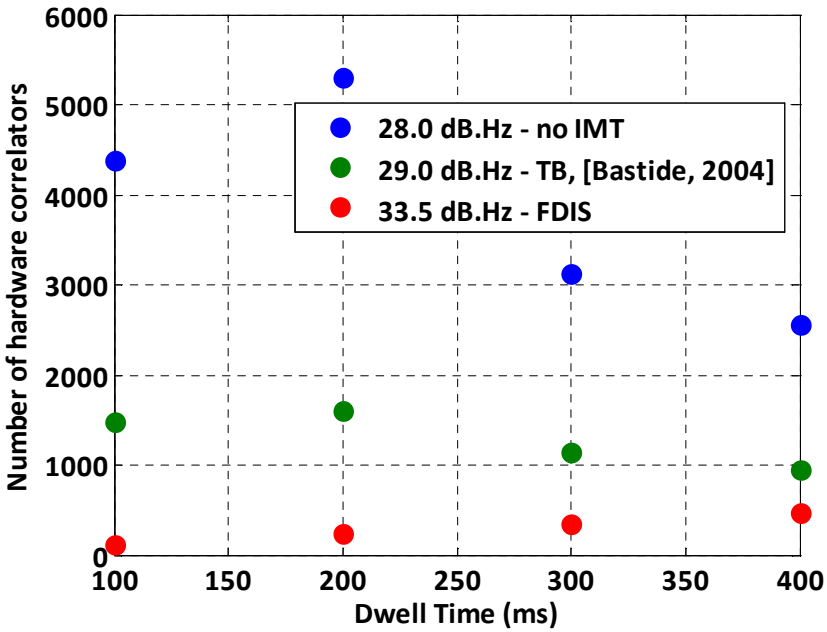

Figure 79: Required Number of Correlators vs. dwell time for subsequent satellite acquisition.

To conclude, the results obtained in paragraph IV.2.1 can be interpreted in two different ways:

- First, the acquisition threshold is reconsidered. FDIS guaranteeing higher C/N_0 values, the thresholds are updated to these latest and GNSS receivers' manufacturers can implement fewer hardware correlators. In this case, C/N_0 margins remain slim. Indeed, if the acquisition threshold is set to 33.5 dB.Hz, the E5a margin will decrease to 0.1 dB (L5 and E5b margins are larger), but the number of correlators required to fulfil civil aviation requirements on acquisition time can be decreased to 500, if short dwell times are used.
- Second, the acquisition thresholds remain the same, and the number of correlators required to perform the minimum acquisition performance also. However, the C/N_0 margins increase, as shown in paragraph IV.5. In this case, the E5a margin equals 4.6 dB (L5 and E5b margins are larger), which is comfortable.

CROSS-CORRELATION RESULTS

The Matlab tool described in paragraph III.3.4.3 has been run in the following conditions:

- The GPS L5 signal is received,
- European hot spot environment (FL 400), with RTCA assumptions about antenna gain,
- Temporal Blanker threshold equals -117.1 dBW,
- FDIS threshold equals -196 dBW/Hz.

Table 26 shows that the maximum values of the cross-correlation functions are lowered by the front end filter, but also the Temporal Blanker and the FDIS. Indeed, the front-end filter induces a decrease of the maximum cross-correlation value of 0.5 dB on both XI and XQ codes. Concerning IMTs, the Temporal Blanker induces an additional decrease of 2.5 dB on both XI and XQ codes, while the FDIS only induces a decrease of 1.3 dB on XI codes, and 1.5 dB on XQ codes. Hence, the threat evoked in paragraph III.3.4.3 does not exist: the maximum possible value of cross-correlations is lower than predicted. In this case, the estimated acquisition time performances are pessimistic, which is not a problem from the civil aviation community point of view.

Table 26: L5 PRN Codes Cross-correlation Susceptibility to IMTs

	XI	XQ
Without Front-end filtering	-26.4 dB	-26.5 dB
Front-end filtering, no IMT	-26.9 dB	-27.0 dB
Front-end filtering, TB Th = -117.1 dBW	-29.9 dB	-30.4 dB
Front-end filtering, FDIS Th = -195 dBW/Hz	-28.5 dB	-28.9 dB

To conclude, the proposed IMT (temporal blanker, FDIS) decrease the level of cross-correlation peaks, resulting in a decrease of the Pfa. As a matter of fact, the effect of IMTs on cross-correlation peaks does not constitute a threat, and the assumptions made in acquisition time simulations are valid.

CONCLUSION

The services provided by the future GPS L5 and the Galileo E5 signals are of great interest for the civil aviation community. More particularly, the interests of these signals lie in the integrity data broadcasted by the E5b signal and the possibility of performing dual-frequency measurements. However, the performances of E5/L5 receivers are degraded by DME/TACAN and JTIDS/MIDS emissions, which constitute interference signals. Investigations conducted to the conclusion that the coexistence of these systems was not possible, especially at high altitude and while flying over so called hot spots, unless GNSS receivers implement an IMT called the temporal blanker. In this case, GNSS receivers fully comply with RTCA and EUROCAE performance requirements for en-route operations, but with slim margins.

The use of more complex IMTs is a good solution to improve these margins, but also induces additional costs. The FDIS is one of these techniques, and the main objective of this PhD thesis was to assess the performances of this technique, and to test it on a prototype receiver.

CONCLUSIONS ON FDIS PERFORMANCES

FDIS has been analyzed as a better pulsed interference mitigation technique than the temporal blanker. From the C/N_0 degradation point of view, GNSS receivers suffer less degradation using FDIS than using the temporal blanker. This improvement has been assessed theoretically, using the Matlab derivation tool, through software simulations, using PULSAR, and through hardware simulations, using the ANASTASIA project Galileo mock-up receiver.

First, the theoretical derivation tool was used to assess the performances of the FDIS. The FDIS and the temporal blanker were tested under the worst case interference scenario defined in [RTCA, 2004]: DME/TACAN hot spot scenario, JTIDS/MIDS IGEB case VIII scenario, and specific antenna gain pattern for negative elevations. The results showed that FDIS performs better than the temporal blanker: the C/N_0 degradations are decreased by 6 dB on E5a/L5, and 3 dB on E5b. However, the tool does not take into account additional losses due to front-end filtering, or AGC imperfections.

The Galileo mock-up receivers developed for the ANASTASIA and the GIRASOLE projects were then used to assess the performances of the studied technique. However, these

receivers were tested under interference conditions different from the ones used in the theoretical derivation tool. Thus, the results obtained with the prototypes can not be compared with the results issued by the theoretical derivation tools. At the time the prototypes were tested, EUROCAE defined new aircraft antenna gain assumptions for negative elevations. Today, this assumption differs from the one considered by RTCA.

The ANASTASIA mock-up receiver could only be tested considering the E5b signal. The tests showed that using the FDIS instead of the temporal blanker brought a decrease of the C/N_0 degradation due to pulsed interferences of 5dB. Moreover, these tests were conducted assuming either a fixed AGC, or a real AGC which regulation is based on an estimation of the signal distribution at ADC output. The tests showed that the performances of both the temporal blanker and the FDIS were improved of 1 dB using a fixed AGC. Considering a fixed AGC is therefore optimistic and not representative of real AGC implementations.

In addition, two different types of AGC were implemented in the ANASTASIA prototype: one based on standard deviation estimations, the other based on distribution estimations. The tests showed that the distribution-based AGC loop was more robust to pulsed interference (the AGC gain bias equals 1.35 dB, considering the EUROCAE interference environment) than standard deviation-based AGC loops (the AGC gain bias equals 10 dB, considering the EUROCAE interference environment). Distribution-based AGC loops are to be implemented in future E5/L5 receivers.

The GIRASOLE prototype was also tested under EUROCAE interference conditions, and considering a real AGC which regulation is based on an estimation of the signal distribution at ADC output. In this prototype, the AGC, the temporal blanker and the FDIS are implemented differently than in the ANASTASIA prototype. The tests showed that the C/N_0 degradations due to pulsed interferences are decreased by 6 dB on E5a and 4 dB on E5b when the FDIS is used instead of the temporal blanker. Moreover, it showed that the E5b signal was less impacted by pulsed interference than the E5a signal, especially when the temporal blanker is considered (a difference of 2 dB is observed).

Finally, PULSAR has been tested under various interference scenarios, in order to validate the results obtained with the theoretical derivation tool and the Galileo prototypes, and so as to be compared to the results proposed in [Bastide, 2004]. In the meantime, the original implementation of PULSAR (that was developed for [Bastide, 2004]) has been modified so as to be as faithful as possible to the ANASTASIA Galileo mock up receiver.

First, PULSAR was tested so as to validate the results obtained with the theoretical derivation tool, in the RTCA interference conditions, using a fixed AGC. All results match, excepted when no IMT is used: the degradations calculated by the theoretical derivation tool are stronger than the degradation obtained through PULSAR simulations. Indeed, this is due to the second quantization in PULSAR, which could not be modelled in the theoretical tool.

Then, PULSAR was tested so as to validate the results presented in [Bastide, 2004]. Thus, the interference scenario is the RTCA one, and the AGC is fixed. The obtained results are

generally speaking not consistent with the ones proposed in [Bastide, 2004]. Indeed, PULSAR implementation changed between the results obtained in [Bastide, 2004] and the results obtained in this PhD thesis. One of the objectives of this PhD being to assess and validate the performances of the ANASTASIA mock-up receiver, PULSAR was tuned and modified so as to be as similar as possible to the quoted receiver. Therefore, the non-centred quantization law has been turned into a centred quantization law, a second quantization has been implemented after IMTs, the AGC loop distribution estimators and filters have been modified, and the sampling frequency has been set to 56 MHz (unknown in [Bastide, 2004]). Moreover, the front-end filters have been modified so as to reduce simulation times. All these modifications might explain the discrepancies observed in the results.

Finally, PULSAR was tested so as to validate the results obtained with the receiver prototypes. AS a matter of fact, the interference scenario defined by EUROCAE was played, and the AGC was regulated. The results were roughly speaking consistent.

Acquisition time simulations were also performed, assuming the worst case interference environment defined by RTCA (DME/TACAN + JTIDS/MIDS, RTCA antenna gain assumptions), and a regulated AGC. In this configuration, the use of FDIS guarantees a minimum C/N_0 of 33.5 dB.Hz for E5a and L5 signals. Then, acquisition time simulations were performed assuming this minimum C/N_0 value. They showed that EUROCAE and RTCA requirements about acquisition time after a power outage during en-route operations could be met using 500 correlators. In [Bastide, 2004], the same simulations were run assuming a C/N_0 of 29 dB.Hz, and show that 1500 to 2500 are required to cope with the requirements. It is to be noticed that the assumed acquisition thresholds are different in these studies: a minimum C/N_0 of 29 dB.Hz is considered in [Bastide, 2004], while this threshold equals 33.5 dB.Hz in this PhD thesis. As a matter of fact, the margins provided in paragraph IV.6 were calculated assuming an acquisition threshold of 29 dB.Hz. Therefore, in case the threshold is set to 33.5 dB.Hz, the provided margins are not valid anymore.

Code and carrier phases tracking performances were assessed. The code and phase tracking accuracies are better using FDIS than the temporal blanker. Moreover, the measured standard deviations match the theoretically derived ones whatever the used IMT, which means that no major distortion is introduced in the tracked signal.

The benefits of implementing weighting windows in the FDIS algorithm have also been shown. Implementing such windows with 50% overlap costs fewer calculations than doubling the window size. Moreover, the C/N_0 is improved by 1 dB when implementing weighting windows instead of doubling the window size.

Finally, link budgets were calculated. The minimum C/N_0 value was derived assuming RTCA interference conditions (DME/TACAN + JTIDS/MIDS and RTCA antenna gain pattern for negative elevations) and a regulated AGC. Thanks to the FDIS, the margin are positive and comfortable (>4 dB) for the three studied signals (L5, E5a, E5b).

RECOMMENDATIONS ON E5/L5 RECEIVERS ARCHITECTURE

The pulsed interference issue raised in this PhD thesis can be solved by implementing an FDIS algorithm using 128 samples in GNSS E5/L5 receivers. In this PhD thesis, the link budgets margins being negative using the temporal blanker, while they are positive using the FDIS. As a matter of fact, the technique can not be used as IMT on GNSS E5/L5 receivers and the FDIS has to be implemented. The FDIS threshold must be set at least 5 dB above the noise floor, or equivalently to -195 dBW/Hz assuming a thermal noise density of -200 dBW/Hz. Moreover, the AGC loop must be robust to pulsed interferences. AGC loops based on distribution estimators, such as the one proposed in paragraph III.3.1.2.3 are a good solution. Finally, the quantization must be designed so as to permit good FDIS operations, in other words offering a sufficient dynamic for pulses processing. The other components of the receiver (antenna, RF front-end, hardware correlators, etc…) must be designed according to the recommendations provided in [EUROCAE, 2007] or [RTCA, 2004], which are supposed to be harmonized (currently, this is not the case for antenna gain patterns assumptions for negative elevations).

OTHER POSSIBLE INTERFERENCE MITIGATION TECHNIQUES

Other signal processing techniques can be adapted to GNSS receivers to mitigate pulsed interferences. Several other mitigation techniques, some operating in the time domain, others in the frequency domain, can be used to solve the E5/L5 pulsed interferences issues.

For example, a modified version of the temporal blanker has been implemented in the GIRASOLE receiver. This mock-up also gathers a frequency-based pulsed interference mitigation technique, which is based on polyphase filters. In [Stitz, 2004], filter-banks are proposed to fight narrowband interferences.

Finally, the FDIS implementation is not the only possible one. In [Young, 1998], several versions of the FDIS algorithm are presented, and should be deeper investigated. For example, the removed frequency bins can be set to the noise floor instead of zero, etc.

ORIGINAL CONTRIBUTIONS REVIEW

The major contributions of the present Ph.D. thesis are the following: the results on pulsed interferences impact on GNSS receivers performances using the Temporal Blanker as IMT or no IMT, proposed in [Bastide, 2004] or [Monnerat, 2000] have been consolidated. A detailed analysis of FDIS algorithm against pulsed interference have been conducted. A theoretical derivation of post-correlation C/N_0 degradation in pulsed interference environment using FDIS as a mitigation technique has been proposed, and the analysis of the

impact of pulsed interference on Automatic Gain Control (AGC) device accuracy is provided. Moreover, the implementation and test of a distribution based AGC showing good pulsed interference robustness on a Galileo mock-up receiver, along with the implementation and test of Temporal Blanker and FDIS algorithms as IMTs on a Galileo mock-up receiver, were performed during the PhD. Then, the analysis of the impact of the FDIS algorithm on PRN codes isolation and tracking loops accuracy was furnished. Finally, the mock-up receiver performance were compared with civil aviation requirements.

FUTURE WORK

In the present PhD thesis, the performances of the FDIS algorithm have been assessed against pulsed interference. In the future, the efficiency of the technique should be tested in case other kind of interferences is received. Narrowband interferences, such as continuous waves (CW) also constitute a threat for GNSS receivers, not only in the E5/L5 band. The performances of the algorithm against such signals could be modelled and assessed through simulations, for example using PULSAR, for all the GNSS signals threatened by CW interference.

The performances of the interference mitigation techniques proposed in the previous paragraph could also be tested and modelled. The performances of these techniques might be better than the FDIS ones, and/or less resource demanding.

The studied IMTs have been tested at FL 400, assuming a flight over the hot spot. The techniques should also be tested during landing operations, when few but very strong pulses are received, and the obtained results compared to civil aviation requirements for landing operations, which are more stringent than en-route ones.

The performances of the temporal blanker have been assessed and as a conclusion, it has been observed that GNSS E5/L5 receivers could not comply with civil aviation requirements, if the pulsed interference are mitigated using the temporal blanker. This is showed by the negative margins presented in the link budget paragraph IV.5. This is a critical conclusion as RTCA SC-159 and EUROCAE WG-62 followed the conclusions of [Bastide, 2004], where E5/L5 GNSS receivers comply with the civil aviation requirements when the temporal blanker is used to mitigate pulsed interference. Thus, these results must be consolidated before concluding that the temporal blanker is not a solution to the E5/L5 pulsed interference issue.

Finally, EUROCAE and RTCA must harmonise their antenna gain assumptions for negative elevations. EUROCAE is currently reconsidering its antenna gain assumptions, and should propose new assumptions soon, following the recommendations of antenna manufacturers.

References

[ANASTASIA] ANASTASIA Consortium, *ANASTASIA SP3 Detailed Project Plan*.

[ANASTASIA, 2008] Anastasia Project Web Site http://www.anastasia-fp6.org.

[Anon, 1997] Anon, *Assessment of Radio Frequency Interference Relevant to the GPS – appendix G*, RTCA, January 1997.

[ARINC, 2005] Anon, Interface Specification – Navstar GPS Space Segment / User Segment L5 Interfaces, ARINC Incorporated, September 2005.

[Bastide, 2002] F. Bastide, O. Julien, C. Macabiau, B. Roturier, *Analysis of E5/L5 acquisition, tracking, and data demodulation thresholds*, Proceedings of the Institute of Navigation GPS, September 2002.

[Bastide, 2003] F. Bastide, D. Akos, C. Macabiau, and B. Roturier, *Automatic Gain Control (AGC) as an Interference Assessment Tool*, ION GPS 2003.

[Bastide, 2003'] F. Bastide, J.Y Tourneret, *DME/TACAN signal autocorrelation computation*, ENAC/STNA/TeSA working note, September 2003.

[Bastide, 2003''] F. Bastide, *Assessment of L5 Receiver Performance in presence of Interference using a Realistic Receiver Simulator*, Proceedings of The Institute of Navigation GPS Meeting, Portland, OR, September 2003.

[Bastide, 2004] F. Bastide, *Analysis of the Feasibility and Interests of Galileo E5a/E5b and GPS L5 Signals for Use with Civil Aviation*, PhD. Thesis.

[Betz, 2000] J.W. Betz, *Effect of narrowband interference on GPS code tracking accuracy*, Proceedings of the Institute of Navigation National Technical Meeting, Anaheim, CA, January 2000.

[Borden, 1951] R.C. Borden, C.C. Trout, E.C. Williams, *Description and evaluation of 100-channel Distance-Measuring Equipment*, Proceedings of the IRE, June 1951.

[Calmettes, 1999] V. Calmettes, *Etude d'adoucissement de spectre pour recepteur GPS*,PhD. Thesis, 1999.

[Capozza, 2000] P. Capozza, B. Holland, *A Single-Chip Narrow-Band Frequency-Domain Excisor for a Global Positioning System (GPS) Receiver*, IEEE journal of solid-state circuits, March 2000.

[Chang, 1982] H. Chang, *Presampling, Filtering, Sampling and Quantization Effects on the Digital Matched Filter Performance*, Proceedings of the International Telemetering Conference, 1982, pp. 889-915.

[Cohen, 1995] L. Cohen, *Time-Frequency Analysis*, 1995.

[DiPietro, 1989] R. DiPietro, *An FFT Based Technique for Suppressing Narrow-Band Interference in PN Spread Spectrum Communications Systems*, ICASSP'89, May 1989

[Ernou, 2003] Y. Ernou, "*E5 band RF Interference Environment and receivers susceptibility*", 6th EUROCAE meeting, working paper 12, Madrid, 8-9 April 2003 .

[ESA, 2008] European Space Agency Web Site, http://www.esa.int

[EUROCAE, 2007] Interim Minimum Operational Performance Specification For Galileo Satellite Positioning Receiver. Eurocae WG-62 works

[European Community, 2003] European Community: *A global strategy for GNSS – the European perspective*, 11th air navigation conference, September 2003.

[Grabowski, 2002] J. Grabowski, C. Hegarty, *Characterization of L5 Receiver Performance Using Digital Pulse blanking*, Proceeding of The Institute of Navigation GPS Meeting, Portland, OR, September 2002

[GSA, 2008] GNSS Supervisory Authority, Galileo Open Service Signal in Space Interferace Control Document, draft 1, 2008.

[Harris, 1978] F. Harris, *On the use of windows for harmonic analysis with the discrete Fourier transform*, Proceedings of the IEEE, January 1978

[Hegarty, 1999] C. Hegarty, C., T. Kim, S. Ericson, P. Reddan, T. Morrissey, and A.J. Van Dierendonck, *"Methodology for Determining Compatibility of GPS L5 with Existing Systems and Preliminary Results"*, Proceeding of the Institute of Navigation Annual Meeting, Cambridge, MA, June 1999

[Hegarty, 2000] C. Hegarty, A.J. Van Dierendonck, D. Bobyn, M. Tran, T. Kim, *Suppression of pulsed interference through blanking*, Proceedings of the Institute of Navigation Annual meeting, June 2000

[Hegarty, 2003] C. Hegarty, M. Tran, A.J. Van Dierendonck, *Acquisition Algorithms for the GPS L5 signal*, Proceedings of the institute of Navigation GNSS Meeting, Portland, OR, September 2003.

[ICAO] ICAO Annex 10, Vol I, Aeronautical telecommunications systems Standards and Recommended Practices.

[IGEB, 2000] IGEB Ad Hoc Working Group 1, Draft report, November 2000.

[Julien, 2005] O. Julien, *Design of Galileo L1F Receiver Tracking Loops*, PhD. Thesis, July 2005.

[Kaplan, 2006] E. Kaplan, Understanding GPS principles and applications, 2006.

[Kinjo, 1997] S. Kinjo, M. Oshiro, H. Ochi, M. Nayeri, *A Robust Frequency-Domain Adaptive Filter with Colored Input Signal*, Conference Record of the Thirty-First Asilomar Conference on Signals, Systems and Computers, November 1997.

[Kolodziejski, 1999] K. R. Kolodziejski and J. W. Betz, *Effect of Non-White Gaussian Interference on GPS Code Tracking Accuracy,* The MITRE corporation technical report MTR99B21R1, June 1999.

[Kunt, 1999] M. Kunt, *Traitement Numérique des signaux*, Traité d'électricité, Volume XX, 1999.

[Landry, 1998] R. J. Landry, V. Calmettes, P. Mouyon, M. Bousquet, A. Renard, A. DePetris, B. Botero, *Theory and performance of the PIRANHA filter*, Statistical Signal and Array Processing, 1998. Proceedings., Ninth IEEE SP Workshop on Volume , Issue , 14-16 Sep 1998.

[Lesthievent, 2000] G. Lesthievent, *Method and Device for Eliminating Spurious Signals in a Direct-Sequence Spread Spectrum Link*, US Patent, March 2000.

[Macabiau, 2002] C. Macabiau, V. Calmettes, W. Vigneau, L. Ries, J-L. Issler, *L5 codes properties*, Proceedings of the ENC GNSS conference, Copenhague, May 2002.

[Macabiau, 2008] C. Macabiau, O. Julien, J.-L. Issler, GNSS Receiver Performance Thresholds for Civil Aviation Users, UE/US RFC meeting, July 2008.

[Monnerat, 2000], Monnerat M., Lobert B., S. Journo, C. Bourga, *Innovative GNSS2 navigation signal*, Proceedings of the Institue of Navigation GPS meeting, Salt Lake City, UT, September 2000.

[Monnerat, 2003] M. Monnerat, P. Erhard, B. Lobert, *Performance Analysis of a GALILEO Receiver Regarding the Signal structure, Multipath, and Interference Conditions*, ION GNSS 2003.

[Nisner, 2003] P. Nisner, *JTIDS Scenarios*, EUROCAE WG 62, Working Paper, April 2003.

[Ouzeau, 2008] C. Ouzeau, C. Macabiau, B. Roturier, M. Mabilleau, *Performance of Multicorrelators GNSS Interference Detection Algorithms for Civil Aviation*, Proceedings of the 2008 National Technical Meeting of the Institute of Navigation, January 2008.

[Perre, 2008] Personal conversation with Jean-Michel Perre, 2008.

[Rebeyrol, 2005] E. Rebeyrol, L. Lestarquit, L. Ries: *BOC Power Spectrum Densities*, Proceeding of the Institue of Navigation NTM meeting, 2005.

[Rebeyrol, 2007] E. Rebeyrol, *Galileo Payload and Signal Optimization*, PhD Thesis, October 2007.

[RTCA, 2001] RTCA SC-159, *Minimum Operational Performance Standards for Airborne Supplemental Navigation Equipment*, 2001.

[RTCA, 2001] RTCA SC-159, *Minimum Operational Performance Standards for Global Positioning System/Wide Area Augmentation System Airborne Equipment*, RTCA DO 229C.

[RTCA, 2004] RTCA SC-159, *Assessment of Radio Frequency Interference Relevant to the GNSS L5/E5a*, RTCA DO 292, July 2004.

[Stephens, 1995] S.A. Stephens*, Controlled-Root formulation for digital phase-locked loops*, IEEE transactions on aerospace and electronic systems, January 1995.

[Stitz, 2004] T. Stitz, M. Renfors, *Filter-Bank-Based Narrowband Interference Detection and Suppression in Spread Spectrum Systems*, EURASIP Journal on Applied Signal Processing, August 2004.

[THAV, 2007] Thales Avionics, *DME tests implementation*, EUROCAE document, 2007.

[Tran, 2001] M. Tran, *Validation of the feasibility of coexistence of the new civil GPS signal (L5) with existing systems*, MITRE paper, February 2001.

[Tran, 2003] M. Tran, C. Hegarty, *Performance Evaluations of the New GPS L5 and L2 Civil (L2C) Signals*, Proceedings of the Institute of Navigation National Technical Meeting, Anaheim, CA, January 2003.

[Vaidyanathan, 1993] P. Vaidyanathan, *Multirate Systems and Filter Banks*, Ed. Prentice Hall P.T.R., 1993.

[Van Dierendonck, 1996] A.J. Van Dierendonck, *GPS receivers*, Global Positioning System: Theory and Application, B.Parkinson and J.J Spilker, JR., Ed ., Washington, D.C.: AIAA, Inc., 1996.

[Van Dierendonck, 1999] A.J Van Dierendonck, J.J Silker Jr, *Proposed New Civil GPS signal at 1176.45 MHz*, Proceedings of the Institute of Navigation GPS meeting, Salt Lake City, Utah, September 1999.

[WP333, 2007] ANASTASIA WP333, *D3333: Receiver Mock-Up Definition file*, ANASTASIA Project public document, 2007.

[Young, 1998] J. Young, *Analysis of DFT-Based Frequency Excision Algorithms for Direct-Sequence Spread-Spectrum Communications*, IEEE Transactions on communications, August 1998.

Appendix A : **AGC Loop Study**

The present appendix presents the AGC loop analyses performed during this PhD thesis. The AGC loop implemented in the ANASTASIA receiver mock-up, which description can be found in paragraph III.3.1.2.3, was designed according to this analysis. The following parameters are studied:

- The loop convergence time,
- Its robustness to pulsed interference,
- Its stability.

These parameters are studied as a function of the loop configuration. Indeed, as already discussed in paragraph III.3.1.2.3, the user can choose:

- The loop mode: distribution or variance,
- The loop gain K,
- The optimal consign value,
- The possibility of using IMTs processed signals.

A.1. Loop Behaviour in Standard Deviation Mode

The state-of-the-art solution for AGC loops is to use a variance estimator. The output of the implemented standard deviation estimator is the following:

$$Estimator = \sum_{k=1}^{N} x^2(k) = N \times \sigma^2 + n(t) \qquad \text{A.1}$$

The estimator output is then processed as set out in paragraph III.3.1.2.3.

A.1.1. Closed Loop Transfer Function

The implemented AGC loop can be modelled as described in Figure 80: the loop input is the optimal gain value in dB, while the output value is G , the gain determined by the loop in dB.

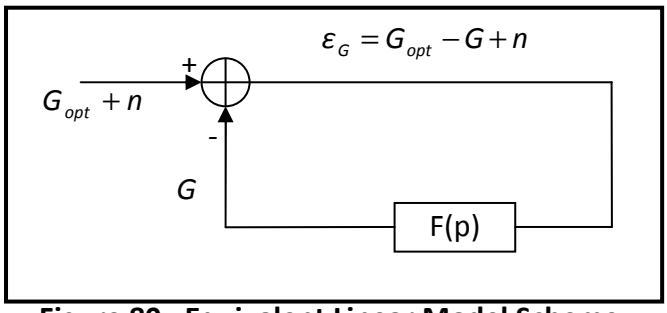

Figure 80 : Equivalent Linear Model Scheme.

The closed loop equation associated to the equivalent loop model would be:

$$G_{dB} = \frac{F(p)}{1+F(p)} G_{opt\,dB}(p) + \frac{F(p)}{1+F(p)} n(p) \qquad \text{A.2}$$

And so the equivalent closed loop transfer function is:

$$\frac{F(p)}{1+F(p)} \qquad \text{A.3}$$

On the other hand, having in mind the implemented AGC loop structure shown in Figure 64. The amplifier is a VGA controlled by the tension v_f. The component implemented in the ANASTASIA receiver can be modelled as follows:

$$G_{dB}(p) = 45 \times v_f(p) - 2{,}5 \qquad \text{A.4}$$

This tension is the output of the RC filter proposed in Figure 81. The filter design was driven by the following specified performances:

- The filter shall have a time constant of 1 ms,
- The loop gain shall equal 0.5,
- The filter shall be a low-pass filter.

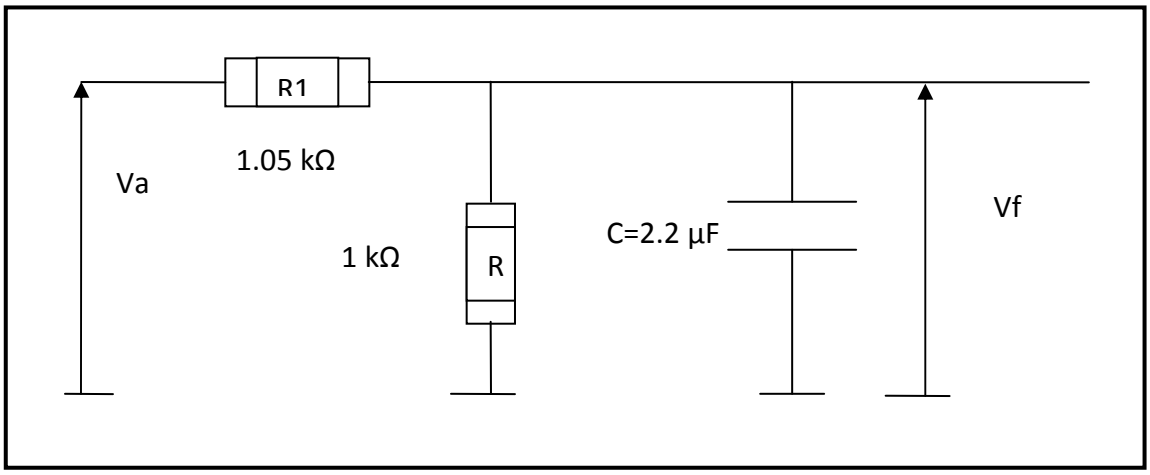

Figure 81: Galileo mock-up receiver implemented RC Filter.

The transfer function of the filter is:

$$\frac{V_f}{V_a} = \frac{\dfrac{1}{\dfrac{1}{R_2} + jCw}}{\dfrac{1}{\dfrac{1}{R_2} + jCw} + R_1} = \frac{1}{(1 + \dfrac{R_1}{R_2}) + jR_1Cw} \qquad \text{A.5}$$

Where V_a is the DAC output tension. In Laplace space, we get:

$$\begin{aligned} H(p) &= \frac{V_f(p)}{V_a(p)} \\ &= \frac{1}{\left(1 + \dfrac{R_1}{R_2}\right) + R_1Cp} \\ &= \frac{1}{\left(1 + \dfrac{R_1}{R_2}\right)} \times \frac{1}{1 + \tau p} \end{aligned} \qquad \text{A.6}$$

Where $\tau = \dfrac{R_1R_2C}{R_1 + R_2}$. Then, the gain can be written

$$G_{dB}(p) = 45 \times H(p) \times v_a(p) - 2{,}5 \qquad \text{A.7}$$

The tension v_d entering the DAC lies in the range [0 2^{16}]. The DAC output, v_a, lies in the range [0 2] V. In our model, we associate this conversion to an amplification which gain equals 1/2^{15}, so that $G_{dB}(p) = \dfrac{45 \times H(p)}{2^{15}} \times v_d(p) - 2{,}5$. The DAC input tension is the output of the standard deviation estimator module, which corresponds to the integrated difference between the calculated standard deviation and the reference value:

$$v_d(p) = \frac{K}{10^{-4} \times p} \times N \times \left(\sigma_{opt}^2 - \sigma^2(p) + n(p)\right) \qquad \text{A.8}$$

Replacing this tension in the AGC gain expression:

$$\begin{aligned} G_{dB}(p) &= 45 \times \frac{K}{10^{-4} \times p} \times H(p) \times N \times \frac{1}{2^{15}} \times \left(\sigma_{opt}^2 - \sigma^2(p) + n(p)\right) - 2{,}5 \\ &= \frac{K \times 45 \times H(p) \times N \times \sigma_{opt}^2}{10^{-4} \times p \times 2^{15}} \times \left(1 - \frac{\sigma^2(p)}{\sigma_{opt}^2} + \frac{n(p)}{\sigma_{opt}^2}\right) - 2{,}5 \end{aligned} \qquad \text{A.9}$$

Assuming that the loop tracking error is small, the function $1 - \dfrac{\sigma^2(p)}{\sigma_{opt}^2}$ is well approximated by $-\log\left(\dfrac{\sigma^2(p)}{\sigma_{opt}^2}\right)$ using a first order Taylor expansion.

$$G_{dB}(p)=\frac{K\times 45\times H(p)\times N\times\log(10)\times\sigma_{opt}^2}{10^{-4}\times 10\times p\times 2^{15}}\times\left(\sigma_{optdB}^2-\sigma_{dB}^2(p)+n'(p)\right)-2{,}5$$
$$=\frac{K\times 45\times H(p)\times N\times\log(10)\times\sigma_{opt}^2}{10^{-4}\times 10\times p\times 2^{15}}\times\left(\sigma_{optdB}^2-\sigma_{indB}^2(p)-G_{dB}^2(p)+n'(p)\right)-2{,}5 \quad \text{A.10}$$

Replacing $\sigma_{optdB}^2-\sigma_{indB}^2(p)$ by $G_{optdB}^2(p)$ and G_{dB}^2 by $2\times G_{dB}$:

$$G_{dB}(p)\left(1+\frac{2\times K\times 45\times H(p)\times N\times\log(10)\times\sigma_{opt}^2}{10^{-4}\times 10\times p\times 2^{15}}\right)$$
$$=\frac{2\times K\times 45\times H(p)\times N\times\log(10)\times\sigma_{opt}^2}{10^{-4}\times 10\times p\times 2^{15}}\times\left(G_{optdB}(p)+n'(p)\right)-2{,}5$$
$$\Rightarrow G_{dB}(p)=\frac{\frac{2\times K\times 45\times H(p)\times N\times\log(10)\times\sigma_{opt}^2}{10^{-4}\times 10\times p\times 2^{15}}}{\left(1+\frac{2\times K\times 45\times H(p)\times N\times\log(10)\times\sigma_{opt}^2}{10^{-4}\times 10\times p\times 2^{15}}\right)}\times\left(G_{optdB}(p)+n'(p)\right) \quad \text{A.11}$$
$$-\frac{2{,}5}{\left(1+\frac{2\times K\times 45\times H(p)\times N\times\log(10)\times\sigma_{opt}^2}{10^{-4}\times 10\times p\times 2^{15}}\right)}$$

So the closed loop transfer function relating the gain in dB to the optimal gain in dB is

$$F(p)=\frac{\frac{2\times K\times 45\times H(p)\times N\times\log(10)\times\sigma_{opt}^2}{10^{-4}\times 10\times p\times 2^{15}}}{\left(1+\frac{2\times K\times 45\times H(p)\times N\times\log(10)\times\sigma_{opt}^2}{10^{-4}\times 10\times p\times 2^{15}}\right)} \quad \text{A.12}$$
$$=\frac{1}{1+\frac{10^{-4}\times 10\times p\times 2^{15}}{2\times K\times 45\times H(p)\times N\times\log(10)\times\sigma_{opt}^2}}$$

Placing this expression in $H(p)$, one obtains:

$$F(p)=\frac{1}{1+\frac{3{,}85\times 10^{-4}}{K}p+\frac{4{,}3\times 10^{-7}}{K}p^2} \quad \text{A.13}$$

This is equivalent to a second order filter.

A.1.2. Time Constant Determination

The theoretical transfer function of a second order filter is:

$$F(p)=\frac{1}{1+\frac{2\xi}{\omega_n}p+\frac{1}{\omega_n^2}p^2} \qquad \text{A.14}$$

Identifying the theoretical transfer function coefficients to the ones calculated in paragraph A.1.1:

$$\begin{cases} \frac{2\xi}{\omega_n}=\frac{3{,}85\times10^{-4}}{K} \\ \frac{1}{\omega_n^2}=\frac{4{,}3\times10^{-7}}{K} \end{cases} \Rightarrow \begin{cases} \xi=\frac{3{,}85\times10^{-4}}{2\times K}\sqrt{\frac{K}{4{,}3\times10^{-7}}}=\frac{0{,}29}{\sqrt{K}} \\ \omega_n=\sqrt{\frac{K}{4{,}3\times10^{-7}}} \end{cases} \qquad \text{A.15}$$

According to theory, when $\xi<1$, the time constant of the corresponding second order filter is given by:

$$\tau_{AGC}=\frac{1}{\xi\omega_n}\approx 2ms, \sqrt{K}>0{,}29 \qquad \text{A.16}$$

It appears that as long as K is greater than 0.53, the loop convergence time equal 2 ms.

A.1.3. Stability

A loop is unstable if the open-loop transfer function equals -1 (its module is 1 and phase is -180°). Figure 82 shows that the implemented loop is stable if K<0.5. Usually, closed loops are regulated so as to preserve a phase margins of 45 degrees. This means that when the open-loop transfer function has a module of one, its phase should not be lower than -135 degrees. K=0.5 is the higher value guaranteeing this condition.

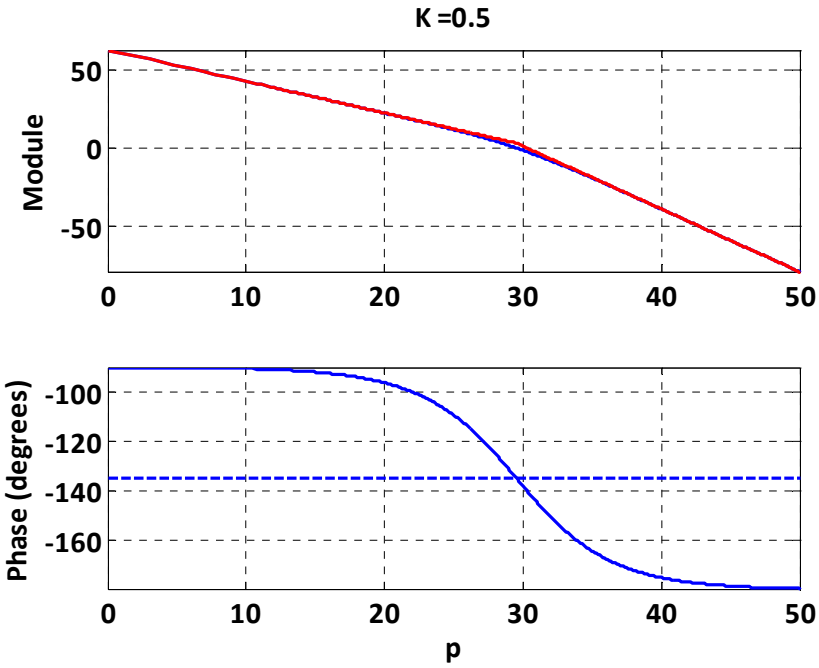

Figure 82 : AGC Open Loop Transfer Function Bode Diagram using variance.

A.1.4. MATLAB Simulation

The described AGC loop has been implemented and tested using MATLAB, so as to test its stability, its robustness to interference and its convergence time.

A.1.1.1.Signal Generation

The loop is tested with a signal composed of thermal noise and interference if desired, considering the E5a/L5 band environment. The thermal noise is white and its density equals -200 dBW/Hz. The sampling frequency being 56 MHz, the power of the generated noise is -142 dBW (-112 dBm).

$$P = \frac{\sigma^2}{50} = \frac{\frac{N_0}{2} \times f_s}{50} \qquad \text{A.17}$$

Then, the signal is filtered using the filter described in paragraph III.3.1.2.1 (the thermal noise power is then approximately -117 dBm), amplified by the preamplifier (29 dB), while cable losses are also applied (5 dB). At this stage, the thermal noise power equals -66 dBm. The objective of the AGC loop is to amplify the noise in such a way that its power goes from -66 dBm to -45 dBm. In this case, the loop converges towards a gain of 10.6 dB.

A.1.1.2.Expected Simulation Results

Before running simulations, one can determine the expected loop convergence value, by computing the signal power as a function of the gain. Figure 83 shows the convergence values in different cases:

- Noise only is present, which represents the nominal case (blue curve),
- Noise and interference are present, and no interference mitigation technique is used (red curve),
- Noise and interference are present, and the temporal blanker is used, setting the threshold to -117.3 dBW (green curve),
- Noise and interference are present, and the temporal blanker is used, setting the threshold to -117.3 dBW, and the blanked samples are not taken into account in the power calculation (black curve).

The loop operates as follows: if the power is lower than the one corresponding to the consign value (-45 dBm), the gain increases. If the power is larger, the gain decreases. Figure 83 shows that:

- Pulsed interferences induce a bias of 6 dB in the gain,
- The use of the temporal blanker decreases the bias by a few dB, but also that if the gain exceeds 15 dB (“divergence zone”), the loop diverges. This solution cannot be implemented in an onboard receiver,
- The solution of neglecting the samples zeroed by the temporal blanker does not have a “divergence zone”. Nevertheless, the gain bias decrease is not significant.

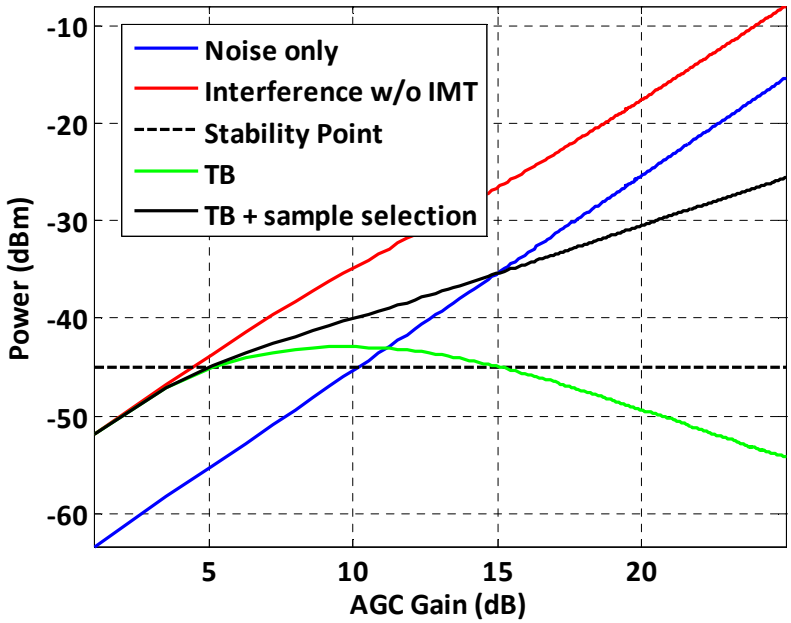

Figure 83: AGC Gain expected behaviour using Temporal Blanker.

Figure 84 is obtained in the same conditions, replacing the temporal blanker by the FDIS (128 samples, threshold set to -195 dBW). It shows that the gain bias using the signal processed by FDIS is lower than 1 dB. However, the presence of a divergence zone prevents us from using such a method.

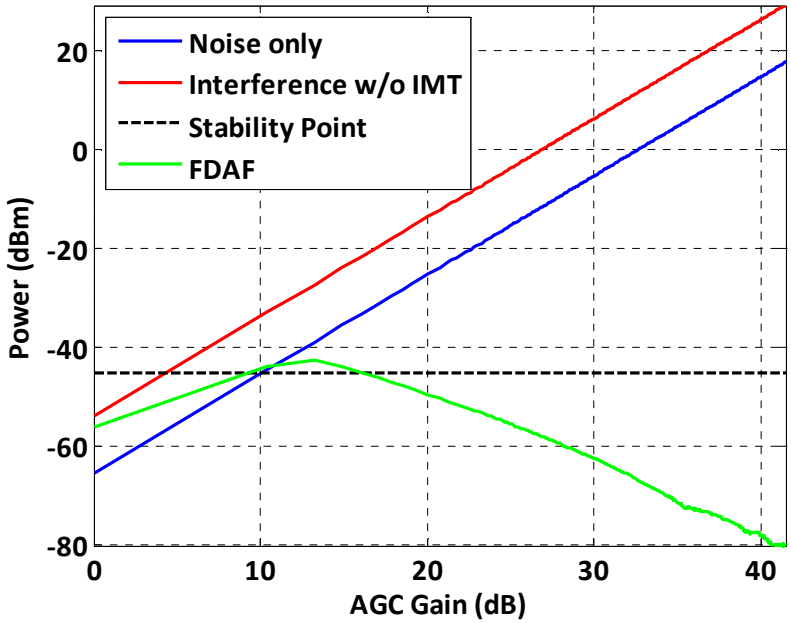

Figure 84: AGC Gain expected behaviour using FDIS.

A.1.1.3.Simulation Results

Figure 85 shows the behaviour of the loop in presence of noise only, and setting the loop gain K to 0.05. The loop converges in few ms towards 10.6 dB.

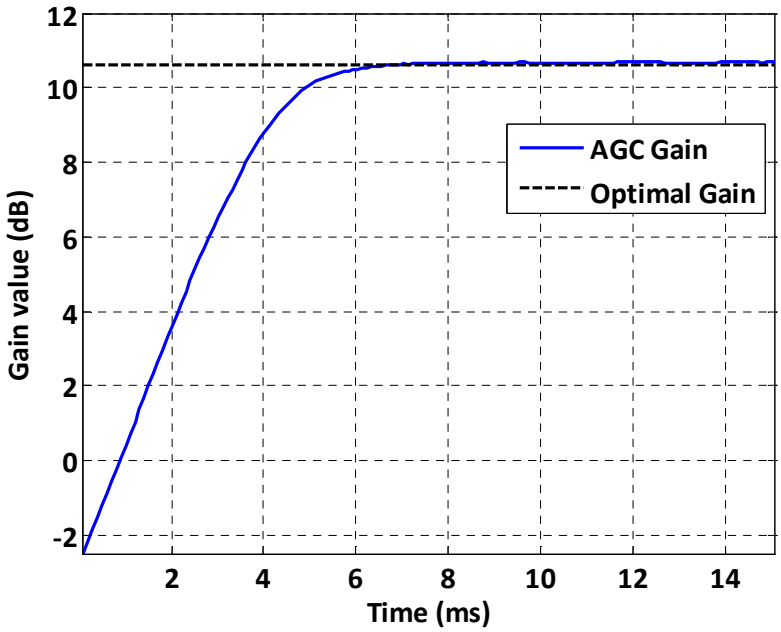

Figure 85: AGC gain with Interference free signal at receiver input using variance estimator.

The same test is run, playing the DME/TACAN hot spot scenario, and using the signal before IMTs processing. The results, given in Figure 86, reveal that the gain is biased by 6 dB, as expected.

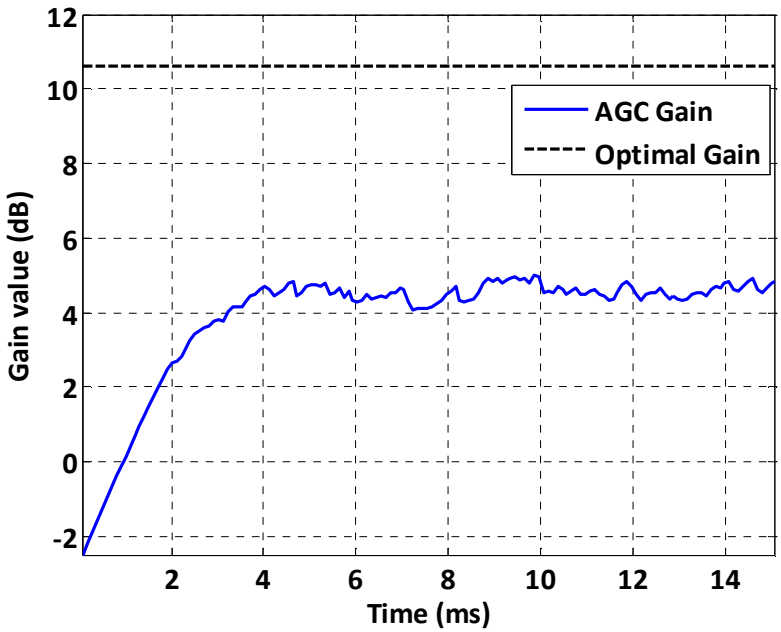

Figure 86: AGC gain with Interference at receiver input using variance estimator.

Figure 87 and Figure 88 confirm the expected performance improvement brought by IMTs: the gain bias is slightly lowered using the temporal blanker, and equals only a few tenths of dB using FDIS. Nevertheless, as said in paragraph A.1.1.2, the loop can diverge in such configurations, which is not acceptable.

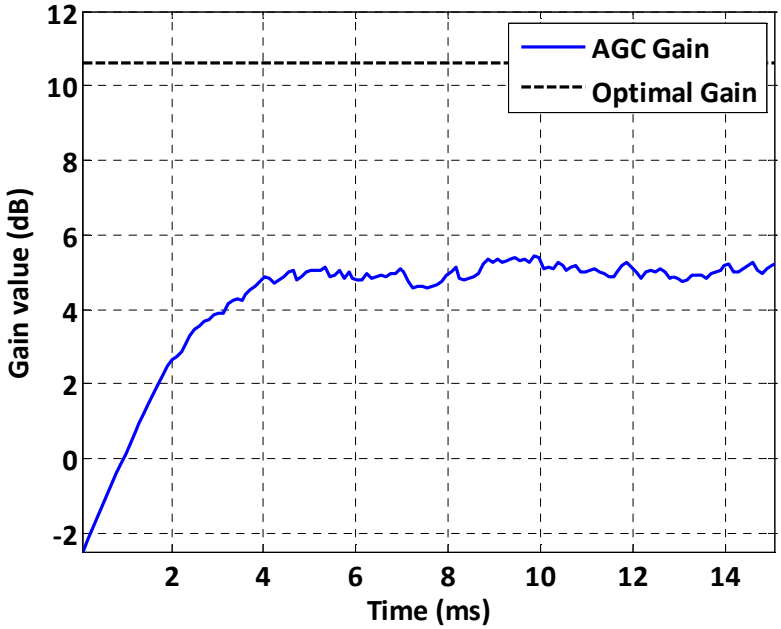

Figure 87: AGC gain with Interference at receiver input using variance estimator and Temporal Blanker.

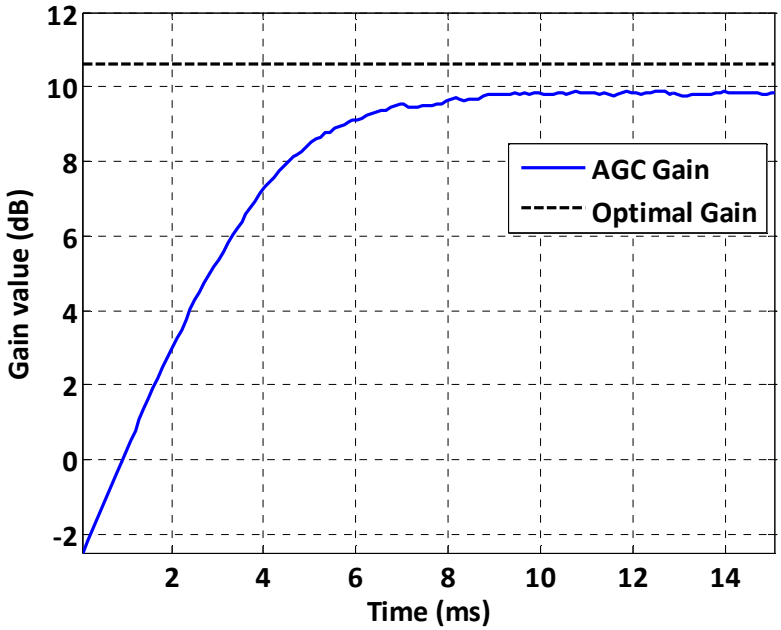

Figure 88: AGC gain with Interference at receiver input using variance estimator and Temporal Blanker.

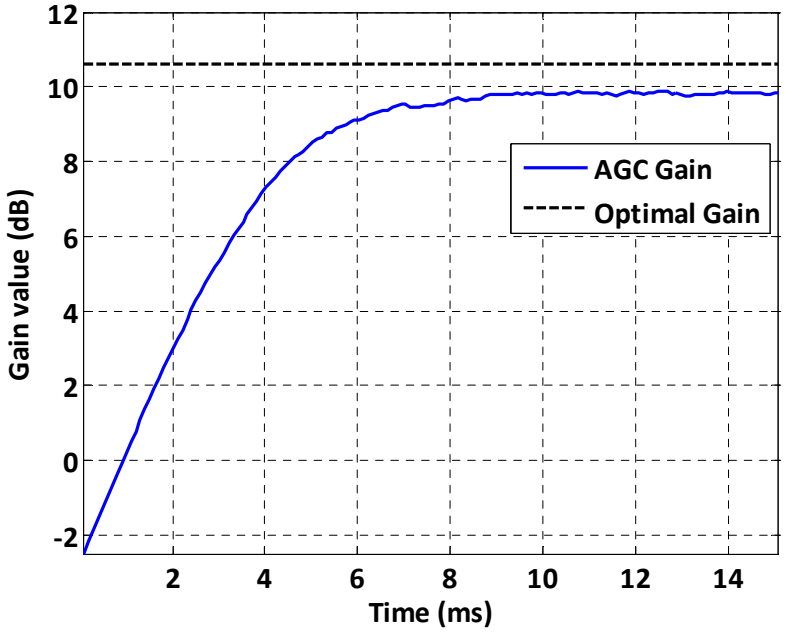

Figure 89 : AGC gain with Interference at receiver input using variance estimator and FDIS.

A.1.1.4.Conclusion

Using the variance estimator is a good option to process interference free signals (acceptable rapidity, good accuracy). As the E5 band is highly disturbed by pulsed interference, it is mandatory to consider the loop performance in this case. As the system shows poor performance in the tested environment, it is required to find another way of designing the loop to build onboard receivers. An alternative to variance estimation, which is a distribution based estimator, might be a good solution for the targeted application.

A.2. Loop Behaviour in Distribution Estimator Mode

The proposed estimator counts, at ADC output, the number of 0, 1 and -1. The proposed estimator is:

$$Estimator = 2 \times n_0 - n_1 - n_{-1} \qquad \text{A.18}$$

This function is monotonous as a function of the gain, as shown in Figure 90. The dashed blue line represents the value used to regulate the loop (consign value), which corresponds to a gain of 10.6 dB. The black line represents the linearization that will be made so as to be able to calculate the loop transfer function. The proposed model is highly non-linear when the gain is far from the desired value.

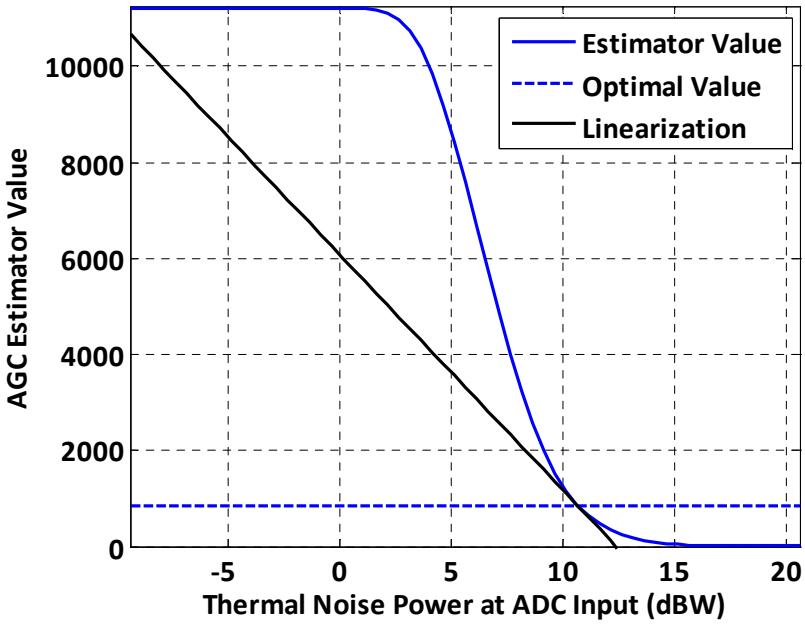

Figure 90 : Distribution Estimator value as a function of the gain.

A.2.1. Closed Loop Transfer Function

The closed loop transfer function is a little bit different from the one shown in paragraph A.1.1 since the linearization of the estimator as a function of the gain is different. Indeed, the linearization proposed in Figure 90 can be written as:

$$dist(G) = 490 \times \left(G_{dB} - G_{optdB}\right) + dist_{opt} \qquad \text{A.19}$$

Then, the same approach than in paragraph A.1.1 leads to the following closed-loop transfer function:

$$F(p) = \frac{1}{1 + \frac{3{,}04 \times 10^{-4}}{K} \times p + \frac{3{,}44 \times 10^{-7}}{K} p^2} \qquad \text{A.20}$$

The total transfer function is equivalent to a second order filter.

A.2.2. Time Constant

The theoretical transfer function of a second order system is:

$$F(p) = \frac{1}{1 + \frac{2\xi}{\omega_n} p + \frac{1}{\omega_n^2} p^2} \qquad \text{A.21}$$

Identifying the coefficients of the denominator one obtains:

$$\begin{cases} \frac{2\xi}{\omega_n} = \frac{3{,}04\times10^{-4}}{K} \\ \frac{1}{\omega_n^2} = \frac{3{,}44\times10^{-7}}{K} \end{cases} \Rightarrow \begin{cases} \xi = \frac{3{,}04\times10^{-4}}{2\times K}\sqrt{\frac{K}{3{,}44\times10^{-7}}} = \frac{0{,}11}{\sqrt{K}} \\ \omega_n = \sqrt{\frac{K}{3{,}44\times10^{-7}}} \end{cases} \quad \text{A.22}$$

According to theory, when $\xi < 1$, the time constant of the corresponding second order filter is given by:

$$\tau_{AGC} = \frac{1}{\xi\omega_n} \approx 5ms, \sqrt{K} > 0{,}11 \quad \text{A.23}$$

In the receiver mock-up this condition is always fulfilled, so that the time constant of the AGC loop is approximately 5 ms if K>0,11.

A.1.5. Stability

The approach is the same than in paragraph A.1.3, that is the open loop transfer function shall not equal -1. In order to avoid that, K is set so that the open loop transfer function module equals one and phase equals -135° (-180°+45°). This K value is the maximum K value assuring a 45° phase margin, so that the system should be designed setting K to lower or equal values.

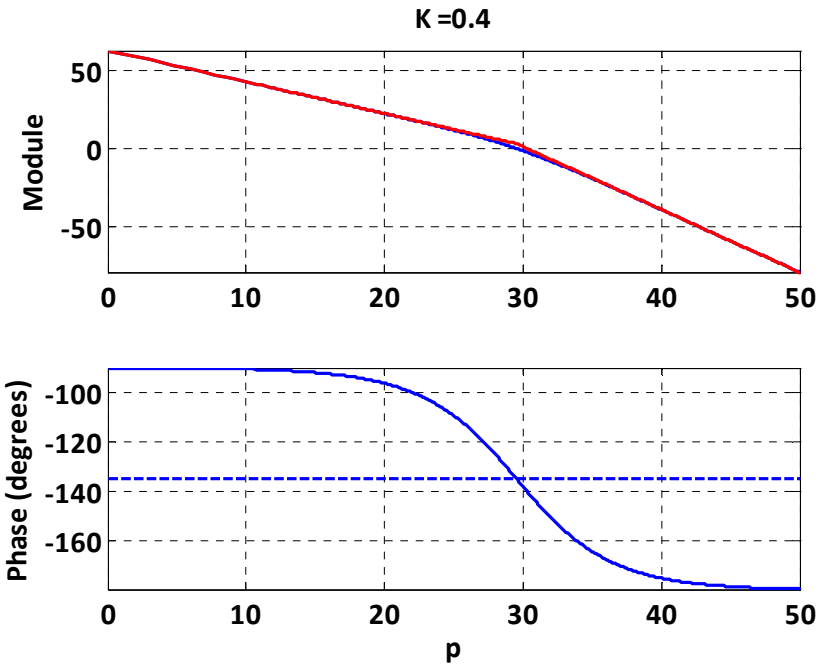

Figure 91 : AGC Open Loop Transfer Function Bode Diagram using distribution estimator.

In this case, the maximum K value assuring 45° phase margin equals 0.4.

A.1.6. Matlab Simulation Results

The same scenario than in paragraph A.1.4 is run, first without any interference or IMT, using a loop gain value of 0.3.

A.1.1.5.Expected Results

As for the standard deviation estimation method, the results using the distribution estimation method can be forecast by analysing the estimator value as a function of the gain. Figure 92 shows that in presence of interference, the estimated gain error is significantly smaller using the distribution estimator (≈2 dB) than the standard deviation estimator (≈6 dB). Moreover, the use of FDIS processed signals in the distribution estimator decreases the gain bias to less than a 0.1 dB, which is somewhat negligible. Nevertheless, the presence of a divergence zone prevents the use of this configuration. The reader would notice that the loop is not studied in case the distribution is estimated after temporal blanking. Indeed, the Temporal Blanker sets high amplitude samples to zero, which cannot be taken into account in the distribution estimation. Therefore the use of the temporal blanker has no effect on the estimator.

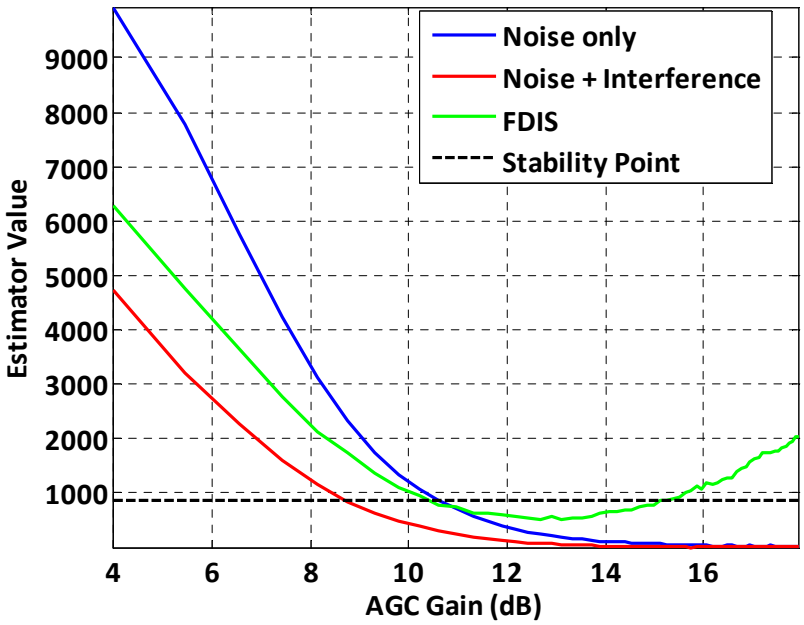

Figure 92 : Distribution Estimator value as a function of the gain.

A.1.1.6.Simulation Results

The loop is tested first in absence of interference. The loop converges within a few milliseconds to the expected value, as shown in Figure 93.

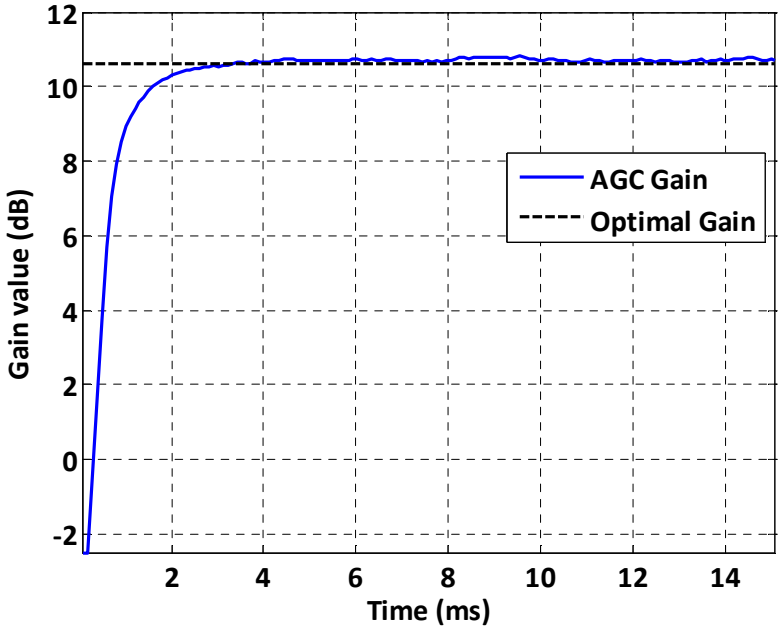

Figure 93 : AGC gain with Interference free signal at receiver input using distribution estimator.

The same test is performed in interference environment, and the results are presented in Figure 94. The system converges rapidly close to the correct value: the error is about 2 dB, meaning that this estimator is far less disturbed by the presence of interference than the variance one. The results are as good as when using the variance estimator with FDIS, but here there is no divergence issue (see Figure 92 red curve).

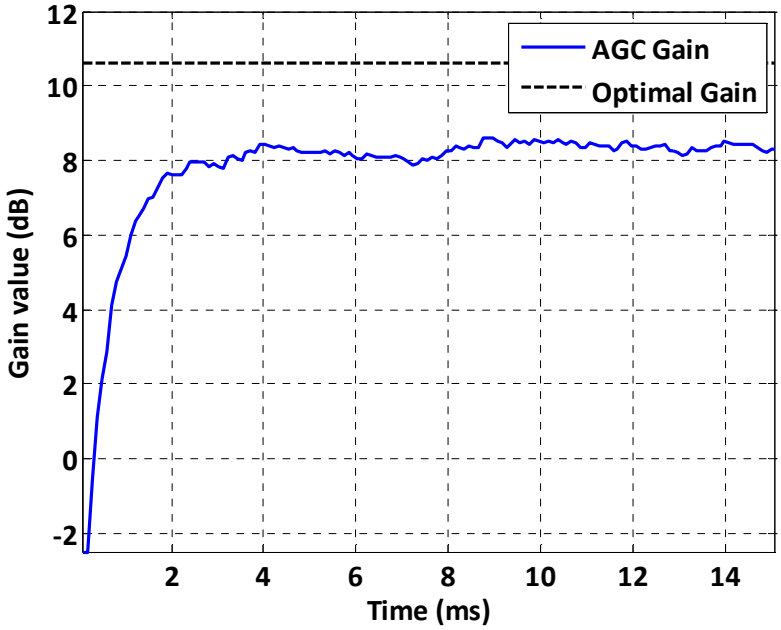

Figure 94 : AGC gain with Interference at receiver input using distribution estimator.

Finally, the loop was tested using the FDIS prior distribution estimation. The results are very good, as shown in Figure 95: the convergence is fast and the gain bias is almost null. However, the loop is not stable if the gain is too large, which is not acceptable.

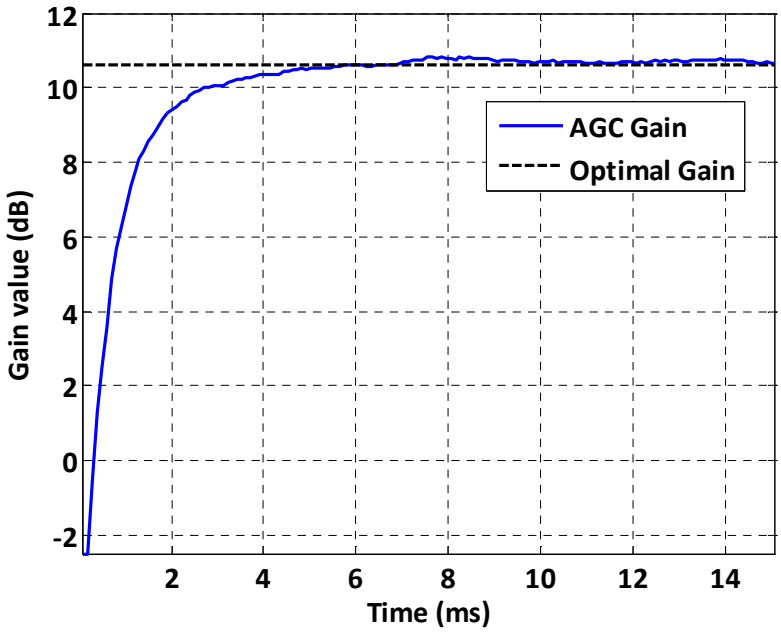

Figure 95 : AGC gain with Interference at receiver input using distribution estimator and FDIS.

A.3. Conclusions and Recommendations

In absence of interference, both techniques are valid, show good convergence speed and stability. Nevertheless, in presence of interference, the variance estimator is highly disturbed and leads to large gain biases (up to 6 dB). This is mitigated using FDIS, but this option is not acceptable as the system can diverge. The distribution estimator is less vulnerable to interferences (gain bias of 2 dB only), making this method the best solution.

To conclude, the best solution is to use a distribution based AGC. The loop gain has to be set to 0.3, and the consign value to 861.

Appendix B : European hot spot DME/TACAN beacons characteristics

Table 27: European hot spot DME/TACAN beacons characteristics.

Frequency (MHz)	Angle of arrival (°)	Power at antenna input (dBW)	Pulse repetition frequency (ppps)	Frequency (MHz)	Angle of arrival (°)	Power at antenna input (dBW)	Pulse repetition frequency (ppps)
1156	-3.6	-116.3	3600	1182	-2.3	-103.2	3600
1156	-4.8	-113.8	3600	1182	-3.9	-99.8	2700
1156	-3.5	-116.6	3600	1182	-4.3	-100.9	2700
1156	-2.7	-118.7	3600	1183	-1.9	-111.8	2700
1157	-1.8	-106.3	2700	1183	-1.7	-112.6	2700
1157	-2.4	-103.6	2700	1183	-4.2	-99.2	2700
1157	-1.8	-108.0	3600	1184	-1.8	-108.3	2700
1158	-1.8	-108.4	2700	1184	-2.5	-102.6	3600
1159	-3.0	-111.8	2700	1184	-1.9	-110.0	3600
1159	-3.8	-98.8	3600	1185	-1.8	-106.4	2700
1160	-1.9	-107.9	2700	1186	-2.1	-105.1	2700
1160	-2.4	-113.9	2700	1186	-2.8	-102.5	2700
1160	-1.6	-106.1	3600	1187	-2.8	-112.5	2700
1161	-3.5	-100.5	2700	1187	-2.6	-113.1	2700
1162	-2.7	-104.8	2700	1187	-3.6	-99.5	3600
1162	-2.9	-104.2	2700	1187	-4.1	-109.3	2700
1163	-1.9	-105.7	2700	1188	-2.0	-115.3	2700
1164	-5.3	-106.0	3600	1188	-2.1	-115.0	2700
1165	-2.6	-109.0	2700	1188	-4.3	-100.9	2700
1165	-1.8	-105.4	3600	1188	-4.1	-109.4	2700
1165	-4.1	-109.2	2700	1190	-3.0	-100.9	2700
1166	-1.7	-105.6	3600	1191	-2.0	-117.4	2700
1166	-2.1	-106.9	2700	1191	-3.0	-105.2	2700
1167	-1.6	-109.3	2700	1191	-3.8	-110.1	2700
1167	-1.7	-105.7	2700	1192	-1.8	-116.5	2700

1168	-4.8	-97.0	3600	1192	-3.7	-100.2	2700
1169	-1.6	-111.2	2700	1192	-2.0	-109.7	3600
1169	-1.9	-107.7	2700	1193	-3.0	-111.9	2700
1169	-2.6	-113.0	2700	1193	-14.4	-108.6	2700
1169	-1.8	-105.4	3600	1193	-2.6	-101.3	3600
1169	-1.6	-106.5	3600	1194	-2.1	-104.1	3600
1170	-3.7	-99.2	3600	1194	-2.5	-113.5	2700
1170	-2.5	-102.5	3600	1195	-1.6	-109.5	2700
1171	-4.8	-98.0	2700	1195	-3.8	-99.1	3600
1172	-2.0	-109.5	2700	1196	-3.6	-99.5	3600
1172	-2.1	-108.8	3600	1197	-1.7	-109.1	2700
1174	-1.8	-105.2	3600	1197	-5.3	-109.2	2700
1175	-1.8	-105.4	3600	1198	-2.0	-109.6	3600
1175	-12.0	-108.1	3600	1200	-1.6	-111.6	2700
1176	-15.3	-99.0	3600	1201	-10.4	-98.5	3600
1177	-1.5	-109.7	2700	1201	-1.5	-109.8	2700
1177	-2.3	-104.1	2700	1202	-2.2	-109.9	3600
1178	-1.8	-116.5	2700	1202	-2.4	-106.2	2700
1178	-2.6	-105.1	2700	1203	-2.0	-105.4	2700
1178	-3.2	-101.5	2700	1203	-2.7	-113.1	2700
1179	-2.6	-113.1	2700	1203	-2.7	-102.0	3600
1179	-7.5	-108.2	3600	1203	-2.0	-107.6	2700
1179	-4.1	-109.2	2700	1204	-2.2	-106.9	2700
1180	-2.0	-111.3	2700	1204	-4.0	-96.6	3600
1180	-2.6	-113.1	2700	1205	-4.9	-96.9	3600
1180	-4.1	-109.3	2700	1206	-2.4	-103.0	3600
1181	-2.6	-113.1	2700	1206	-2.3	-108.5	3600
1181	-2.6	-100.3	3600	1207	-2.6	-103.5	2700
1181	-4.1	-109.3	2700	1207	-1.7	-110.0	2700
1181	-1.6	-111.3	3600	1208	-1.9	-112.2	2700

Appendix C **: Résumé en Français**

Les organismes de standardisation de l'aviation civile (l'OACI, RTCA, EUROCAE) mènent actuellement des études sur l'utilisation des Systèmes de navigation par satellite fournissant une couverture globale, tels GPS ou Galileo, en tant que moyen de navigation embarqué unique. L'OACI regroupe l'ensemble de ces systèmes de navigation satellitaires et de leurs systèmes d'augmentation sous la dénomination GNSS. Pour des raisons de sécurité évidentes, les performances des récepteurs GNSS embarqués doivent garantir des minima propres à chaque phase de vol et chaque procédure d'approche. Ces exigences de performances sont spécifiées dans les spécifications des performances opérationnelles minimales, documents publiés (ou en cours de publication) par les autorités sus-citées.
Le GNSS est en passe d'être amélioré par la diffusion de nouveaux signaux. Parmi eux, les signaux Galiléo E5 et GPS L5 devraient permettre l'amélioration du service de navigation par satellite. Cependant, ces signaux seront émis dans une bande déjà utilisée par des systèmes Radiofréquences. Il est donc primordial de s'assurer de la possibilité de la cœxistence de ces systèmes. Plus particulièrement, il est nécessaire de s'assurer que les récepteurs GNSS embarqués utilisant les signaux sus-cités respectent les exigences de performance. La menace principale au bon fonctionnement des récepteurs GNSS utilisant les signaux E5/L5 a été identifiée comme étant les émissions pulsées des systèmes DME, TACAN, JTIDS et MIDS. Sans moyen de lutte contre ces interférences, les performances des récepteurs GNSS embarqués peuvent être dégradées de manières significatives, empêchant les récepteurs de se conformer aux exigences de sécurité sur l'ensemble du monde, et plus particulièrement sur des « points chauds » ayant été identifiés comme les lieux ou l'impact de ces interférences sur lesdits récepteurs est la plus importante. Deux techniques de réduction d'interférences ont été proposées pour lutter contre cette menace, le Blanker temporel et le Frequency Domain Interference Suppressor (FDIS).
Le Blanker temporel est une technique de traitement du signal consistant en un simple test de puissance, relativement simple à mettre en œuvre et dont la capacité de réjection des interférences a été démontrée suffisante pour assurer exigences de l'aviation civile dans toutes les phases de vols sur l'ensemble du monde pour les récepteurs GPS et Galiléo utilisant respectivement les signaux L5 et E5, dans [Bastide, 2004]. Toutefois, cette technique permet de respecter les exigences avec une marge faible, dans les environnements les plus riches en interférences, autrement dit les « points chauds ».
En revanche, le FDIS est une technique de lutte contre les interférences pulsées beaucoup plus exigeante en termes de ressources, puisque basée sur l'excision des interférences dans le domaine fréquentiel. Cependant, elle permet une amélioration sensible des performances du récepteur, et donc une augmentation des marges vis-à-vis des exigences fixées par l'Aviation Civile.

Le FDIS a été proposé comme une alternative au blanker temporel, mais ses problèmes d'implantation et ses performances n'ont été que peu étudiés. La dissertation a pour but de participer à cette étude de performance afin de valider son intérêt. Le plan de la thèse est le suivant : tout d'abord, les signaux de navigation, Galiléo E5a/E5b et GPS L5, les interférences pulsées, ainsi que leur impact sur les performances des récepteurs GNSS sont présentés. Ensuite, une description des techniques de suppression d'interférences (blanker temporel, FDIS), leurs caractéristiques théoriques et les dégradations de performances subies par un récepteur GNSS utilisant ces techniques en présence d'interférences pulsées sont présentées. Les conditions dans lesquelles ont été obtenues ces performances, c'est à dire le choix des scénarios joués ainsi que des paramètres observés, ou encore les outils de simulation sont décrits. La conclusion résume l'analyse des performances.

C.1. Description des signaux

Les signaux GNSS diffusés dans la bande étudiée sont GPS L5 et Galileo E5. Le signal GPS L5 est émis autour de la fréquence porteuse 1176,45 MHz, et modulé en QPSK. Le signal Galileo E5 est émis autour de la fréquence centrale 1191,18 MHz, et modulé en AltBOC(15,10). E5 est composé des signaux E5a et E5b, respectivement modulés autour de 2 sous porteuses de fréquence 1176,45 MHz et 1207,14 MHz. Les signaux interférents (DME, TACAN, JTIDS, MIDS) sont émis sur toute la bande de Service de RadioNavigation Aéronautique (SRNA) qui leur est allouée (960 – 1215 MHz). La Figure 96 représente les spectres des signaux E5 et L5, ainsi que la bande de fréquence SRNA à l'intérieur de laquelle les signaux interférents sont susceptibles d'être émis. Cette figure met en évidence l'omniprésence des interférences dans la bande du signal utile.

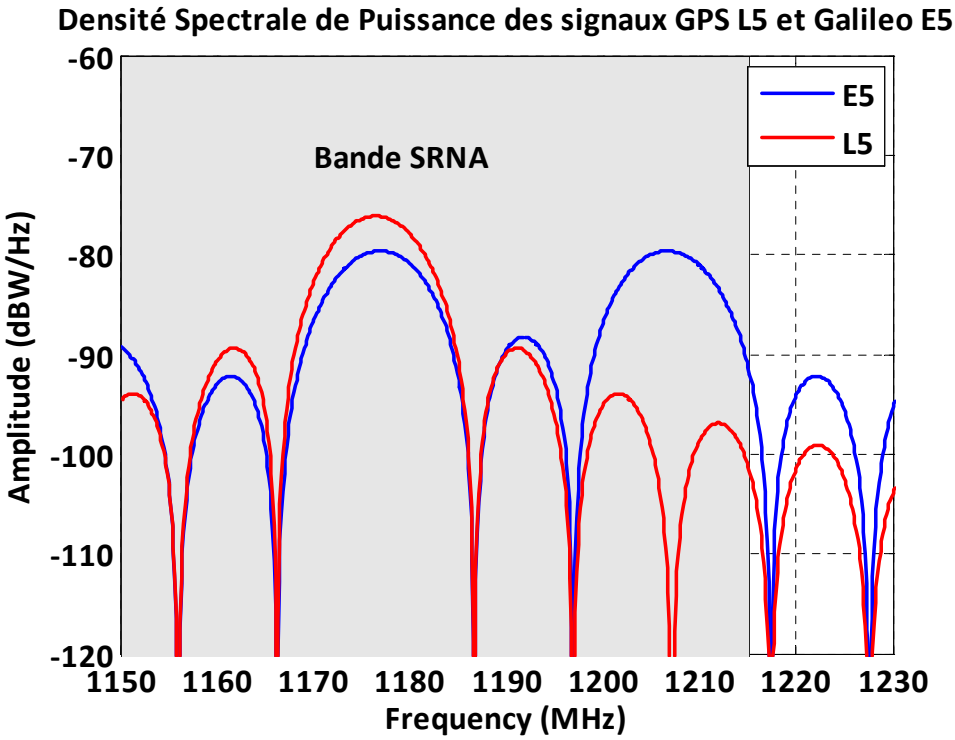

Figure 96: Occupation de la Bande E5/L5 par les signaux GNSS et SRNA.

Les interférences pulsées émises dans la bande étudiée sont issues des systèmes DME, TACAN, JTIDS et MIDS. Les systèmes DME, et leur équivalent militaire TACAN, sont composés d'interrogateurs embarqués et de balises terrestres. Un dialogue (interrogation/réponse) entre les deux équipements permet à l'utilisateur de mesurer la distance le séparant de la balise sol, dont il connaît la position. Les signaux émis par les balises sont les seuls à être émis dans la bande étudiée, et prennent la forme de paires de pulses gaussiens modulés par un cosinus. Les représentations temporelles et spectrales de ces signaux sont données Figure 97. L'étroitesse du spectre des signaux DME/TACAN par rapport au spectre GNSS est remarquable.

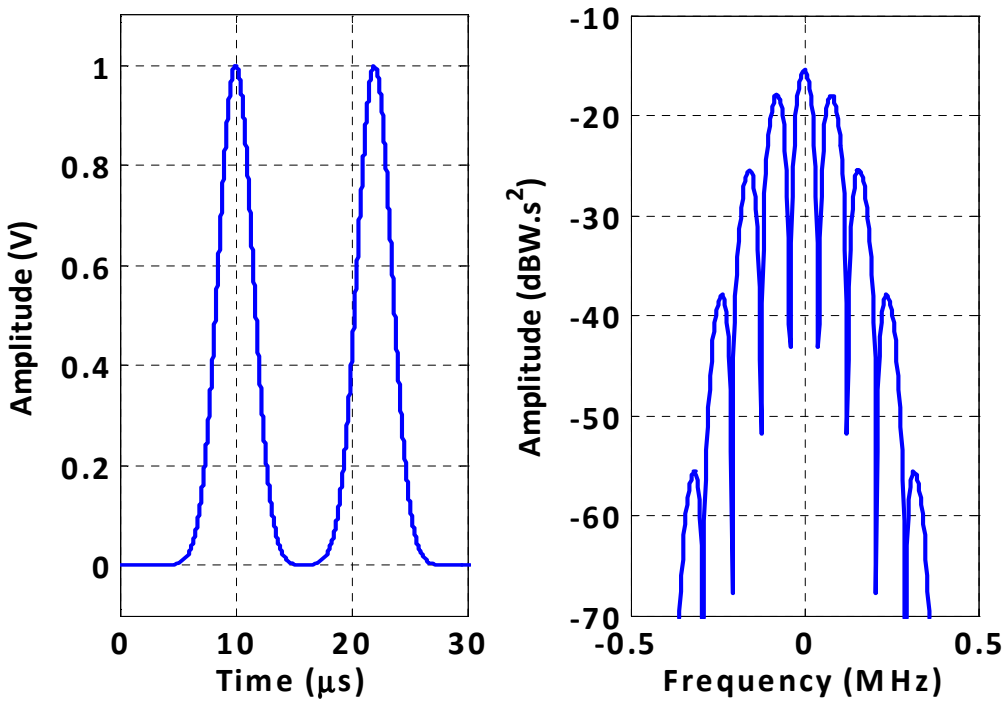

Figure 97: Représentations Temporelles et Spectrales des Signaux DME/TACAN.

Les systèmes JTIDS et MIDS sont des systèmes militaires, constituant des plateformes de communication de données tactiques. Les signaux sont composés de pulses rectangulaires modulés par un cosinus. Les caractéristiques temporelles et spectrales des signaux JTIDS/MIDS sont présentées Figure 98. Ici encore, l'étroitesse du spectre des signaux JTIDS/MIDS par rapport au spectre GNSS est remarquable.

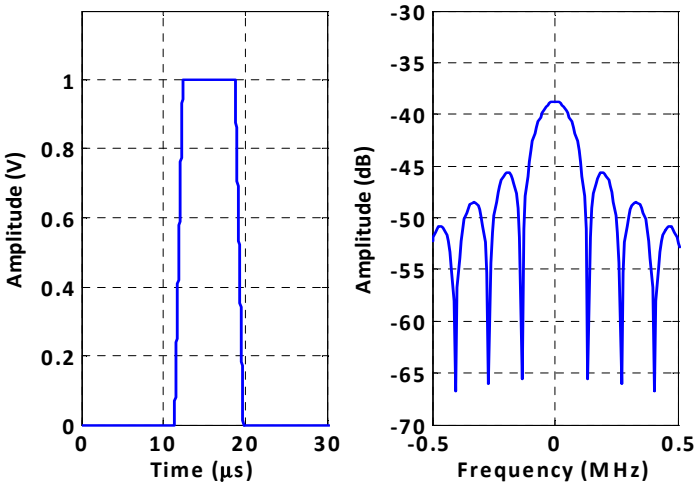

Figure 98: Caractéristiques Temporelles et Spectrales des Signaux JTIDS/MIDS.

C.2. Description des Effets des Interférences sur les Récepteurs GNSS

L'architecture des récepteurs GNSS est présentée Figure 99. Le fonctionnement de la plupart des étages des récepteurs peut être perturbé par la réception d'interférences :

- La réception d'interférences peut provoquer la saturation du préamplificateur, voire l'endommager, si la puissance desdites interférences est trop élevée. Les préamplificateurs des récepteurs E5/L5 seront conçus pour supporter les puissances maximales attendues.
- La réception d'interférences peut aussi provoquer la saturation du quantificateur. Le nombre de bits des quantificateurs implémentés dans les récepteurs E5/L5 sera augmenté pour traiter linéairement les interférences pulsées.
- Le fonctionnement de la boucle de Contrôle Automatique de Gain (CAG) est perturbé. Il est nécessaire de proposer des techniques de traitement du signal permettant de s'affranchir de ces perturbations.
- Les sorties de corrélateurs sont perturbées. Ces sorties étant utilisées pour mesurer les pseudo-distances, calculer la position et démoduler les données, il est primordial d'atténuer les perturbations induites par ces interférences. Cette opération est effectuée par des techniques de réduction d'interférences (en anglais Interference Mitigation Techniques, IMT).

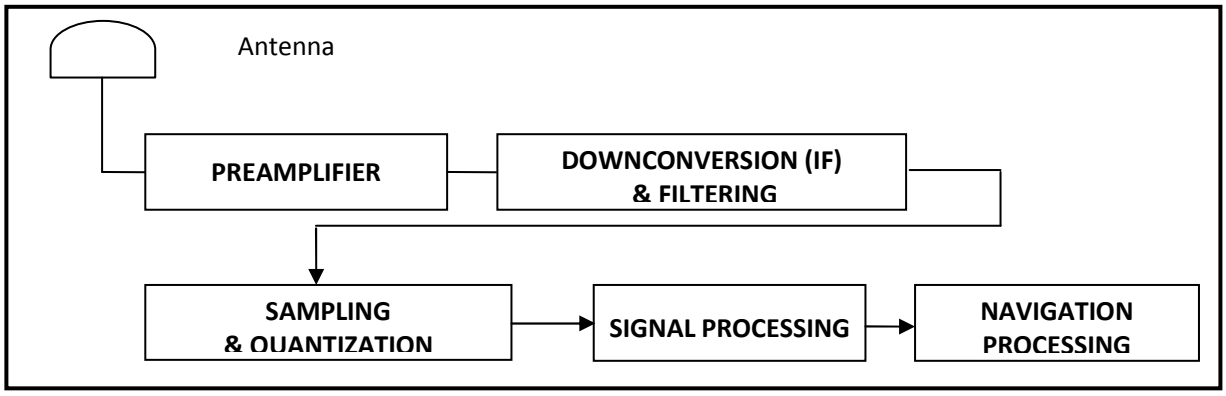

Figure 99: Architecture des Récepteurs GNSS.

C.2.1. Effet des Interférences sur la Boucle de CAG

La boucle de CAG a pour rôle d'adapter la puissance du signal en entrée de quantificateur de façon à minimiser la dégradation du signal due à la quantification. Les pertes de quantification dépendent de la loi de quantification utilisée et des caractéristiques du signal entrant. En absence d'interférences, le signal est dominé par le bruit thermique. Etant donné la distribution Gaussienne du signal et une loi de quantification, la dégradation subie est fonction de la puissance du signal entrant le Convertisseur Analogique Numérique (CAN). La CAG estime la puissance du signal en sortie de CAN et donc le gain à appliquer pour minimiser la dégradation. La Figure 100 représente la boucle de CAG, et montre que le signal utilisé pour estimer le gain à appliquer est observé en sortie de CAN, avant toute IMT. La boucle de CAG ne profite donc pas de l'atténuation des interférences opérée par les IMTs.

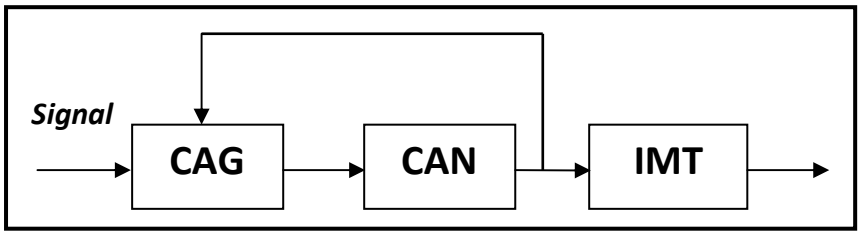

Figure 100: Boucle de CAG.

La Figure 101 représente les pertes dues à la quantification en fonction de la puissance du signal entrant, et confirme l'existence d'un minima. Ces pertes, calculées en sortie de corrélateurs, supposent la réception de bruit blanc gaussien uniquement. Les CAG classiques, basées sur des estimateurs de puissance, sont ainsi fortement biaisées par la réception d'interférences, ce qui entraîne une augmentation des pertes de quantification, d'autant plus importante que la puissance des interférences reçues l'est. Dans cette thèse, une CAG basée sur une estimation de la distribution est proposée pour s'affranchir de ce problème.

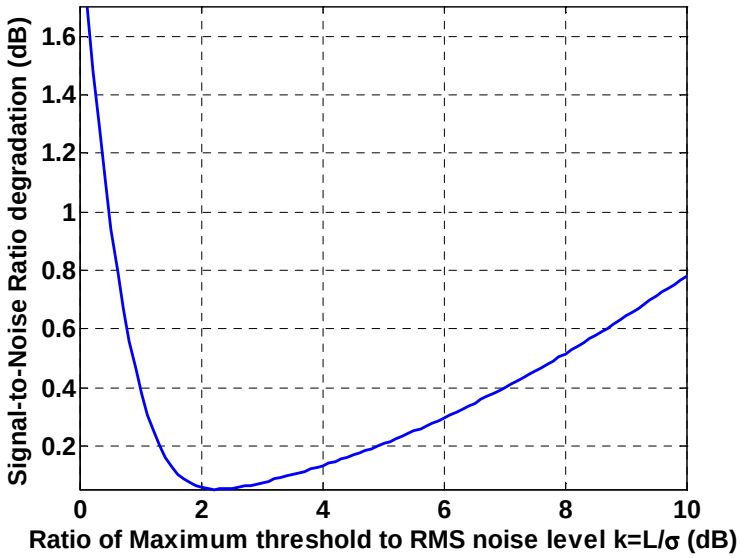

Figure 101: Pertes de Quantification en fonction de l'écart type du signal entrant.

C.2.2. Effet des Interférences Pulsées sur les Sorties de Corrélateurs

L'effet des interférences pulsées, ou plus largement des interférences à bande étroite, sur les sorties de corrélateurs peut être modélisé [Van Dierendonck, 1996] par un bruit blanc gaussien de densité $N_{0,I}$ dont l'expression est :

$$N_{0,I} = \sum_k P_k \times C_I(\Delta f_k)$$
$$C_I(\Delta f_k) = \int_{-\infty}^{+\infty} S_{I,k}(f) \times S_C(f) df \qquad \text{B.1}$$

Où :

- P_k est la puissance moyenne de l'interférence,

- $C_{I,k}$ est le coefficient d'interférence,
- $S_{I,k}$ est le spectre normalisé du signal interférant,
- S_C est le spectre normalisé du signal GNSS.

Cette densité augmente la densité de bruit totale affectant les sorties de corrélateurs. Cette quantité sera par la suite utilisée dans le calcul du C/N_0, une mesure du rapport entre la puissance du signal sur la densité de bruit, largement utilisé pour évaluer les performances du récepteur.

C.3. Techniques de Lutte contre les Interférences

Les techniques de lutte contre les interférences sont destinées à diminuer l'impact des interférences sur les récepteurs GNSS, et plus particulièrement sur les sorties de corrélateurs. L'utilisation de telles techniques a pour but de réduire la densité de bruit blanc gaussien ajouté par les interférences. La première IMT à avoir été proposée s'appelle le Blanker Temporel. Cette technique, considérée par les organismes de standardisation de l'Aviation Civile (EUROCAE, RTCA) comme une référence, repose sur l'hypothèse selon laquelle la distribution du signal est Gaussienne. Ainsi, l'amplitude du signal est supposée ne pas dépasser quelques sigmas. Il est donc possible de déterminer un seuil en amplitude, au-delà duquel le signal est considéré corrompu par une interférence. Les échantillons concernés sont alors remplacés par des zéros. La Figure 102 montre un exemple du traitement d'un signal composé d'une interférence et d'une paire de pulses DME (ou TACAN) par le blanker temporel.

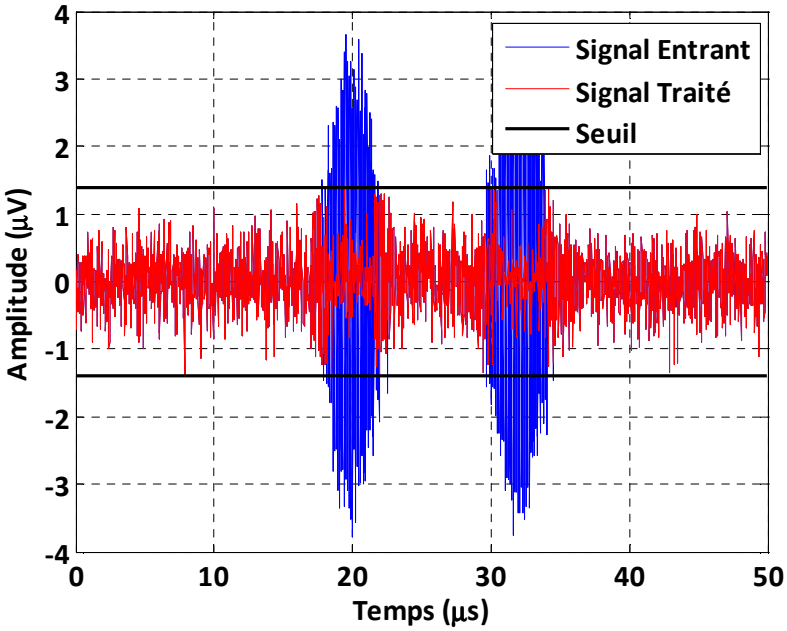

Figure 102: Illustration du Fonctionnement du Blanker Temporel.

La deuxième technique de réduction d'interférences étudiée est appelée Frequency Domain Interference Suppressor (FDIS). La technique repose sur une estimation du

spectre du signal à partir de quelques échantillons (calcul de la transformée de Fourier), et suppose la présence de bruit blanc uniquement. De la même manière que pour le blanker temporel, le signal est supposé être composé de bruit thermique, et donc blanc, uniquement (le signal utile est négligeable avant corrélation). Il est donc possible de déterminer un seuil en amplitude dans le domaine fréquentiel, au-delà duquel le signal est considéré corrompu par une interférence. Les canaux fréquentiels concernés sont alors remplacés par des zéros, et le signal temporel est retrouvé par calcul de la transformée de Fourier inverse. La Figure 103 montre un exemple du traitement d'un signal composé d'une interférence et d'une paire de pulses DME (ou TACAN) par le FDIS.

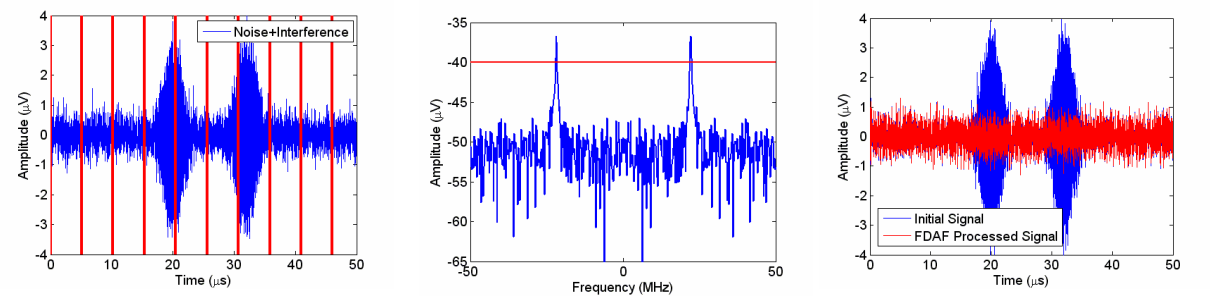

Figure 103: Illustration de fonctionnement du FDIS.

C.4. Description des Outils de Simulation

C.4.1. PULSAR

PULSAR est un simulateur de récepteur GNSS logiciel, développé sous Labview. Dans le cadre de cette thèse, cet outil est utilisé pour évaluer les performances des techniques proposées dans le paragraphe précédent, ainsi que l'impact de la boucle de CAG sur les performances des récepteurs GNSS. Par ailleurs, cet outil est utilisé pour valider les résultats obtenus avec les autres outils utilisés (maquette, outil de prédiction) lors de l'étude.

Le simulateur est composé d'un générateur de signaux et d'un récepteur GNSS. Le générateur de signaux simule les signaux Galileo E5a, E5b, et GPS L5. Ces signaux sont obtenus en modulant les codes d'étalement en QPSK autour d'une fréquence intermédiaire (FI) de 14 MHz, avec une fréquence d'échantillonnage de 56 MHz. Le générateur simule également un bruit thermique, à l'aide d'une fonction Labview permettant de générer des bruits blancs Gaussiens. Enfin, il génère les interférences pulsées DME/TACAN et/ou JTIDS/MIDS, selon les scénarios fixés par la RTCA ou l'EUROCAE.

Le récepteur GNSS est composé d'un filtre équivalent en FI, d'une boucle de CAG, des IMTs décrites précédemment (Blanker Temporel et FDIS), de corrélateurs, de boucles de poursuite de code et de phase, et enfin d'un estimateur de C/N_0. L'interface graphique présentée en Figure 104 permet à l'utilisateur de paramétrer le récepteur et de suivre les mesures de C/N_0 en temps réel.

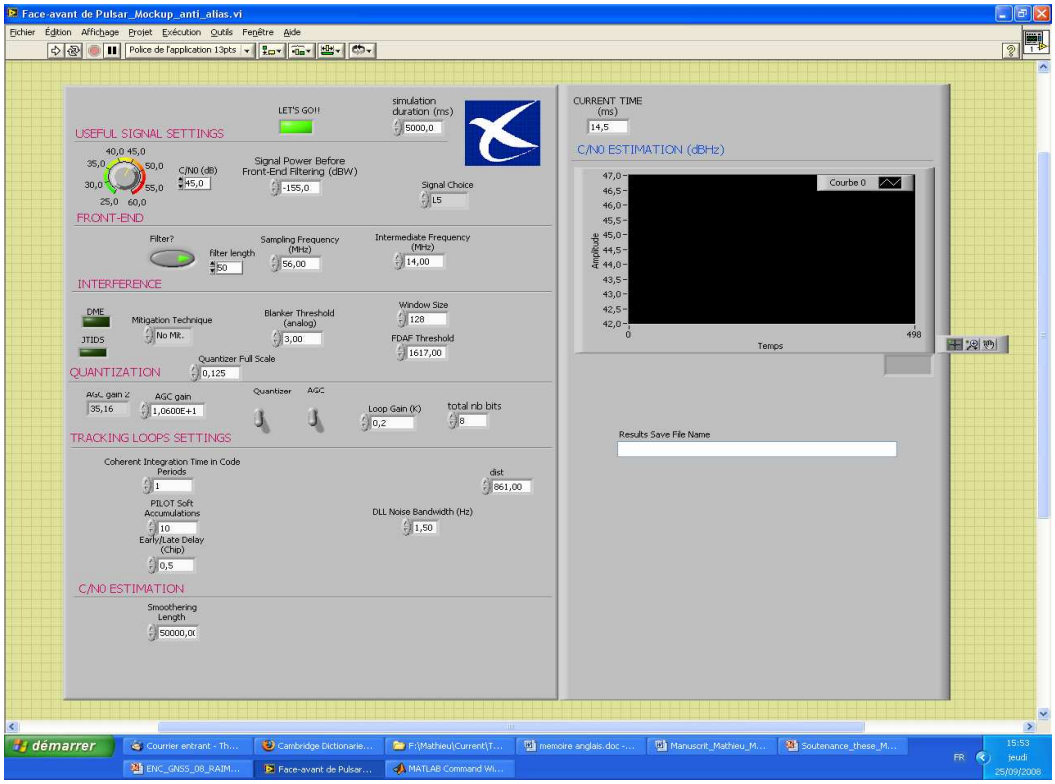

Figure 104: Face Avant de PULSAR.

Lors des simulations, la densité du bruit est réglée à -200 dBW/Hz, et la puissance du signal reçu à -155 dBW (voie pilote uniquement). Il en résulte un C/N_0 de 45 dB-Hz. La fréquence d'échantillonnage est fixée à 56 MHz, et les filtres équivalents en FI sont d'ordre 50 et respectent les masques fournis par l'Aviation Civile, voir Figure 105 et Figure 106.

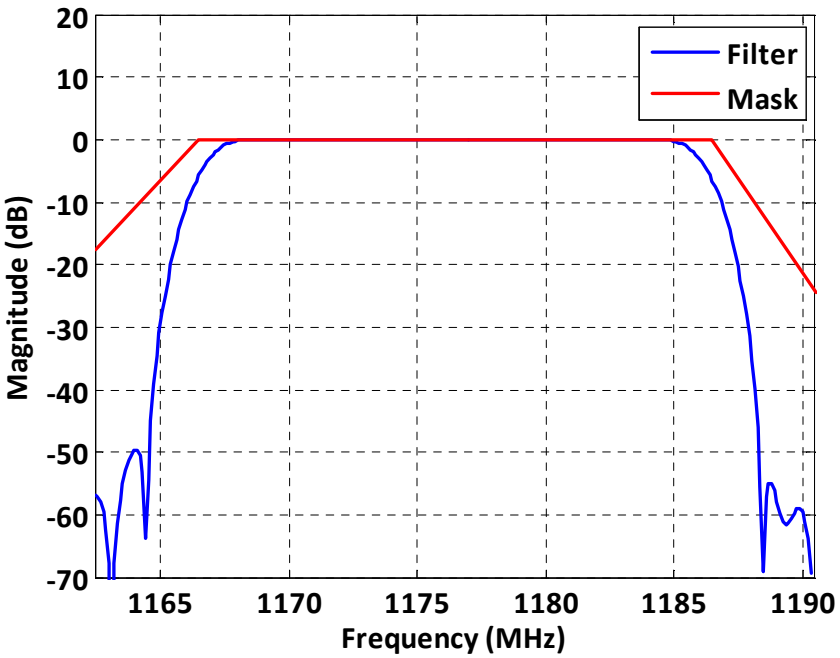

Figure 105: Module de la Fonction de Transfert du Filtre équivalent FI utilisé pour les signaux E5a et L5.

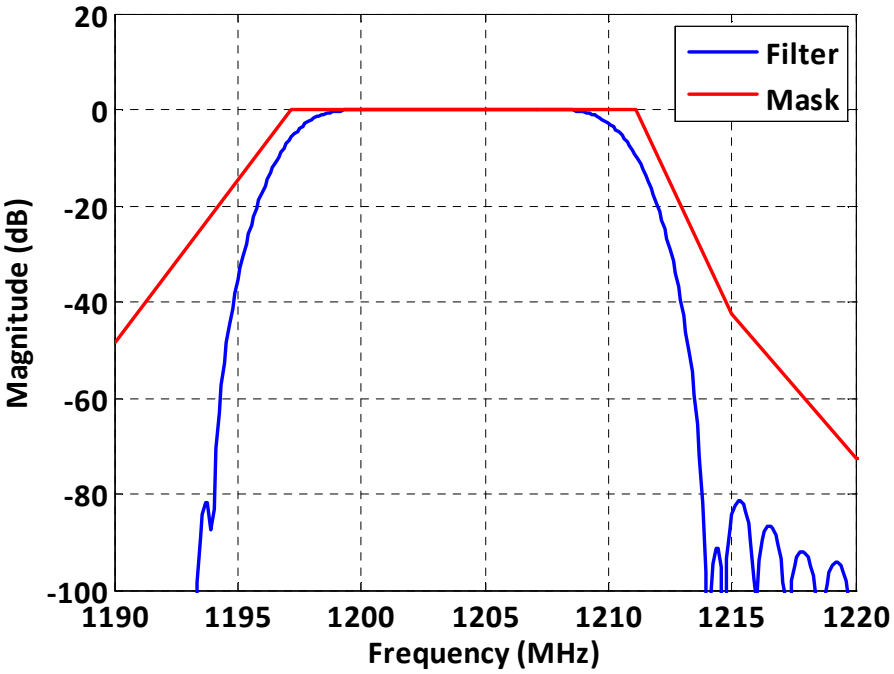

Figure 106: Module de la Fonction de Transfert du Filtre équivalent FI utilisé pour les signaux E5a et L5.

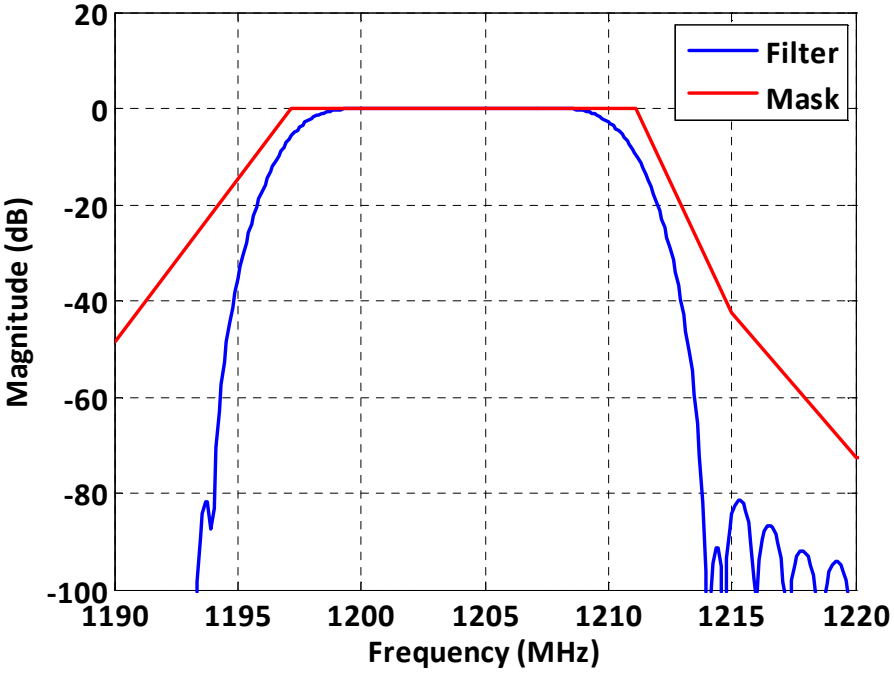

Figure 107: Module de la Fonction de Transfert du Filtre équivalent FI utilisé pour le signal E5b.

Les estimateurs de puissances étant fortement biaisés par les interférences, la CAG implémentée dans PULSAR est basée sur un estimateur de distribution, moins sensible aux interférences pulsées. L'estimateur implémenté s'écrit :

$$\varepsilon = 2 \times N_0 - N_1 - N_{-1} \qquad \text{B.2}$$

Où:

- N_0 est le nombre de zéros compté en sortie de CAN durant 100 µs,
- N_1 est le nombre de 1 compté en sortie de CAN durant 100 µs,
- N_{-1} est le nombre de -1 compté en sortie de CAN durant 100 µs.

La densité de probabilité d'un bruit Gaussien, représentée Figure 108 pour une puissance de bruit de -75 dBW, est estimée pour diverses puissances et utilisée pour calculer la valeur de l'estimateur précédemment présenté. Cette correspondance est présentée Figure 109.

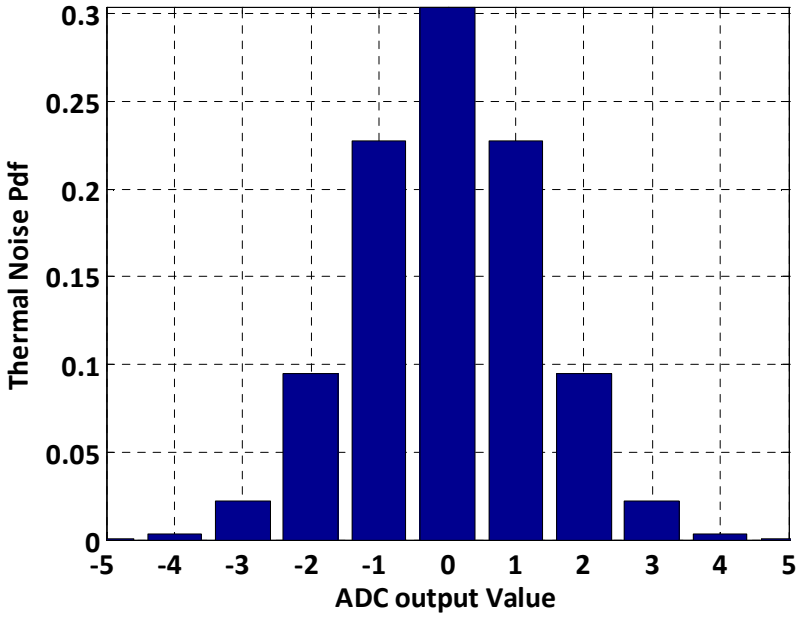

Figure 108: Distribution d'un bruit Gaussien en sortie de CAN.

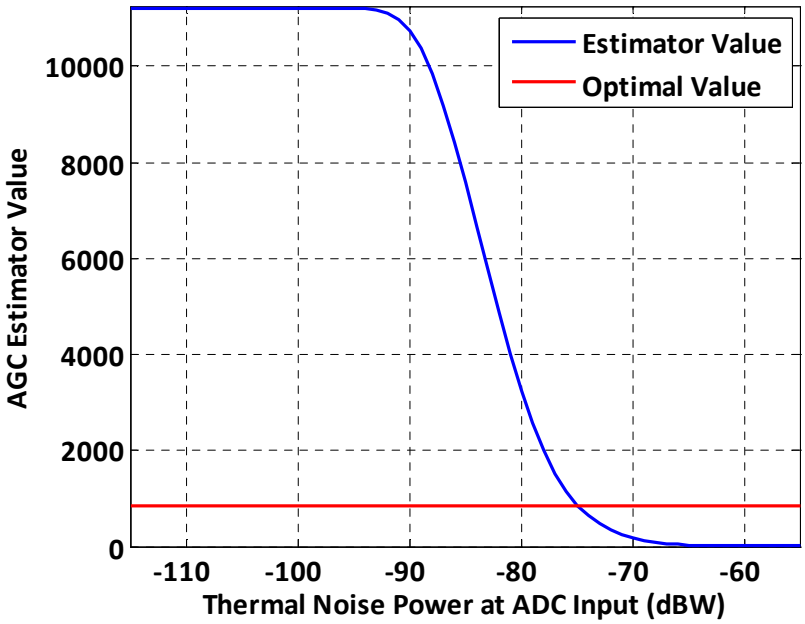

Figure 109: Valeur de l'estimateur proposé en fonction de la puissance de bruit.

Les interférences sont générées selon les scénarios de « pire cas » définis par la RTCA ou l'EUROCAE. La quantité et la puissance de signaux DME/TACAN reçus étant une fonction de la position, ces scénarios correspondent à un lieu appelé « hot spot ». En Europe, les coordonnées du « hot spot » sont 50° Nord et 9° Est. L'appareil, survolant le lieu à une altitude de 40 000 pieds, reçoit les émissions de toutes les balises DME/TACAN émettant dans son horizon radio-électrique. La puissance des signaux reçus est atténuée par le gain d'antenne des balises DME/TACAN, les pertes de propagation en espace libre, ainsi que par l'antenne du récepteur. L'instant de réception de chaque paire de pulse est déterminée aléatoirement, suivant une loi de Poisson. Ce procédé permet la génération de collisions entre paire de pulses, phénomène très fréquent en opérations. Le diagramme utilisé pour les antennes des balises DME/TACAN est montré Figure 110, et celui utilisé pour les antennes GNSS l'est Figure 111. Plus exactement, la Figure 111 représente les hypothèses de pire cas proposées par la RTCA ainsi que les hypothèses proposées par l'EUROCAE. Dans cette étude, l'hypothèse prise par la RTCA est retenue. Les signaux JTIDS/MIDS sont générés suivant le scénario numéro VIII définit par l'IGEB (Interagency GPS Executive Board).

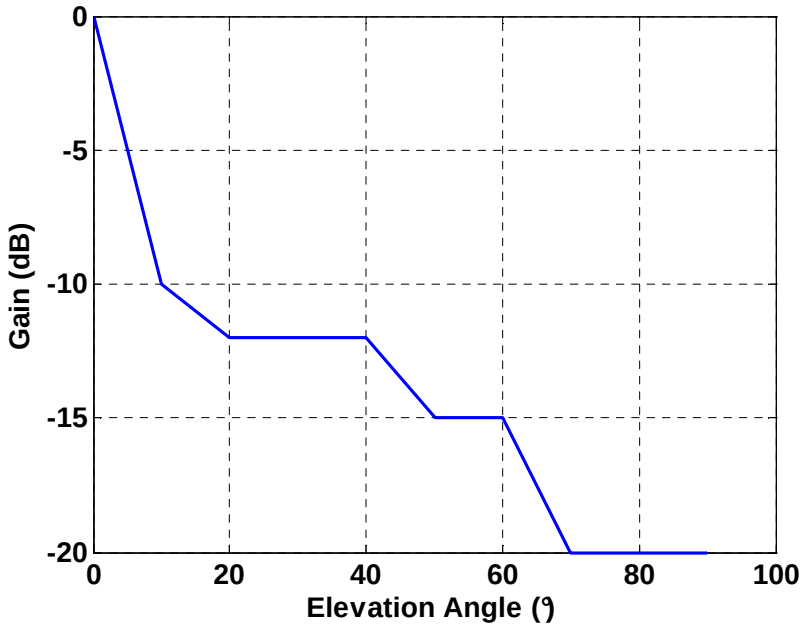

Figure 110: Diagramme d'antenne des Balises DME/TACAN.

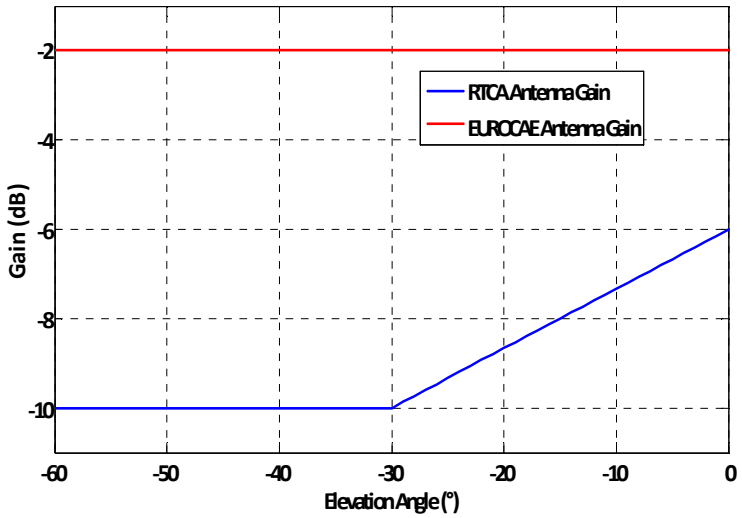

Figure 111: Diagramme d'antenne GNSS embarqué pour les élévations négatives.

C.4.2. Outil de prédiction de dégradation de C/N_0

L'outil de prédiction permet de déterminer les pertes de C/N_0 dues à la réception de signaux DME/TACAN, en fonction de la position de l'utilisateur, et de la technique de réduction d'interférences utilisée. Le calcul de la dégradation sur le C/N_0 en sortie de corrélateur se décompose en trois parties:

- La dégradation du signal utile due à l'utilisation d'IMTs,
- La dégradation du bruit thermique due à l'utilisation d'IMTs,
- L'augmentation de la densité du bruit due aux interférences.

$$\frac{C}{N_0} = \frac{C_{IMT}}{N_{0,IMT} + \sum_k N_{0,DME/TACAN,k,IMT}} \qquad \text{B.3}$$

Cet outil a été utilisé avec le blanker temporel puis le FDIS, afin d'estimer leurs performances sur toute l'Europe. Lors des tests, le seuil du blanker temporel est réglé sur -117.1 dBW sur E5a/L5 et -120 dBW sur E5b. Ces seuils ont été définis dans [Bastide, 2004] comme optimisant les performances du blanker temporel. Le seuil du FDIS, quand a lui, a été réglé sur -195 dBW/Hz, et le nombre d'échantillons utilisés dans le calcul de la FFT à 128. Les dégradations de C/N_0 sont prédites sur toute l'Europe, pour les signaux E5a et L5 Figure 112 pour le blanker temporel et Figure 113 pour le FDIS. Les résultats obtenus au hot spot sont comparés avec les simulations PULSAR, effectuées dans les mêmes conditions et présentées Table 28. Cette dernière montre une forte corrélation entre les résultats obtenus avec PULSAR et l'outil de prédiction. De plus, les performances obtenues avec le FDIS sont nettement meilleures (6 dB au hot spot) que celles obtenues avec le blanker temporel, et ce partout en Europe.

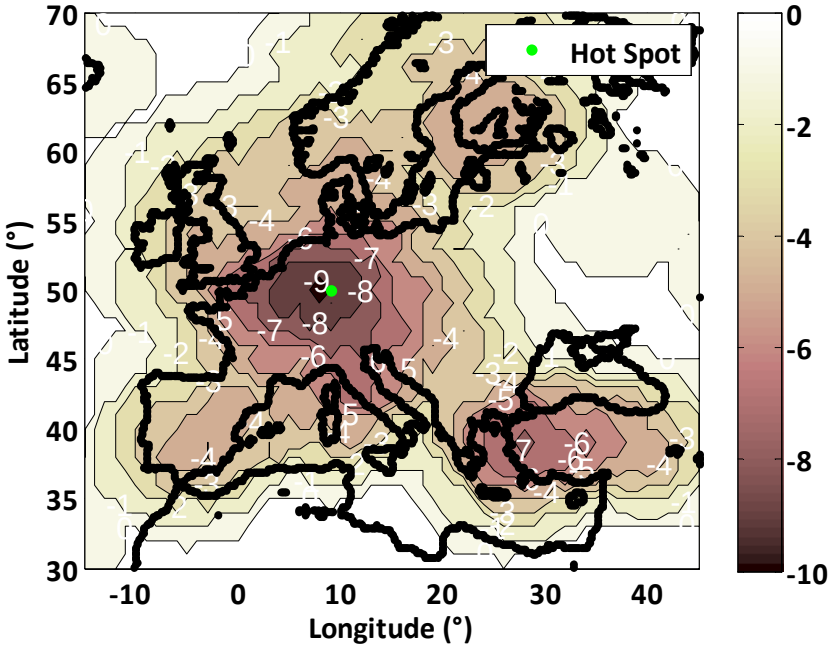

Figure 112: Performances du blanker temporel sur l'Europe pour les signaux E5a/L5.

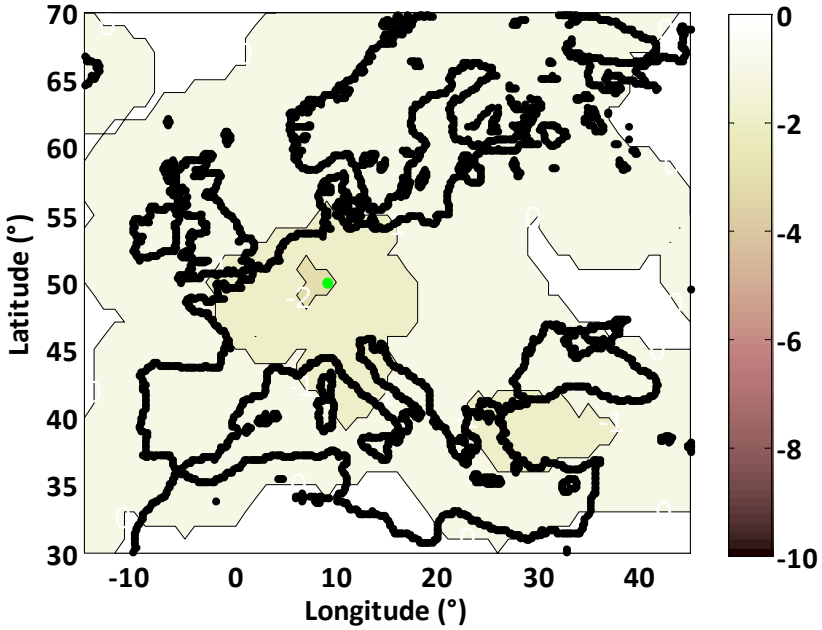

Figure 113: Performances du FDIS sur l'Europe pour les signaux E5a/L5.

Table 28 Dégradations de C/N_0 avec le blanker temporel et le FDIS au hot spot pour les signaux E5a/L5 obtenus avec PULSAR et l'outil de prédiction.

	PULSAR	Théorie
BT	8.8 dB	9.0 dB
FDIS	3.0 dB	2.2 dB

Les mêmes tests ont été effectués avec le signal E5b. Les résultats obtenus sont présentés Figure 114 et Figure 115, et comparés aux simulations PULSAR dans la Table 29. Une fois de plus, les résultats obtenus avec le FDIS sont nettement meilleurs (4 dB) que ceux obtenus avec le blanker temporel. On pourra noter que la corrélation entre les résultats obtenus avec PULSAR et avec l'outil de prédiction est faible pour le FDIS, ceci étant du à la non prise en compte dans l'outil de prédiction de l'étroitesse de la bande du filtre utilisé dans PULSAR.

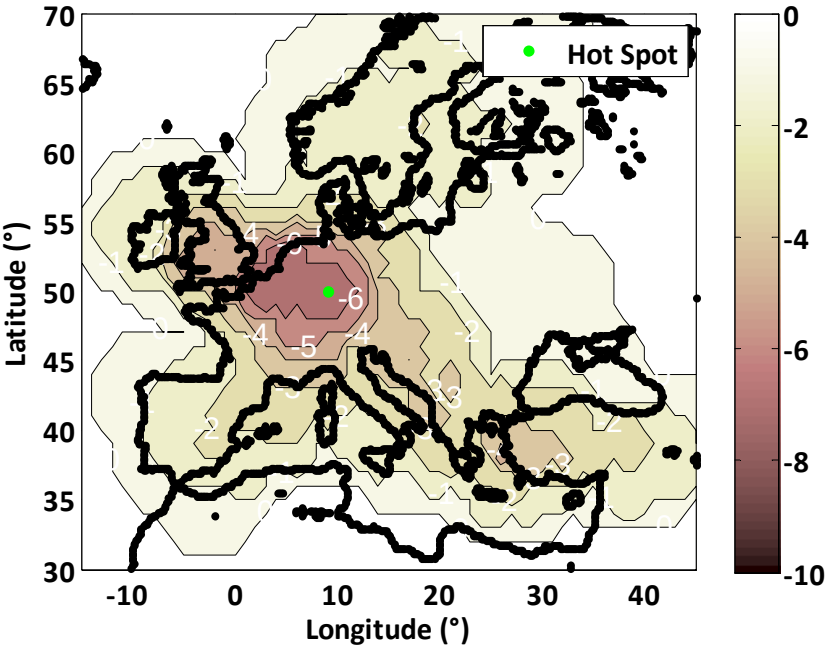

Figure 114: Performances du blanker temporel sur l'Europe pour le signal E5b.

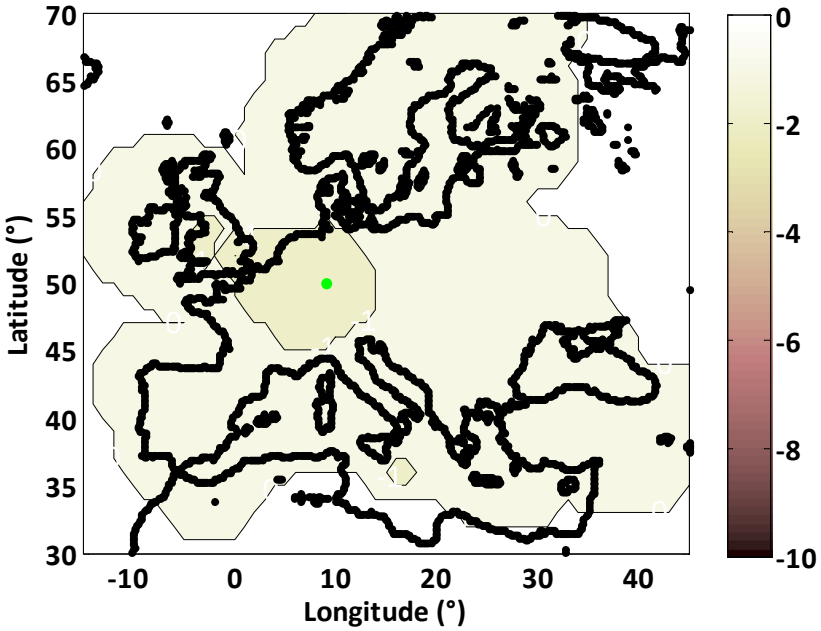

Figure 115: Performances du blanker temporel sur l'Europe pour le signal E5b.

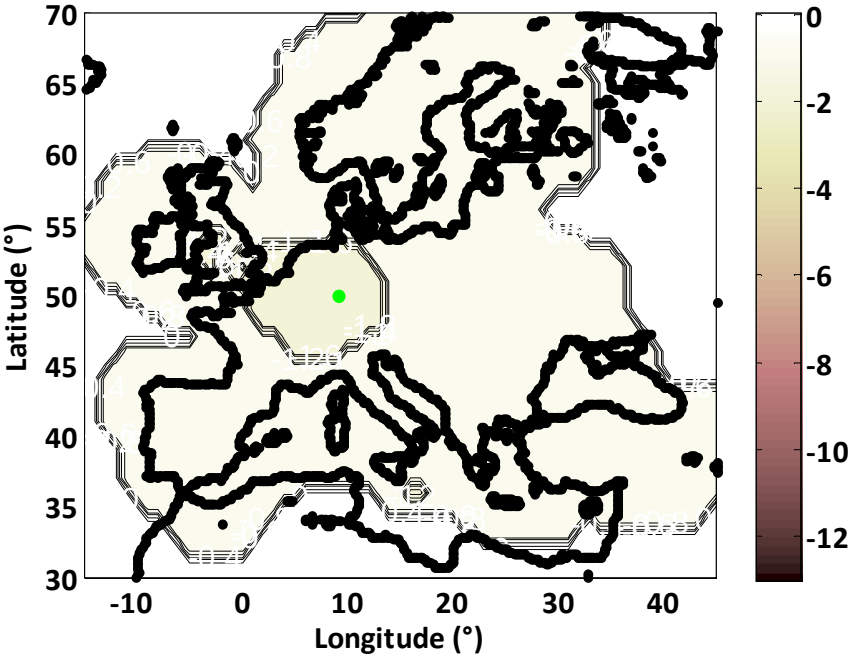

Figure 116: Performances du FDIS sur l'Europe pour le signal E5b.

Table 29: Dégradations de C/N_0 avec le blanker temporel et le FDIS au hot spot pour le signal E5b obtenus avec PULSAR et l'outil de prédiction.

	PULSAR	Théorie
BT	6.1 dB	6.0 dB
FDIS	0.3 dB	1.9 dB

C.4.3. Maquette ANASTASIA

La maquette de récepteur Galileo bifréquence E1/E5 embarqué produite pour le projet ANASTASIA comporte une boucle de CAG dont la régulation peut être effectuée à l'aide d'un estimateur de puissance ou d'un estimateur de distribution. Par ailleurs, les techniques de réduction d'interférences présentées précédemment sont disponibles et peuvent être activées au travers de l'interface utilisateur. Ce dernier a le choix entre:

- Aucune technique,
- Le Blanker Temporel,
- Le FDIS – 128 échantillons.

Les filtres implémentés dans la tête HF respectent les exigences de l'Aviation Civile. La fréquence d'échantillonnage est de 62.5 MHz, et les signaux sont descendus en fréquence puis traités autour d'une fréquence intermédiaire de 14 MHz. Les résultats obtenus lors du test de la maquette en conditions de hot spot Européen sont présentés dans la Table 30. On notera que les hypothèses de diagramme d'antenne utilisées pour ces tests sont les

hypothèses définies par l'EUROCAE (gain d'antenne de -2 dBi pour toute élévation négative). Les résultats présentés dans le paragraphe précédent, obtenus avec les hypothèses de gain d'antenne définies par la RTCA, ne sont donc pas comparables à ceux-ci. Les instants d'arrivées des paires de pulse sont générées avec une loi uniforme. La maquette, configurée pour acquérir et poursuivre le signal Galileo E5b, est testée dans deux configurations de CAG : (1) régulée et (2) fixe. Si la CAG est fixe, le gain est réglé sur la valeur minimisant les pertes de quantification, et les effets de la sensibilité de la boucle aux interférences ne sont pas ressentis. Dans le cas où la boucle est régulée, les performances sont diminuées d'au moins 1 dB, quelque soit l'IMT utilisée. Par ailleurs, l'utilisation du FDIS à la place du blanker temporel apporte une amélioration de 6 dBs. Enfin, l'augmentation du nombre d'échantillons utilisés pour le calcul de la FFT n'améliore pas les performances de l'algorithme, ce qui est en contradiction avec la théorie. Ceci est dû à la faible quantité de ressources allouées au calcul des FFT.

Table 30: Comparaison des performances au hot spot pour le signal E5b obtenus avec la maquette ANASTASIA, avec scénario d'interférences EUROCAE.

IMT / Seuil	Dégradation du C/N_0 (Hot Spot, CAG régulée)	Dégradation du C/N_0 (Hot Spot, CAG fixe)
Pas d'IMT	12.5 dB	N/A
BT /-120 dBW	11.5 dB	9.7 dB
FDIS 64 /-160 dBW/Hz	5.5 dB	4.7 dB
FDIS 128 /-160 dBW/Hz	6.4 dB	N/A
FDIS 256 /-163 dBW/Hz	5.7 dB	4.7 dB
FDIS 512 /-163 dBW/Hz	5.7 dB	4.2 dB

Les mesures relatives à la sensibilité de la boucle de CAG aux interférences sont présentées dans la Table 31. Les sorties des estimateurs (de puissance ou de distribution) sont converties en tensions, constituant la commande de l'amplificateur de CAG. Les mesures de ces tensions montrent que l'estimateur de distribution est nettement plus robuste aux interférences que l'estimateur de puissance. L'utilisation de l'estimateur de distribution est donc indispensable.

Table 31: Performances de la boucle de CAG de la maquette ANASTASIA.

	Tension de Commande CAG		Différence gain CAG
	Sans Int.	Avec Int.	
Estimation de puissance	2.20 V	0 V	-10 dB

Estimation de distribution	2.08 V	1.96 V	-1.35 dB

C.5. Exigences Aviation Civile

Les exigences de performances définies par l'Aviation Civile peuvent être exprimées sous formes de seuils de C/N_0. Ces seuils sont présentés dans la Table 32.

Table 32: Seuils de C/N_0 pour les signaux GPS L5 et Galileo E5a et E5b.

	Acquisition	Poursuite	Démodulation des Données
L5	29.0 dB.Hz	27.0 dB.Hz	27.0 dB.Hz
E5a	29.0 dB.Hz	N/A	22.5 dB.Hz
E5b	29.0 dB.Hz	N/A	29.7 dB.Hz

Il est nécessaire que les récepteurs GNSS respectent ces conditions, quelque soit la phase de vol. Plus particulièrement, ces conditions doivent être respectées au-dessus du hot spot, en considérant le scénario de pire cas en interférence (puissance des signaux et gain d'antenne minimum, DME/TACAN hot spot FL 400 + scénario JTIDS/MIDS numéro VIII de l'IGEB). Par ailleurs, la CAG doit être considérée comme régulée. Le bilan de liaison correspondant est proposé Table 33. Ce bilan montre que seul le FDIS permet de respecter les exigences de l'Aviation Civile en terme de C/N_0 pour les 3 signaux étudiés. Au regard de ce bilan de liaison, le blanker temporel n'est pas suffisant et le FDIS est indispensable.

Table 33: Bilan de Liaison.

	Pas d'IMT			Blanker Temporel			FDIS		
Signal	L5	E5a	E5b	L5	E5a	E5b	L5	E5a	E5b
Puissance du Signal (dBW)	-155.0	-155.0	-155.0	-155.0	-155.0	-155.0	-155.0	-155.0	-155.0
Pertes d'Imp. (dB)	-2.0	-2.0	-2.5	-2.0	-2.0	-2.5	-2.0	-2.0	-2.5
Gain ant. min. (dB)	-4.5	-4.5	-4.5	-4.5	-4.5	-4.5	-4.5	-4.5	-4.5
Densité de bruit eff. (dBW/Hz)	-188.8	-189.1	-190.9	-189	-189.4	-193.1	-194.8	-195.2	-196.1
C/N0 Eff. (dB.Hz)	27.3	27.6	28.9	27.5	27.9	31.1	33.3	33.7	34.1
C/N0 Requis (dB.Hz)	29.0	29.0	29.7	29.0	29.0	29.7	29.0	29.0	29.7

Marge (dB)	-1.7	-1.4	-0.8	-1.5	-1.1	+1.4	+4.3	+4.7	+4.4

C.6. Temps d'acquisition

Une des exigences de performances formulées par les organismes de standardisation de l'Aviation Civile concerne le temps de réacquisition. En effet, suite à une coupure d'alimentation, le récepteur doit être capable de fournir une position valide en moins de 5 minutes, avec une probabilité de 0,99. Ces conditions correspondent à une réacquisition en opération en route. Etant donné une configuration de récepteur minimale, la communauté de l'Aviation Civile a déduit de cette exigence des seuils de C/N_0, en deçà desquels les récepteurs n'atteignent plus les performances exigées. Plus précisément, les configurations minimales des récepteurs (le nombre de corrélateurs requis pour l'acquisition) ont été déduites des C/N_0 minimum garantis, étant donné la menace constituée par les interférences pulsées. Le FDIS permettant de garantir des C/N_0 plus élevés, des simulations de Monte-Carlo ont été effectuées afin de déterminer le nombre de corrélateurs minimum nécessaire pour remplir les exigences de performance en terme d'acquisition. L'étude est divisée en deux sous parties : (1) le nombre de corrélateurs minimum nécessaire à l'acquisition du 1er satellite en moins d'1 minute avec une probabilité de 0.99 est recherché, en considérant le C/N_0 minimum garanti avec le FDIS. (2) le nombre de corrélateurs minimum nécessaire à l'acquisition du 2ème au 4ème satellite en moins de 30 secondes chacun avec une probabilité de 0.99 est recherché, en considérant le C/N_0 minimum garanti avec le FDIS. Les temps alloués à l'acquisition des différents satellites sont différents car les conditions d'acquisition sont différentes (incertitude réduite après l'acquisition du 1er satellite). Les nombres de corrélateurs obtenus sont présentés Figure 117 pour le 1er satellite et Figure 118 pour les suivants. L'opération la plus contraignante en terme de nombre de corrélateur est l'acquisition du 1er satellite. De plus, il apparaît que le nombre de corrélateurs nécessaires à l'acquisition est de 500 si le FDIS est utilisé, au lieu de 1500 à 2500 si le blanker temporel est utilisé, selon [Bastide, 2004]. L'utilisation du FDIS permet un gain considérable en terme de nombre de corrélateurs.

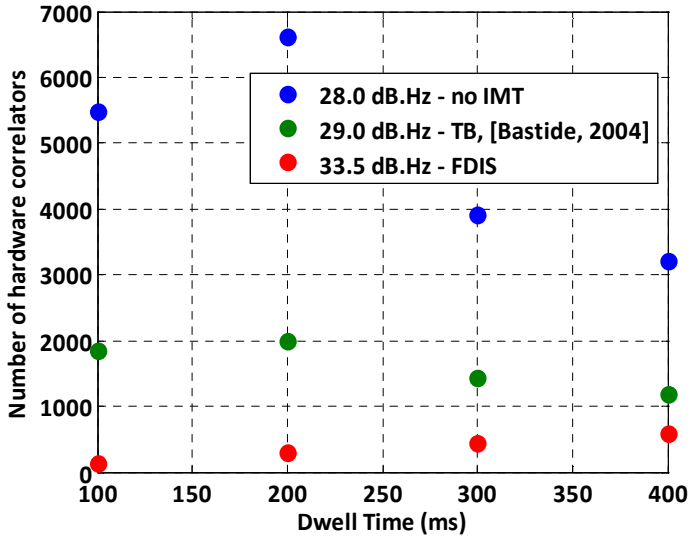

Figure 117: Nombre de Corrélateurs Requis pour l'Acquisition du premier satellite, en fonction du C/N_0 et du temps d'intégration non cohérent.

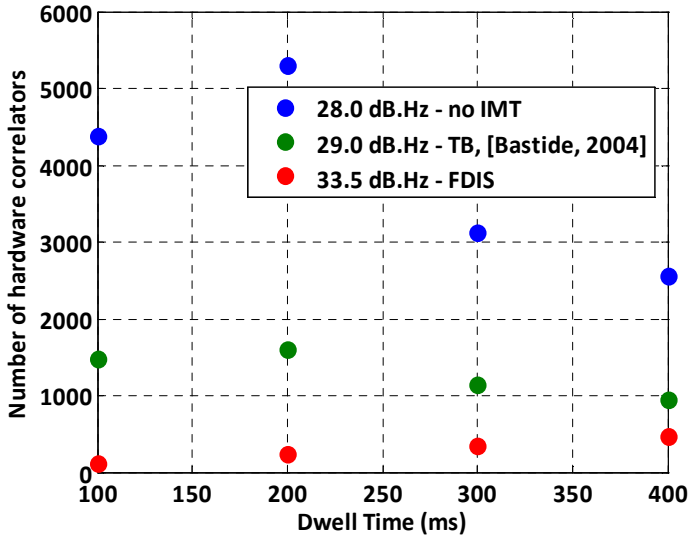

Figure 118: Nombre de Corrélateurs Requis pour l'Acquisition du premier satellite, en fonction du C/N_0 et du temps d'intégration non cohérent.

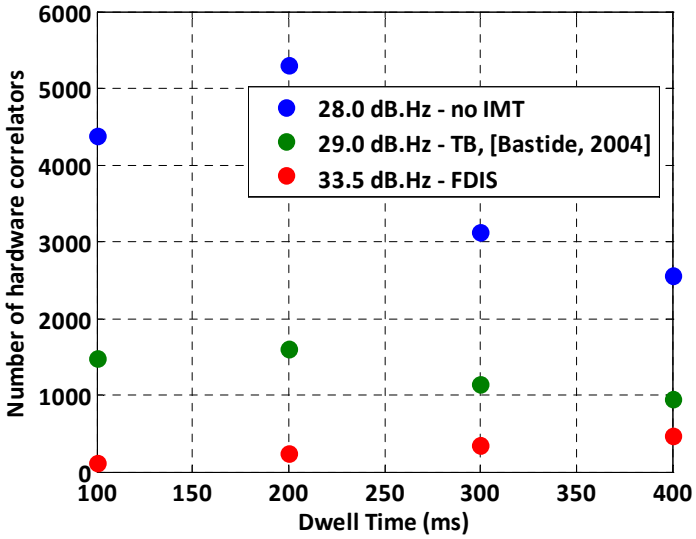

Figure 119: Nombre de Corrélateurs Requis pour l'Acquisition des satellites, en fonction du C/N_0 et du temps d'intégration non cohérent.

C.7. Conclusion

Les services fournis par les futurs signaux GPS L5 et Galileo E5 sont d'un grand intérêt pour la communauté de l'aviation civile. Plus particulièrement, les intérêts de ces signaux résident dans les données d'intégrité diffusées par le signal E5b et la possibilité d'effectuer des mesures bifréquence GPS L1/L5 ou Galileo E1/E5. Toutefois, les performances des récepteurs E5/L5 sont dégradés par les émissions DME/TACAN et JTIDS/MIDS, qui constituent des interférences. Les investigations passées menèrent à la conclusion que la coexistence de ces systèmes n'est pas possible, plus particulièrement à haute altitude (40 000 pieds) pendant le survol des «points chauds», à moins que les récepteurs GNSS ne mettent en œuvre une IMT appelée blanker temporel. Dans ce cas, les récepteurs GNSS respectent les exigences de performances pour les opérations en route fixées par la RTCA et l'EUROCAE, mais avec de minces marges.

L'utilisation d'IMTs plus complexes est une bonne solution pour améliorer ces marges, mais induit également des coûts supplémentaires. Le FDIS est l'une de ces techniques, et l'objectif principal de cette thèse était d'évaluer les performances de cette technique, puis de la tester sur un prototype de récepteur Galileo embarqué.

Le FDIS a été analysé comme étant une technique de réduction d'interférences pulsées plus efficace que le blanker temporel. Du point de vue de la dégradation du C/N_0, les récepteurs GNSS souffrent de plus faibles dégradations en utilisant le FDIS qu'en utilisant le blanker temporel. Cette amélioration a été évaluée de manière théorique, à l'aide d'un outil de prédiction développé sous Matlab, par le biais de simulations logicielles, en utilisant PULSAR, et par le biais de simulations « hardware », en utilisant la maquette de récepteur Galileo conçue pour le projet ANASTASIA. Dans les trois cas, l'utilisation du FDIS (128 échantillons,

seuil à -195 dBW/Hz) permet de réduire les dégradations du C/N_0 dues aux interférences pulsées en utilisant le blanker temporel de 4 ou 5 dB sur les signaux L5, E5a ou encore E5b.